Sensitivity and control of a pneumatic force transducer

A proof of principle

Jorrinde A.L. Lambers

Delft University of Technology

Sensitivity and Control of a Pneumatic Force Transducer

A proof of principle

by

J.A.L. Lambers

to obtain the degree of Master of Science
at the Delft University of Technology,
to be defended publicly on Friday September 27, 2019 at 10:00 AM.

Student number:	4307283	
Project duration:	February 25, 2019 – September 27, 2019	
Thesis committee:	Dr. ir. Dick H. Plettenburg,	TU Delft, supervisor
	Prof. dr. Frans C.T. van der Helm,	TU Delft

An electronic version of this thesis is available at http://repository.tudelft.nl/.

Preface

This thesis contains all the results I have obtained during my graduation project. I enjoyed working on it for the past 7 months. During this project, many people have helped me. I would like to thank my supervisor, Dick Plettenburg, for his guidance through each stage of the process. I learned a lot. I also would like to thank Jos van Driel from the 3mE meetshop. He helped me coding the LabView simulations and made sure I could extract all the relevant data from it. It was a good and at the same time educational collaboration. I also want to thank Jan van Frankenhuyzen for his advice and help during the prototyping phase. Further, thanks to everyone at the IWM Workshop. They supported me to manufacture and assemble the prototype. I want to say thank you to my subjects that all voluntarily participated in the experiments. Thanks to them I was able to derive relevant data. At last, I want to show gratitude to Hans Pop, who is an employee at Festo NL (Festo Didactic). He helped me brainstorm to find the correct valve.

Contents

Introduction

People that miss an upper limb caused by a birth defect, disease or trauma can make use of an upper-limb prosthesis. There are different types of prostheses, namely passive, externally powered or body-powered. Passive prostheses are often worn from a cosmetic point of view and only have passive functions. Externally powered prostheses make use of an external energy source (e.g. electricity). Body-powered prostheses can be actuated purely mechanical by body movements.

Feedback is essential for correct prosthetic control as it results in more efficient control since the user feels what he/she is doing. Body-powered prostheses have an advantage over externally powered devices, because they provide feedback to the user. However, feedback can also be added to an external system by adding sensors and/or actuators [3]. In this article, a design will be presented that will control a prosthesis with body movements and will be powered externally.

A body-powered prosthesis is often controlled with a figure-of-nine harness (see Figure 1). When the shoulder moves (elevation and protraction), the Bowden cable pulls a 'switch' that will in result open or close the prosthesis, depending on whether the prosthesis is voluntary opening or voluntary closing. The pulling force on the wire automatically provides physical feedback to the user.

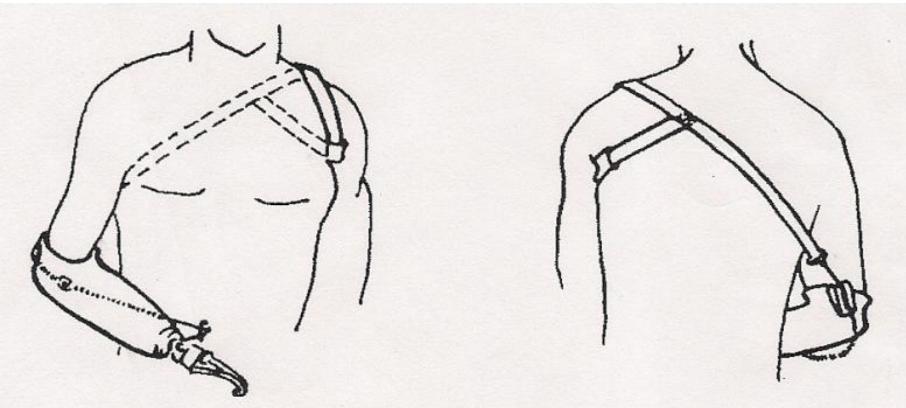

Figure 1: Example of a figure-of-nine harness, which controls a prosthesis via shoulder movement [1]. The prosthesis is attached with a Bowden cable to a harness that is placed on the contralateral shoulder. When the shoulder is moved upwards and/or forwards (elevation and/or protraction), a pulling force will act upon the Bowden cable, forcing the prosthetic hand to open or close.

Despite the fact that the cables have the advantage of providing feedback, there are also disadvantages to this design. The cables could irritate and cut the skin, for example at the armpit. This partly causes the high rejection rate (20-40%) of body-powered prosthetic devices [4]. Another reason for this high rejection rate is the high activation force that is needed to control the prosthesis, which could lead to fatigue [31]. One other complain is the high mental load that is needed to control a prosthesis. This could be caused by inappropriate feedback. There could be a modality mismatch between the feedback and where the feedback is provided. The sensory information needs to be perceived at a conscious level. The Central Nervous System (CNS) now has to match and interpret different information sources together, which demands a high mental load [3]. These problems show that many more improvements need to be made in the field of upper-limb prosthetics.

Problem Statement
As was mentioned before, problems arise when controlling a body-powered prosthesis. The main problems that occur are:

1. Discomfort (e.g. skin irritation)
2. High activation forces
3. High mental load

Many attempts have been made to improve the design of the body-powered prosthesis and to reduce/remove the problems mentioned above. Some of these solutions can be found in Part III: Literature study. However, these solutions did not seem to be sufficient to completely compensate for the problems. An example of a redesign of the figure-of-nine harness is invented by Latour [19], see Figure 2. Skin anchors are attached to the scapula. The prosthesis is actuated and by shoulder movements. It will still provides proprioceptive feedback, decreasing the mental load. This design decreases the discomfort for the wearer. Vardy et al. [35] continued with this design and they were able to decrease the activation forces.

Figure 2: The Ipsilateral Scapular Cutaneous Anchor System designed by Latour [19] [26].

Objective
The main objective of this thesis is:

Design and prototype the control and actuation system of a body-powered prosthesis and test its usefulness to place this system on the back/shoulder of the user.

The starting point of this new design was the study conducted by Vardy et al. [35]. In this thesis a proof of principle will be presented. It will be researched whether it is possible to place the total system (the pneumatic force transducer and displacement measurement device) on the back, where Vardy et al. [35] still placed the system on the table. A prototype will be built and tested. The results will be compared with the study of Vardy et al. [35], to evaluate if this new system performs equally good or even better than the system of Vardy et al. [35].

Reader's guide
This thesis report is divided intro three parts. In the first part, the scientific article will be presented (Part I). Herein the final design will be explained and tested. Experiments were performed to investigate whether the system provides appropriate proprioceptive feedback by measuring and calculating the sensitivity. A second experiment was executed to assess the accuracy of the displacement control (hand opening/closing). The results of these experiments will be discussed and compared with Vardy et al. [35].

The second part will consist of the appendices (Part II). In Chapter 1, an overview of the appendices will be provided. Chapter 2 will show the analyses that were done on the topic of this thesis. Before the final design was created, it was needed to perform small-scale literature studies on different topics, namely on the target group, the forces of the shoulder, the anatomy and movements of the shoulder, and the biomechanical properties of the skin.

In Chapter 3, the criteria that were set for the final design are shown. Chapter 4 shows the design phase of this thesis. Results of brainstorm sessions are displayed. Also, the three final concepts will be explained and presented. A Harris profile and weighted criteria were used to choose the final concept.

The concept proposal of the final design is presented in Chapter 5. All main components of the system are discussed in detail.

Chapter 6 presents more elaborate information on the research design and methods of the experiments. Also, extra information about the results will be presented (see Chapter 7). The biggest challenges of the design are presented in Chapter 8. In Part I (Article), some recommendations will be mentioned, but a more extensive list will be presented in Chapter 9.

To provide all the information on the final design, SolidWorks drawings are included in Chapter 10. The data of the experiments were analysed with the program Matlab. The code written for these analyses can be seen in Chapter 11.

In Part III, the literature study will be presented. This study was conducted prior to the experiments that were executed in Part I. In this review, it was researched what kind of pneumatic actuators were available and were suitable for the final design in this thesis (Part I). It was also investigated how physical feedback could be provided by pneumatic actuators.

PART I

Article

Exploring the Accuracy of Sensitivity and Position Control for a Pneumatic Force Transducer for Upper-limb Prosthetics

Lambers, J.A.L.
Delft University of Technology

Abstract

Current upper-limb prostheses are often rejected as a result of high activation forces that are needed for control. Another reason for rejection is the absence of appropriate proprioceptive feedback. In this study, a pneumatic control system was designed that decreased the activation forces and where proprioceptive feedback was provided. The system was placed on the back of the user and was actuated by shoulder movements. The design has been evaluated on two aspects, namely the sensitivity, determined by the Just Noticeable Difference (JND) and the Weber Fraction (WF), and the displacement (re-)production accuracy (e.g. opening/closing of the prosthetic hand). Ten healthy, right-handed male subjects performed both experiments. The sensitivity was assessed by a reminder task where two forces were compared. Four reference force levels were used: 2, 4, 6, and $8N$. This resulted in WF values of: 18% for $2N$, 4% for $4N$, 3% for $6N$, and 2% for $8N$. The results for the three higher forces agreed with literature. To evaluate the displacement accuracy the Absolute Displacement Error (ADE), the Relative Displacement Error (RDE), and the Displacement Variability (DV) were measured for three different reference displacements: $5mm$, $10mm$, and $20mm$. The results show that the control of the system is accurate enough for object manipulation and the relative error was lower than 1% for each reference displacement. This design may be the next step in controlling prosthetic hands.

body-powered prosthesis - pneumatics - proprioceptive feedback - sensitivity - displacement accuracy

Introduction

A body-powered hand prosthesis is controlled by shoulder and/or elbow movements. Users frequently complain about discomfort when using a traditional figure-of-eight or figure-of-nine harness [4] [5]. They also criticize the high activation forces and high mental load that are needed to control the prosthesis. The high cognitive effort is caused by the lack of appropriate feedback [1]. Hence, current designs within the field of body-powered prostheses should be improved. The comfort for the wearer needs to be increased, control forces should be lowered, and the system should provide sufficient (proprioceptive) feedback.

This article will proceed on existing designs that have attempted to improve the body-powered control system. Latour [15] increased comfort by inventing an anchor system that does not incorporate a figure-of-eight or figure-of-nine harness. Vardy et al. [22] enhanced this design, and lowered the activation forces. From pilot studies performed by Vardy et al. [22] it was concluded that forces between 2 and $10N$ were most suitable as control forces. Forces below $2N$ were considered too low for sufficient control, and forces above $10N$ were classified as uncomfortable.

In this study, a pneumatic force transducer and displacement measurement device was placed on the back and shoulder of the user. The experiments will serve as a proof of principle to see whether it is effective to put the total system on the body of the user. The system should meet criteria, of which the most important are:

1. The system should be able to control the opening and closing of a body-powered prosthetic hand.
2. It should provide proprioceptive force feedback and displacement feedback.
3. The system should be lightweight, maximally $400g$.
4. The dimensions should be limited and should not exceed 223x346x50mm [9].
5. The force sensitivity should be sufficient and should be comparable to the results of Vardy et al. [22].
6. The displacement accuracy should be

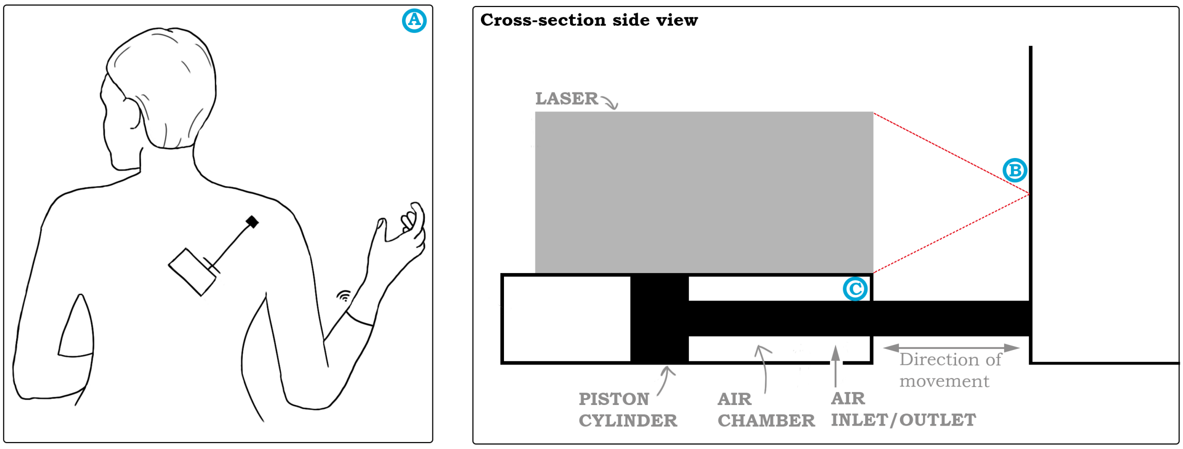

Figure 1: A schematic overview of the system is presented in this figure. A. The figure shows how the system is attached to the back of the user. B. The distance is detected and measured by the laser sensor and is sent to the prosthesis. This distance is caused by the shoulder movement, causing the piston to move sideways. C. To provide proprioceptive feedback, the pressure in the air chamber can be increased, such that a resistance is felt by the user when moving his/her shoulder.

satisfactory and the relative displacement error should not exceed 1%.

There are three types of actuators: pneumatic, electric and hydraulic. In this study, a pneumatic actuator is used because it is lighter than the other two types of actuators [17]. Electronic systems are heavier due to their added battery weight. They are also incompatible with water and other liquids. Hydraulic systems tend to be heavy due to the need of a pump to achieve a certain hydraulic pressure. Another reason why pneumatic systems were chosen is that it is the safest option. Electronic systems could ignite a spark. Hydraulic systems operate with a chemical fluid or water. A pneumatic system only uses gas or air. If the system leaks, it is less problematic if gas/air escapes then leaking chemicals/water [16].

Vardy and Plettenburg [21] determined what the best control location was to place a harness for an upper-limb prosthesis. They resulted in a system that was located on the scapula and was attached to the skin at the upper right corner and next to vertebrae. It is desired that the shoulder movement, that controls the prosthesis, generates the largest change in distance between the two attachments. This will create the highest resolution possible between the shoulder displacement and hand opening/closing. It was concluded by Vardy and Plettenburg [21] that shoulder elevation and protraction yielded the largest change in distance. The average maximum distance was 35mm. This control location and shoulder movement were used in this prototype.

The design in this article is a master-slave system where the master system is worn directly onto the body and is actuated by shoulder movements. The slave system is the externally powered prosthesis, which is a voluntary opening and closing hand, see Figure 1A. When the shoulder protracts and elevates, the piston will slide inside the cylinder. The displacement of the shoulder is detected and measured by a laser sensor. This displacement data is sent to the prosthesis, causing the hand to open or close (see Figure 1B). Figure 1C shows how proprioceptive feedback is provided. When a specific force is measured at the prosthetic hand, the pressure inside the air chamber will be increased. The pressure is regulated by a proportional pressure valve. The user now needs to exert a higher activation force to move his/her shoulder. This will in turn induce proprioceptive feedback.

In this article, the sensitivity of the shoulder was researched. The (re-)production of the shoulder movement was also investigated. For both these objectives, two separate research questions were formulated. The research question concerning the first objective was: 'What is the sensitivity for the force feedback used in this system for prosthetic control?'. The second objective was researched by posing the following question: 'What is the accuracy of position control, in terms of displacement perception and reproduction for prosthetic control with this system?'.

Methods

Two experiments were performed. The first experiment focused on the sensitivity of the shoulder. The second experiment was performed to investigate the accuracy of position control. Both experiments were carried out by moving the right shoulder, namely with shoulder elevation and protraction. The experiments were completed in a single session by the same subject separated by a short break and lasted 1.5 hours in total. Forces were kept sufficiently low to avoid fatigue.

Participants

Ten healthy right-handed males aged between 23 and 31 (mean: 26.6) completed both experiments. It was chosen to only include male subjects to have a homogeneous group of participants. The physical capability between males and females differ, causing variations in force reproduction [10]. Therefore, only male subjects were included.

Subjects provided informed consent and both experiments were approved by the local ethics committee.

Setup

The same setup was used for both experiments. The setup can be seen in Figure 2. LabView (2018, V18.0) was used to simulate the opening/closing of the prosthetic hand. The program also provided visual feedback to the subject during the experiments. The data was stored and analysed in Matlab (R2016b). The system was attached to the body at two points. One next to the vertebrae and the other on the upper right corner of the right shoulder.

When the subject protracted and elevated his shoulder, the cylinder (1) moved. The laser (2) (micro-epsilon, optoNCDT 1401) measured the displacement of the shoulder and sent it via an AD-converter (placed on the table) (National instruments, USB6002) to the computer (placed on the table) (HP, Elitebook 8570w). A proportional pressure valve (3) (Festo, VEAA-L-3-D9-Q4-V1-1R1) was attached to the pneumatic piston cylinder (1) and received signals from the computer (also via the AD-converter). The air was supplied by a gas tank where the pressure was set at $6bar$. The air was then supplied via the valve (3) to the air chamber inside the cylinder (1).

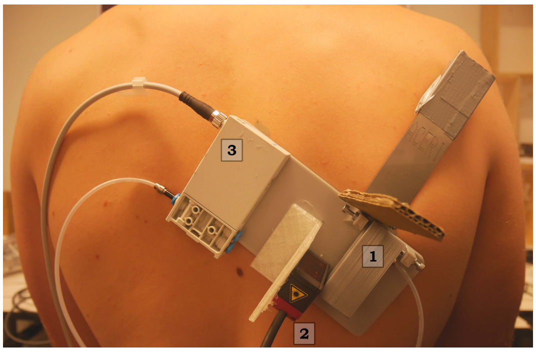

Figure 2: The setup for both experiments with 1. Piston cylinder, 2. Laser sensor, and 3. Proportional valve.

Before the experiments started, the subject got familiar with the actuator. When the subject was accustomed with the system, the experiments started.

Methods experiment 1: Sensitivity

The sensitivity of the system was investigated by measuring the Just Noticeable Difference (JND) and calculating the Weber Fraction (WF). The JND is the smallest perceivable difference in intensity. The WF is the ratio between the JND and the original stimulus magnitude and provides information about the level of precision, hence how well a small change in force is perceived by the subject. A WF of 0.01 (or 1%) indicates that the subject can detect a difference in stimulus intensity of 1% of the original stimulus [11]. A low WF yields a high level of precision, because it indicates that a small variation in stimulus can be detected.

To determine the WF, four reference forces were used, namely 2, 4, 6 and $8N$. These forces were the same as were applied by Vardy et al. [22] to be able to compare the results accurately. A reminder task was used to measure sensitivity when comparing two stimuli. On each trial, the standard (reference force) was presented first followed by the comparison (test force) [14]. The magnitude of this test force deviated a fixed percentage from the reference force, namely ±3.5%, ±7%, ±10.5%, ±14%, and ±17.5%. This yields the forces that can be seen in Table 1.

In Figure 3, the procedure of this first experiment is displayed. In step 1, the subject was asked to relax his shoulder. In step 2, the subject was instructed to move his shoulder (elevate/protract) and to reach a certain target displacement. This displacement was

Reference force(N)	Test force(N)									
	-17.5%	-14%	-10.5%	-7%	-3.5%	+3.5%	+7%	+10.5%	+14%	+17.5%
2	1.65	1.72	1.79	1.86	1.93	2.07	2.14	2.21	2.28	2.35
4	3.30	3.44	3.58	3.72	3.86	4.14	4.28	4.42	4.56	4.70
6	4.95	5.16	5.37	5.58	5.79	6.21	6.42	6.63	6.84	7.05
8	6.60	6.88	7.16	7.44	7.72	8.28	8.56	8.84	9.12	9.40

Table 1: Reference forces(N) together with their corresponding test forces(N).

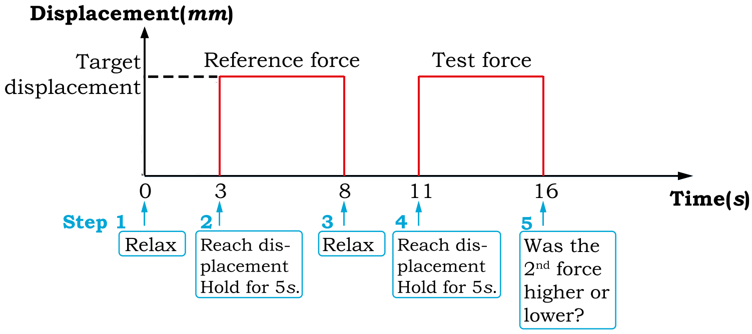

Figure 3: Visual time-line of experiment 1 with the x-axis: time(s) and the y-axis: displacement(mm). After 3$seconds$, the user is told to move his shoulder and hold it for 5$seconds$. After that, the shoulder can be relaxed for 3$seconds$. This movement is repeated, but now with the test force applied to the system. At the end, it is asked if the second force was higher or lower.

made visual on the computer screen by showing a 'progress bar'. During this step, the reference force was applied to the system by increasing the pressure inside the air chamber. This position was kept constant for 5$seconds$ (isometric contraction). In step 3, the subject was asked to relax for 3$seconds$ (depression and retraction of the shoulder). He then again needed to move his shoulder to reach the same target displacement. In this step (4), the test force was applied to the system by increasing/decreasing the pressure. After 5$seconds$, the subject could relax and needed to answer the following question: 'Was the second force higher or lower than the first force?'. One trial was now executed for one reference force and one test force.

Four blocks of the four reference forces were presented to each subject. The order of reference forces within these blocks was randomized within-subjects and between-subjects. Each block then holds all the four reference forces, together with their 10 tests forces. The order of test forces was also randomized within-subjects and between-subjects. In total, this yields: 4 (blocks) x 4 (reference forces) x 10 (test forces) = 160 trials.

It was chosen to keep the target displacement constant. This way same-sized objects were simulated, but with a different stiffness.

Data analysis experiment 1

After the experiment, the number of trials where the test force was identified as larger than the reference force was counted per subject and divided by the number of repetitions, which was 4. Now, for each reference force and corresponding test force the average response per subject was calculated. This data was pooled for all the subjects and a logistic psychophysical curve was fitted for each of the reference forces. A psychometric function models the relationship between the change in physical stimulus and the forced-choice response of the subject.

The JND was calculated by determining the relative differences in force (ΔF) corresponding to 25% and 75% success probability in the psychometric graph. The formula as presented in Equation 1 was used.

$$JND = \frac{(\Delta F(75\%) - \Delta F(25\%))}{2} \qquad (1)$$

To calculate the WF, the JND was divided by the reference force and multiplied by 100 to receive a percentage, see Equation 2.

$$WF = \frac{JND}{F_{reference}} * 100\% \qquad (2)$$

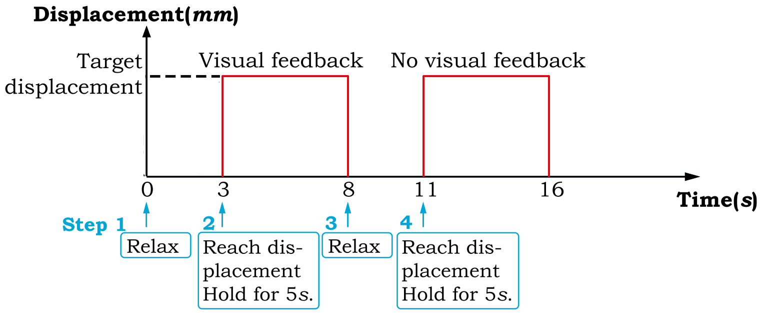

Figure 4: Visual time-line of experiment 2 with the x-axis: time(s), and the y-axis: displacement(mm). After 3$seconds$, the user is told to move his shoulder and hold it for 5$seconds$. This is repeated without visual feedback.

Methods experiment 2: Accuracy of position control

In experiment 2, it was researched how well a subject could reach a certain target displacement with and without visual feedback. Three reference shoulder displacements were used namely: 5mm, 10mm and 20mm. In each trial, the subject was instructed to achieve a certain displacement (step 1), with visual feedback on the screen where the target displacement was shown, see Figure 4. This position needed to be held for 5$seconds$ (isometric contraction). Then, the subject could relax for 3$seconds$ (step 2). The subject was instructed to achieve the same target displacement, but now without visual feedback (step 3). This was repeated 10 times per reference displacement, resulting in 30 trials in total. The order of reference positions was counterbalanced between subjects.

Data analysis experiment 2

To remove transition effects between steps, the first 2.5$seconds$ and the last 0.5$seconds$ were removed from each trial. The data was sampled with a frequency of 50Hz. The data was analysed to measure the following features:

1. Absolute Displacement Error (ADE), which is the absolute difference between the mean of the data and the target displacement.
2. Relative Displacement Error (RDE), which is the relative difference between the mean of the data and the target displacement.
3. Displacement Variability (DV), which is the standard deviation of the produced error.

This experiment was performed to see how well a subject could reach a certain displacement and how accurately this displacement could be reproduced without visual feedback. The measurement data shows if the control of the prosthesis will be as intended and if displacements are perceived correctly.

Results

Experiment 1: Sensitivity

Figure 5 shows the psychometric curve of the pooled data for each reference force. The curves show the probability of a response (test force identified as larger than the reference force) as a function of the relative difference between the reference force and test force (test force factor). For the reference force 2N, the data is extrapolated to correctly calculate the JND and WF. These results show JND values of 0.35, 0.15, 0.17, and 0.15 and WF values of 18%, 4%, 3%, and 2%. It can be seen that larger differences in force were detected more frequently than smaller differences.

Experiment 2: Accuracy of position control

In Figures 6, 7, and 8 the results of the second experiment can be seen. The Figures 6 and 7 show that the absolute (ADE) and relative (RDE) error is noticeable lower in the presence of visual feedback compared to the blind reproduction trials. As can be seen in Figure 8 there is less variability in the blind reproductions than for the visual productions for the displacements 5mm and 10mm. However, this difference is relatively small.

Figure 6 shows the results of the ADE. It can be seen that these results are to some extent similar for each displacement. The absolute error does not increase or decrease when the displacement was increased. However, when looking at the results of the RDE (see Figure 7), it can be seen that there is a differ-

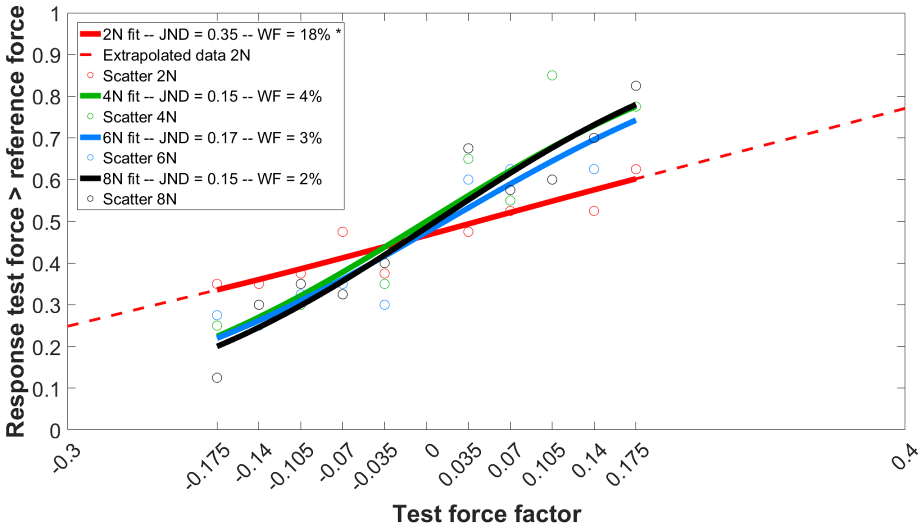

Figure 5: Psychometric curves for the pooled data for all the four reference forces. *The JND and WF for the reference force 2N were calculated with the extrapolated data. This, because the 25% and 75% success probability were not reached.

ence in relative error between the displacements. Relatively, the 20mm displacement is performed more accurately than the 5mm.

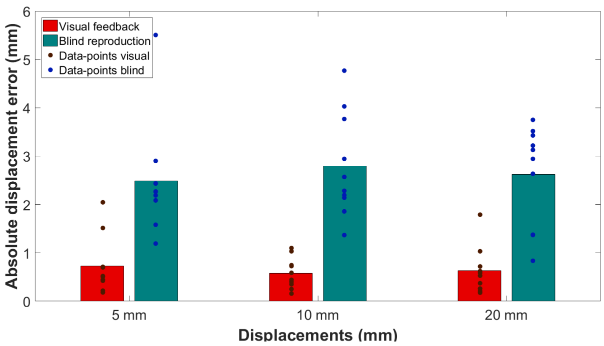

Figure 6: The Absolute Displacement Error (ADE) is presented in mm for each of the three displacements. The ADE is the average of all the subjects together.

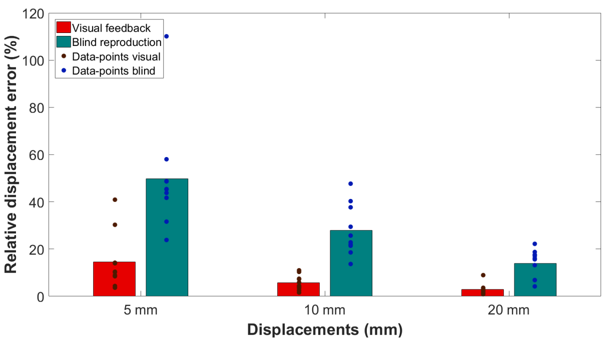

Figure 7: The Relative Displacement Error (RDE) is presented in % for each of the three displacements. The RDE is the average of all the subjects together.

Figure 7 displays that there is relatively less variability in error for the 20mm displacement than in the lower displacements. This can be seen when looking at the individual data-points of the subjects.

Figure 8 shows that the results per subject are quite similar. However, for the 20mm displacement, there is one outlier for the visual production and for the blind reproduction. This was one subject, that only had difficulty in the highest displacement, and was therefore not removed from the data-set.

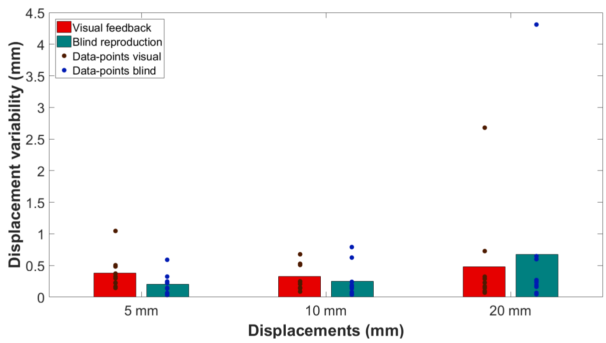

Figure 8: The Displacement Variability (DV) is presented in mm for each of the three displacements. The DV is the average of all the subjects together.

Discussion

Experiment 1: Sensitivity

The goal of the first experiment was to investigate how well a subject can detect force variations. The sensitivity was tested for four reference forces. Results show that differences in force were less accurately detected for the reference force 2N than for the other three reference forces. A success probability of 25% and 75% was not reached for the lowest reference force. Hence, the JND could not be calculated correctly according to Equation 1. Therefore, the fitted data was extrapolated to calculate the JND.

High friction values inside the pneumatic cylinder could cause the poor results of the $2N$ force. This friction was caused by O-rings inside the cylinder. The friction for the $2N$ force was $5.083N$, which is 250% of the reference force. The friction for the $8N$ was $5.590N$, which is 62% of the reference force. This shows that this friction force was relatively more prominent for the lower reference force. This could justify why the sensitivity results were worse for the $2N$ than for the higher reference forces. A suggestion is to decrease O-ring clamping, which in turn will lower the friction forces. The friction for the $2N$ could decrease to $3.727N$ (186% of the reference force), and could decrease to $4.234N$ for the $8N$ (53% of the reference force).

Another recommendation is to seek for another valve with a higher pressure range. When the maximum pressure value increases, the cylinder diameter can be decreased, which will in turn lower the friction.

Pressure value inaccuracies, caused by the pressure regulating valve, were detected. It was concluded that the analogue output of the valve did not precisely correspond to the input. These inaccuracies were not consistent and therefore the pressure levels differed little between trials. This causes the force to be variable between trials. However, these differences were small, namely an average relative force error of 0.15% for the $2N$ reference force, and no error for the $8N$. This however shows that the error has a larger effect on the lower forces than on the higher forces. Nevertheless, an error of 0.15% is truly small and will probably not affect the results. Therefore, these inaccuracies do not explain the poor results for the $2N$.

There was variability between subjects with one extreme outlier. One participant had much difficulty and scored low on all the four reference forces compared to other subjects. When removing this subject from the data, it resulted in JND-values of 0.30, 0.15, 0.16, and 0.14, and in WF-values of 15%, 4%, 3%, and 2%. All the results improved slightly. Nevertheless, there is still a high JND and WF measured for the reference force $2N$. To check if the subject removed from the dataset was truly an outlier, it is suggested to repeat the experiment with more subjects, to see if outliers are naturally filtered out.

Compared to Vardy et al. [22], the reference force of $2N$ scored worse. Vardy et al. [22] had JND and WF values of 0.14 and 7% for $2N$, 0.11 and 3% for $4N$, 0.16 and 3% for $6N$, and 0.17 and 2% for $8N$. The $4N$ barely scored worse in this study. The sensitivity for the reference forces $6N$ and $8N$ is comparable to Vardy et al. [22]. The results show that the system performs equally good for higher forces. The aim is to have a sufficient sensitivity for lower forces. This, because a range with higher forces is not desired, because fatigue is then more likely to occur as the user needs to withstand higher forces during the day.

No JND or WF data on the protraction and elevation of the shoulder was found in literature. However, some perception experiments with the shoulder were identified. Yet, it needs to be stated that the JND and WF can be calculated in different ways. This then varied between articles. This needs to be kept in mind when comparing results.

Hurmuzlu et al. [13] evaluated the shoulder sensitivity and performed an experiment with the following reference forces: $4.4N$, $8.9N$, $13.4N$, and $17.8N$. This resulted in the following WF-values: 50%, 12.5%, 17%, and 6%. The high WF-values were probably caused by the internal friction of the haptic device. Nevertheless, these values are higher than found in this article. This suggests that the system employed in this article yields a higher sensitivity.

Schmidtler and Körber [19] showed based on a literature review, that the lower the reference force, the higher the Weber Fraction. They investigated the human perception in the upper arm and torso while manipulating a robot. This does agree with the results in this article.

It was encountered that stick-and-slip occurred at high pressures. This agrees with an article from Belforte et al. [3]. He showed that with increasing pressure, the average friction force also increases. Stick-and-slip behaviour will be explained later in detail.

Debats et al. [8] investigated how perceptual precision is dependent on neural noise. The absolute noise determines motor precision. It was concluded that the absolute noise increased with the reference force. The higher the absolute noise, the lower the motor precision. However, concluded by Debats et al. [8] perceptual precision does not depend on absolute noise but on the relative noise. This agrees with the results found in this article. The WF decreases when the reference force increased, suggesting that the relative noise also decreased.

Experiment 2: Accuracy of position control

The second experiment was designed to investigate how well a user can control the opening/closing of their prosthetic hand. It was also researched if visual feedback is essential in position control. The results show that precise movements were harder to control. It further demonstrates that visual feedback was needed to control the opening/closing of the hand. Visual feedback had a relative larger effect on smaller displacements when looking at the RDE. However, it needs to be stated that possibly a learning curve will occur. This could result in better blind reproduction results [6] [12]. Nonetheless, this hypothesis needs to be tested in future research.

The results demonstrate that the absolute displacement for the visual production for all the three displacements was around $0.6mm$ (with Standard Deviation (SD): $0.5mm$) and around $2.6mm$ (with SD: $1.1mm$) for the blind reproduction. This shows that position control is reasonably accurate. However, to see if the control is accurate enough for object manipulation, experiments should be performed while handling a prosthesis performing daily life activities.

Stick-and-slip behaviour was observed during the position control of precise movements. This could be caused by high static friction values and could explain why smaller displacements were relatively harder to control. Just before the piston moves, static friction is established on the contact surface of the pneumatic cylinder. When the exerted force on the system (by the subjects' shoulder) exceeds the static force, the piston starts to move. The friction force quickly decreases due to the Stribeck effect. The Stribeck friction is a non-linear low-velocity friction that contributes to the stick-and-slip behaviour [2]. This effect causes the friction coefficient to promptly decline when the static force is exceeded, causing the piston to rapidly accelerate creating a 'slipping' overshoot [23]. Subjects carefully and slowly protracted/elevated their shoulder to reach the smallest target displacement. When an overshoot took place, subjects wanted to compensate for this error by again slowly moving their shoulder, exciting once more the stick-and-slip behaviour.

Thompson and Robbins [20] likewise showed that there is a drop in static friction as the velocity increases. To check this statement, the average speed was calculated per subject and then pooled together to calculate the total average speed for the $5mm$ displacement and the $20mm$ displacement. The speed for the $5mm$ displacement was $3.75mm/s$, while the velocity was $11.91mm/s$ for the $20mm$ displacement. This shows that the velocity was lower for the smallest displacement, which could explain why stick-and-slip was more apparent in those trials.

There are several approaches to decrease stick-and-slip behaviour. To decrease this behavior at low velocities, the static force should be lowered. This could be done by applying lubrication to the system [7] [20]. In this prototype, a silicone based lubrication was used to decrease the friction. However, in the future, perhaps more research should be conducted on the use of lubrication.

Another option to decrease the sticking behavior is by optimizing the pneumatic cylinder. In this design, it is chosen to clamp the O-rings with 10% of their thickness. However, according to Plettenburg [18], this clamping could be decreased, namely to 8±2%. This will decrease the static forces at all velocities. In this design, the static friction at maximum pressure was $5.843N$. With O-ring clamping of 6%, the friction will be $4.378N$. This is a decrease of approximately $1.5N$. However, decreasing the O-ring clamping will increase the chance of leakage. It is therefore recommended to optimize this O-ring clamping, and repeat the experiments to see if leakage occurs.

As was also mentioned before, it is also possible to increase the maximum pressure, which would decrease the size of the cylinder diameter. Hence, the static friction will be lowered.

Summary discussion

Many recommendations for future research have been proposed. The design of the cylinder should be improved to reduce stick-and-slip behaviour. Another valve with higher maximum pressures should be used. The cylinder diameter could then decrease, causing the friction to also decrease. This could presumably improve the sensitivity of lower reference forces and the displacement accuracy of smaller displacements.

Furthermore, it is suggested to perform more experiments, to see if these is a high in-between subjects variability, to check if learning effects occur, and to see if the systems works accordingly when controlling an actual hand prosthesis.

Conclusion

The results presented in this article indicate that with this prototype the reference forces $4N$, $6N$, and $8N$ have a comparable sensitivity as the prototype of Vardy et al. [22]. The reference force $2N$ has a lower sensitivity, causing this force to not provide proper proprioceptive feedback. It is desired to keep the forces as low as possible, because this results in a reduced chance on fatigue. However, as stated in the discussion, some aspects of the prototype need to be investigated in future research to fully conclude that a force of $2N$ is not applicable.

There is appropriate position control and the system is accurate for object manipulation. A criterion was set that the relative displacement error should not exceed 1%. The results in this article show that this value is not exceeded. However, in future research the system should be tested with the user clamping objects to see if these displacement errors are low enough.

This interface for haptic control may be the next step in controlling prosthetic hands. This study provided a proof of principle and is a first step in the right direction. More research should be conducted on the system, especially on the lower forces, and the design should be optimized.

References

[1] C. Antfolk, M. D'Alonzo, B. Rosén, G. Lundborg, F. Sebelius, and C. Cipriani. Sensory feedback in upper limb prosthetics. *Expert Reviews of Medical Devices*, 0(1):45–54, 2013.

[2] B. Armstrong-Helouvry. Stick-slip arising from stribeck friction. *Proceedings., IEEE International Conference on Robotics and Automation*, 1990.

[3] G. Belforte, G. Mattiazzo, S. Mauro, and L.R. Tokashiki. Measurement of friction force in pneumatic cylinders. *Tribobest journal*, 10(1):33–48, 2003.

[4] Elaine A. Biddiss and Tom T. Chau. Upper limb prosthesis use and abandonment: A survey of the last 25 years. *Prosthetics and Orthotics International*, 31(3): 236–257, 2007.

[5] Elaine A. Biddiss, D. Beaton, and Tom T. Chau. Consumer design priorities for upper limb prosthetics. *Disability and Rehabilitation: Assistive Technology*, 2 (6):346–357, 2007.

[6] H. Bouwsema, C.K. Van der Sluis, and R.M. Bongers. Changes in performance over time while learning to use a myoelectric prosthesis. *Journal of NeuroEngineering and Rehabilitation*, 11(16), 2014.

[7] H. Chang, C. Lan, C. Chen, T. Tsung, and J. Guo. Measurement of frictional force characteristics of pneumatic cylinders under dry and lubricated conditions. *Przeglad elektrotechniczny (Electrical Review)*, 88(7):261–264, 2012.

[8] N.B. Debats, I. Kingma, P.J. Beek, and J.B.J. Smeets. Moving the weber fraction: The perceptual precision for moment of inertia increases with exploration force. *PLoS ONE*, 7(9), 2012.

[9] DINED. Dutch adults 2004, age 20-60, male and female. *Retrieved from https://dined.io.tudelft.nl/en/database/tool*, 2004.

[10] R.M. Enoka and J. Duchateau. Muscle fatigue: what, why and how it influences muscle function. *Journal Physiology*, pages 11–23, 2008.

[11] T.D. Fechner. Elemente der psychophysik. 1, 1860.

[12] L.H.B. Huinink, H. Bouwsema, D.H. Plettenburg, C.K. Van der Sluis, and R.M. Bongers. Learning to use a body-powered prosthesis: changes in functionality and kinematics. *Journal of NeuroEngineering and Rehabilitation*, 13(90), 2016.

[13] Y. Hurmuzlu, A. Ephanov, and D. Stoianovici. Effect of a pneumatically driven haptic interface on the perceptional capabilities of human operators. *Presence*, 7(3):290–307, 1998.

[14] E. Lapid, R. Ulrich, and T. Rammsayer. On estimating the difference limen in duration discrimination tasks: A comparison of the 2AFC and the reminder task. *Perception & Psychophysics*, 70(2):291–305, 2008.

[15] D. A. Latour. Method for anchoring prosthetic and orthotic devices. *US8821588 B2 Patent*, 2014.

[16] A. Parr. Hydraulics and pneumatics: A technician's and engineer's guide. 2011.

[17] B. Peerdeman, G. Smit, S. Stramigioli, D. Plettenburg, and S. Misra. Evaluation of pneumatic cylinder actuators for hand prostheses. *IEEE RAS/EMBS International Conference on Biomedical Robotics and Biomechatronics*, 2012.

[18] D.H. Plettenburg. A sizzling hand prosthesis. *PhD-Thesis*, 2002.

[19] J. Schmidtler and M. Körber. Human perception of inertial mass for joint human-robot object manipulation. *ACM Trans. Appl. Percept.*, 15(3), 2018.

[20] P. A. Thompson and M. O. Robbins. Origin of stick-slip motion in boundary lubrication. *Science*, 250(4982):792–794, 1990.

[21] A.N. Vardy and D.H. Plettenburg. Control locations for harnesses used in upper limb prostheses. *MEC14- Redefining the Norm*, pages 271–274, 2014.

[22] A.N. Vardy, M. Boone, and D.H. Plettenburg. Perceptual and control properties of a haptic upper-limb prosthetic interface. *MEC17 - A Sense of What's to Come*, 2017.

[23] Y. Wakasawa, Y. Ito, and H. Yanada. Friction and vibration characteristics of pneumatic cylinder. *The 3rd International Conference on Design Engineering and Science*, pages 155–159, 2014.

PART II

Appendix

Contents Appendix

1 Introduction

In this Part, the Appendix will be presented. All the steps of the design cycle will be presented, as can be seen in Figure 1.1. First, small-scale literature studies were performed to provide the reader with supplementary background information. This will be presented in Chapter 2: Analysis. Chapter 3 shows the criteria that were set for the prototype and for the final design. These criteria were then translated to ideas and concepts, see Chapter 4. Ideas will be presented, from which concepts were developed. With the use of a Harris profile and a weighted criteria method, the final concept is chosen. This design is explained in detail in Chapter 5 (Concept Proposal). All the specifications of the design will be discussed here. Chapter 6 shows additional information on the research design. In Part I (Article) the test setup was already discussed. However, in Chapter 6 extra material about the experiments will be presented if the reader desires more information. This is also the case with the results, which are presented in Chapter 7. The most important results were discussed in the Article. Yet, extra information is presented in this chapter as well as all the calculations. Chapter 8 will present the two main challenges that were encoutered during the experiments. Chapter 9 will present recommendations made for future research. Chapter 10 shows all the SolidWorks drawings of the prototype. In Chapter 11, the Matlab code will be provided.

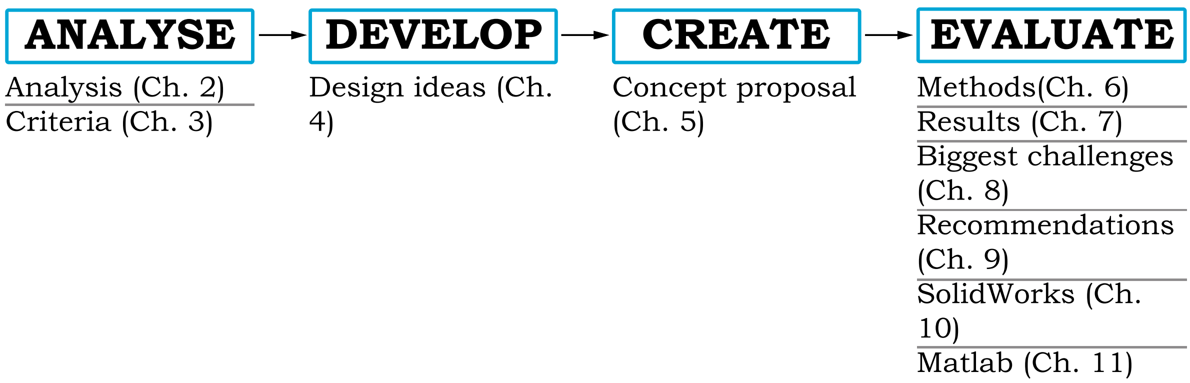

Figure 1.1: An overview of the design cycle that was followed during this master's thesis.

2
Analysis

As mentioned in the introduction of this thesis, the objective was to design and prototype the control and actuation system of a body-powered prosthesis and test its usefulness to place this system on the back/shoulder of the user. In this chapter, the scope of this assignment is specified by defining the target group. Also, some topics of interest will be mentioned. Some of these topics were analysed further in other sections of this chapter.

2.1. Scope

First, the target group will be specified. This group is based on the targeted subjects for the experiment. The following criteria for the target group were set:

1. *ADL (activities of daily living)*
   A force of $35N$ should be reached when controlling the prosthesis. This maximum force is set based on the ADL tasks and based on the pinch force needed to pull up a sock [11].
2. *Gender*
   The prototype in this thesis is only developed for male subjects. Eventually it would be the goal to design the system for both genders. However, this makes the design more intricate, because there are differences between the genders when it comes down to maximum force and maximum displacement. Men can exert higher maximum forces than females. However, in the daily life tasks that were set in this thesis, maximum forces are not needed. However, this difference in maximum force creates another contrast between male and female concerning the muscle fatigue according to Hicks et al. [12]. This is caused by the fact that females have a lower muscle mass, which requires them to use less O_2 during contraction than men. This is supported by other articles that state that males have a greater muscle fatigue, when exerting the same relative force (% of maximum force) ([8], [16]). Females have a lower maximum force, which causes the relative force of males to be higher. Men have a higher muscle mass, which causes them to activate more mass to achieve the same relative force as females. This provokes larger intramuscular pressures and greater occlusion of blood flow, causing women to be able to sustain a contraction for a longer duration, especially for lower contraction intensities [8].
   Monod [24] showed that 20% of the maximum voluntary force can be applied without fatigue. This is called the critical force. A force higher than this 20% causes fatigue, which is generated by ischaemia inside the muscle. Ischaemia is a lack of oxygen in the muscles. This critical force increases when the muscle does not need to exert a force for a long period of time. The shorter the contraction time, the higher the critical force. Hichert [11] also states that a fatigue free force for females and males is between 15-20% of their maximum force. This yields a fatigue free force for females of $38N$, while for males it is $66N$.
3. *20-30 years of age*

The system will be designed for users aged between 20 and 30 years. This is done, because there are differences in physical capacity when concerning age. Maximum physical capacity is between the age of 20 and 30 years. Muscle strength declines after the 30th life year. After the age of 50, this decline will accelerate. However, some articles state that this accelerated decline already starts at the age of 40 [14]. Therefore, it is chosen to keep the age of the target group between 20-30 to make sure that the accelerated decline has not started yet.

2.2. Interesting topics

In this section, some interesting topics will be mentioned and discussed.

1. *Available pneumatic systems*
It needs to be researched what the available pneumatic systems were. This is widely discussed in the Literature study in Part III. It is discussed which systems are applicable for the design in this masters thesis.
2. *Shoulder forces*
It is also of importance to know how much force a shoulder can provide. This makes it essential to investigate where the system should be attached to. It needs to be researched what the best control locations on the shoulder are.
3. *Proprioceptive feedback*
It is important to understand the biology that determines how humans sense. How does it work? What kind of sensors play a role in proprioceptive feedback? How can these be of use in the design of the system? This will be discussed in section 2.4.1.
4. *Movements of the shoulder*
It is of importance to know which muscles are used during protraction and elevation of the shoulder. Also, the anatomy of the muscles is of interest.
5. *Biomechanical properties of the skin*
In the system of Latour et al. [18] stickers are used to attach the system to the body. However, are stickers the only option? What are the other possibilities? How does the skin react to stretch?
6. *Sensitivity of the shoulder*
This is of importance, because of the feedback that will be provided by the system. How well does a user feel the difference between forces? And what is the range of these forces? This topic will be investigated in experiment 1.
7. *Accuracy of position control*
It is essential to know if the position control of the prosthesis is accurate enough. Can the user control the opening and closing of the hand precisely without any visual feedback? This topic will be investigated in experiment 2.

2.3. Forces

Sufficient forces to operate an externally powered prosthesis are between 2 and 10N, while maintaining a sufficient level of proprioceptive feedback [35]. This shows that there are no high actication forces needed to achieve appropriate proprioceptive feedback. However, there is a trade-off between low activation forces and the accuracy of sensation. L.A. and Hunter [17] stated that smaller forces (% of Maximum Voluntary Contraction (MVC)) were overestimated. At 50% MVC forces were most accurately estimated. It is desired to keep the operational forces as low as possible to not induce fatigue. However, the lower the forces, the less accurate the estimate of forces. Therefore, in this article, it is researched if forces varying from 2-10N are sufficient for accurate proprioceptive feedback.

Forces will not only be presented to the shoulder muscles, but also on the skin. These forces are dependent on the biomechanical properties of the skin. These will be discussed in paragraph 2.4.3.

2.4. Shoulder

In this section, proprioceptive control will be discussed. This background information is required to fully comprehend how the feedback mechanisms work. Then, the possible movements of the shoulder were analysed. At last, the biomechanical properties of the skin were investigated. This, because the system will be directly attached to the skin.

2.4.1. Proprioceptive control

Proprioceptors are position sense receptors and occur in skeletal muscles, tendons, joints, ligaments and in connective tissue coverings of bones and ligaments [21]. There are several proprioceptive receptors of which golgi tendon organs and muscle spindles are the most important. Golgi tendon organs are located in the tendons and they measure tension. Spindles are located in the muscles and measure muscle length. Signals from these receptors are sent to the the primary somatosensory cortex in the brain. Neurons in the brain are able to identify the body regions that are stimulated. This is called spatial discrimination [21].

According to Feyzabadi et al. [10], the shoulder has a better force discrimination (lower Weber Fraction) than the wrist and elbow joints. This possibly can be explained by the fact that the shoulder has more muscles, which can help in the proprioception. All the shoulder muscles contain tendons, which contain golgi tendon organs [21]. This could support the assumption of Feyzabadi et al. [10] that the shoulder has a better proprioception. More muscles means more golgi tendon organs, which in turn means more receptors to signal back to the brain where neurons will convert this signal into a spatial discrimination. However this is not further tested yet. A higher number of muscles involved could perhaps improve the ability to discriminate forces.

Salles et al. [29] states that muscle spindles are better in position detection when the muscles are trained. Strength training causes them to become more sensitive [27]. Physical exercise does not change the number of mechanoreceptors, but induces morphological adaptations in the muscle spindle. This could result in an increased accuracy of position detection.

Fatigue decreases the level of accurate proprioception in the shoulder [7]. Fatigue should therefore be avoided and forces should be kept below $40N$ [11]. However, this is the case in the experiments performed in this thesis where forces are kept below $10N$.

2.4.2. Movements of the shoulder

There are several motions the shoulder can make. Vardy and Plettenburg [34] identified locations on the shoulder that exhibit a large relative displacement during shoulder movement. They performed the experiments with five different shoulder motions, namely: elevation, depression, protraction, retraction and a combination of elevation and protraction. In the prototype of this thesis, this shoulder displacement is translated to the opening/closing of the hand prosthesis. Therefore, a larger relative displacement could afford a higher resolution for position control. The subject will control the prosthetic hand with shoulder motion. From the study of Vardy and Plettenburg [34] it was concluded that a combination of protraction and elevation was most effective for this type of control. The highest average displacement could be reached, namely $35mm$. Shoulder protraction is also used in the traditional harness design control.

There are many muscles in the posterior thorax that will create the movements of the shoulder and scapula. The muscles that stabilize and control the protraction and elevation motion are shown in Table 2.1. The function of these muscles are in short mentioned in this table. The anatomy of the shoulder muscles is presented in Figure 2.1, where the muscles of Table 2.1 are visualized.

Muscle	Function
m. trapezius	stabilizes, elevates, retracts and rotates scapula
m. levator scapulae	elevates/adducts scapula
mm. rhomboids	stabilize scapula, elevation of the scapula
m. serratus anterior	small elevation (upper fibers), protraction (lower fibers)
m. supraspinatus	protraction, and stabilizes humerus
m. deltoideus	protraction (middle fibers), and stabilizes (front and back fibers)

Table 2.1: Most important posterior shoulder muscles and their function [15] [21].

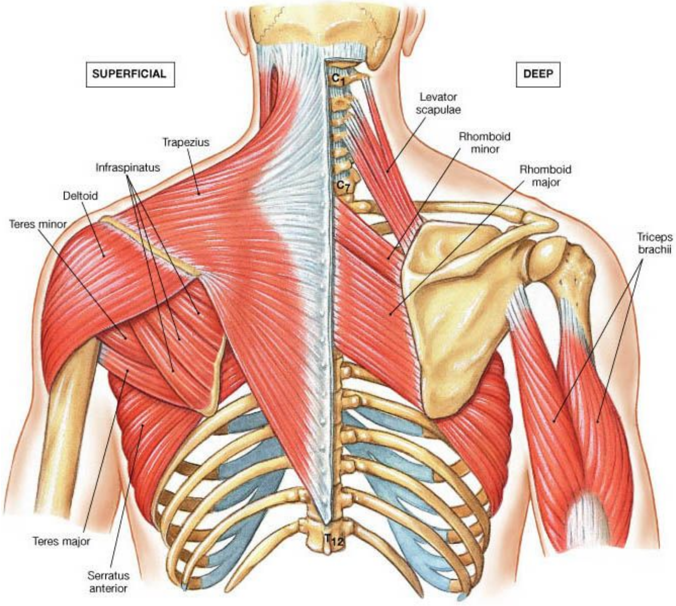

Figure 2.1: Anatomy of the shoulder with all the muscles presented from Table 2.1 [20].

For future designs, it could be possible to use both shoulder blades for control. One shoulder could then control the hand opening/closing, and the other shoulder could control flexion/extension or pronation/supination.

2.4.3. Biomechanical properties of the skin

As mentioned before, the forces on the skin are dependent on the biomechanical properties of the skin. The most important structural components of the dermis (skin) are collagen, elastin and ground substance [13]. Collagen has high tensile strength, is stiff and lacks extensibility. The component elastin is responsible for the ability of the skin to come back to its original shape after deformation.

The elasticity and stretch-ability of the skin is not equal for everyone and changes over time. These properties diminish after the age of 30, causing the skin to be more stiff [2]. The Young's Modulus for younger people is around $4.2x10^5 Nm^{-2}$ and for the older people around $8.5x10^5 Nm^{-2}$. However, these values differ quite much between studies (sometimes with a factor of 3000) [6]. Therefore, this property is difficult to estimate and analyse.

Skin thickness also influences the biomechanical properties of the skin. The thickness varies with location, age and sex [13]. Elderly often have a thinner skin because less collagen and ground substance are synthesized in the dermis. The thickness of the skin declines with 6% per decade. The elastin and collagen networks degenerate, which decreases the skin's ability to recover from stress [28]. This causes the skin to be more stiff. The thickness is typically greater in men than in woman for any given location, because it has a greater collagen content.

3 Criteria

Two lists of criteria that the actuator should meet were set. The first list contains the criteria that were set for the prototype in this article. The second list contains the criteria which the final system should meet in the future. The first list of criteria is as follows:

1. The system should function as the control system of a body-powered hand prosthesis and should be able to control the opening and closing of a prosthetic hand.
2. The actuator should provide proprioceptive force feedback.
3. The actuator should be pneumatically driven.
4. The actuator should be safe to operate as no places where clothing can get stuck are allowed.
5. The actuator should not physically harm the user.
6. The part of the system that is placed on the back should weigh maximally $400g$.
7. The actuator should be maximally 223x346mm in width and height. The thickness should be limited and should not be more than 50mm [5].
8. The design should have round edges to not harm the user.
9. The material of the device should not irritate the skin.
10. The attachment to the skin should be disposable.

As mentioned before, the second list of criteria is set for a final design. These criteria can be seen as recommendations for future research. The second list of requirements is:

1. The system should have a wireless connection with the prosthesis.
2. The actuator should consist of a soft material.
3. The actuator should be easy to apply, donning and doffing should be done within $120 seconds$.
4. The actuator should be practical in use. It should not stand in the way of daily life activities, for example it should not interfere with the back of a chair when sitting down.
5. The system should be able to be used for a whole day, without the need of changing the air supply.
6. The system needs to be cleaned easily. It needs to be handily brushed with an alcohol wipe.
7. The system should be able to sustain friction from clothing.
8. The system should be able to endure a temperature of 30 degrees $Celsius$.
9. The latency time of the system (control and feedback) should be maximally 300ms in order to let the prosthesis feel as the users own hand [30].
10. The actuator should be waterproof, it should sustain perspiration and/or rain.
11. Easy to operate, the system should be able to be used correctly within $1 month$.
12. The actuator should have a long durability.
13. Behave reliably with no unexpected or jerky movements. Mechanical joints should be sufficiently lubricated.
14. The battery must last a whole day (24$hours$), before recharging.
15. Gas tank should preferable be placed on the body, such that no long wires are present.

The tank should therefore be as small as possible.
16. The device should look appealing to the user.

4 Design ideas

It is widely discussed in the literature study which kind of pneumatic systems are available (see Part III). This study was used as a starting point for the design phase. During this phase, a morphological chart was generated (Figure 4.1) [33]. This chart shows ideas for the functionalities of the system such as: measure displacement, change force/pressure/resistance, create pressure, change in distance, measure force, and measure change in flow/pressure.

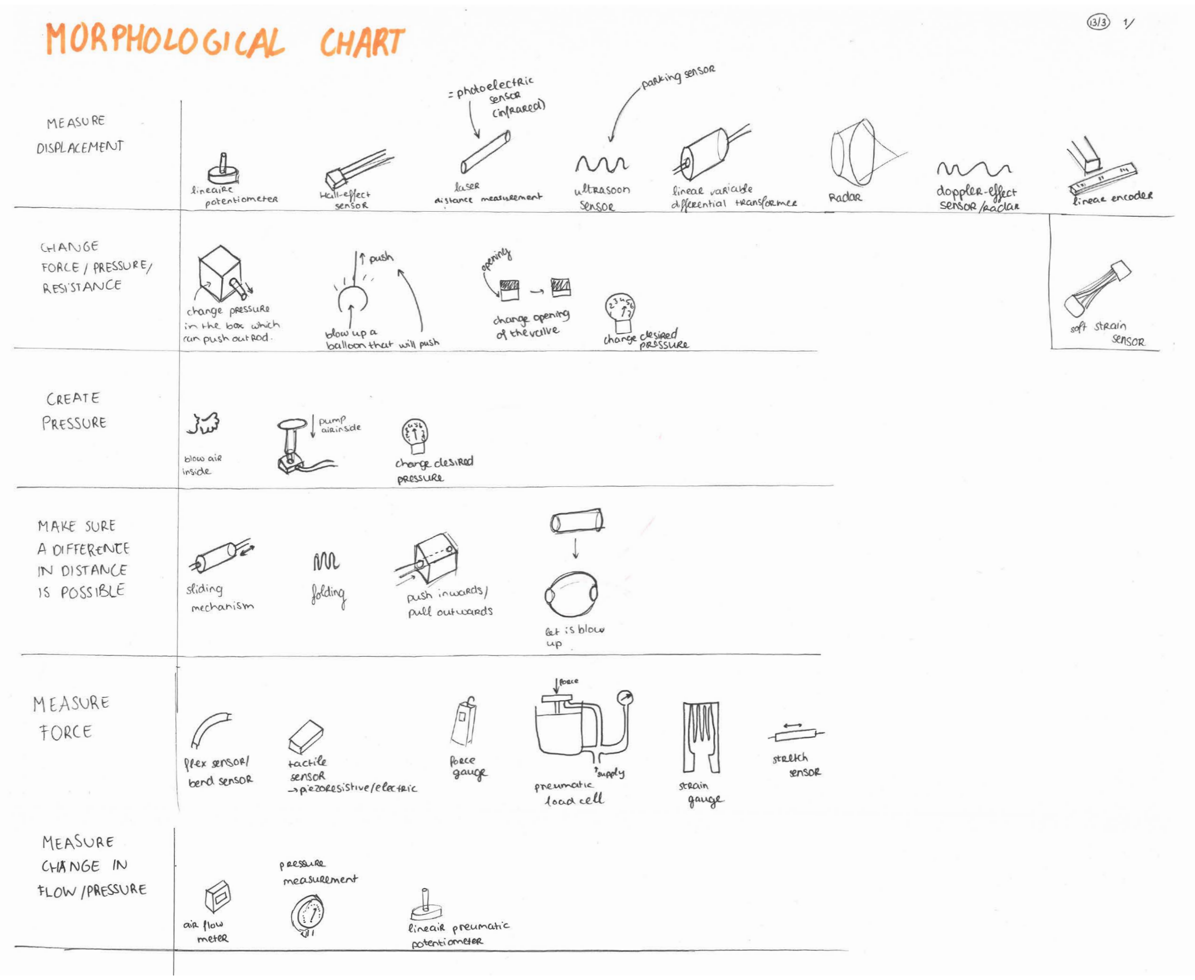

Figure 4.1: Morphological chart which shows solutions for the following functionalities: measure displacement, change force/-pressure/resistance, create pressure, change in distance, measure force, and measure change in flow/pressure.

Another method (How-To's) was used to come up with design ideas. In this method, questions on how to realise certain functionalities are posed [33] The results of these first two questions are shown in Figure 4.2. The questions are:

1. How to send info/signals back and forth?
2. How to create feedback (pneumatically)?

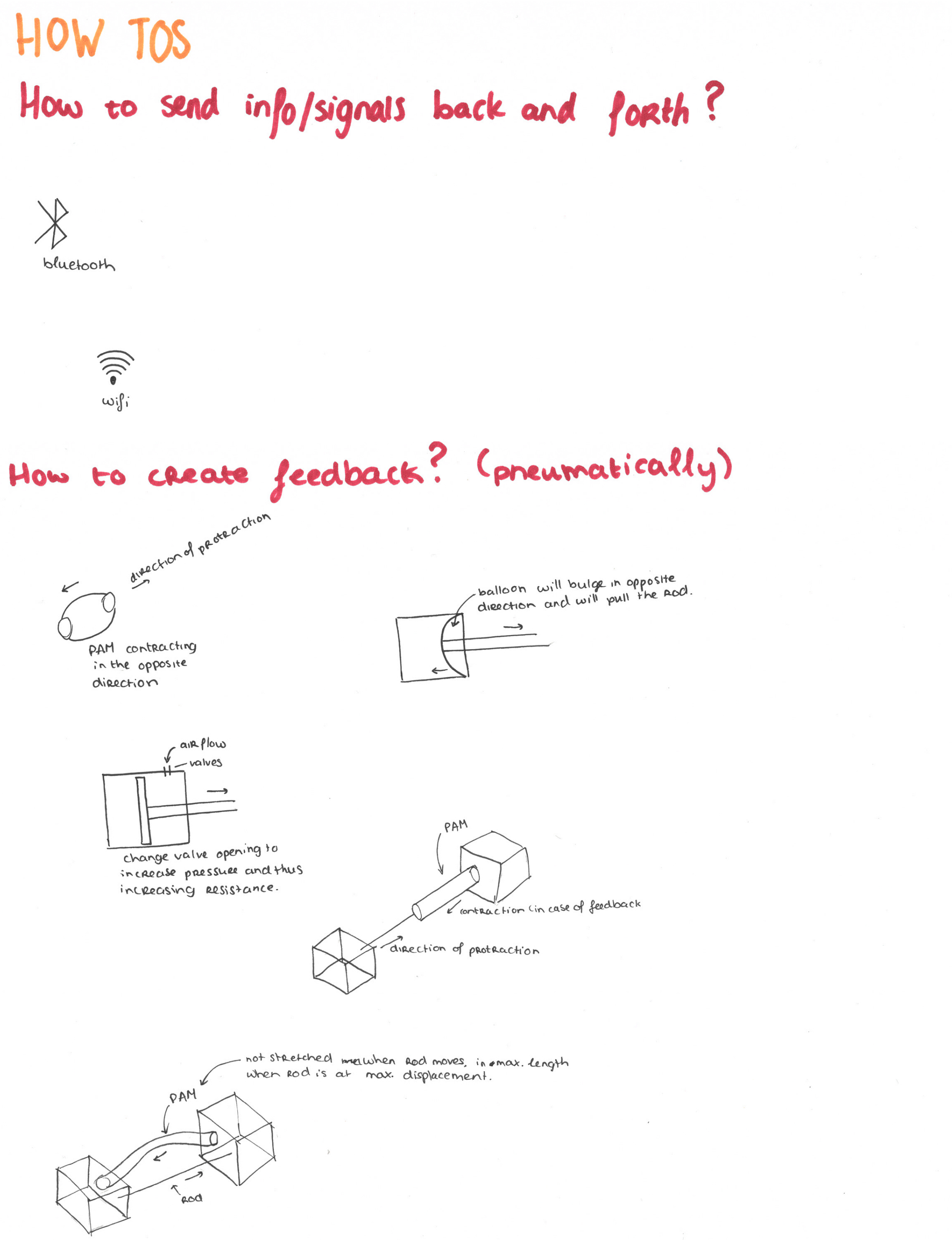

Figure 4.2: Drawings of the results of the How-To's questions: 1. How to send info/signals back and forth?, and 2. How to create feedback (pneumatically)?.

The third and fourth questions are:

3. How to attach something directly onto the body?
4. How to supply energy/gas?

Figure 4.3 displays the results of the brainstorm session on these questions.

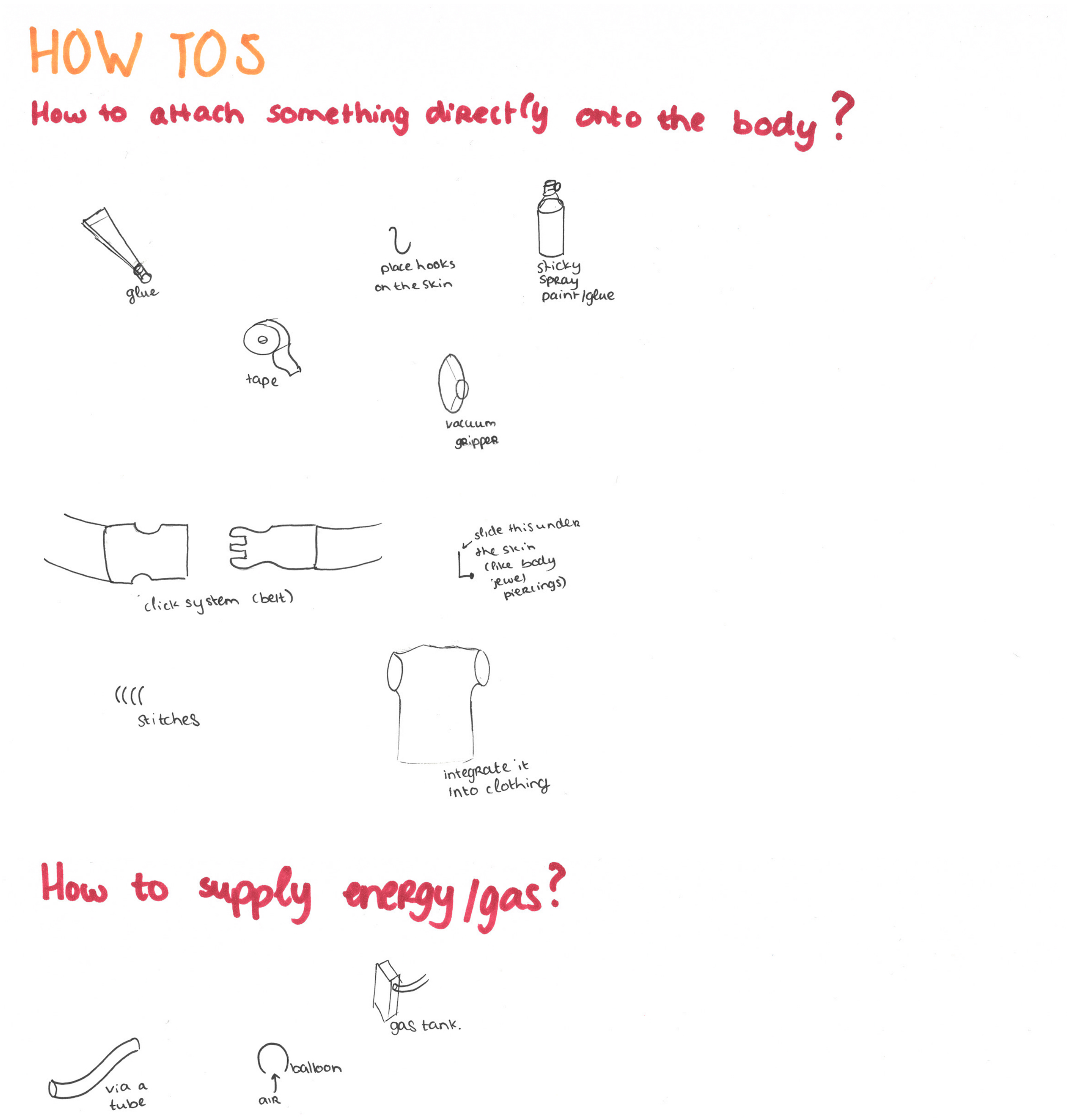

Figure 4.3: Drawings of the results of the How-To's questions: 3. How to attach something directly onto the body?, and 4. How to supply energy/gas?.

The last two questions that were posed are:

5. How to store energy/gas?
6. How to create motion in the system?

Figure 4.4 shows the results of these last two questions.

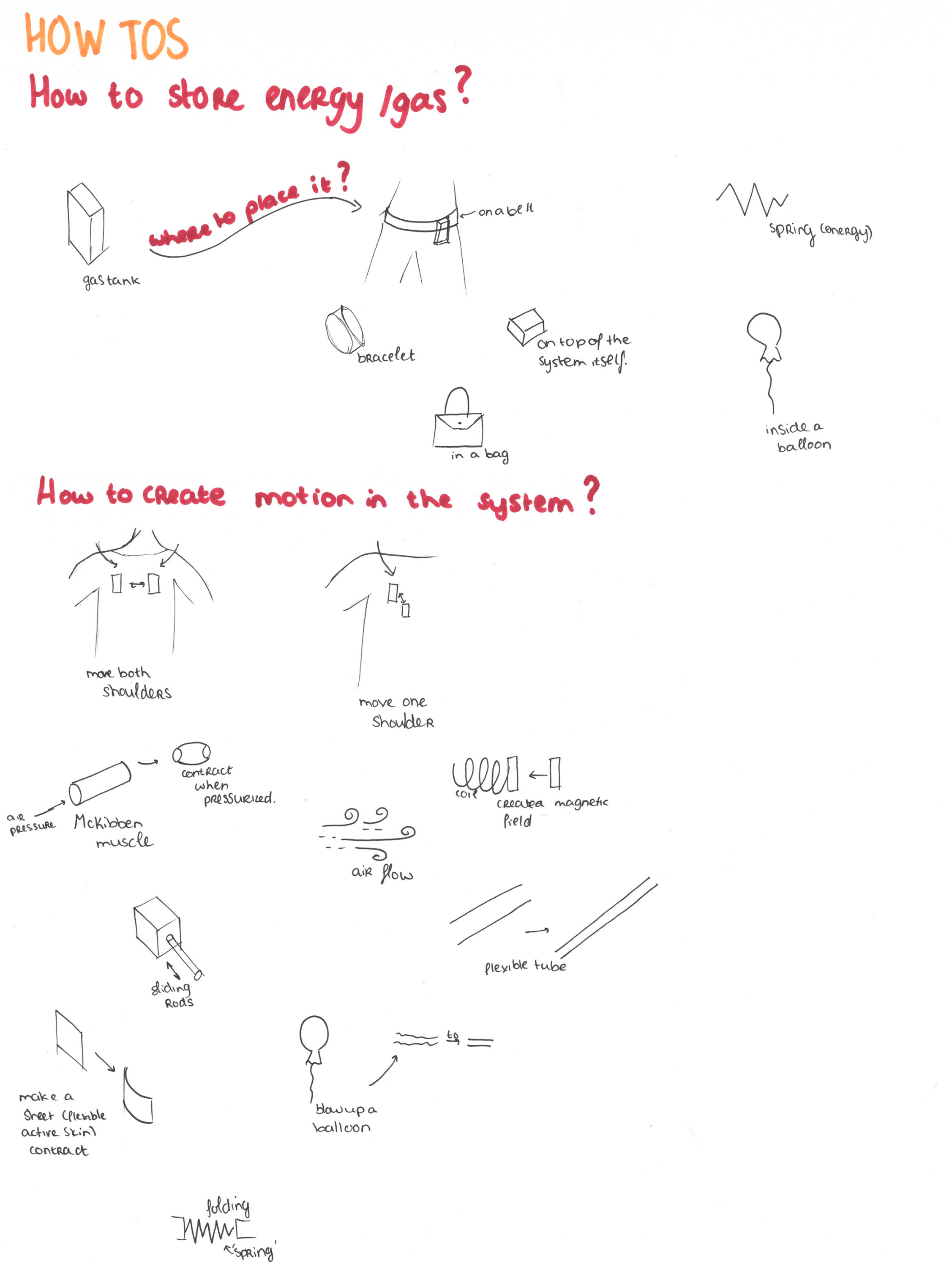

Figure 4.4: Drawings of the results of the How-To's questions: 5. How to store energy/gas?, and 6. How to create motion in the system?.

From the results of the morphological chart and the How-To's, ideas were subtracted and developed. In Figure 4.5, the first 2 ideas are presented. Idea 1 represents a system with a Pneumatic Artifical Muscle (PAM) that contracts to provide the force feedback. Sensors are integrated in the hardware to measure the displacement.

The second idea shows a design with a Pneumatic Balloon Acuator (PBA) that is pressurized to create resistance in the system. This way, the motion of the shoulder is hindered, which establishes proprioceptive force feedback.

Both ideas can be placed on one shoulder, where the movements protraction and elevation create the motion in the system. However, both ideas can also be placed on both shoulders.

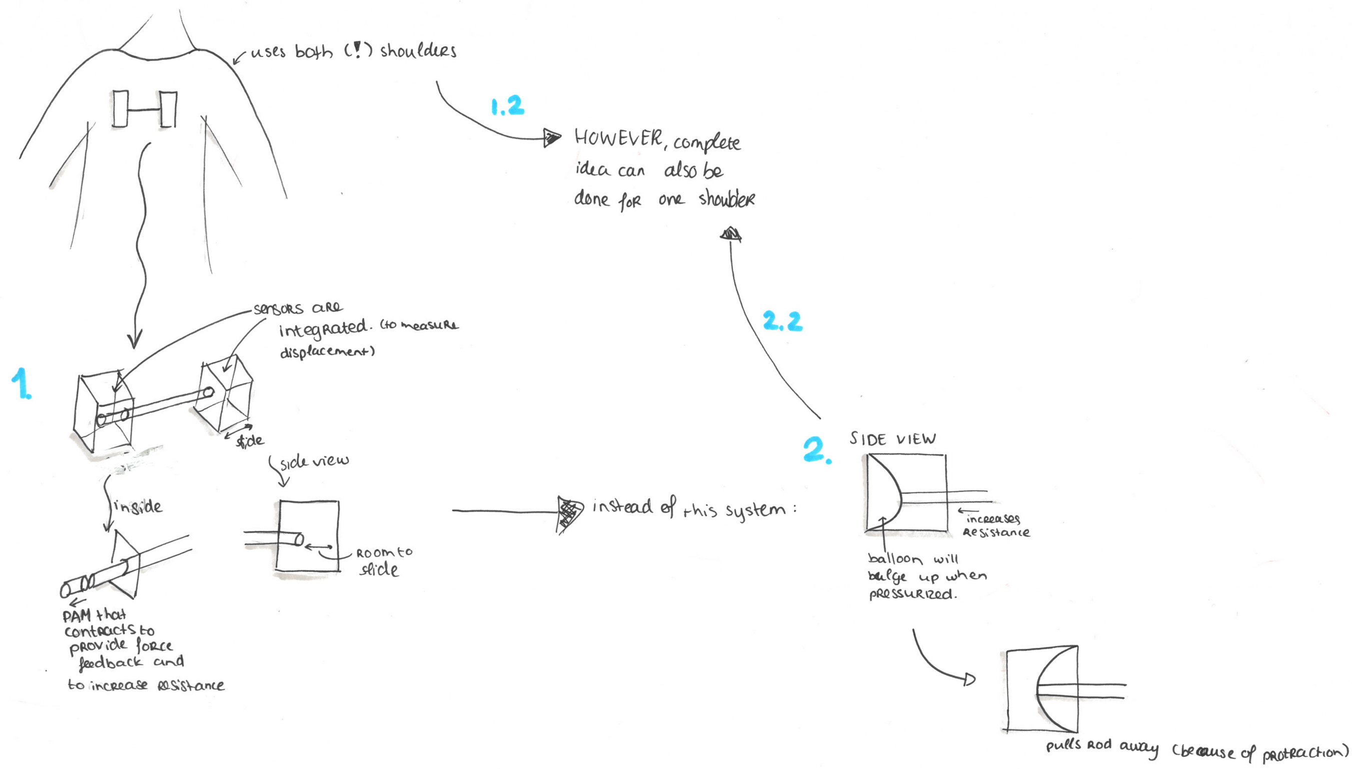

Figure 4.5: First ideas. Idea 1: Pneumatic Artificial Muscle (PAM). Idea 2: Pneumatic Balloon Actuator (PBA).

In Figure 4.6 ideas 3 to 7 are presented. The third idea shows a version of a pneumatic load cell. During protraction, the pressure inside the air chamber changes. The air could escape through the nozzle of the valve, where a pressure gauge is placed. This gauge measures the pressure relating it to the distance travelled (caused by the shoulder movement).

Idea 4 presents a design with a 'hook' incorporated. This hook pulls the valve open to let air flow into the chamber. A force or flow sensor measures how much air flows into the system. This is related to the displacement. Idea 5 is a new version of idea 4 where a force gauge is placed on top of the valve and hook. This gauge measures the force that is exerted during protraction. The force is related to the displacement.

The next idea (idea 6) shows a flexible active skin. In this skin small Pneumatic Artificial Muscles (PMAs) are placed that will contract when pressurized to exert force feedback. Stretch sensors are also integrated into the thin skin to measure the stretch. This stretch is related to the motion (and thus the displacement) of the shoulder.

The last idea in Figure 4.6 shows a design with a POT-meter. This meter measures the displacement by rotating during protraction. On the other side of the bar, a PAM is integrated into the design, to create the proprioceptive feedback.

Figure 4.7 shows the last four ideas. These will be explained on the next page.

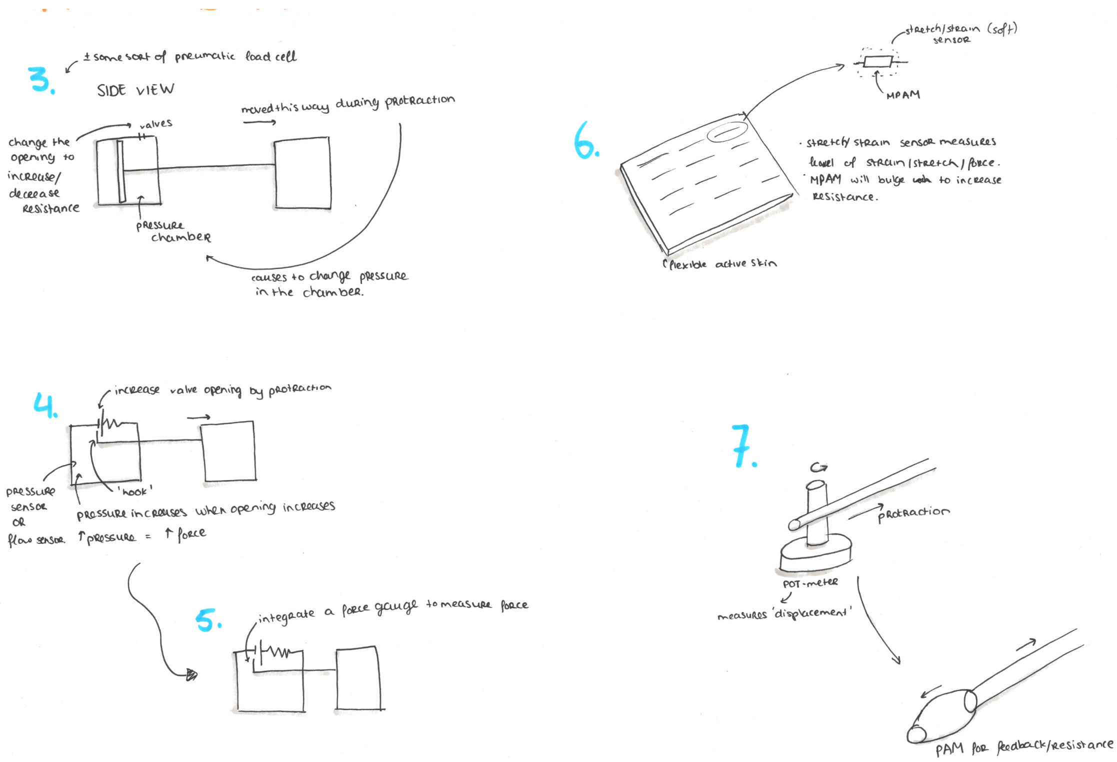

Figure 4.6: First ideas. Idea 3: Pneumatic load cell. Idea 4: Valve-hook. Idea 5: Force gauge. Idea 6: Flexible Active Skin. Idea 7: POT-meter.

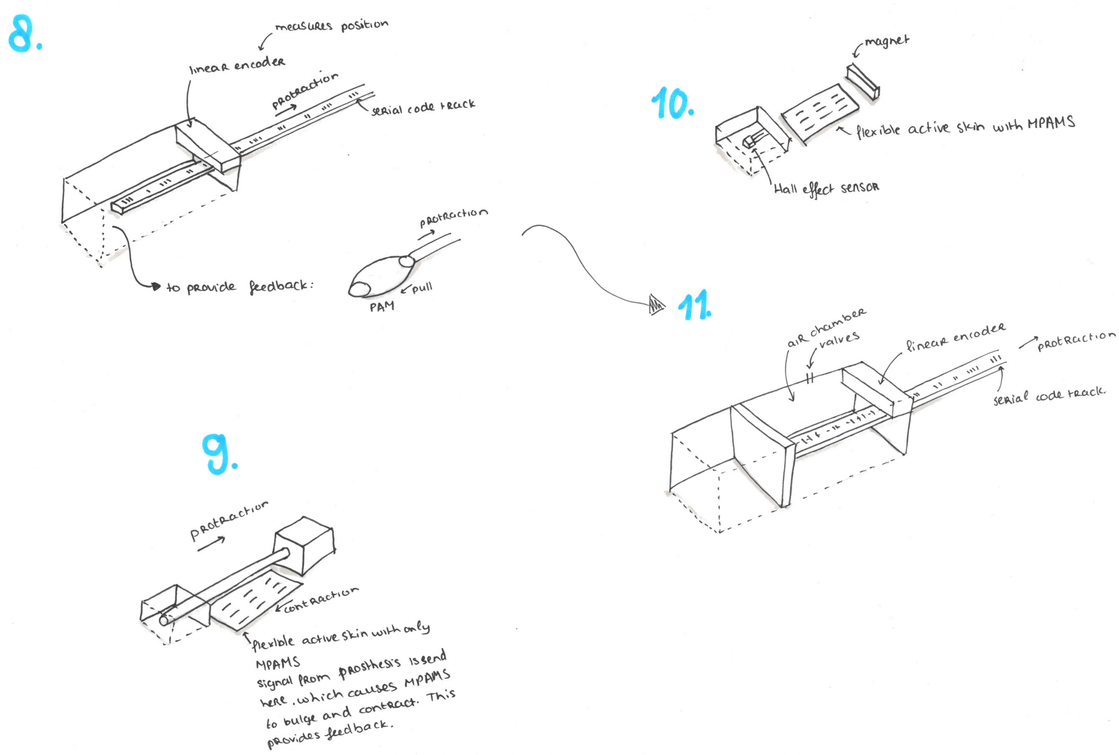

Figure 4.7: First ideas. Idea 8: Linear encoder. Idea 9: Flexible active skin with rod. Idea 10. Flexible active skin with an hall effect sensor. Idea 11. Linear encoder with an air chamber.

Idea 8 shows a system with a linear encoder. This encoder can measure the position based on the serial code that is placed on the rod. During protraction, this rod will move. Inside the chamber, a PAM is incorporated to provide feedback.

The ninth idea is a combination of the flexible active skin and a rod. The flexible active skin has small Pneumatic Artificial Muscles that will contract when pressurized. The rod is attached at both sides of the shoulder. On the ends of the rod, a sensor is placed to measure the displacement.

Idea 10 shows the combination of a flexible active skin and a hall effect sensor. The hall effect sensor will measure the displacement based on the strength of a magnetic field.

The last idea (idea 11) is a combination of a linear encoder and a piston-cylinder. The linear encoder will measure the displacement. The piston-cylinder has a chamber, through which air can flow. A valve will increase/decrease the pressure to create proprioceptive feedback.

Some of these ideas were combined and further developed. Idea 3 was further developed and can be seen in Figure 4.8. While developing this idea, some questions arose. How large will the magnet be? What is the minimal/maximal distance of a hall effect sensor? How large will the gas tank be, and where is it be placed? The answers to these questions need to be given when this concept is chosen.

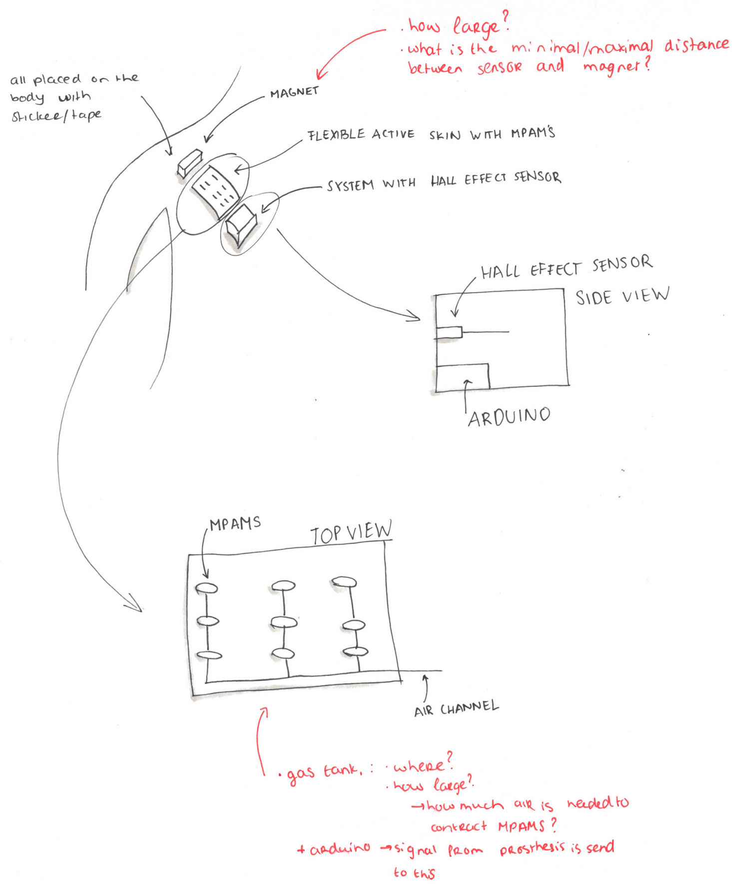

Figure 4.8: Idea 3 further developed. This idea contained a hall effect sensor with flexible active skin.

Figure 4.9 shows a more detailed drawing of idea 9. This idea had a POT-meter that measured the displacement. The POT-meter rotates when the piston rod moves (caused by shoulder protraction and elevation). Force feedback is provided by changing the air pressure inside the chamber. When the air pressure increases, the movement of the shoulder will be resisted and a higher activation force is needed to protract the shoulder.

Figure 4.10 shows how idea 10 was further developed and will be explained below the figure.

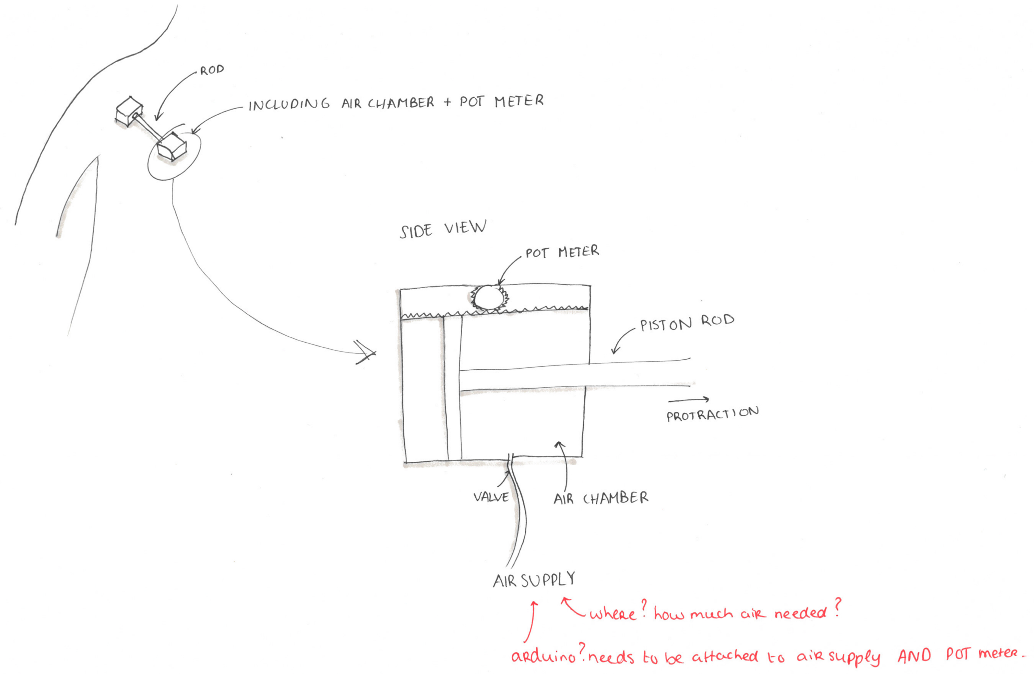

Figure 4.9: Idea 9 further developed. This idea contained a POT-meter that measures the displacement. The pressure in the air chamber is controlled via the opening/closing of the valve, creating a higher/lower pressure in the chamber.

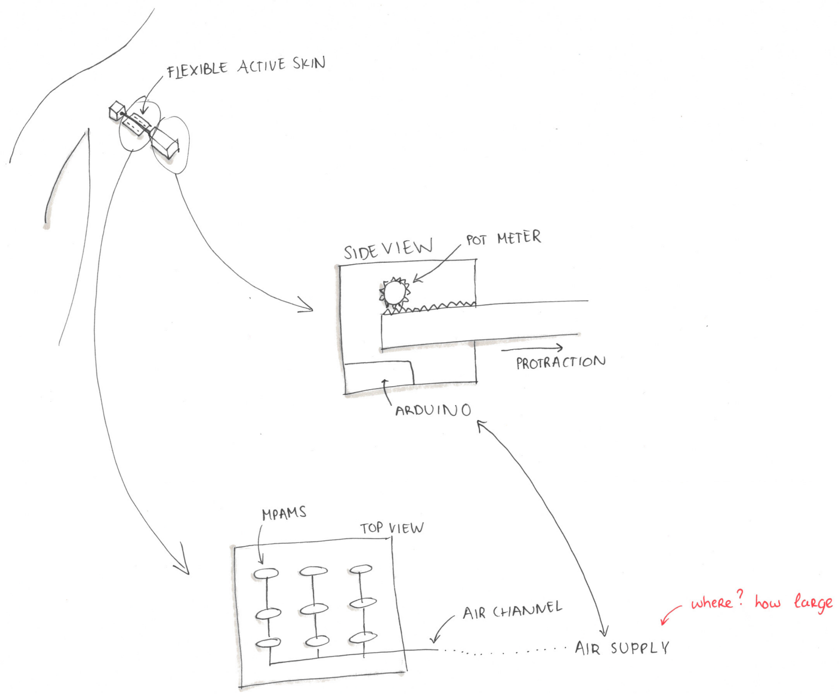

Figure 4.10: Idea 10 further developed. This idea included a POT-meter and a flexible active skin.

The design in Figure 4.10 had a POT-meter that was rotated by the rod. This rod moved when the shoulder was protracted. An Arduino will function as an AD-converter, by converting the POT-meter input to displacement values. This will then be sent to the prosthesis, and will control the opening/closing of the hand. The Arduino will also send pressure input values to the air supply valve. The Arduino will therefore control the force feedback provided by the system. When air is supplied to the air channels, the MPAMS (miniature PAMs) will inflate and contract.

In Figure 4.11 it can be seen how idea 11 was detailed. This design measured the displacement via a linear encoder. A serial code was placed on the piston rod. The linear encoder will read this code and will relate it to the displacement of the shoulder. This information is converted in the Arduino and sent to the prosthesis. The Arduino also controls the air pressure inside the air chamber.

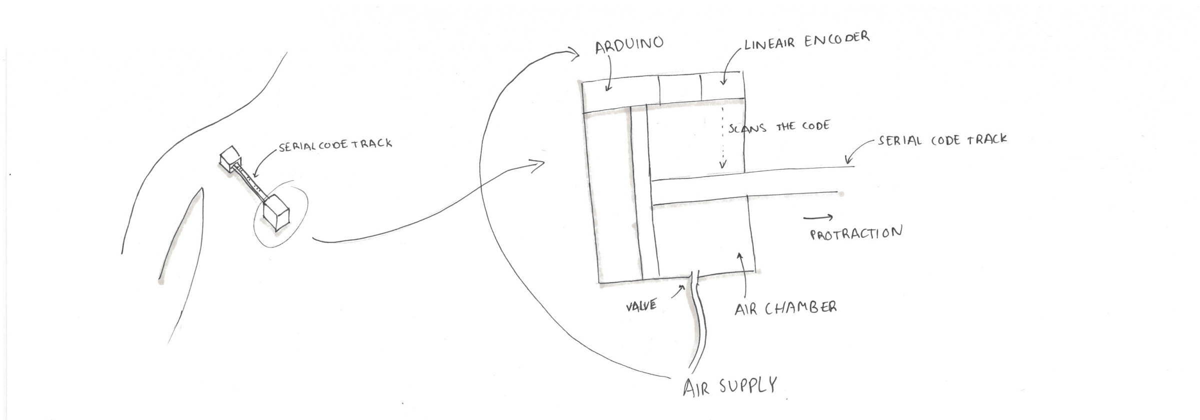

Figure 4.11: Idea 11 further developed. This system contained a linear encoder together with a pressure chamber.

Three final concepts were realized. The first concept can be seen in Figure 4.12. This concept has a linear encoder to measure the displacement and a PAM to create force feedback.

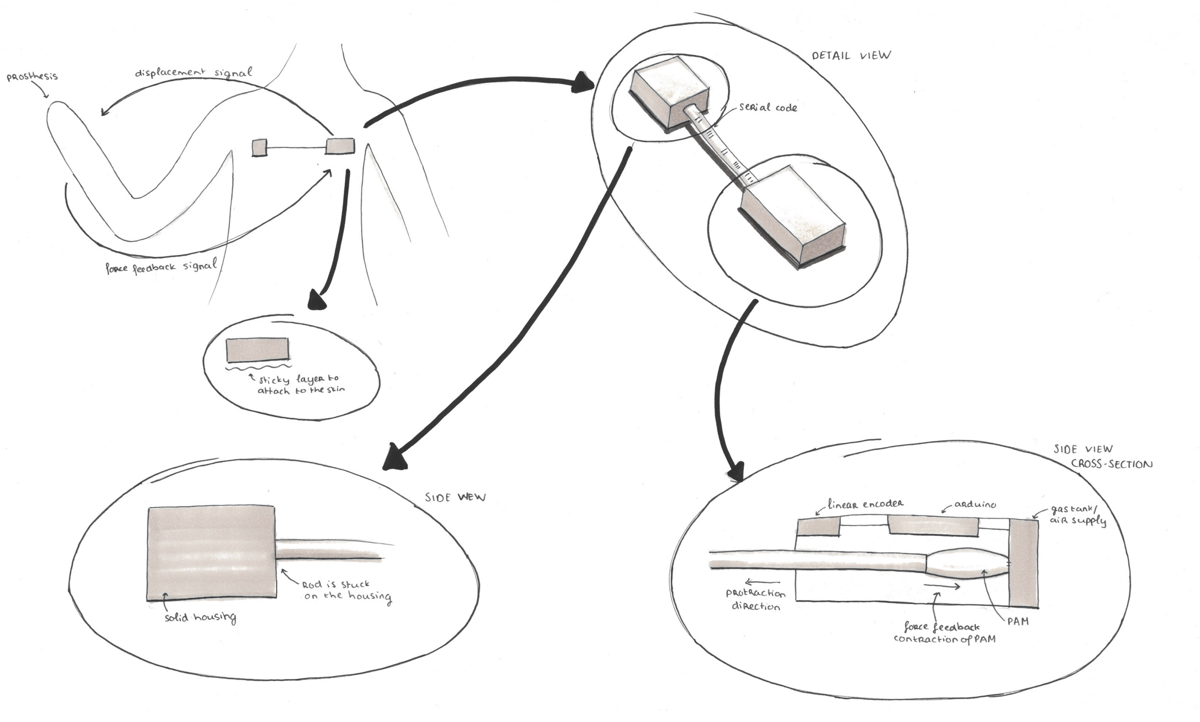

Figure 4.12: Concept 1, with a linear encoder to measure the displacement and a PAM to create force feedback.

The second concept is presented in Figure 4.13. A hall effect sensor will measure the distance and a pneumatic piston-cylinder will create feedback.

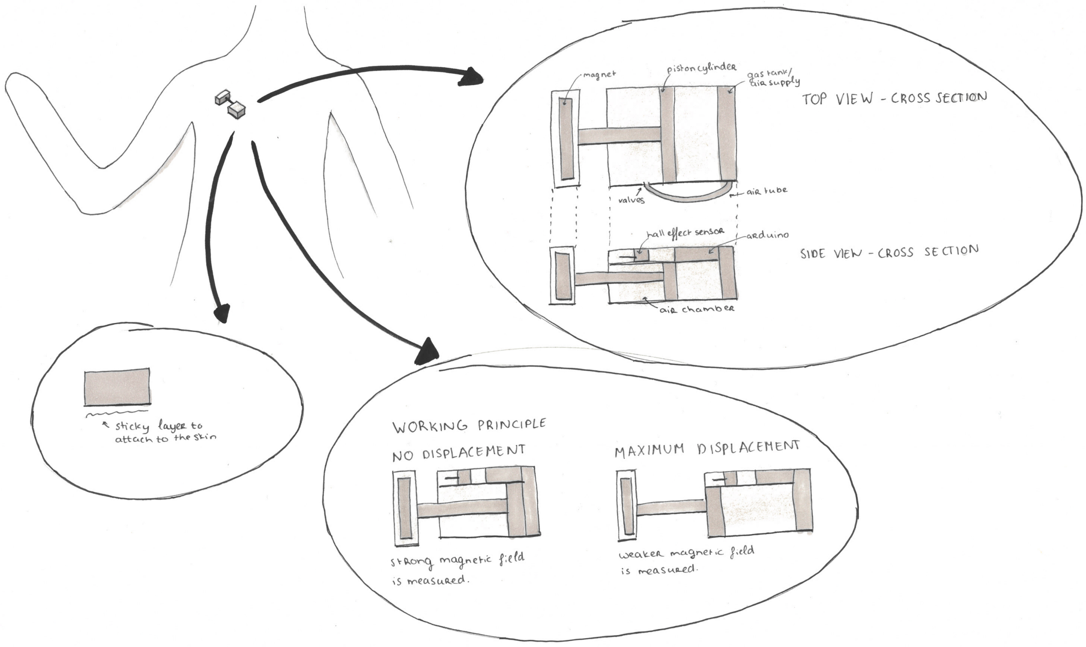

Figure 4.13: Concept 2, with a hall effect sensor to measure the displacement and a pneumatic piston-cylinder to create force feedback.

Figure 4.14 shows the final design of the third concept. This concept has a flexible active skin with MPAMs incorporated. A hall effect sensor will measure the displacement.

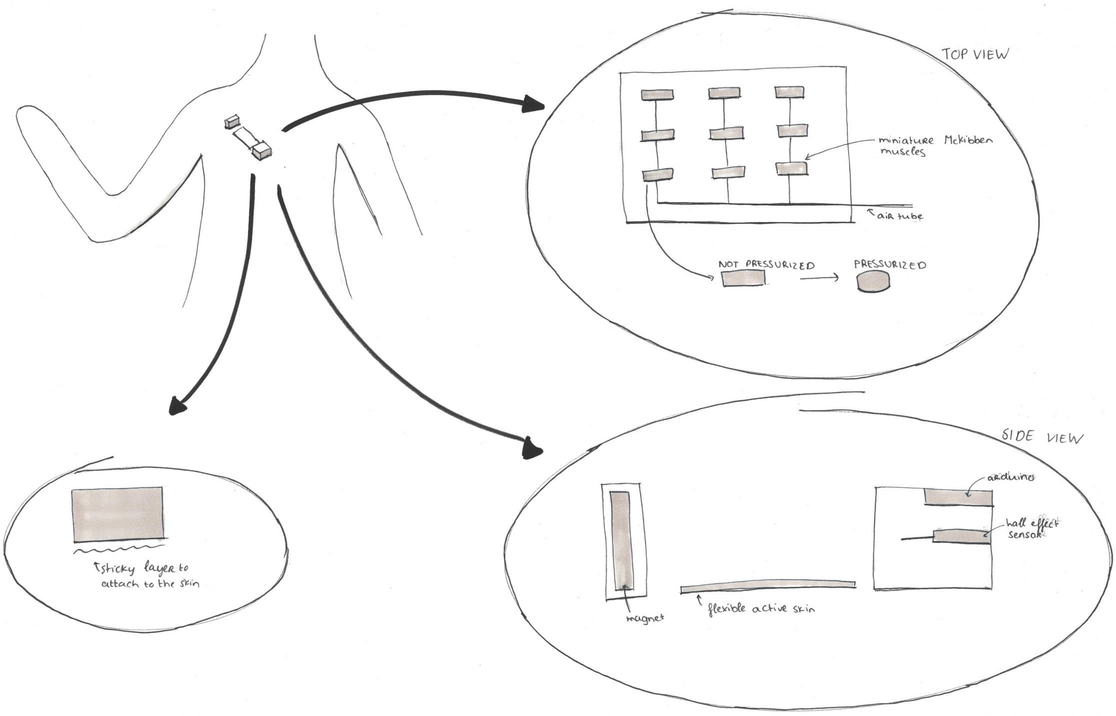

Figure 4.14: Concept 3, with a hall effect sensor to measure the displacement and flexible active skin with MPAMs to create force feedback.

To determine which of these concepts will be chosen and further developed into a prototype, two decision methods were combined and used, namely a Harris profile and a weighted criteria method [33]. For these methods, both criteria lists were used. This, because eventually this system needs to be optimized to fulfill all the criteria in the long run. The result can be seen in Figure 4.15. Eventually concept 2 is chosen even though concept 3 has more points. This is because concept 3 is a very difficult new, innovative design, which will take more time than is stated for this project. However, it is recommended for future research to also develop, built and test a prototype of concept 3.

Criteria	**Weighting factor**	**CONCEPT 1**					**CONCEPT 2**					**CONCEPT 3**				
		--	-	+	++		--	-	+	++		--	-	+	++	
Control prosthesis	8			■	■	16			■	■	16			■	■	16
Proprioceptive feedback	8			■	■	16			■	■	16			■	■	16
Wireless	8			■		8			■		8			■		8
Pneumatically driven	8			■	■	16			■	■	16			■	■	16
35*N* supply force	8			■		8			■		8			■		8
Safe	7			■		7			■		7			■		7
Max. 400*g*	7			■	■	14			■		7			■		7
Max. size 223x346x50*mm*	7		■			-7			■	■	14			■		7
No physical harm	5			■		5			■		5			■		5
Soft material	5		■			-5		■			-5			■		5
Latency time max. 300*ms*	5			■		5			■		5			■		5
Reliable (no jerky movements)	3			■		3			■		3			■		5
Round edges	3			■		3			■		3			■	■	6
Easy to apply	3		■			-3			■		3			■		3
No irritation to the skin	3			■		3			■		3			■		3
Able to be used for a whole day	3			■		3			■		3			■		3
Practical	2			■		2			■		2			■	■	4
Easy to operate	1			■	■	2			■	■	2			■	■	2
Disposable attachment	1			■		1			■		1			■		1
Sustain friction	1			■		1			■		1			■		1
Sustain temperature of 30 degrees	1			■		1			■		1		■			-1
Waterproof	1		■			-1			■		1			■		1
Easily cleaned	1			■		1			■		1			■		1
Long durability	1			■		1			■		1			■		1
Total score	**100**					**100**					**122**					**130**

Figure 4.15: Harris profile and weighted criteria [33].

5

Concept Proposal

5.1. Changes made in concept

Some changes are made to the design of the concept. After a meeting with Jos van Driel, I came to the conclusion that a hall effect sensor is not applicable in this design, because a hall effect sensor measures distances of $micrometers$, and not $millimeters$. The displacement that will be reached in this design (maximally $35mm$) is therefore too high to measure for a hall effect sensor. Hence, a laser sensor will be used.

It was intended to use an Arduino as an AD-converter in the design. However, an Arduino is less compatible with LabView (a visual coding program). An AD-converter of the brand National Instruments was more compatible with Labview. That is why this AD-converter will be used in the prototype.

5.2. Final design

First, the final design will be presented briefly. In Figure 5.1, the design can be seen. In Figure 5.2 a cross-section of the design is shown. The components of the system are now more visible. All the components will be discussed in the next section.

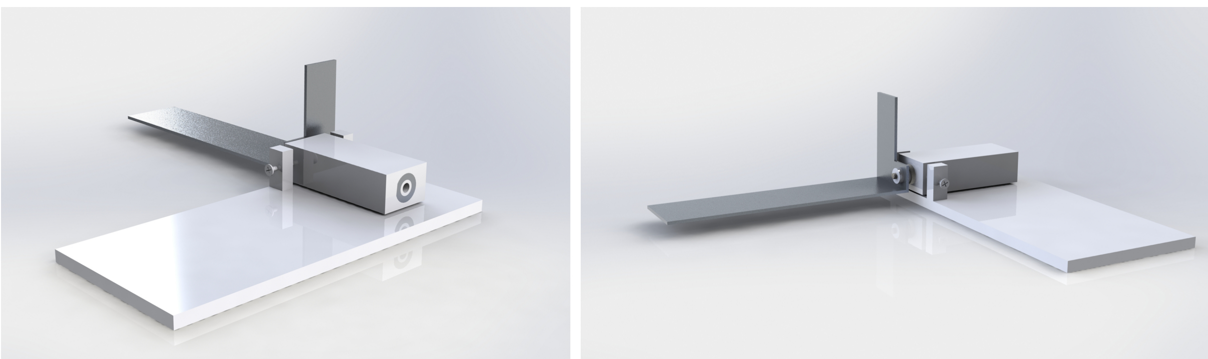

Figure 5.1: Two side-views of the total system with the different main components visible.

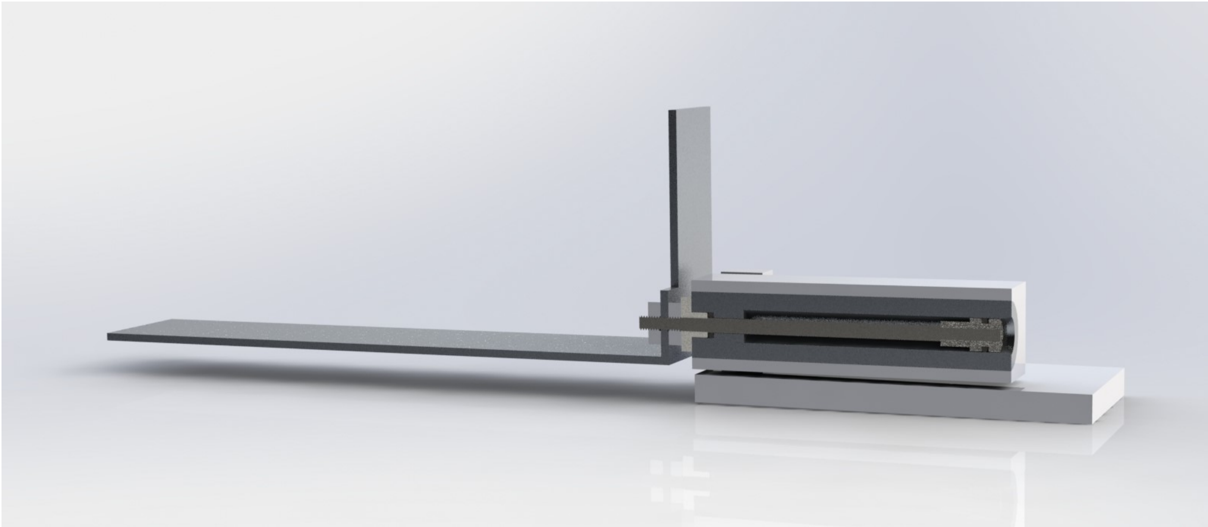

Figure 5.2: A SolidWorks render of a cross-section of the system.

A usage scenario was developed to demonstrate how the system works. In the scenario, the user lifts an imaginary object. Some relationships between variables will be mentioned, but will not be explained in detail. This will be done later on in this chapter.

1. The user wants to pick up an object that has a width of $20mm$. Hence the prosthetic hand should close with $50mm$, because the maximum opening of the hand is $70mm$.
2. The user protracts and elevates the shoulder joint with a displacement of $25mm$. The prosthesis will now close with $50mm$, leaving an opening of $20mm$. This, because the relation between the prosthesis closing and displacement of the shoulder is the following: $70mm$:$35mm$, which is the same as: $2mm$:$1mm$. This means that $1mm$ displacement of the shoulder means $2mm$ of hand opening/closing.
3. The prosthetic hand closes and the object is lifted. The object has a weight of $2.04kg$, which results in a force of $20N$.
4. This force should be fed back to the user by exerting a force on the shoulder joint. As will be explained later on, the relation between the force at the prosthesis and the force at the shoulder joint is the following: $35N$:$10N$. This results in a force of $\frac{20}{3.5} = 5.7N$. This force should be exerted by the force transducer on the shoulder joint.
5. This force will be fed back to the shoulder by increasing the pressure inside the air chamber of the piston-cylinder. With the formula shown in Equation 5.1 the pressure (in bar) will be calculated in Equation 5.2. The formula will be explained in detail later on in this chapter.

$$\rho(bar) = \frac{F(N)}{A(mm^2)} \times 10 \quad (5.1)$$

$$\rho = \frac{5.7}{\frac{\pi}{4} \times 6^2 - \frac{\pi}{4} \times 3^2} \times 10 \approx 2.68 \quad (5.2)$$

   This resulted in a pressure of approximately $2.68bar$.
6. This pressure signal is sent via the AD-converter to the valve which will control and regulate the pressure inside the air chamber.
7. Now the user feels a force acting on the shoulder joint, providing the proprioceptive force feedback.
8. When the object is released, the force reduces to $0N$. The pressure will also reduce. This will be done by opening the exhaust, causing the pressure to drop to atmospheric pressure, which is $1013.25mbar$.

5.3. Components

In this section, all main components of the system will be discussed. In Table 5.1, the components can be seen, together with the brand and a short explanation of their function.

Component	Brand	Function
Piston-cylinder	Customized	Facilitating movement
O-rings	Supplied by the TU Delft	Seal, avoiding leakage
Air supply	Supplied by the TU Delft	Makes it possible to create a certain pressure
AD-converter	National instruments	Controlling the input and output signals
Valve including pressure sensor	Festo	Regulating air pressure
Laser sensor	AE sensors	Measuring the displacement
Base	Customized	All parts are attached to this base

Table 5.1: All the components of the system, together with their brand and function.

5.3.1. Piston-cylinder

A circular piston-cylinder was designed for this system. The piston is kept as small as possible to limit the total thickness, which was set as a criteria. The dimensions of the piston-cylinder can be seen in Appendix Chapter 10. All the SolidWorks drawings are presented in that chapter.

The piston-cylinder needs two seals, to create a non-leaking system. In a schematic cross-section of the piston-cylinder in Figure 5.3, it can be seen where these two seals will be located. Two O-rings will be used of which one has dimensions of 4x1mm, with 4mm being the internal diameter and 1mm being the cord thickness. This creates a total diameter of 6mm. The other O-ring has dimensions of 3x1mm.

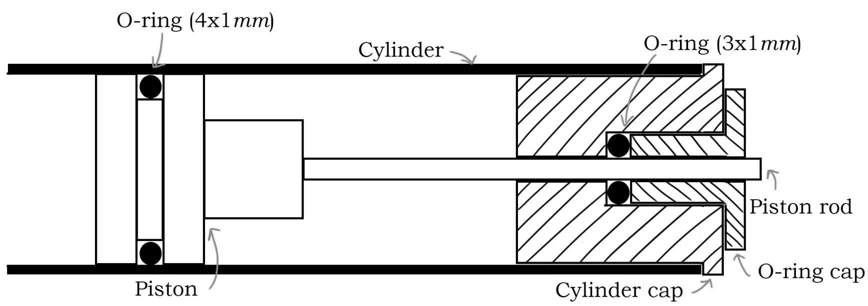

Figure 5.3: Schematic cross-section drawing of the O-rings placed inside the piston-cylinder. Two O-rings are used, namely one of 4x1mm and 3x1mm.

5.3.2. Air supply

Optimal gas supply pressure is invariable with the cycle time, with the length of the pipeline, and with the loading conditions according to Plettenburg [25]. This optimal gas supply was set at 1.25MPa. However, the proportional valve was a limitation in this prototype. This valve has a maximum pressure of 6bar, which is 0.6MPa. Therefore, this optimal gas supply pressure cannot be reached and the maximum pressure will be 6bar.

The air supply was provided by a gas tank that was located at the TU Delft. The pressure at this tank could be set at a certain level, which was 6bar in this case.

5.3.3. AD-converter

The AD-converter will control the input and output signals of the system, see the block-scheme in Figure 5.4. It will receive an input signal from the computer. This input signal will contain the force (reference force or test force) that needs to be reached. This force signal will be converted to a voltage, that will be sent to the valve. This voltage signal is directly related to the pressure that needs to be reached inside the air chamber for that certain force.

The AD-converter also receives an input signal from the laser sensor, containing information about the personal displacement of the subject. This signal will be sent to the computer, which will display this personal displacement on the computer screen.

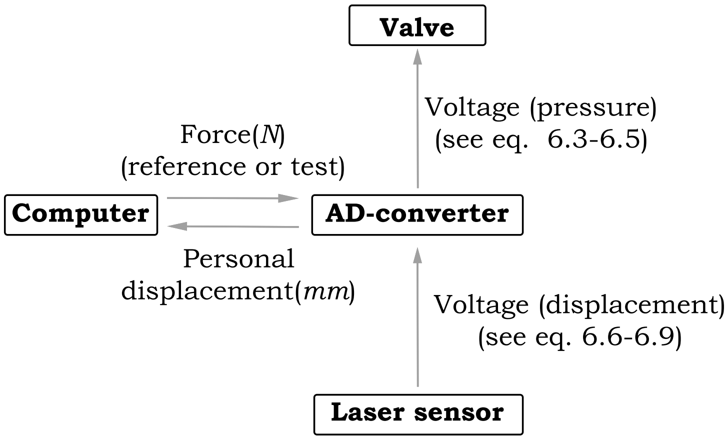

Figure 5.4: Simplified block scheme of the AD-converter. The AD-converter will receive information from the computer about the force. This value is converted to a voltage and will be sent to the valve. The AD-converter also receives displacement information form the laser sensor, which will be sent to the computer.

As could be seen in Figure 5.4, the AD-converter receives an input signal from the computer to send an output signal to the valve. This input signal will be the test force or reference force in $Newton$. This force then needs to be converted to a pressure value, see Equation 5.3.

$$\rho = \frac{F}{A} \times 10 \tag{5.3}$$

With F = force (N), and A = effective area (mm^2). The pressure is multiplied by 10 to get a unit of bar instead of MPa.

The area of the piston-cylinder is calculated as presented in Equation 5.4.

$$A = \frac{\pi}{4} \times 6^2 - \frac{\pi}{4} \times 3^2 \tag{5.4}$$

The area of the piston is $6mm^2$ and the area of the piston rod is $3mm^2$.

With equation 5.3 and 5.4 the pressure value in bar can be calculated. The pressure now has to be converted to a voltage value, which will be send to the valve as an input signal. The valve has a range of 0-6bar and the valve has a range of 0-10V. This results in that 1bar equals to $\frac{10}{6}$ V. Therefore, to translate the pressure value to a voltage value it needs to be multiplied by $\frac{10}{6}$, see Equation 5.5.

$$Pressure(involtage) = \rho \times \frac{10}{6} \tag{5.5}$$

The pressure is now converted to a voltage signal. The valve will now regulate and control the pressure inside the air chamber.

As was explained, the laser will also send an input signal to the AD-converter. The AD-convert can only receive a voltage signal. Therefore this voltage signal is first converted to a current.

$$I = \frac{U}{R} \tag{5.6}$$

With U = $Voltage$ input signal and R = resistance in $k\Omega$. The resistance in this laser sensor is 0.469$k\Omega$. The current is in mA (Equation 5.7).

$$I = \frac{U}{0.469} \tag{5.7}$$

The current of the laser sensor has a range of 4-20mA. Therefore, an offset of 4mA is subtracted from the calculated current, see Equation 5.8.

$$I = I - 4 \tag{5.8}$$

Now we have a range of 0-16mA, that needs to be converted to a distance. The laser sensor has a measurement range of 50mm. The current therefore needs to be multiplied by $\frac{50}{16}$, which equals to 3.125 (see Equation 5.9).

$$Displacement = I \times 3.125 \tag{5.9}$$

5.3.4. Valve

The proportional pressure valve will regulate and control the pressure inside the air chamber. The valve that will be used is a VEAA piezo-valve from Festo [9]. This because it is the smallest valve that was found at the moment. Another advantage of this valve is that a pressure sensor is already incorporated and thus no separate sensor is needed. The pressure in the air chamber should be measured to regulate and control the pressure inside the chamber, such that it reaches the set-point value.

Some of the specifications of the valve can be seen in Table 5.2. It shows that the valve has a pressure range of 0-6bar, which is enough because a maximum pressure of 4.4bar is reached in the experiments. The set-point input signal range is 0-10V, which was already explained in detail in Section 5.3.3 (AD-converter).

Dimensions	15x54.5x85mm
Standard nominal flow rate	7-13L/min
Actuation type	Electrical with piezo-element
Product weight	55g
Nominal operating voltage	24V DC
Set-point input signal	0-10V
Accuracy of analogue output	2%
Pressure range	0-6bar

Table 5.2: Specifications of the 3 way proportional valve (VEAA-L-3-D9-Q4-V1-1R1) [9].

A piezo-valve is a bending actuator with a ceramic piezo-element. This element is polarised in a strong electric field during a polarisation process. This causes the electric field to be directed to one side. When a voltage is applied to the material after this process, it will deform along the electric field lines. When the material bends, the valve will open as can be seen in Figure 5.5 [36].

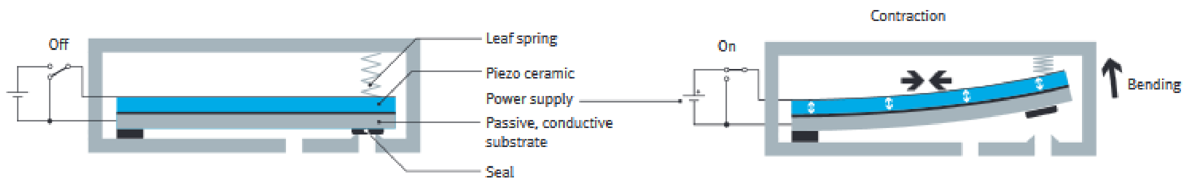

Figure 5.5: Schematic drawing of the function of a piezo-valve [36]. When a voltage is applied to the piezo ceramic material it will bent causing the valve to open.

In Figure 5.6 the functionality of the valve can be seen. Port 1 is for the compressed air, port 2 the working air and port 3 the exhaust air. When port 1 and 2 are connected, the compressed air will flow into the air chamber (via port 2). When the pressure needs to be decreased, port 2 and 3 will be connected causing the air to exhaust. Other symbols are explained in the figure itself.

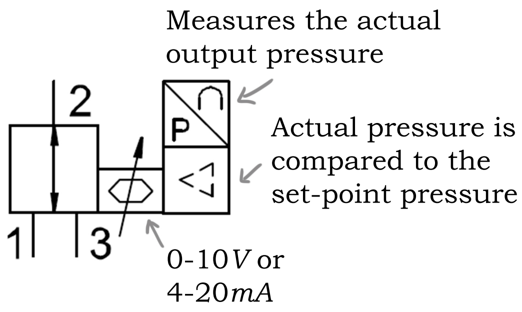

Figure 5.6: Schematic drawing of the valve showing the functionality. Port 1: Compressed air. Port 2: Working air. Port 3: Exhaust air.

5.3.5. Laser sensor

To measure the displacement, a laser sensor was incorporated. Figure 5.7 shows how the laser sensor works. The laser has a measuring range of 50mm, but has an offset of 45mm. This causes to start the measuring range at 45mm and end at 95mm.

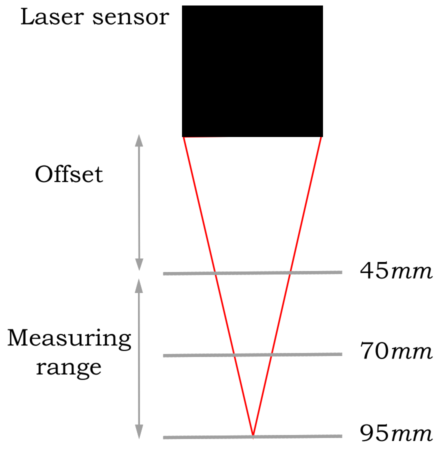

Figure 5.7: Schematic drawing of the working principle of the laser sensor.

Table 5.3 shows some specifications of the laser sensor. As was already mentioned before in Section 6.3.3 (AD-converter), the output signal range is 4-20mA or 1-10V.

Dimensions	50x65x20mm
Measuring range	50mm
Linearity	±0.2%
Measuring rate	1kHz
Laser safety class	class 2 IEC 60825-2 2001 11
Product weight	100g
Nominal operating voltage	24V DC
Output signal (mA)	4-20mA
Output signal (V)	1-10V

Table 5.3: Specifications of the laser sensor [23].

The laser can measure a distance between 0-50mm, which is desired in this prototype. As was mentioned before, Vardy and Plettenburg [34] determined that on average a maximum displacement of 35mm is made with protraction and elevation of the shoulder. According to Smit et al. [32] the maximum hand opening/closing is 70mm. This holds a relationship as can be seen in Figure 5.8 between the displacement of the shoulder and opening/closing of the hand (displacement prosthesis). This causes a displacement of 1mm at the shoulder (input signal) to be 2mm at the prosthesis (output signal), assuming that there is a linear relation between the displacement at the shoulder and displacement at the prosthesis. It is investigated if there could be a non-linear relation between the two variables. This means that for example it will require more effort to close the hand when it is almost closed already, than for example closing the hand with a few mm from maximum opening. However, such relation was not found in literature and it is therefore assumed that the relation is linear.

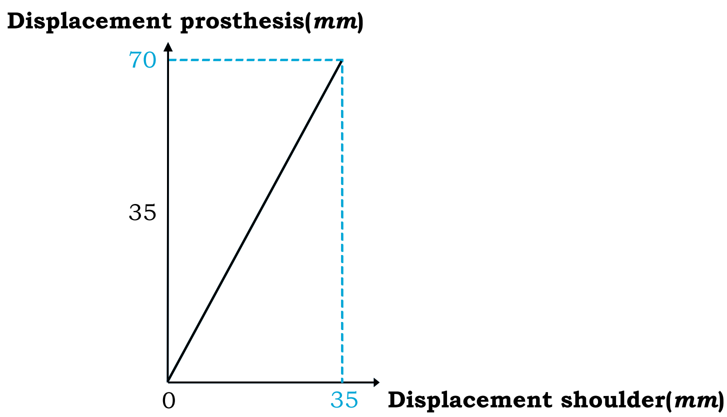

Figure 5.8: Graph showing the relation between the displacement at the prosthetic hand(mm) and the displacement at the shoulder(mm).

5.3.6. Base

The laser sensor and valve need to be placed on top of a base, such that they are in exactly the same place for each subject. For this reason, a base is designed. In this section, the base of the system will be explained. Two versions of this base were made. These two will be explained in Chapter 8. In this Chapter, only the final version will be presented.

The base can be seen in Figure 5.9. The cylinder is fixed inside a block, that is attached to the base via a hinge joint. The block (with the cylinder) can now rotate, and move along with the curvature of the shoulder (see Figure 5.10).

Figure 5.9: Base showing that the cylinder is fixed inside a block, but is able to to rotate because of the hinge joint.

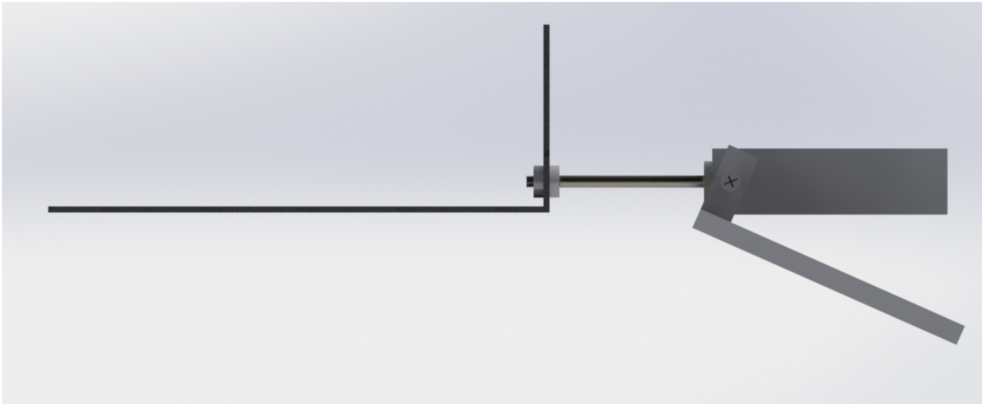

Figure 5.10: Base showing that the cylinder is fixed inside a block, but is able to to rotate because of the hinge joint as can be seen in this side-view.

5.3.7. Attachment to the skin

The complete system is attached to the skin. Latour [19] attached her Anchor system with special double-sided wig tape. This tape is on one side attached to the skin and on the other side to the system. The base is made of polyethylene on which the tape is adhered. The tape is removable, such that is can be replaced after each subject for hygienic reasons.

The system is attached to the skin at two places, as can be seen in Figure 5.11; one next to the vertebrae and the other on the upper right corner of the right shoulder.

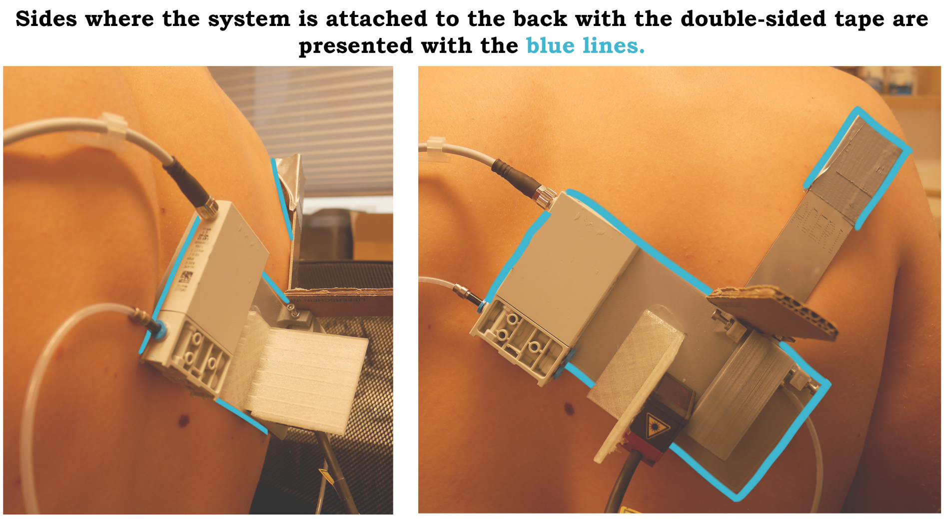

Figure 5.11: This Figure shows where the system is attached to the body. It is attached with special double-sided tape. The blue lines represent the places where the double-sided tape is attached to.

5.4. Forces

Pilot studies from Vardy [35] reveal that static forces up to $10N$ were most comfortable and forces below $2N$ were regarded too low for accurate control. Therefore, this range of forces was also adopted in the research experiment in this article.

As was mentioned before, the reference/test force is an input signal from the computer to the AD-converter. The force that needs to be reached for ADL tasks is $35N$ [11]. This force should be fed back to the shoulder. As was also mentioned is that the forces on the shoulder will maximally be $10N$ [35]. This holds the following relation: $35N$:$10N$. This means that $1N$ at the shoulder equals a force of $3.5N$ at the prosthetic hand. This relation is presented in a graph in Figure 5.12.

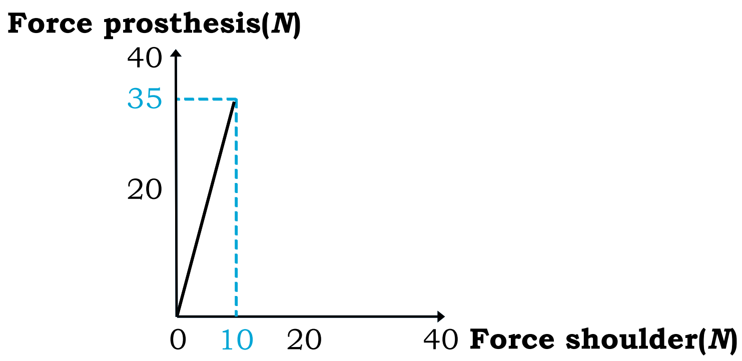

Figure 5.12: Graph of the relationship between the force at the prosthetic hand and the force at the shoulder.

5.5. Dimensions

The total dimensions of the system are 155x85x50.5mm. The system was made as small as possible, but is still quite large. However, the size of the system is essentially caused by the size of the sensors. As a consequence of the laser, the plate, attached at the upper right shoulder, has a height of 50.5mm (see Chapter 10 for the SolidWorks drawing). This, because otherwise the laser could not correctly measure the distance. The height of the plate was even extended, to be sure that the laser was always able to measure the distance correctly.

The valve determines the width of the system (85mm). This shows that both sensors are fairly large.

As will be mentioned later on in Chapter 9 (Recommendations), the design needs to be optimized to decrease the size.

All the dimensions of all the components can be seen in Chapter 10. For each part, a 2D SolidWorks drawing is presented.

5.6. Material and total weight

In Table 5.4 the material for the most important parts can be found. All the materials for each sub-component can be found in Chapter 10. The materials are provided in the bill of materials on the 2D SolidWorks drawings.

Component	Material
Cylinder	Aluminium
Piston-rod	Stainless steel
O-rings	Rubber
Valve including the pressure sensor	Fibre-reinforced plastic
Base	Polyethylene

Table 5.4: The materials of the main components.

The total weight of the system is 272g.

5.7. Criteria

To check if the system met all the criteria set at the start of this research, a table is presented (see Table 5.5). The Table shows that the system fulfills almost all the criteria. Only the limited size was not met. The thickness was limited to 50mm. However, the thickness in the system was 50.5mm. As was already explained in Section 5.5 (Dimensions), the design should be optimized to lower the thickness and size of the system.

The results in Table 5.5 also show that the system is light enough. However, 272g on your back during the whole day will presumably too much. This could therefore be improved in the future.

Criteria	**+/-**	**Comment**
Control system	+	
Proprioceptive force feedback	+	With increasing pressure inside the air chamber.
Pneumatically driven	+	
Safe	+	The design was approved by the local ethics committee.
Maximum weight: 400g	+	System is 272g.
Maximum size: 223x346x50mm	+/-	The size is now: 155x85x50.5mm, which is slightly too thick.
Round edges	+	
Not irritate the skin	+	Minimally, only a little bit of red skin but was gone after a few $minutes$. Special removal spray was used to dissolve the glue of the tape. This decreased irritation.
Disposable attachment	+	The tape could be removed after each experiment.

Table 5.5: This table shows if the system checks all the criteria that were set at the beginning of this thesis.

6 Methods

In this Chapter, an elaborate overview of the research design for both experiments will be presented. Figure 6.1 shows the test design and how the system is placed on the back/shoulder of the subject. The numbers in Figure 6.1 represent the following:

1. Piston-cylinder, which slides when the shoulder protracts/elevates.
2. Laser sensor, which measures the displacement.
3. Valve, which controls and regulates the pressure inside the air chamber.

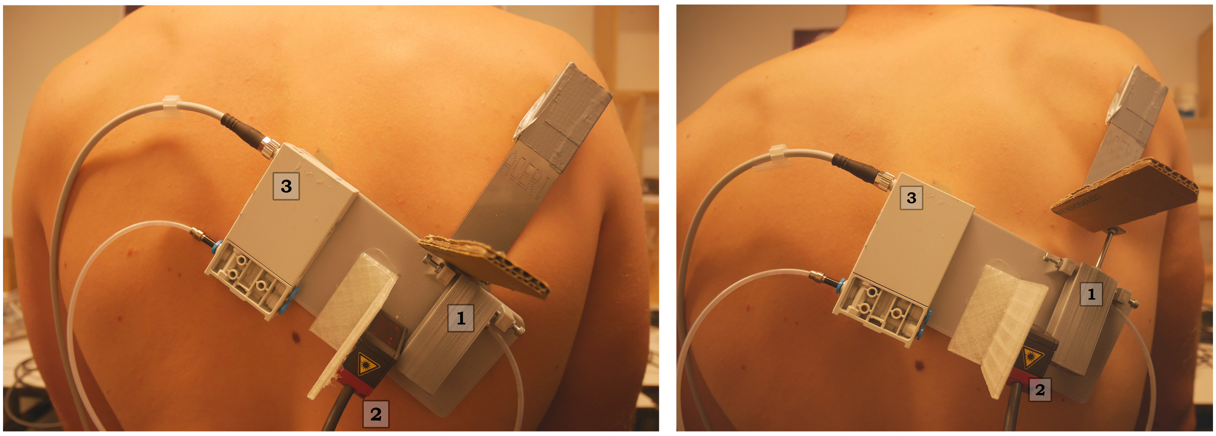

a) Closed system. Shoulder is at rest.

b) Open system. Shoulder is protracted and elevated.

Figure 6.1: An overview of the test setup that was used during both experiments. The components that are displayed are: 1. Piston-cylinder, 2. Laser sensor, 3. Valve.

Attached to the laser sensor and the valve is the AD-converter. As already explained in Chapter 5, this converter receives input signals from the laser sensor and computer, and sends signals to the valve. The wiring of the AD-converter can be seen in Figure 6.2.

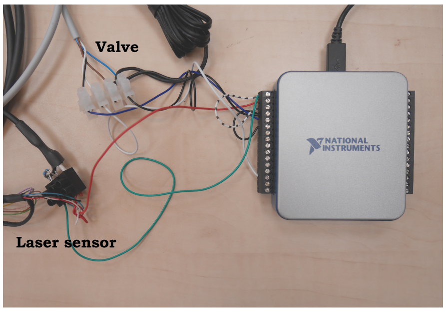

Figure 6.2: The wiring of the AD-converter (National Instruments). The laser sensor and valve are connected to the AD-converter.

The air supply gas tank was provided by the TU Delft and can be seen in Figure 6.3. The compressed air is set at $6 bar$. The maximum pressure that will be reached during the experiment is $4.4 bar$.

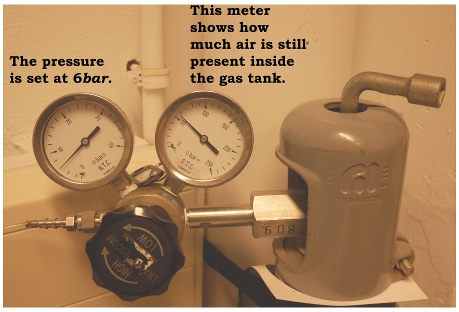

Figure 6.3: Air supply gas tank that was provided by the TU Delft. The compressed air was set at $6 bar$.

6.1. Experiment 1: Sensitivity

During this experiment, subjects had to sense the difference between the reference force and test force. A schematic overview of this test design can be seen in Figure 6.4. One trial is performed when one reference force is compared to one test force. In total, 10 trials will be executed per reference force. This will be done for each reference force. When all the reference forces are tested, one block is executed. This block will be repeated four times.

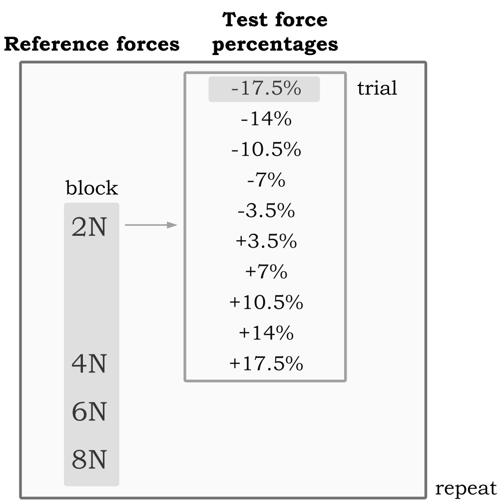

Figure 6.4: A schematic overview of the test design. One trial is performed when one reference force is compared to one test force. All the reference forces together form one block. This block is repeated four times.

A LabView simulation was programmed for each experiment. Figure 6.5 shows the screen the subject sees during the first experiment. Progress bars were displayed to show the target displacement and the personal displacement. The subject needed to reach the target displacement.

The two buttons next to the displacement bars needed to be clicked after one trial was performed. The subject needed to determine whether the second force was higher or lower than the first force.

After 10 trials, one reference force block was performed. Four blocks were executed. Then, the subject had a break for 5 *minutes*. During this break, the bar (with the text *break* above it) would count down the *seconds* that were still left.

A stop-button was also implemented. If the subject felt uncomfortable, the experiment could be aborted by pressing the stop-button.

The progress of the experiment was presented on the lower right corner. The number of trials, forces and repeats were shown.

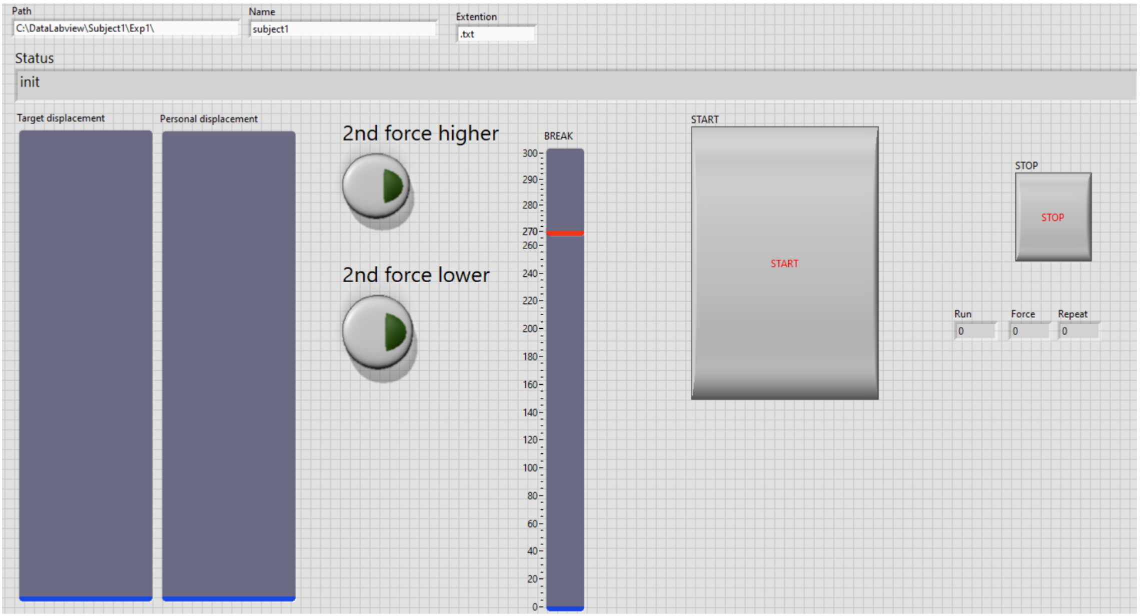

Figure 6.5: A screenshot of the LabView program for experiment 1.

6.1.1. Psychometric curve

In this section, it will be explained how the psychometric curve in the results needs to be interpreted. A psychometric curve models the relationship between the change in force and the forced-choice responses of the subjects.

As can be seen in Figure 6.6, the y-axis shows the response when the test force was stated to be larger than the reference force by the subjects. To the right of the Point of Subjective Equality (PSE) the graphs shows how well the subjects correctly indicated the test force to be larger than the reference force. The positive fest factor indicates that the test force was indeed higher than the reference force.

On the left of the PSE, the graph shows how many the subjects detected the test force as higher than the reference force. However, here the subjects are wrong. The test factor is negative, resulting in a lower test force than reference force. Thus, this percentage represents the incorrect responses of subjects.

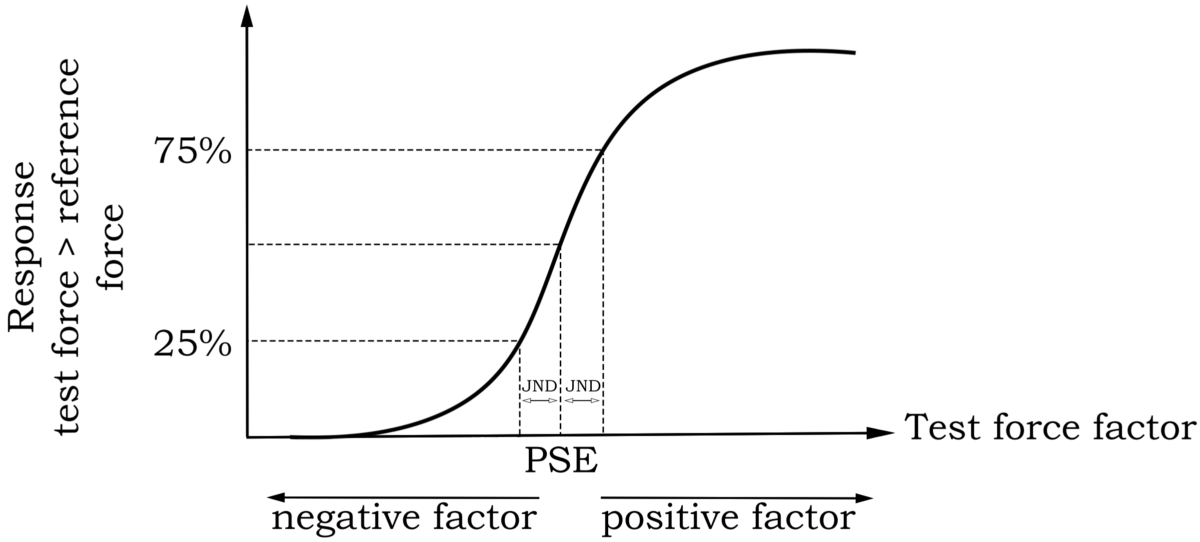

Figure 6.6: Explanation of a psychometric curve, showing the Point of Subjective Equality (PSE), the 25% and 75% success probability and the JND's.

As was mentioned in the Article (Part I), the JND was calculated as provided in Equation 6.1.

$$JND = \frac{(\Delta F(75\%) - \Delta F(25\%))}{2} \tag{6.1}$$

Together with Figure 6.6, Equation 6.1 can be explained. This equation takes the JND of the positive test factor (75%) and the JND of the negative test factor (25%), and divides them by 2 to get the average JND. The 25% success probability in this graph actually shows the result when 75% of the subjects corresponded correctly, because 25% of the subjects indicated that the test force was higher than the reference force (which is incorrect).

The reason why the 25% success probability is subtracted from the 75% success probability is because the test force factor at the 25% is negative. However, we want to add the test force factors and divide them by 2 to receive the JND, and thus the values are subtracted from each other, resulting in a summation.

6.2. Experiment 2: Accuracy of position control

Figure 6.7 shows the screen of the LabView simulation for experiment 2. In this experiment the subject needed to reproduce the target displacement with and without visual feedback.

When the subject received visual feedback, the target displacement bar showed the target and the personal displacement bar shows the movement of the subject. The user needed to reach the target. When visual feedback was switched off, both bars were not presenting the displacements. Hence, the user truly needed to reproduce the displacement on his own sensation.

A stop-button was also integrated in this experiment, such that the experiment could be terminated at all times.

The data in Experiment 2 was sampled with a frequency of $50Hz$. This number was based on how many times a human-being can open and close his/her hand in one second. This was assumed to be 5 times. Therefore, a sampling frequency of $50Hz$ would be sufficient.

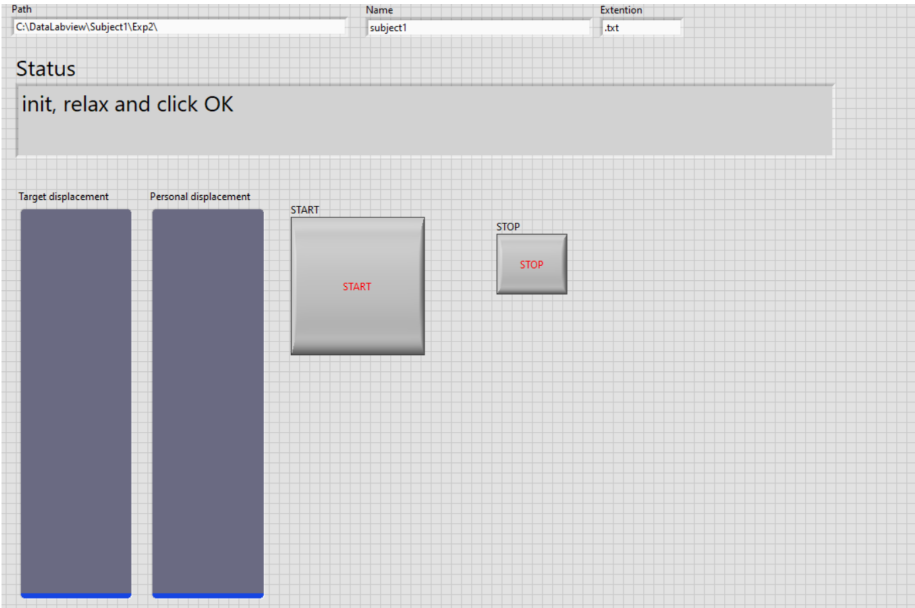

Figure 6.7: A screenshot of the LabView program for experiment 2.

7 Results

The main results were presented in the article (Part I). In this chapter, more elaborate results will be presented.

7.1. Experiment 1: Sensitivity

As was mentioned in Part I (Article), the sensitivity of the shoulder was investigated. In this section, the variability between subjects will be discussed. The design and clamping of the O-rings will also be mentioned and the inaccuracy of the proportional valve will be shown.

7.1.1. Variability between subjects

It was stated in the article that there was a high variability between subjects. This is shown in Figures 7.1, 7.2, 7.3, and 7.4. Figure 7.1 displays the variability for the reference force $2N$. It shows that when comparing this figure to the figures of the other three forces, the variability is higher. This variability seems to be larger for higher positive test force factors than for higher negative test forces.

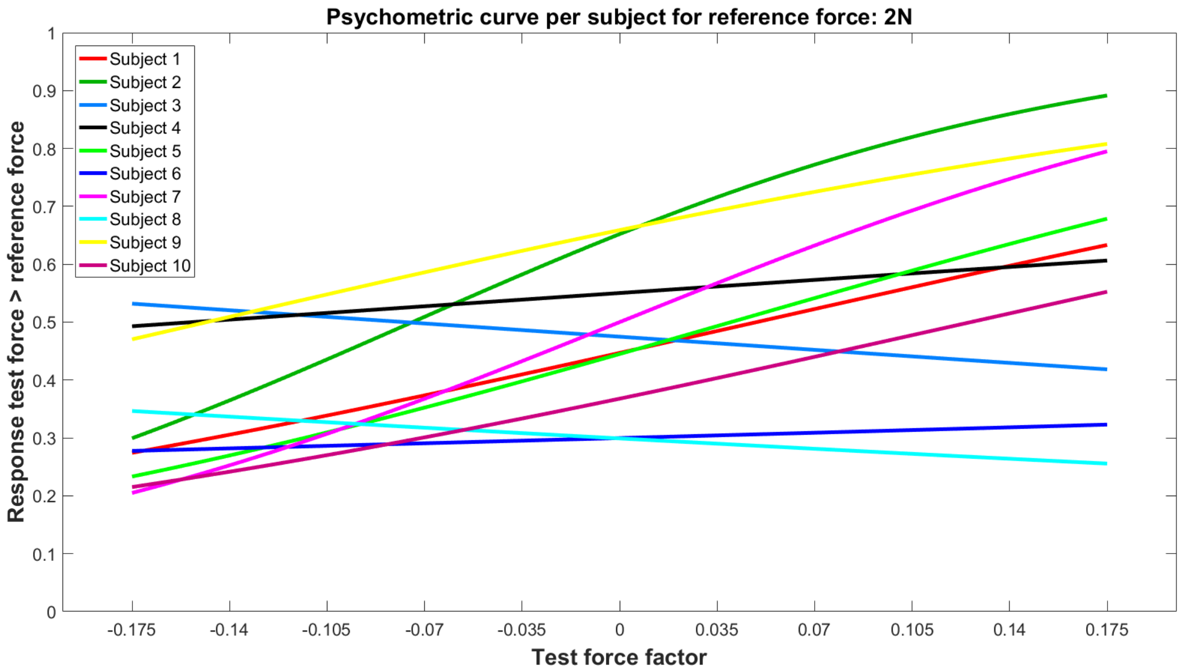

Figure 7.1: Results for the sensitivity experiment for the reference force $2N$ for all the subjects.

The psychometric curves for the reference force $4N$ show less variability (see Figure 7.2) than for the $2N$. The curves of all the subjects in $4N$ have the same shape. For the $6N$ and $8N$ the shapes become even more similar (see Figure 7.3 and 7.4). This suggests that for each subject a larger difference in force was better felt than smaller differences.

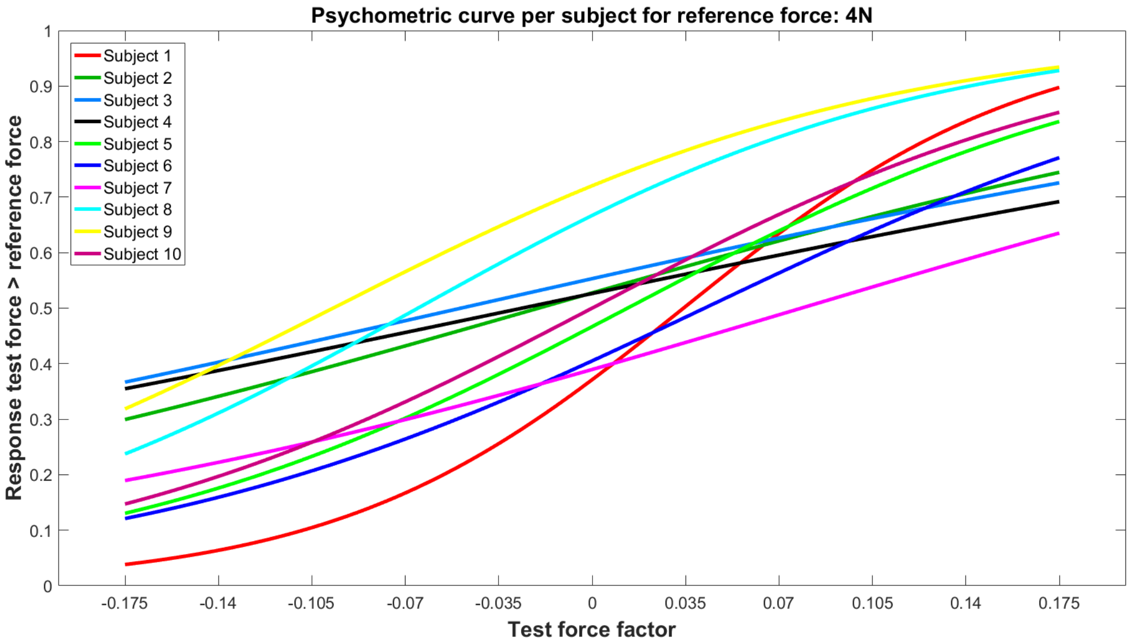

Figure 7.2: Results for the sensitivity experiment for the reference force $4N$ for all the subjects.

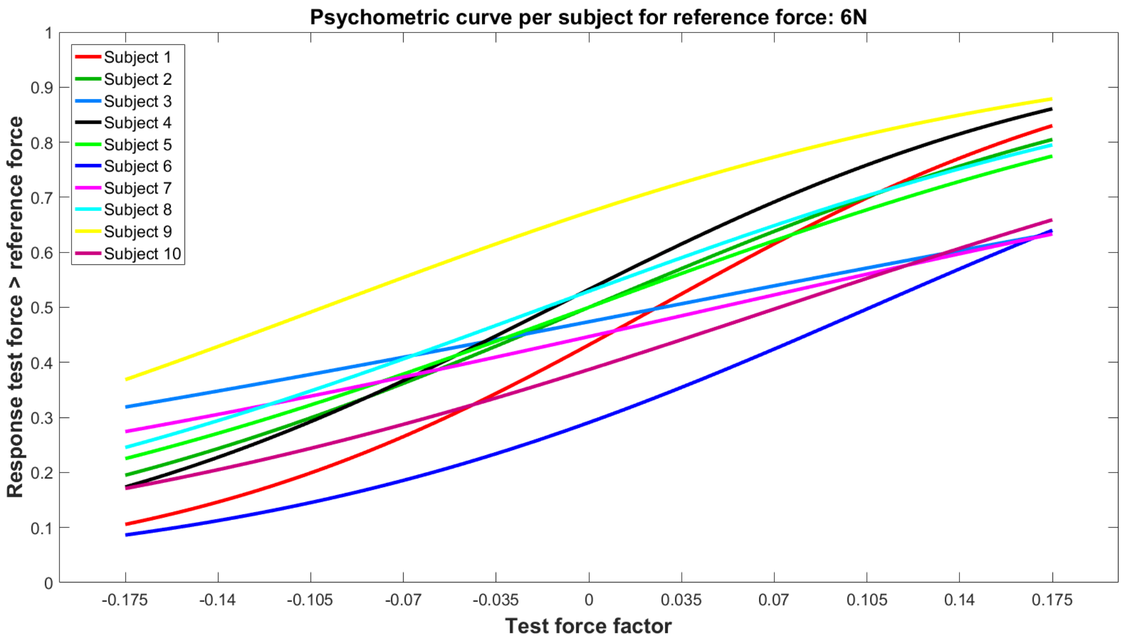

Figure 7.3: Results for the sensitivity experiment for the reference force $6N$ for all the subjects.

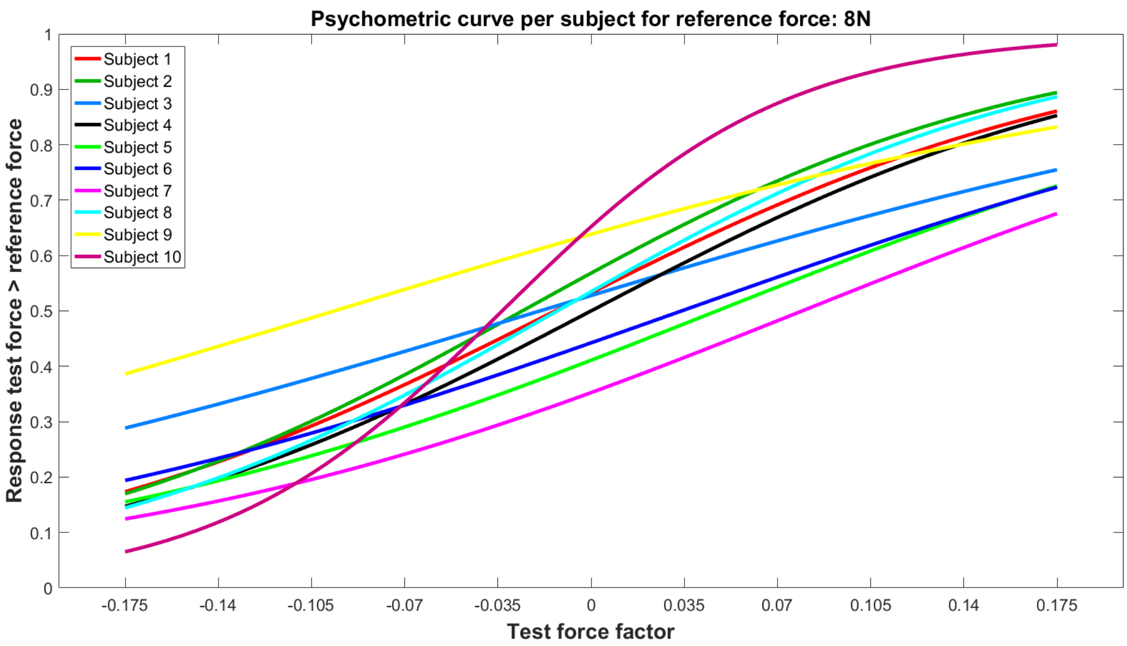

Figure 7.4: Results for the sensitivity experiment for the reference force 8N for all the subjects.

In Part I (Article), it was discussed that subject 3 was removed from the data as he was considered to be an outlier. As can be seen in Figure 7.1 this subject scored very low on all the test force factors for the 2N reference force. The non-fitted results of this subject can be seen in Table 7.1. It shows that he scored a bit higher for some test factor forces than presented in Figure 7.1. However, these higher results were compensated by other bad results, resulting in a bad score in total when the curve was fitted through these data-points.

Test factor force	Score
-0.175	0.75
-0.14	0.25
-0.105	0.25
-0.07	0.50
-0.035	0.75
+0.035	0.75
+0.07	0.50
+0.105	0.25
+0.14	0.25
+0.175	0.5

Table 7.1: The data for subject 3 for the reference force 2N.

As a result of the removal of one subject from the dataset, the psychometric curve for all the fitted data was different, as can be seen in Figure 7.5. It shows that the JND and WF values were improved. Table 7.2 illustrates the difference between the data with all the subjects and the data with one subject removed. The coordinates show the percentages of when the reference force was marked as higher than the test force. It can be seen that when all the subjects were included, only the reference force of 2N did not reach the 75% success probability. Reference force 6N is very close to 75%. When the one subject is removed, all the reference forces, except the 2N reach the 75%, as is also the case for the 25%.

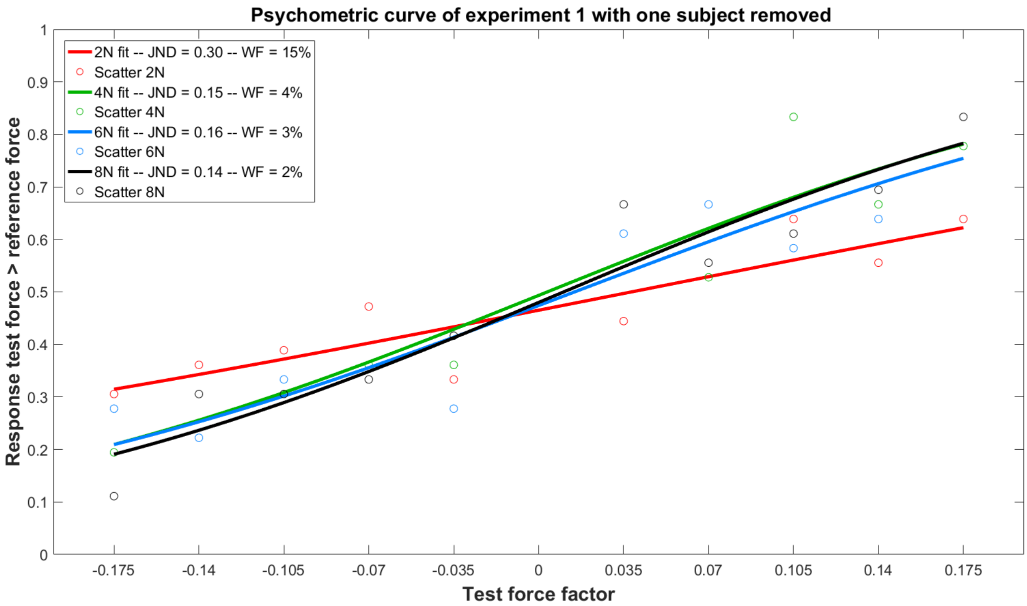

Figure 7.5: The psychometric curve of experiment 1 with one subject removed.

	Reference force(N)	**Test force > reference force at first datapoint(%)**	**Test force > reference force at last datapoint(%)**
All subjects	2	33.57	60.20
	4	22.42	77.58
	6	21.98	74.27
	8	20.01	78.02
One subject removed	2	31.46	62.23
	4	20.95	78.17
	6	20.93	75.44
	8	19.08	78.32

Table 7.2: Comparison of the results when all the subjects were used to fit a psychometric curve on and when one subject was removed. The first and last data-point were compared.

It was also stated that the JND and WF were calculated with the fitted data. They can also be calculated with the data-points that were measured. However, as mentioned before, not all reference forces reached the 75% and/or 25% success probability. When this is the case, the closest value to these percentages was chosen. In Table 7.3 a comparison can be seen between the JND and WF calculated from the fitted data and calculated using the measured data-points. The results in the table show that this difference in calculation only influences the reference force $2N$. This is caused by the fact that the $2N$ reference force did not reach a success probability of 25% and 75%.

Reference force(N)	**JND(N) and WF(%) calculated from the fitted data**	**JND(N) and WF(%) calculated with the measured data-points**
2	0.3507 - 17.54	0.1750 - 8.75
4	0.1548 - 3.87	0.1547 - 3.87
6	0.1652 - 2.75	0.1624 - 2.71
8	0.1450 - 1.81	0.1452 - 1.81

Table 7.3: Comparing the JND(N) and WF(%) from the fitted data and when the first and last data-points were taken.

7.1.2. O-ring

As was mentioned in the article (Part I) the O-rings caused friction inside the cylinder. There are two O-rings inside the cylinder as was explained in Chapter 5.3.1. The friction force for both O-rings will be calculated. The friction force of the O-ring can be calculated as in Equation 7.1 [25].

$$F_f = f_c \times L + f_h \times A \tag{7.1}$$

F_F = O-ring friction force (N)
f_c = friction factor due to O-ring compression (N/mm)
L = length of seal rubbing surface = $\pi \times D_c$
f_h = friction factor due to fluid pressure (N/mm^2)
A = projected area of seal = $\frac{\pi}{4} \times (D_c)^2 - (D_p)^2$
D_c = cylinder bore diameter (mm)
D_p = piston groove diameter (mm)

The values of the variables were determined from graphs provided by Plettenburg [25].

If all variables are substituted by the sub-formulas, the O-ring friction force is calculated with the formula provided in Equation 7.2.

$$F_f = f_c \times (\pi \times D_c) + f_h \times (\frac{\pi}{4} \times (D_c)^2 - (D_p)^2) \tag{7.2}$$

When all the values are entered in the formula, it results in the O-ring friction force(N), see Equation 7.5. The maximum friction factor due to fluid pressure is taken. This means that a situation is calculated when the pressure is maximized.

$$F_f = 0.12 \times \pi \times 6 + 0.07 \times \frac{\pi}{4} \times (6^2 - 4.2^2) \tag{7.3}$$

$$F_f \approx 2.262 + 1.009 \tag{7.4}$$

$$F_f \approx 3.270 \tag{7.5}$$

The first O-ring causes a friction force of $3.270N$. The $2.262N$ is the friction force when the cylinder is not pressurized. This friction force is increased with $1.009N$ when maximally pressurized. However, there is also a second O-ring. This one was was placed to seal the air chamber completely. This O-ring also has a friction force that can be seen in Equation 7.8.

$$F_f = 0.12 \times \pi \times 4.79 + 0.07 \times \frac{\pi}{4} \times (4.79^2 - 3^2) \tag{7.6}$$

$$F_f \approx 1.806 + 0.767 \tag{7.7}$$

$$F_f \approx 2.573 \tag{7.8}$$

The second O-ring results in a friction force of $2.573N$.

In total, the friction force when maximally pressurized is $5.843N$. When no pressure is applied to the system the total O-ring friction force is $4.068N$.

The variable f_c was the friction factor due to O-ring compression. The higher the compression, the higher this factor, and thus the higher the friction. In the prototype, it was chosen to clamp the O-ring with a percentage of 10%. However, stated by Plettenburg [25], the compression could be around 8% ±2%.

A compression of 8% will results in an f_c of 0.1. When the compression even decreases more until 6% the f_c is 0.08. This would result in a friction force for the first O-ring of $2.517N$ ($1.508N$ without pressure, $1.009N$ addition when pressurized) and a friction force for the second O-ring of $1.861N$ ($1.204N$ without pressure, $0.657N$ addition when pressurized). This results in a total friction force of $4.378N$. The total force decreases with almost $1.5N$ when pressurized. The total O-ring friction when no pressure is applied to the system is now $2.712N$, which is a decrease of approximately $1.3N$.

It is therefore strongly recommended to decrease the O-ring compression in order to reduce the friction force. However, there is a trade-off between O-ring friction and leakage. The lower the O-ring compression (the lower the O-ring friction), but the higher chance on leakage. Plettenburg [25] mentions that with zero O-ring squeeze could result in zero leakage. However, O-ring clamping becomes more important at lower pressures, which is the case in this design. Therefore, the clamping could probably not be decreased to 0%.

7.1.3. Static friction for 2N and 8N

As was explained in Part I (Article), high static frictions are acting on the cylinder. These static frictions could explain why the results for the 2N reference force were worse than for the 8N reference force. These static frictions were calculated with the O-ring friction, as was done in the paragraph 7.1.2. In this paragraph, the static friction for the reference forces 2N and 8N will be calculated and compared. Also, the friction forces will be calculated for both reference forces when O-ring clamping is decreased to 6%.

Static friction 2N

First, the maximum pressure will be calculated as in Equation 7.17 and 7.10.

$$\rho = \frac{F}{A} \times 10 \tag{7.9}$$

$$\rho = \frac{2}{\frac{\pi}{4} \times 6^2 - \frac{\pi}{4} \times 3^2} \times 10 \approx 0.94 \tag{7.10}$$

A force of 2N results in a pressure of approximately 0.94bar. This value will determine the friction factor due to fluid pressure. This factor is read from a graph provided by Plettenburg [25].

The Equations 7.1 and 7.2 will be used in this paragraph to calculate the static friction of the two O-rings.

$$F_f = 0.12 \times \pi \times 6 + 0.04 \times \frac{\pi}{4} \times (6^2 - 4.2^2) \tag{7.11}$$

$$F_f \approx 2.262 + 0.577 \tag{7.12}$$

$$F_f \approx 2.839 \tag{7.13}$$

The first O-ring causes a friction force of 2.839N. The static friction caused by the second O-ring will be calculated in Equations 7.14, 7.15, and 7.16.

$$F_f = 0.12 \times \pi \times 4.79 + 0.04 \times \frac{\pi}{4} \times (4.79^2 - 3^2) \tag{7.14}$$

$$F_f \approx 1.806 + 0.438 \tag{7.15}$$

$$F_f \approx 2.244 \tag{7.16}$$

The second O-ring causes a static friction of 2.244N. The total static friction force for the reference force 2N is then: $F_f = 2.839 + 2.244 = 5.083N$. This is a approximately 2.5 times the reference force (250%).

When the O-ring clamping is reduced to 6%, it will decrease the friction. It will result in a friction force of 2.085N for the first O-ring (2.085N without pressure, 0.577N addition with pressure). The second O-ring causes a friction force of 1.642N (1.204N without pressure, 0.438N addition with pressure). This results in a total friction force of 3.727N. This is approximately 186% of the reference force. This value is still quite high, however is a quite large decrease (from 250% to 186%).

Static friction $8N$
First, the maximum pressure will be calculated as in Equation 7.18.

$$\rho = \frac{F}{A} \times 10 \tag{7.17}$$

$$\rho = \frac{8}{\frac{\pi}{4} \times 6^2 - \frac{\pi}{4} \times 3^2} \times 10 \approx 3.77 \tag{7.18}$$

A force of $8N$ results in a pressure of approximately $3.77bar$. This results in a friction factor due to fluid pressure of $0.06N/mm^2$. The results of the calculations for the static friction of both O-rings can be seen in Equations 7.21 and 7.24.

$$F_f = 0.12 \times \pi \times 6 + 0.06 \times \frac{\pi}{4} \times (6^2 - 4.2^2) \tag{7.19}$$

$$F_f \approx 2.262 + 0.865 \tag{7.20}$$

$$F_f \approx 3.127 \tag{7.21}$$

The first O-ring causes a friction force of $3.127N$.

$$F_f = 0.12 \times \pi \times 4.79 + 0.06 \times \frac{\pi}{4} \times (4.79^2 - 3^2) \tag{7.22}$$

$$F_f \approx 1.806 + 0.657 \tag{7.23}$$

$$F_f \approx 2.463 \tag{7.24}$$

The second O-ring causes a friction force of $2.463N$. This results in a total friction force of $5.590N$ when the reference force of $8N$ needs to be applied to the system. This is 62% of the reference force.

When the O-ring clamping is reduced to 6%, it will decrease the friction. It will result in a friction force of $2.373N$ for the first O-ring ($1.508N$ without pressure, $0.865N$ addition with pressure). The second O-ring causes a friction force of $1.861N$ ($1.204N$ without pressure, $0.657N$ addition with pressure). This results in a total friction force of $4.234N$. This is approximately 53% of the reference force. This is a decline of approximately 11%.

Table 7.4 is provided to compare the results between the friction of both reference forces. This shows that the friction for both reference forces do not differ a large amount. However, this causes the friction force to be relatively larger for the lower reference force ($2N$) than for the higher reference force ($8N$). It could explain why the $2N$ sensitivity results are less accurate than the sensitivity for the $8N$.

	Reference force: 2N	**Reference force: 8N**	**2N with 6% clamping**	**8N with 6% clamping**
Pressure (bar)	0.94	3.77	0.94	3.77
Friction (N)	5.083	5.590	3.727	4.234
Percentage of reference force (%)	250	62	186	53

Table 7.4: Results of calculations of the O-ring friction for the two reference forces $2N$ and $8N$.

7.1.4. Inaccuracy valve

As was mentioned in the Article (Part I), the valve is slightly inaccurate. The output voltage does not fully comply with the actual measured voltage of the valve. This suggests that the pressure is not consistent. To show how large this inaccuracy is, some pressure values were compared. Table 7.5 shows the results of different trials from one subject to present the inaccuracy of the valve. It shows that the inaccuracy is larger for the $2N$ reference force than for the $8N$ reference force, namely an average relative error of 0.15% for the $2N$ reference force, and on average almost no error for the $8N$ reference force. This shows that this inaccuracy has a larger effect on the lower forces than on the higher forces. However, an error of 0.15% is very small and will probably not affect the results. It also needs to be stated that these relative error values are determined based on these 4 trials. To fully capture the inaccuracy of the valve, all data-points should be analysed.

		Reference OUT	Actual ref. OUT	Difference ref. and act.(%)	Test OUT	Actual test OUT	Difference test and act.(%)	Difference ref. and test OUT(%)	Difference act. ref. and act. test OUT(%)
1	$\rho(bar)$	0.094	0.095	1.1	0.0910	0.0914	0.40	-3.50	-3.61
	F(N)	2.000	2.010	0.50	1.930	1.938	0.41	-3.50	-3.61
2	$\rho(bar)$	0.094	0.095	1.1	0.0778	0.078	0.26	-17.5	-17.7
	F(N)	2.000	2.010	0.5	1.650	1.654	0.24	-17.5	-17.7
3	$\rho(bar)$	0.377	0.377	0.0	0.3641	0.3642	0.03	-3.5	-3.5
	F(N)	8.001	8.004	0.04	7.721	7.723	0.03	-3.50	-3.51
4	$\rho(bar)$	0.377	0.378	0.27	0.311	0.312	0.32	-17.51	-17.46
	F(N)	8.001	8.007	0.07	6.600	6.611	0.17	-17.51	-17.43

Table 7.5: Some of the output and actual data values of the pressure valve. It shows 4 trials. 1. Test factor force -3.5% for the reference force $2N$. 2. Test factor force -17.5% for the reference force $2N$. 3. Test factor force -3.5% for the reference force $8N$. 4. Test factor force -17.5% for the reference force $8N$. This table compares the inaccuracies of the valve.

7.2. Experiment 2: Accuracy of position control

In this section, more elaborate results of experiment 2 will be shown. First, the precise values for the measurements (ADE, RDE and DV) will be presented. After that, the velocity values for the $5mm$ and $20mm$ displacement per subject are presented.

7.2.1. ADE, RDE and DV

In the Article (Part I), only the graphs for the second experiment were provided and no data values from the results were presented. In Table 7.6 the results are presented for all the three measurements and all the three displacements for both the visual and blind experiment. For the ADE and RDE, also the Standard Deviation (SD) is provided to show in what range the individual subject values scatter. It shows the variability between subjects.

Table 7.6 show that the Absolute Displacement Error (ADE) is comparable for all the three displacements for both visual and blind. It shows that absolutely the $10mm$ was performed best for the visual production. However, relatively the $20mm$ scored better. There is less variability for the larger displacement than for the lower displacement. This can be seen from the SD-values, which provide information about the dispersion of the data-points.

The Displacement Variability (DV) is the highest for the largest displacement, and also higher for the blind reproduction than for the visual production.

	ADE(mm)				RDE(%)				DV(mm)	
	Visual	SD	Blind	SD	Visual	SD	Blind	SD	Visual	Blind
5mm	0.73	0.59	2.49	1.16	14.53	11.88	49.71	23.22	0.38	0.21
10mm	0.58	0.32	2.79	1.08	5.79	3.17	27.92	10.75	0.33	0.25
20mm	0.63	0.48	2.62	1.04	2.87	2.32	13.85	5.59	0.48	0.68

Table 7.6: Results for all the three measurements (ADE, RDE, and DV) for both the visual production and blind reproduction. The SD for the ADE and RDE results is also provided, to show variability. These results are provided for all the three displacements ($5mm$, $10mm$, and $20mm$).

To investigate how well this data-set of ten participants represent the total target group, the Standard Error (SE) is calculated. This will provide information on how precise and accurate the measurement is. The SE is calculated for each measurement and for each displacement. The results can be seen in Table 7.7. With these SE values, we can calculate the 95% confidence interval [22]. The lower limit of this interval is calculated as provided in Equation 7.25 and the upper limit is calculated as in Equation 7.26. The mean of the data-sets can be found in Table 7.6.

$$Upperlimit = mean + (SE \times 1.96) \tag{7.25}$$

$$Lowerlimit = mean - (SE \times 1.96) \tag{7.26}$$

Combining Equation 7.25 and 7.26 with the results presented in Table 7.7, the 95% confidence interval can be calculated. These intervals are presented in Table 7.8. These intervals show that the values could still differ quite much. The width of the intervals is the largest for the smallest displacement ($5mm$), especially the blind reproduction intervals. It is also presented that for each measurement and each displacement, the blind reproduction trials have the largest intervals, suggesting that the results of the total population could differ quite much. To create more reliable results, more participants should conduct the experiments.

	ADE(mm)		RDE(%)		DV(mm)	
	Visual SE	**Blind SE**	**Visual SE**	**Blind SE**	**Visual SE**	**Blind SE**
5mm	0.19	0.37	3.76	7.34	0.08	0.05
10mm	0.10	0.34	1.01	3.40	0.07	0.08
10mm	0.15	0.33	0.73	1.88	0.25	0.41

Table 7.7: Results of the Standard Error (SE) for all the three measurements (ADE, RDE, and DV) for both the visual production and blind reproduction. The STD for the ADE and RDE results is also provided, to show how correct these measurements were. These results are provided for all the three displacements ($5mm$, $10mm$, and $20mm$).

	ADE(mm)		RDE(%)		DV(mm)	
	Visual	**Blind**	**Visual**	**Blind**	**Visual**	**Blind**
5mm	[0.36;1.10]	[1.76;3.22]	[7.16;21.90]	[35.32;64.10]	[0.22;0.54]	[0.11;0.31]
10mm	[0.38;0.78]	[2.12;3.46]	[3.81;7.95]	[21.26;34.58]	[0.19;0.47]	[0.09;0.41]
20mm	[0.34;0.92]	[1.97;3.27]	[1.44;4.30]	[10.17;17.53]	[0.00;0.97]	[0.00;1.48]

Table 7.8: The 95% confidene interval for all the three measurements (ADE, RDE, and DV). The intervals are provided for each of the three displacements ($5mm$, $10mm$, and $20mm$).

7.2.2. Velocity per subject for 5mm and 20mm displacement

As was mentioned in the Article (Part I), there was a difference in speed(mm/s) for the $5mm$ displacement and the $20mm$ displacement, see Table 7.9.

Subject	Speed(mm/s) for the 5mm displacement	Speed(mm/s) for the 20mm displacement
1	2.79	16.89
2	1.72	8.44
3	3.16	18.55
4	8.45	19.58
5	3.86	12.85
6	1.31	5.94
7	3.92	4.76
8	7.27	19.48
9	2.95	7.30
10	2.04	11.31
Average	3.75	11.91

Table 7.9: Results for the velocity for the $5mm$ displacement and $20mm$ displacement for all the subjects.

This difference in speed could explain why stick-and-slip behaviour was more apparent for the smallest displacement. A low velocity could induce sticking behaviour. It was stated in the Article that the average speed was $3.75 mm/s$ for $5 mm$ displacement, and $11.91 mm/s$ for $20 mm$ displacement. The individual values per subject are provided in Table 7.9. It shows that there is variability between the subjects for both displacements. However, every subject had a higher velocity for the larger displacement.

8 Biggest challenges

During the design process, some problems and challenges arose. The two main challenges for this design were the elasticity of the skin and the curvature of the shoulder. At first, the base was a rigid structure in which the cylinder was fixed, as can be seen in Figure 8.1. The problem that arose with this first version of the base was that when the shoulder moved back (from maximal protraction) the piston did not slide back inside the cylinder. This problem is illustrated in Figure 8.3. In this version, a protrusion is also added, because the curvature of the shoulder was too large for the system to overcome because of its rigid nature.

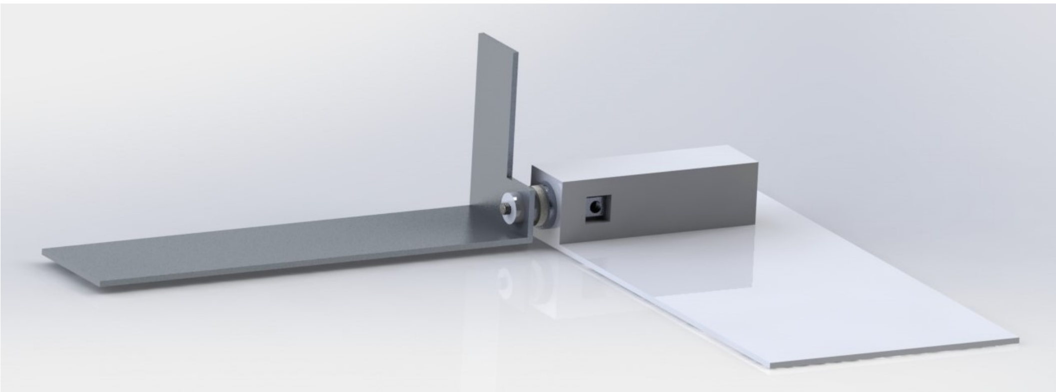

Figure 8.1: Base version 1 showing that the cylinder is fixed on a rigid structure.

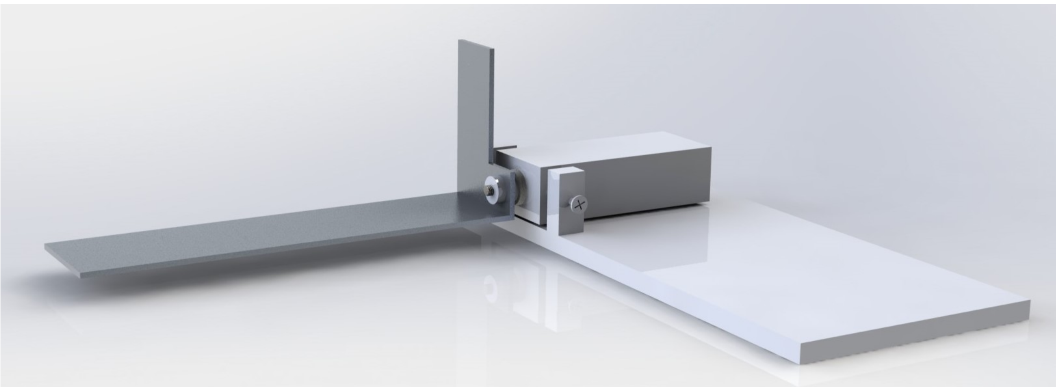

Figure 8.2: Base version 2 showing that the cylinder is fixed inside a block, but is able to to rotate because of the hinge joint.

As can be seen in Figure 8.3, the force of the shoulder is not in the linear direction of the piston. Therefore, the piston will try to go in sideways. This causes a high resistance force at the inner surface of the cylinder. This inner friction was apparently higher than the skin resistance (see Figure 8.3). This was concluded from pilot experiments. For all pilot subjects, the piston did not move and the skin stretched. This problem caused the system to work inappropriate, so a redesign was made.

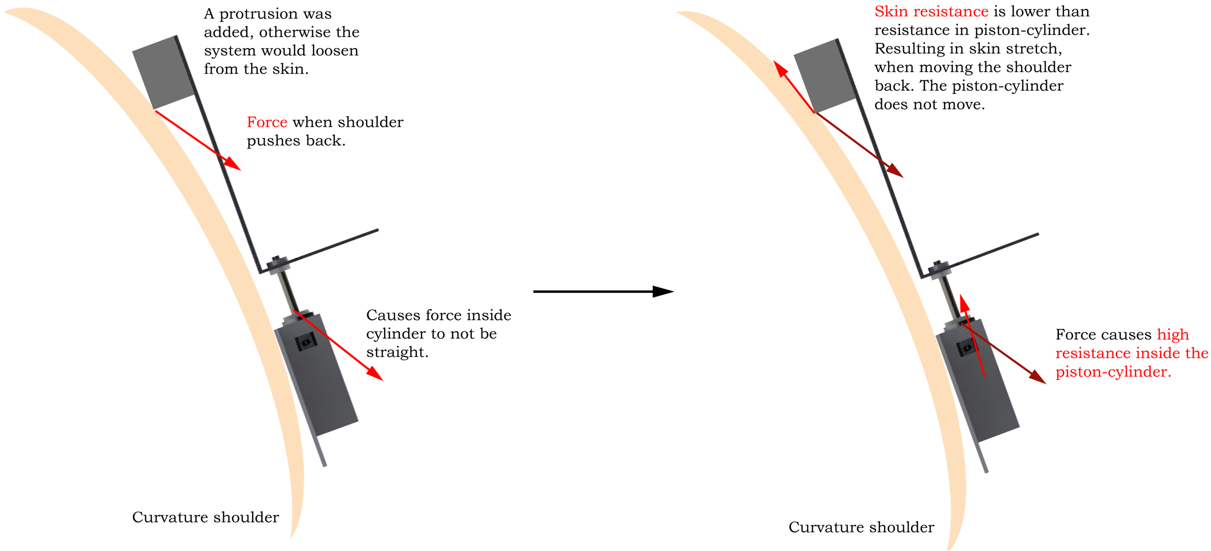

Figure 8.3: A schematic drawing of the forces that act on the system for the first version of the base.

This redesign can be seen in Figure 8.2. When the shoulder protracts, the hinge joint causes the total system to rotate. When the shoulder is now moved retracted, the pushing force is in the direction of the piston-cylinder, see Figure 8.4. This design showed to be success full. It will function appropriately when the curvature of the subject's shoulder is different from another subject.

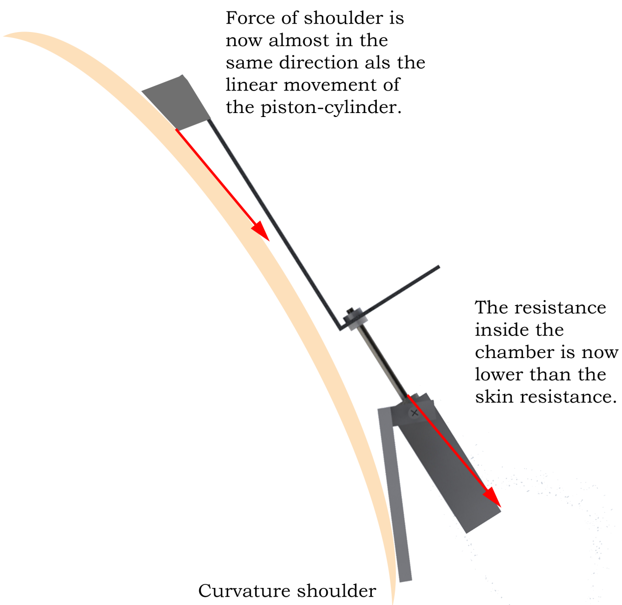

Figure 8.4: A schematic drawing of the forces that act on the system for the second version of the base.

9 Recommendations

The main recommendations were already mentioned in the Article (Part I). However, some more recommendations for future research could be made.

It was mentioned that the average maximum shoulder displacement for elevation and protraction was 35mm. The highest target displacement in the experiment was 20mm. However, some participants mentioned that this 20mm displacement already felt as their maximum. This shows the variability between subjects. It is therefore suggested design a system with an adjustable maximum displacement, or to customize each design in the future.

As an AD-converter, a quite large National Instruments was implemented. This converter was too large to place on the back of the user. Therefore, in the future it is recommended to design a Printed Circuit Board (PCB). This PCB can be specially designed for this system, such that no unnecessary additional functionalities are implemented. This will probably radically decrease the size.

The laser sensor used in this design was quite large. Possibly, this could be designed much smaller. Perhaps it is possible to integrate a laser inside the base of the system. It would thus be suggested to develop these ideas more in the future. This will decrease the total size of the system as perhaps not such a high plate is needed anymore.

Three concepts were developed during this thesis. One concept was very promising, but was deemed to difficult for a thesis project. This deign was the flexible active skin with the miniature PAMs integrated. Nevertheless, this design still sounds very promising, and it is therefore recommended to further develop this idea.

In this design, it was assumed that there was a linear relation between the displacement of the prosthesis (opening/closing) and the displacement of the shoulder. However, it could be interesting to consider a non-linear relation. This could result in easier control for precise movements. When the hand needs to be closed almost maximally, 1 mm at the shoulder could maybe also mean 1mm at the prosthesis. This would make control more precise and accurate. However, when the range of the shoulder displacement is still 0-35mm, control will be less precise at the start of closing the hand.

10

SolidWorks

In this Chapter, all the SolidWorks 2D drawings will be presented. In Table 10.1 it is presented which SolidWorks drawings are shown in this Chapter. It is also provided on which page a certain drawing can be found.

Drawing number	Component	Figure number	Page
1	Plate	10.1	72
2	Rod	10.2	73
3	Cylinder	10.3	74
4	Cap cylinder	10.4	75
5	Cap O-ring	10.5	76
6	Piston	10.6	77
7	Assembly part 1	10.7	78
8	Assembly part 2	10.8	79
9	Total assembly (part 1+2)	10.9	80
10	Base version 1	10.10	81
11	Base version 2 plate	10.11	82
12	Base version 2 block	10.12	83
13	Assembly base version 2	10.13	84
14	Assembly with base version 1	10.14	85
15	Assembly with base version 2	10.15	86

Table 10.1: Overview of all the SolidWorks drawings of the components. This Table shows where all the drawings can be found in this Chapter.

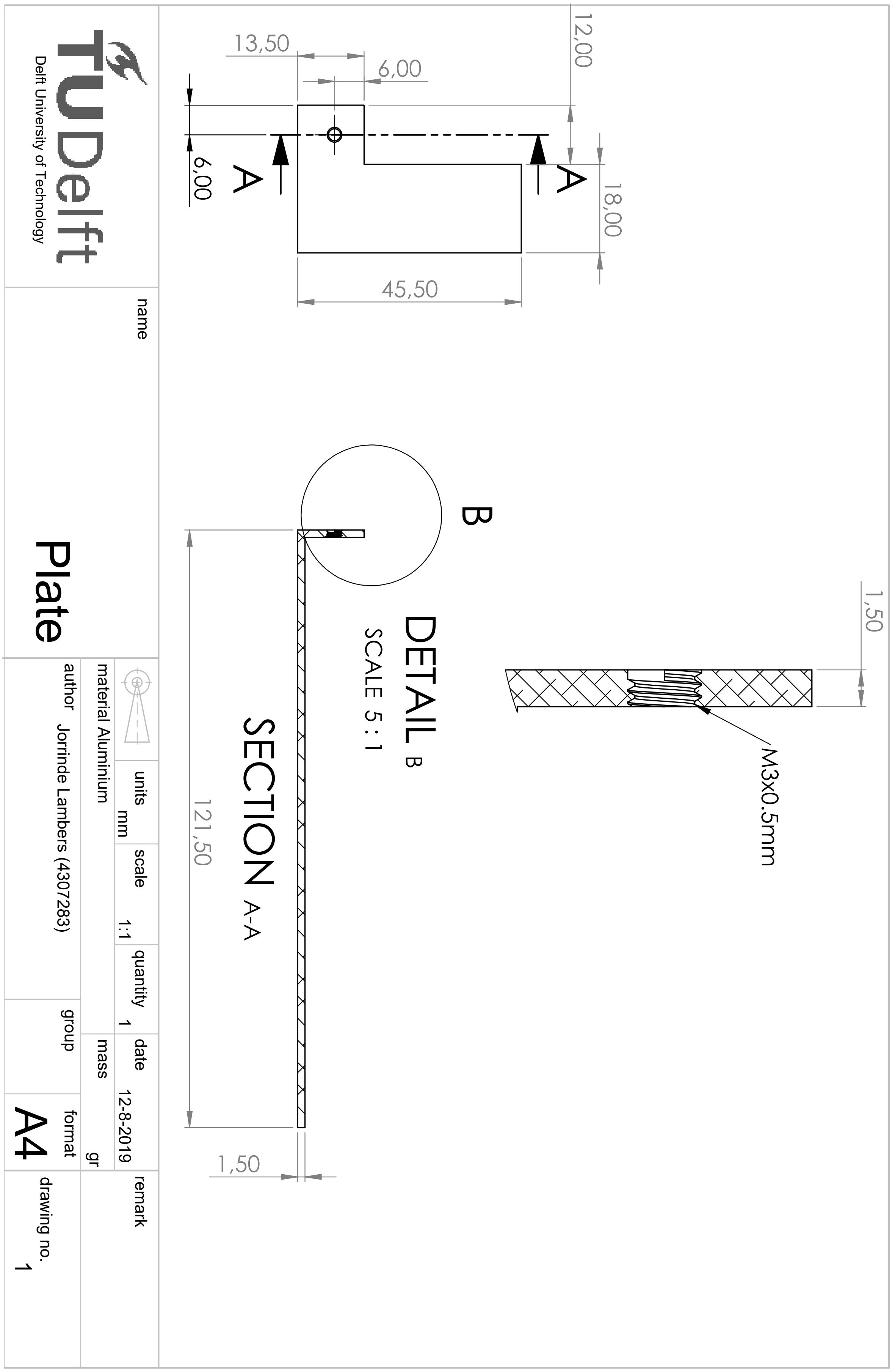

Figure 10.1: SolidWorks drawing of component number 1: Plate.

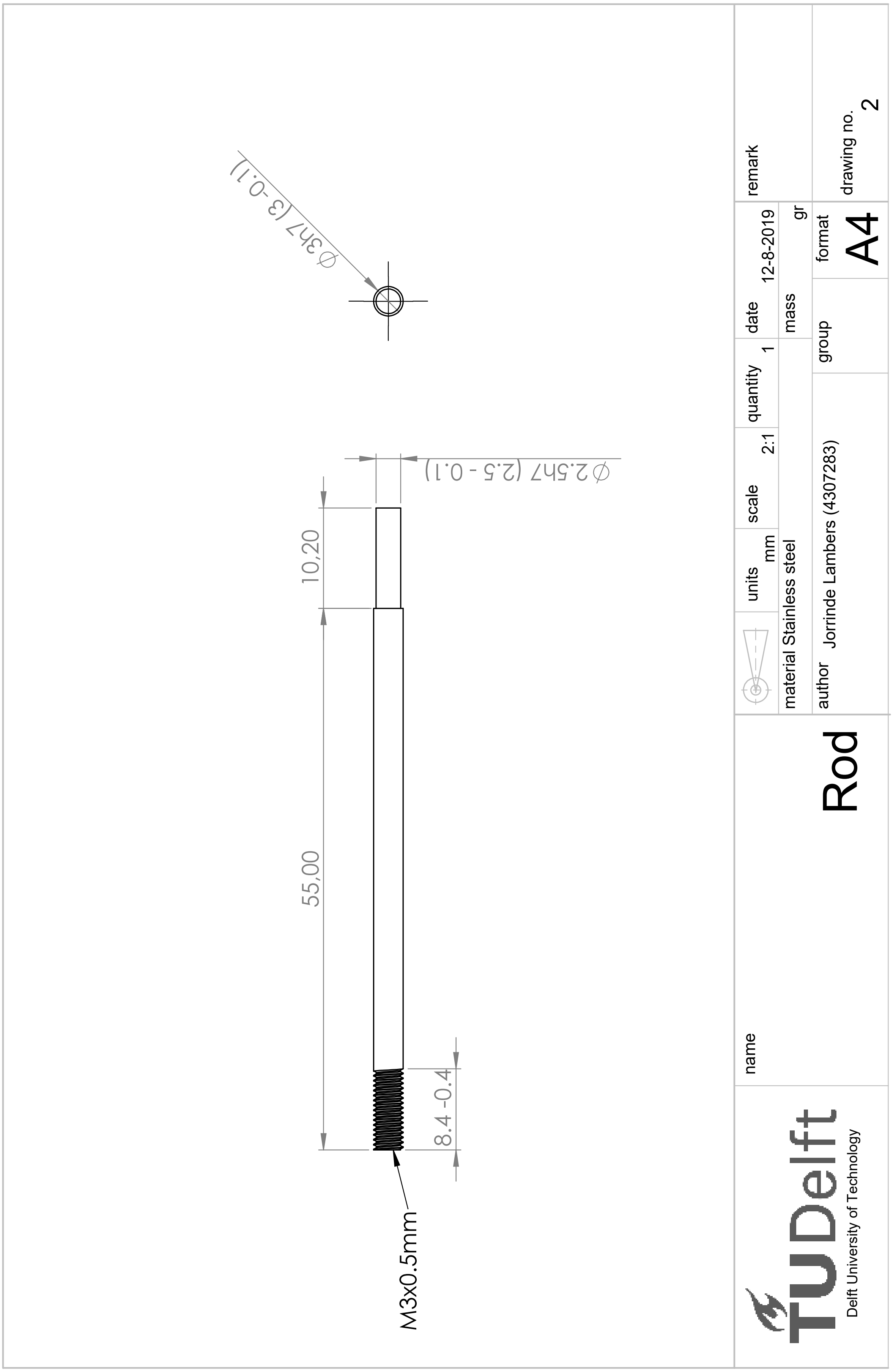

Figure 10.2: SolidWorks drawing of component number 2: Rod.

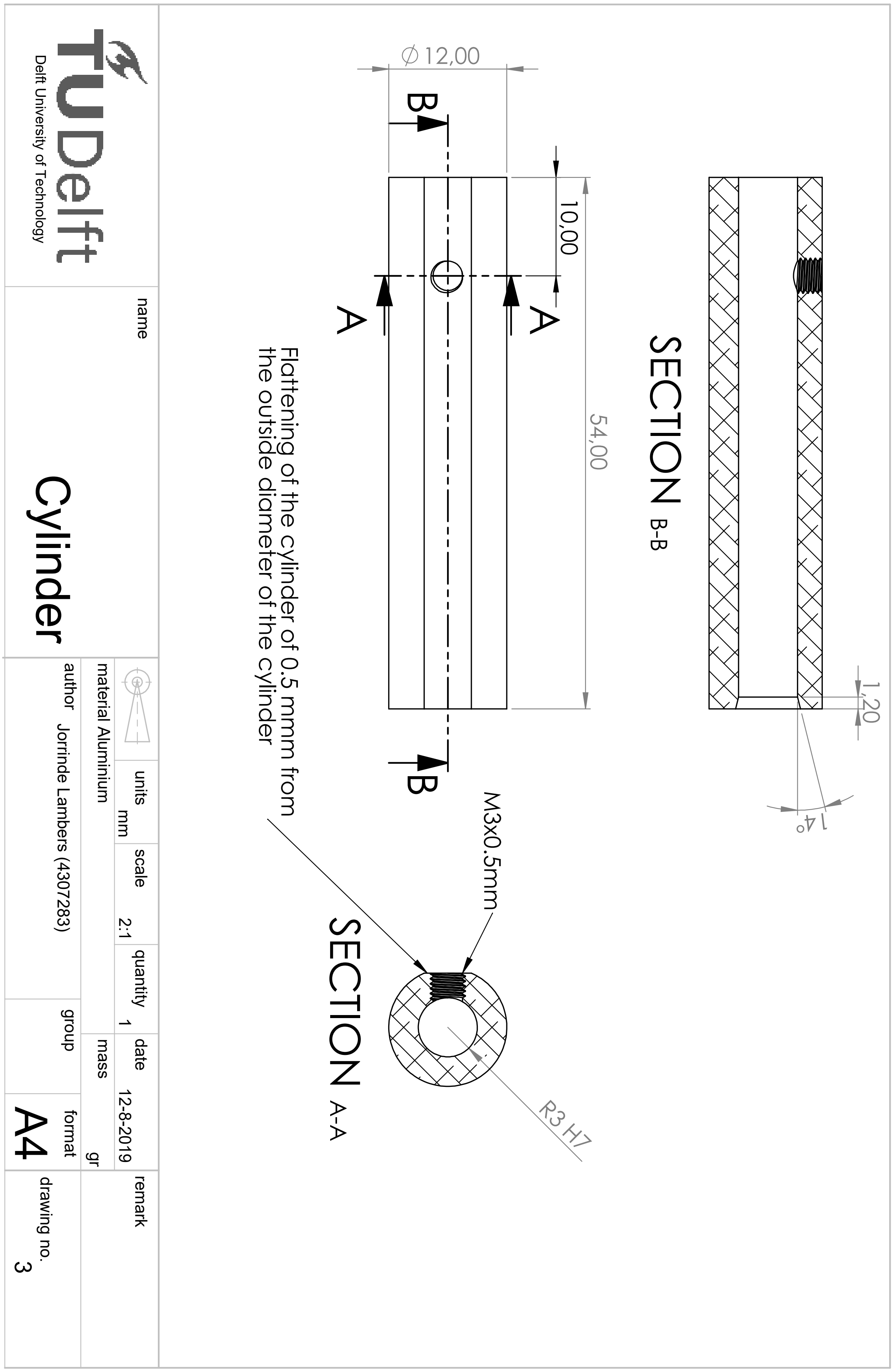

Figure 10.3: SolidWorks drawing of component number 3: Cylinder.

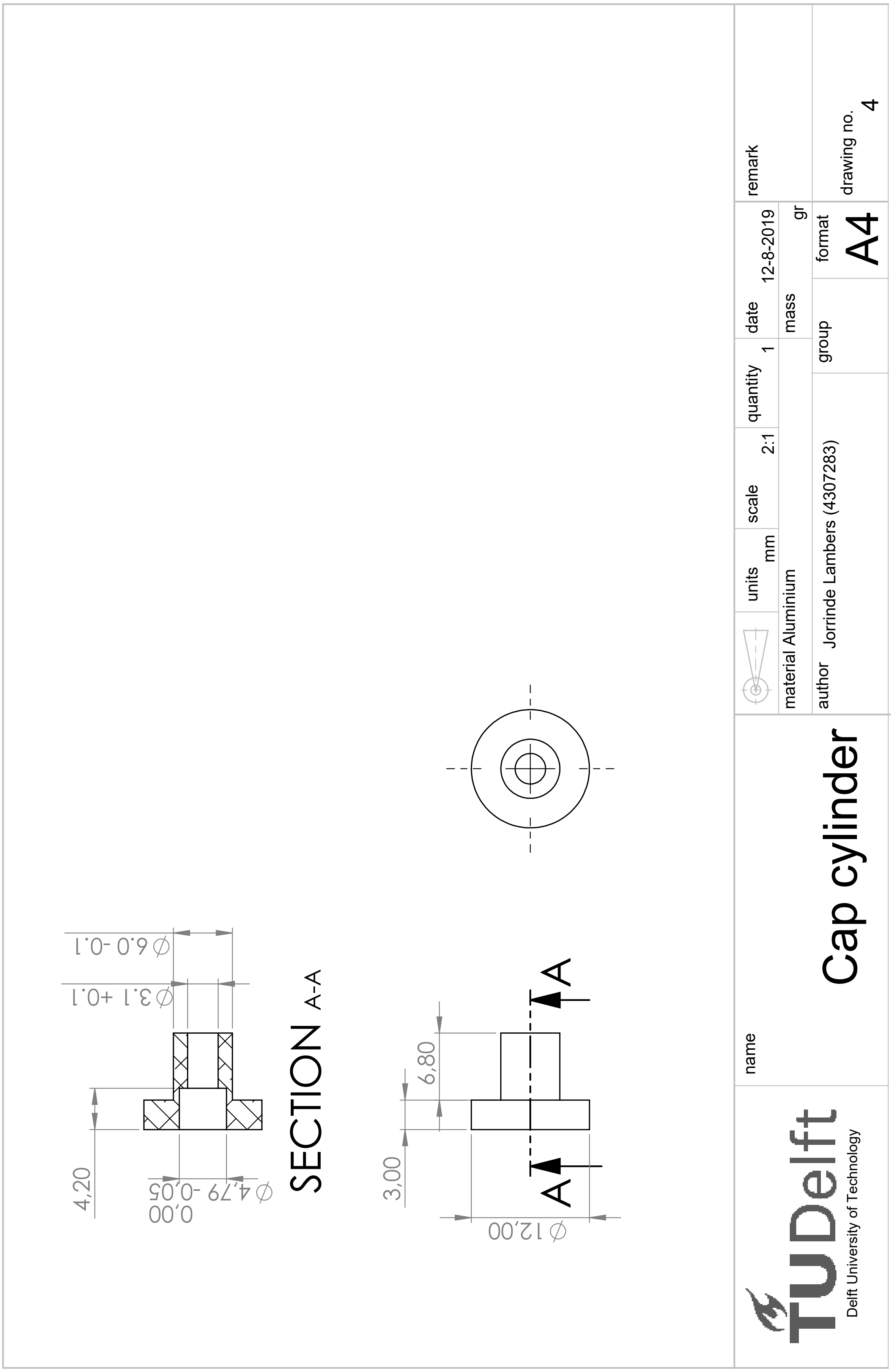

Figure 10.4: SolidWorks drawing of component number 4: Cap cylinder.

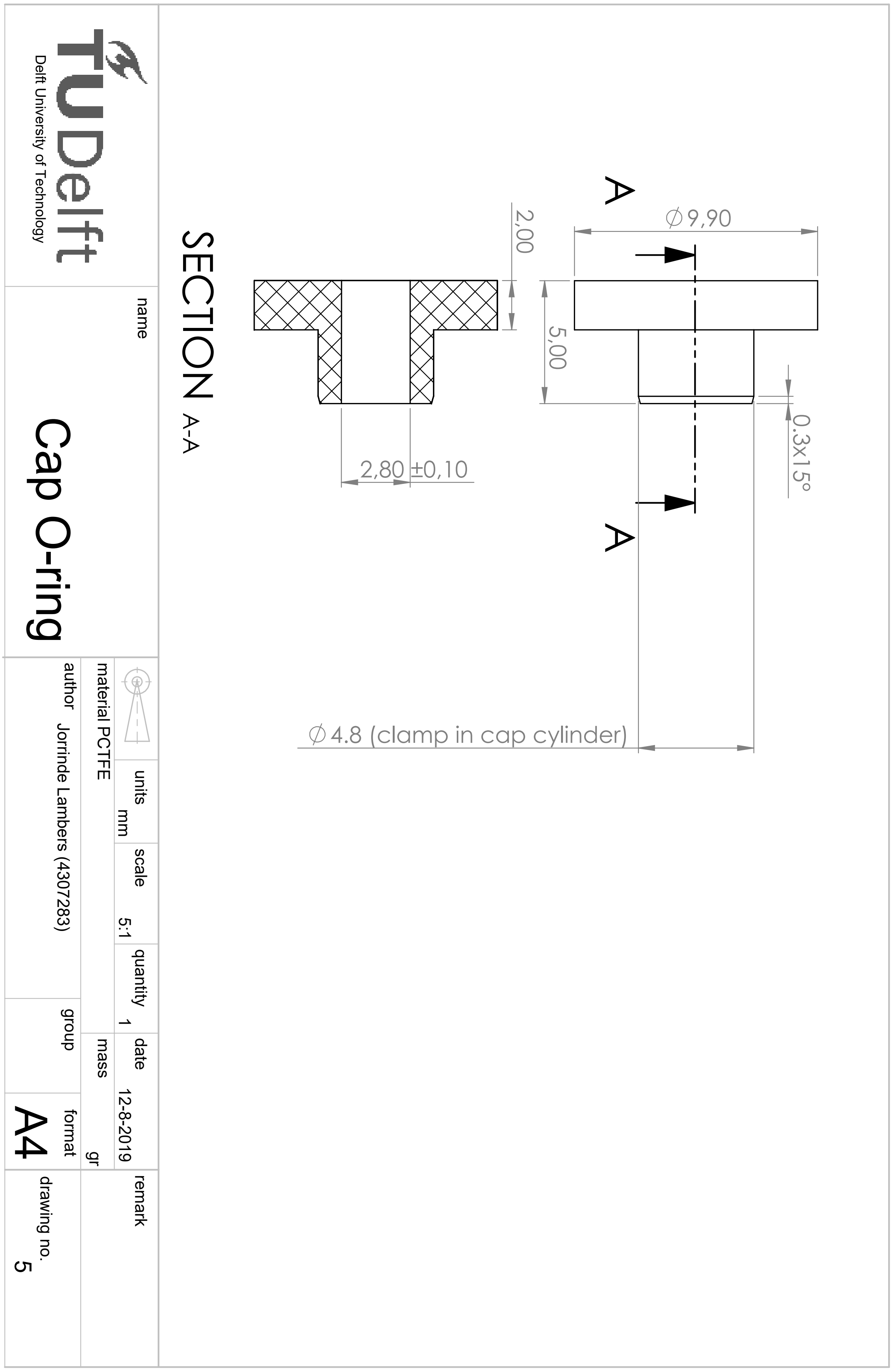

Figure 10.5: SolidWorks drawing of component number 5: Cap O-ring.

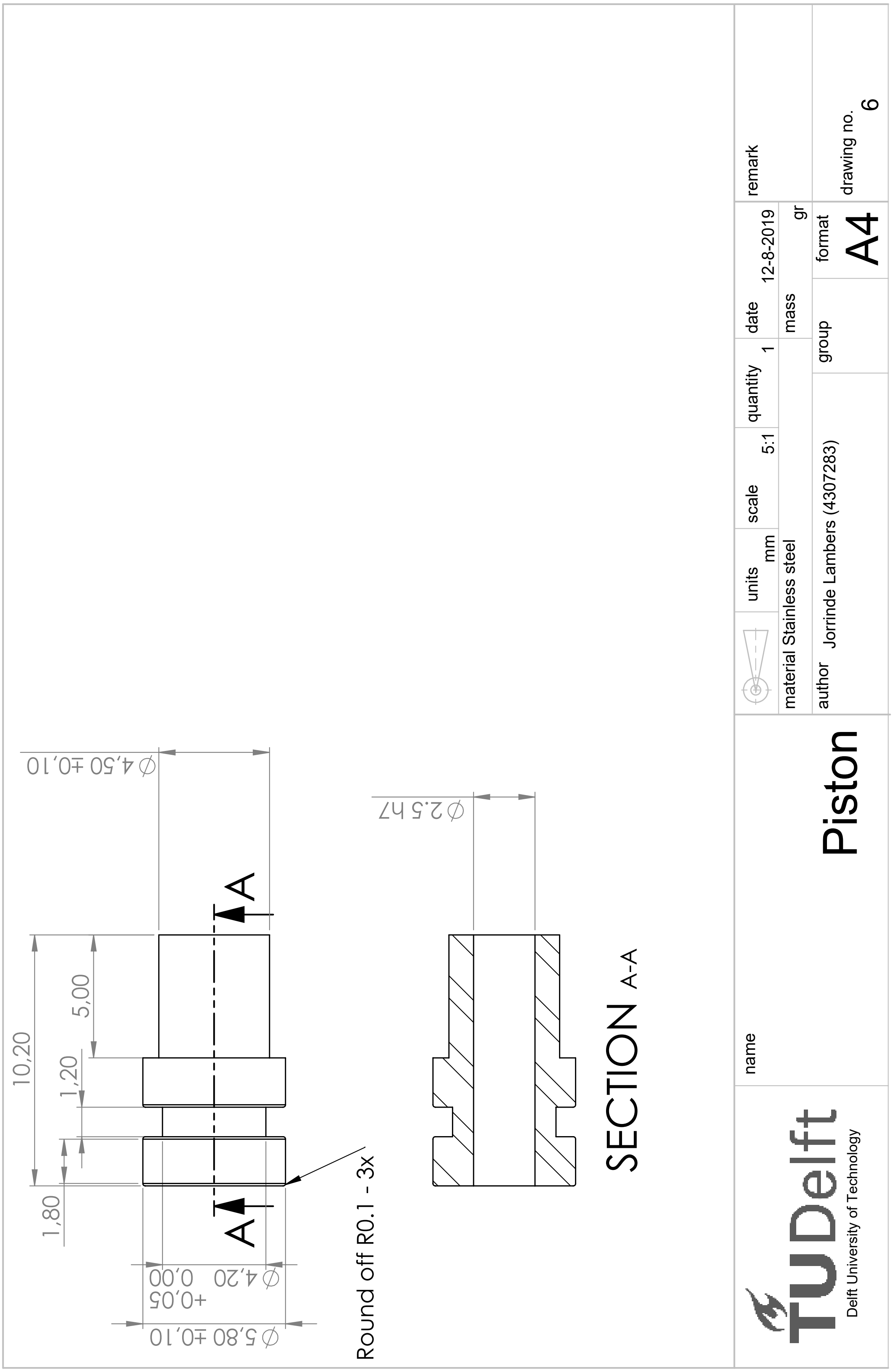

Figure 10.6: SolidWorks drawing of component number 6: Piston.

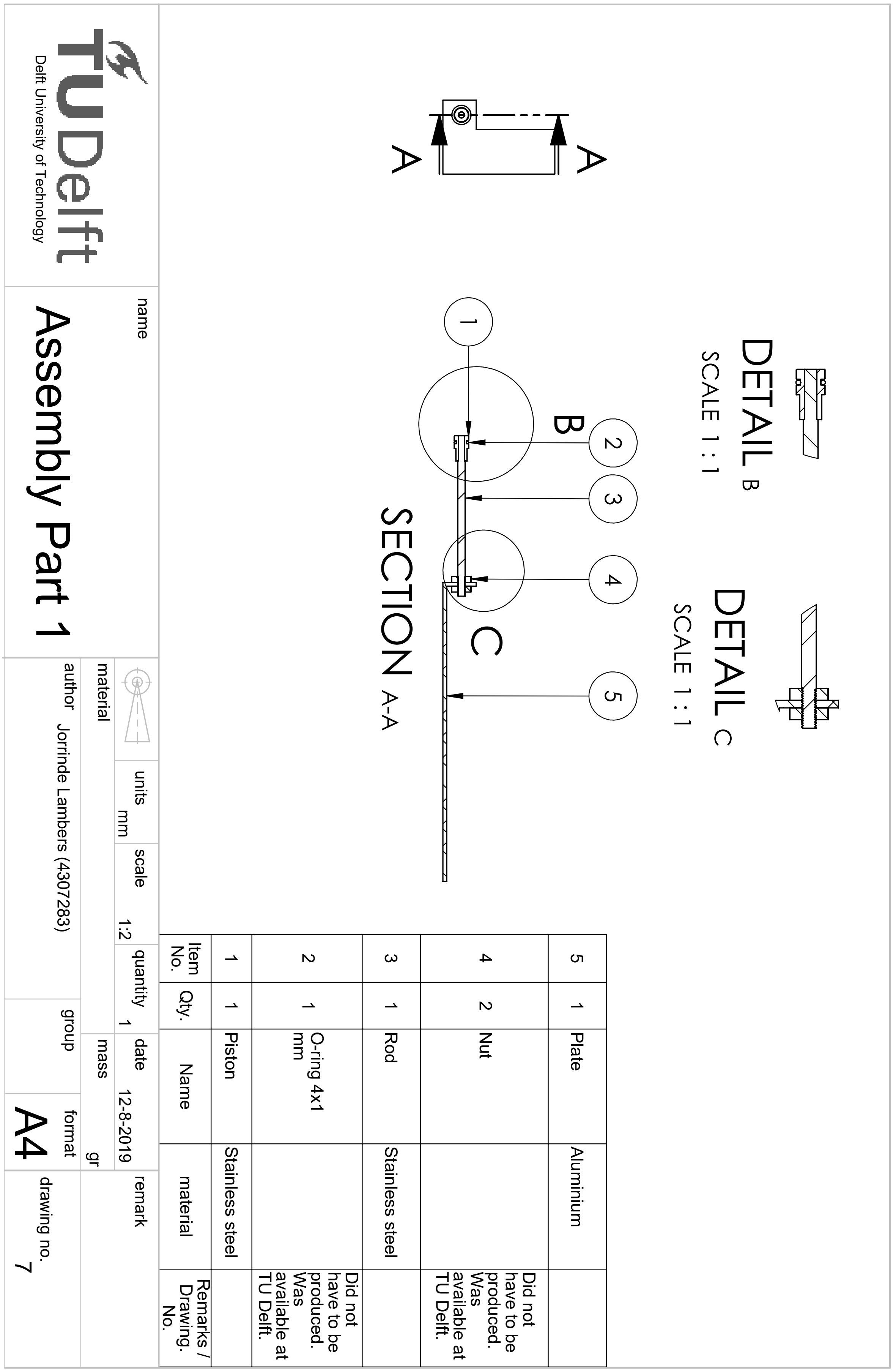

Figure 10.7: SolidWorks drawing of the assembly of part 1, containing the piston, rod and plate.

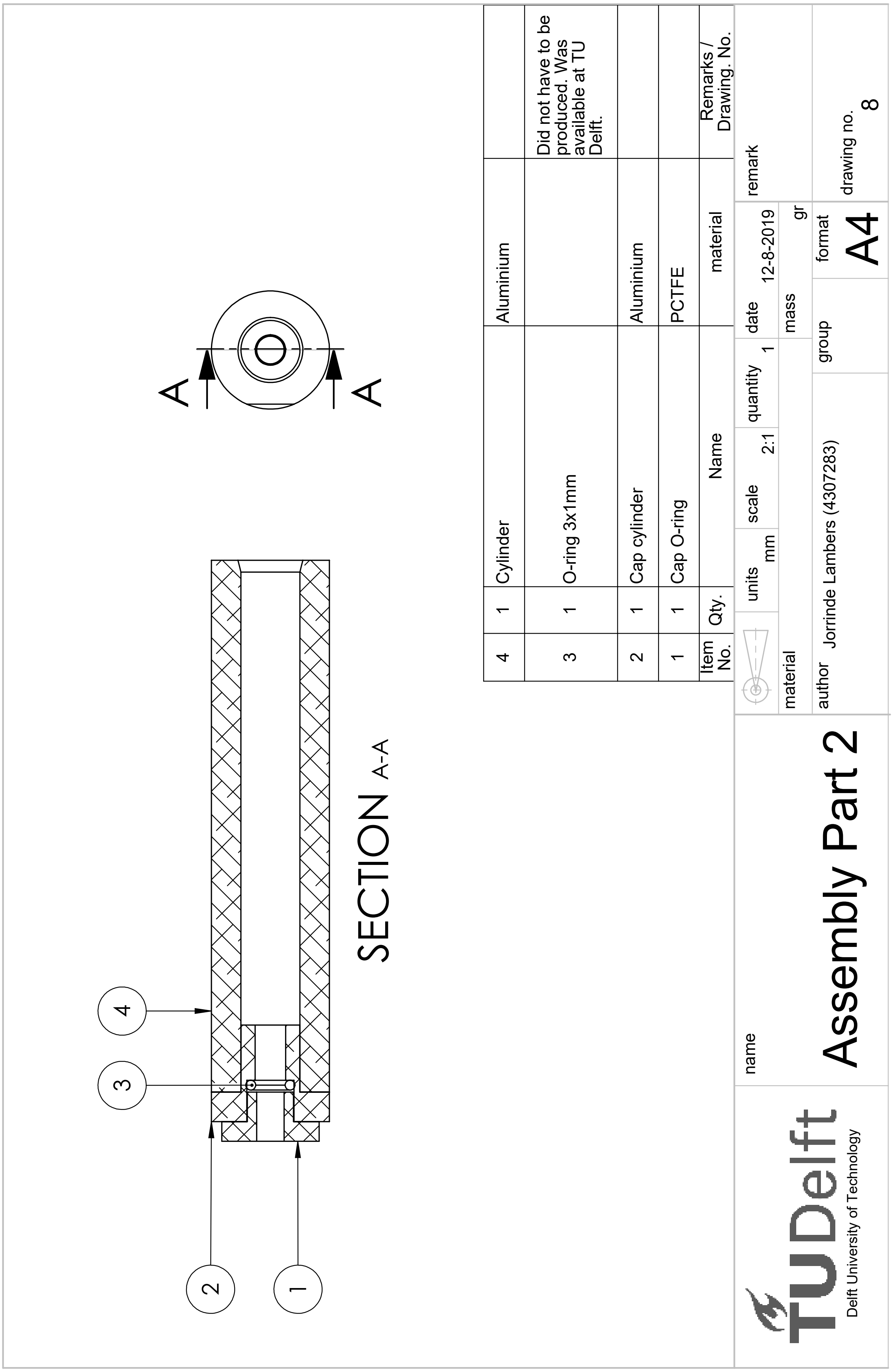

Figure 10.8: SolidWorks drawing of the assembly of part 2, containing the cylinder, cap cylinder, and cap O-ring.

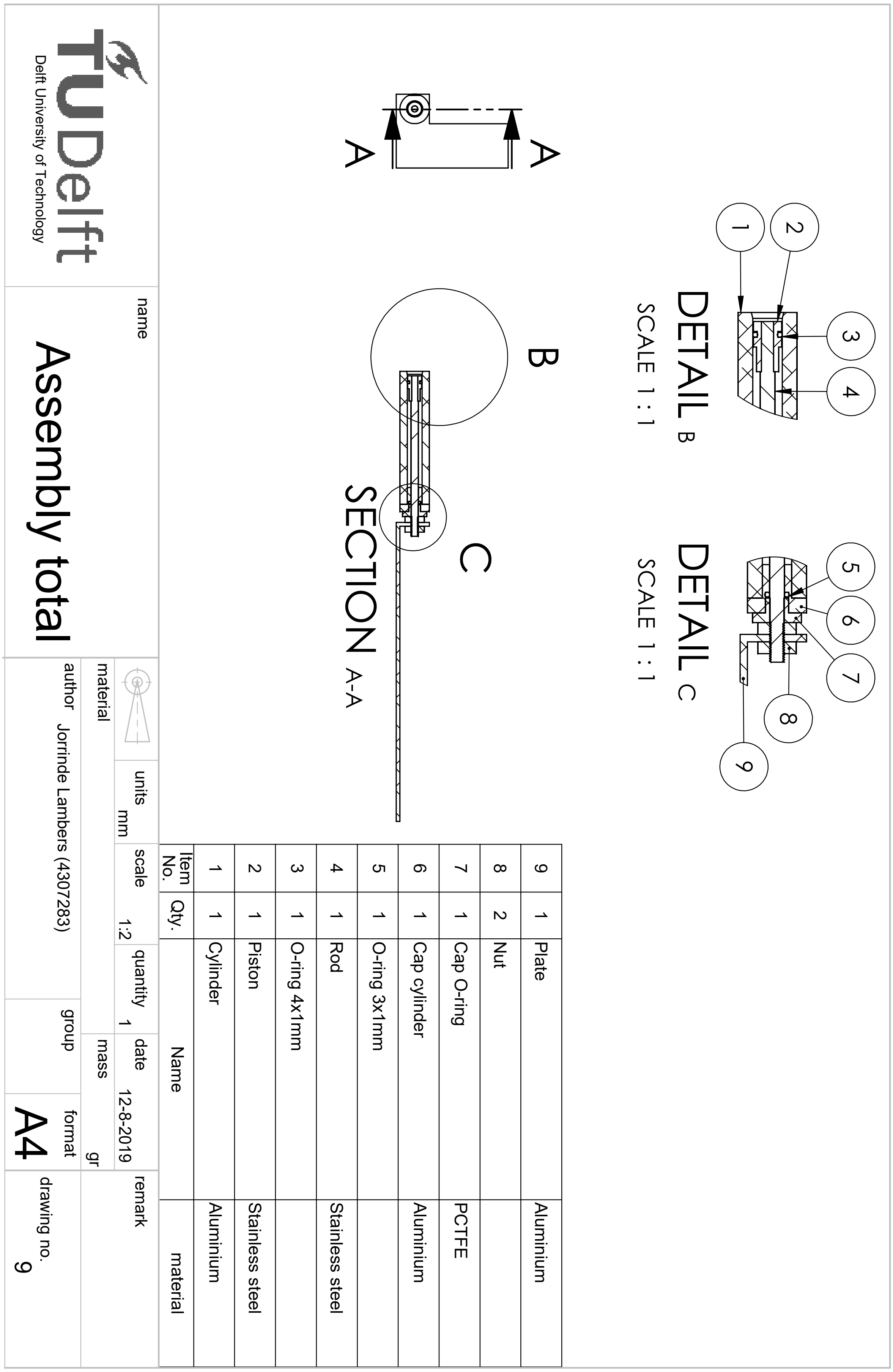

Item No.	Qty.	Name	material
1	1	Cylinder	Aluminium
2	1	Piston	Stainless steel
3	1	O-ring 4x1mm	
4	1	Rod	Stainless steel
5	1	O-ring 3x1mm	
6	1	Cap cylinder	Aluminium
7	1	Cap O-ring	PCTFE
8	2	Nut	
9	1	Plate	Aluminium

Figure 10.9: SolidWorks drawing of the total assembly (part 1 + part 2).

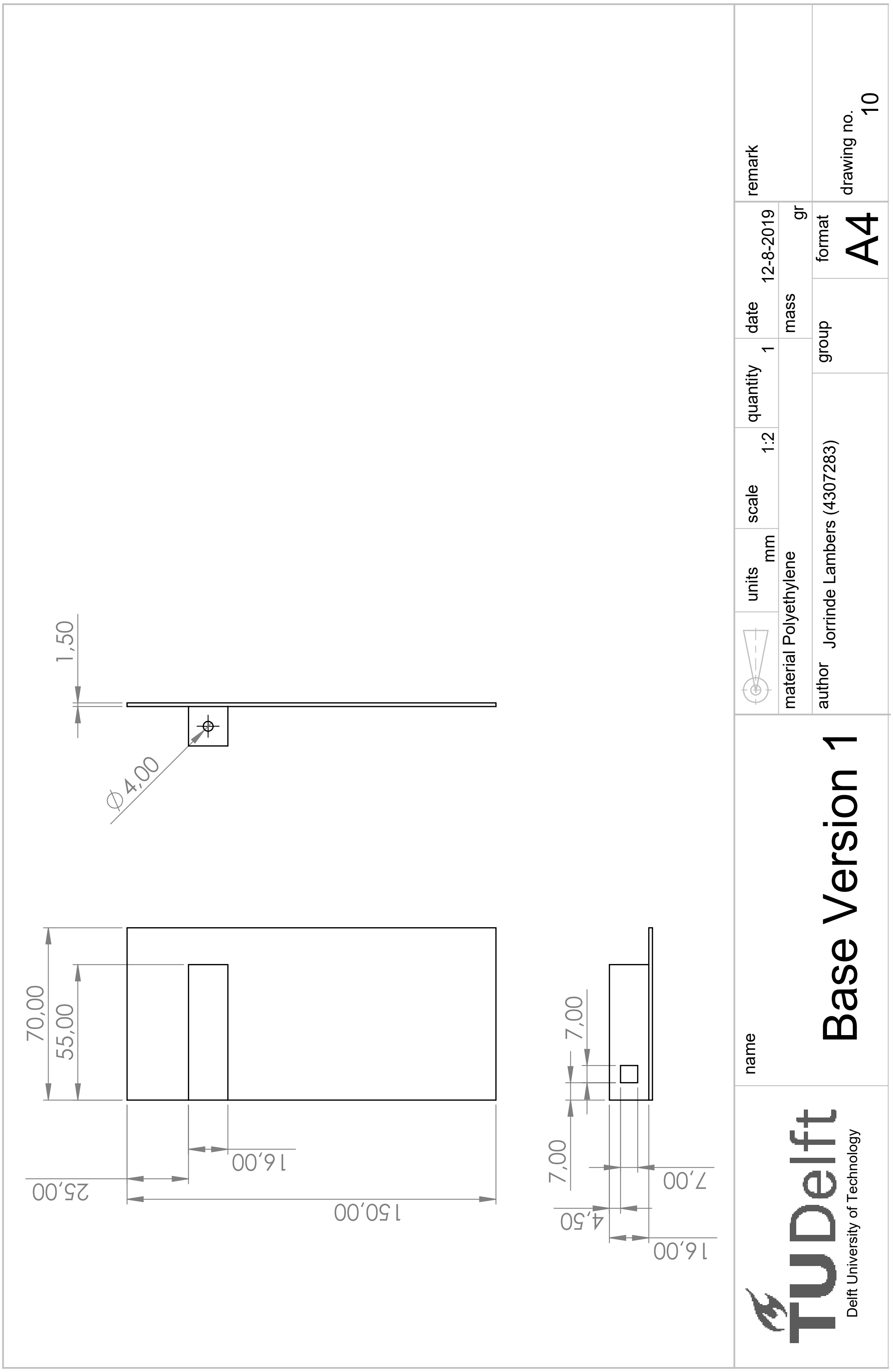

Figure 10.10: SolidWorks drawing of the base version 1.

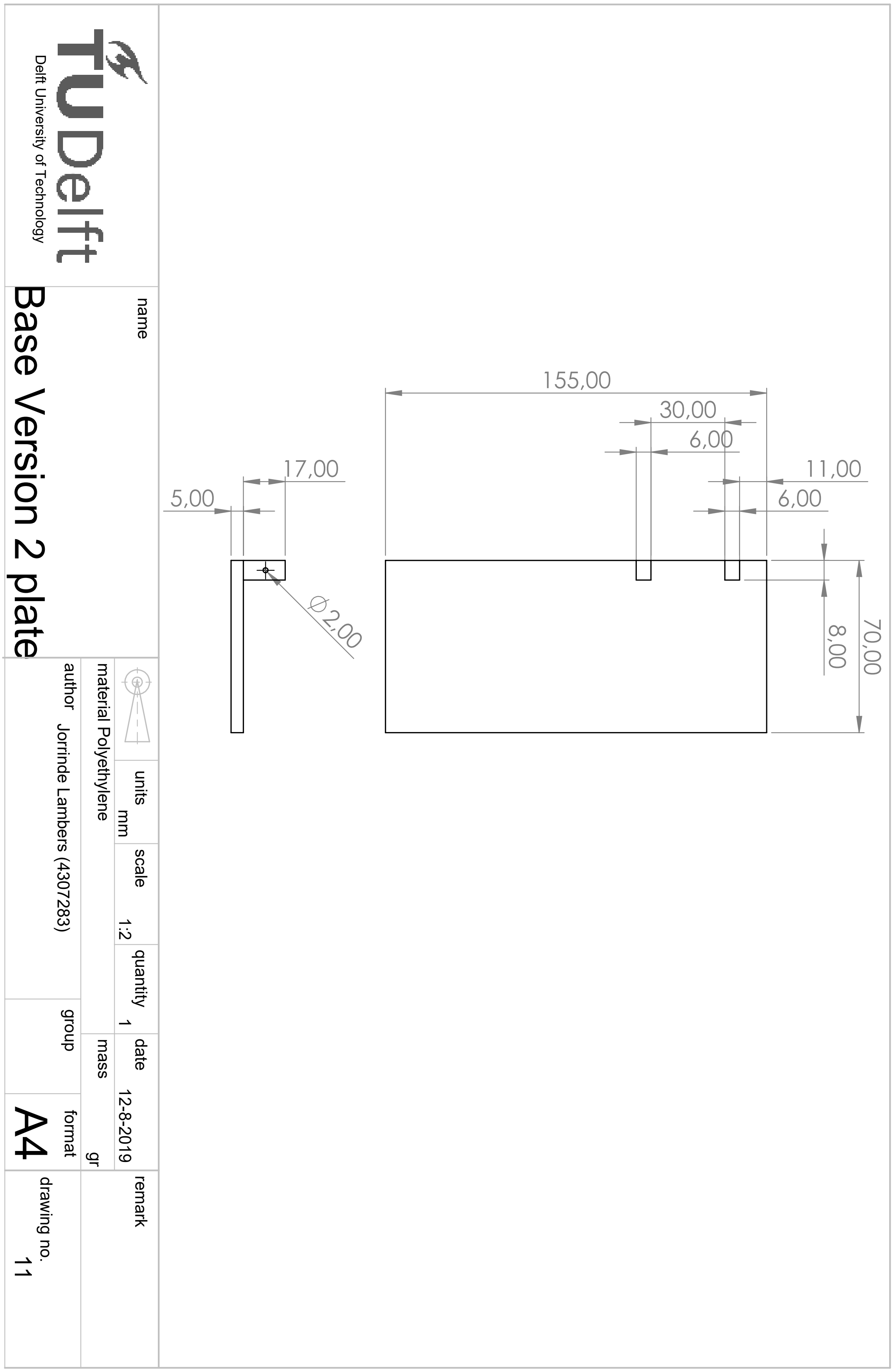

Figure 10.11: SolidWorks drawing of the plate of base version 2.

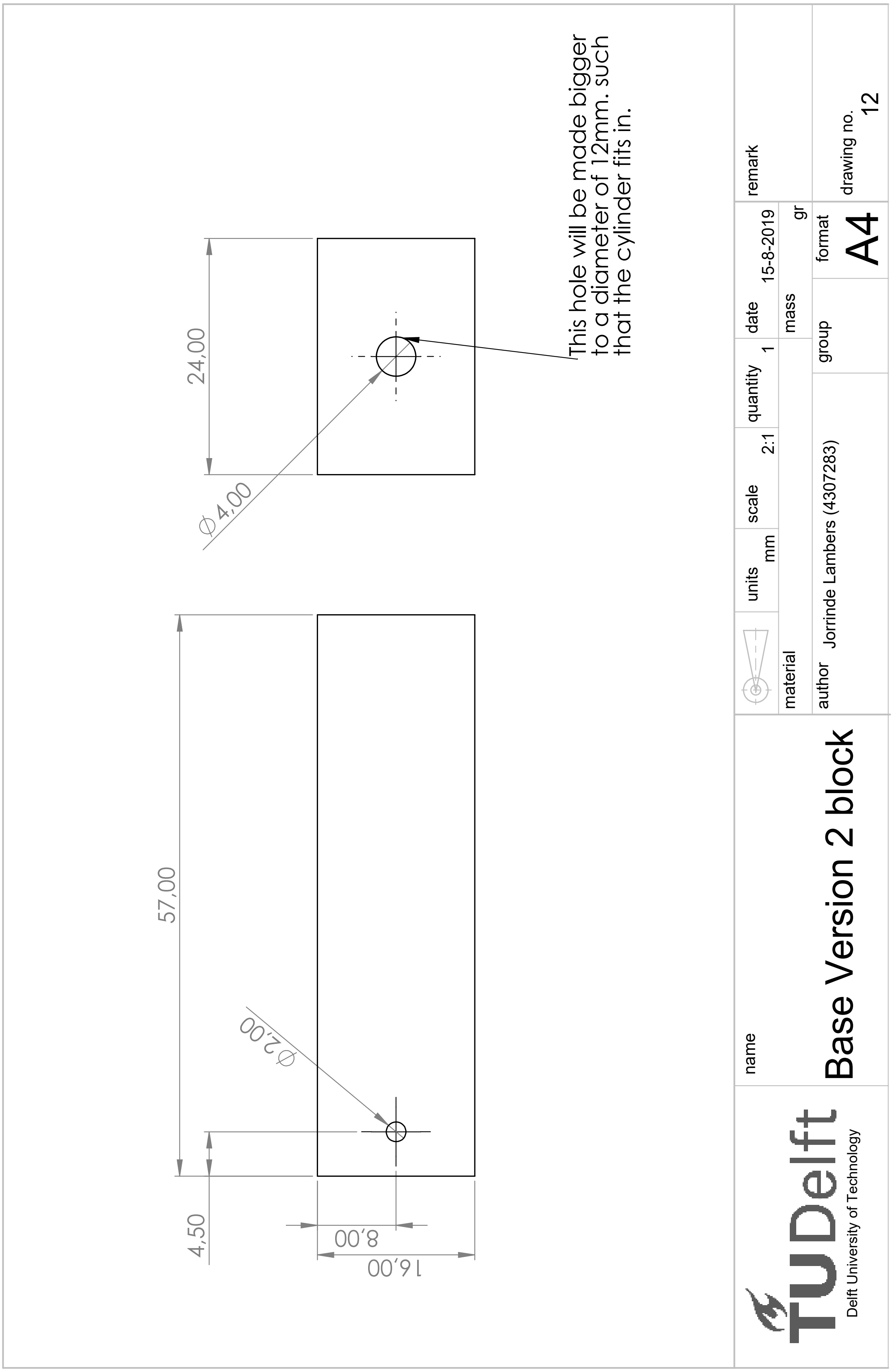

Figure 10.12: SolidWorks drawing of the block of base version 2.

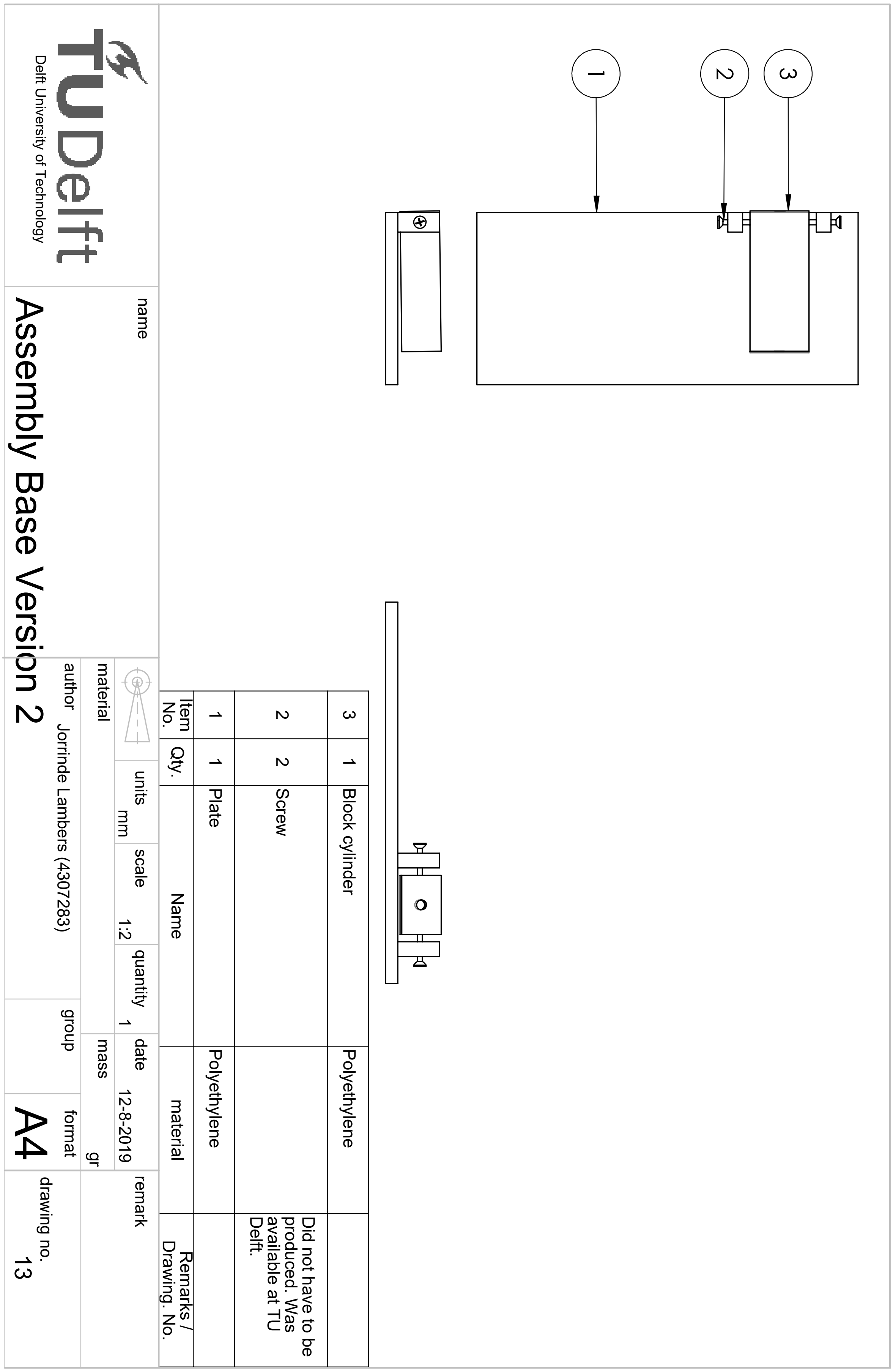

Figure 10.13: SolidWorks drawing of the assembly of base version 2 (plate + block).

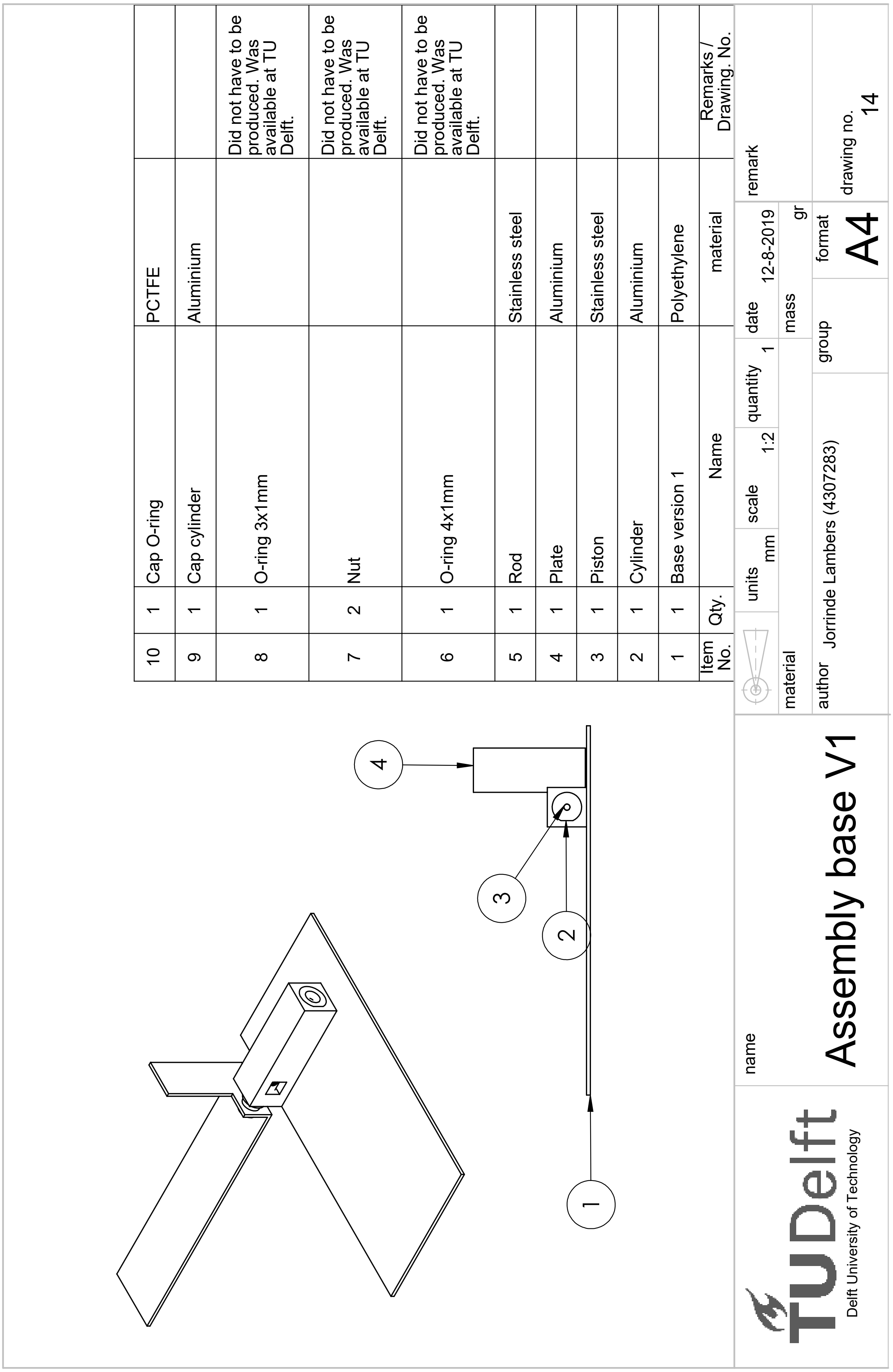

Item No.	Qty.	Name	material	Remarks / Drawing. No.
10	1	Cap O-ring	PCTFE	
9	1	Cap cylinder	Aluminium	
8	1	O-ring 3x1mm		Did not have to be produced. Was available at TU Delft.
7	2	Nut		Did not have to be produced. Was available at TU Delft.
6	1	O-ring 4x1mm		Did not have to be produced. Was available at TU Delft.
5	1	Rod	Stainless steel	
4	1	Plate	Aluminium	
3	1	Piston	Stainless steel	
2	1	Cylinder	Aluminium	
1	1	Base version 1	Polyethylene	

Figure 10.14: SolidWorks drawing of the total assembly with base version 1.

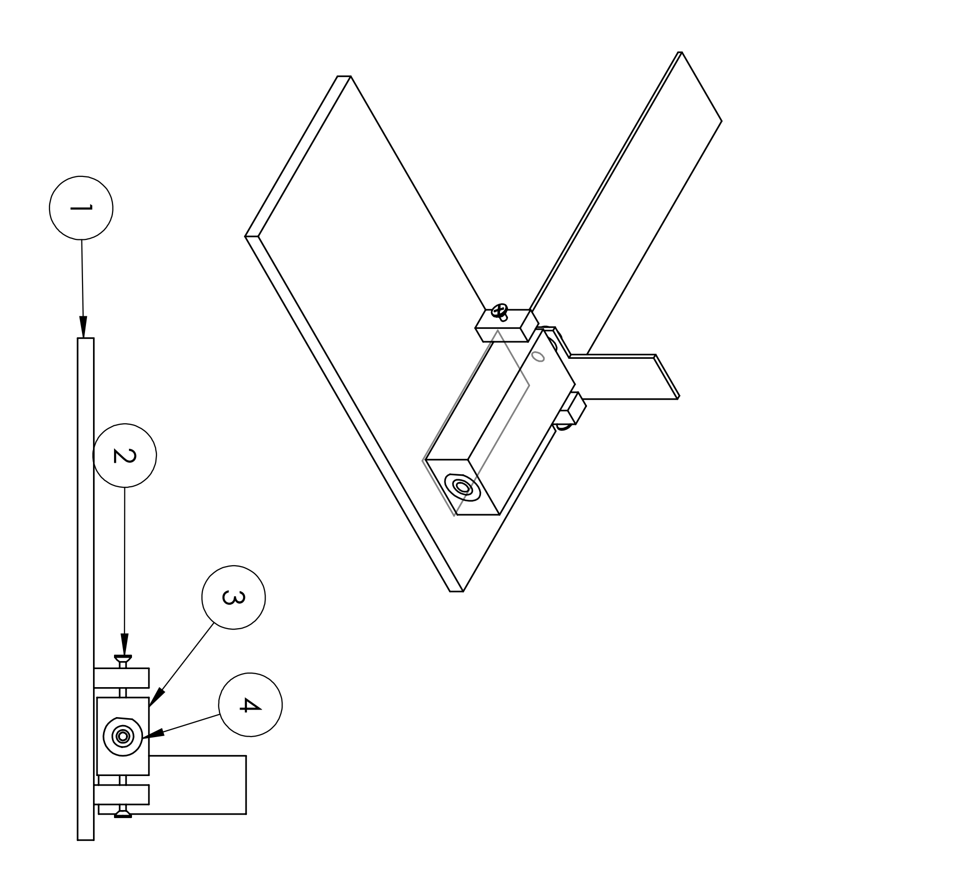

Item No.	Qty.	Name	material	Remarks / Drawing. No.
1	1	Base version 2 plate	Polyethylene	
2	2	Screw		Did not have to be produced. Was available at TU Delft.
3	1	Base version 2 block	Polyethylene	
4	1	Cylinder	Aluminium	
5	1	Plate	Aluminium	
6	1	Rod	Stainless steel	
7	1	Piston	Stainless steel	
8	1	O-ring 4x1mm		Did not have to be produced. Was available at TU Delft.
9	2	Nut		Did not have to be produced. Was available at TU Delft.
10	1	O-ring 3x1mm		Did not have to be produced. Was available at TU Delft.
11	1	Cap cylinder	Aluminium	
12	1	Cap O-ring	PCTFE	

TU Delft
Delft University of Technology

name: Assembly base V2

units	scale	quantity	date	remark
mm	1:2	1	12-8-2019	

material
mass: gr

author: Jorrinde Lambers (4307283)
group
format: A4
drawing no. 15

Figure 10.15: SolidWorks drawing of the total assembly with base version 2.

11 Matlab code

As was explained before Matlab (R2016b) was used to store and analyse the data. Two separate files were created for the experiments. Section 11.1 shows the files for experiment 1, and Section 11.2 will provide the code for experiment 2.

For the second experiment, it is chosen to only show the code for one subject, because the code was relatively long. The first steps (step 1-3) will only show the code for one subject. The data is then later pooled together for all subjects in step 4. From this point, all the code is presented.

11.1. Experiment 1

```
%% Results experiment 1: Sensitivity
% Jorrinde Lambers (4307283)
% Experiments took place: 8/7/2019 - 17/7/2019
clear all
close all
clc
%% Procedure of this code
% 1. Load all the txt files per subject, per test force and trial. This
% results in 4x4 = 16 files per subject, and in total 16x10=160 files.
% 2. Create a matrix of the data per reference force per testsubject
% 3. Count the times when the test force was identified as larger than
% the reference force and divide the count by the number of trials.
% 4. Fit a psychometric curve onto each subjects data, to be able to calculate the JND ...
    per subject
% 5. Calculate the JND per reference force per subject
% 6. Pool all the data together
% 7. Create the scattered data points
% 8. Create the psychometric function plot
% 9. Extrapolate the data
% 10. Calculate the JND and WF per reference force for the fitted curve
% 11. Plot psychometric fitted curves
% 12. Psychometric curves per reference force (to show variability between subjects)
%% Step 1: Load in the txt files
% put it into one big cell 3dimensions, participants x forces x repetitions
% = 10 x 4 x 4
NumberOfParticipants = 10;
NumberOfRepetitions  = 4;
Forces          = 2:2:8;
NumberOfForces = 4;
DataMatrix = cell(NumberOfParticipants,length(Forces),NumberOfRepetitions);

for nParticipant = 1 : NumberOfParticipants
    k = 1;
    for Force = Forces
        for nRepetitions = 1 : NumberOfRepetitions
            FileName  = strcat('subject',num2str(nParticipant),'ref',{' ...
                '},'force_',num2str(Force),'_',num2str(nRepetitions),'.txt');
```

```
            TempOpenString = string(FileName);
            TempOpen    = fopen(TempOpenString);
            TempData    = textscan(TempOpen,'%f%f%f%f%f%f%f%f%f','CollectOutput',1);
            DataMatrix(nParticipant,k,nRepetitions) = TempData;
        end
        k = k + 1;
    end
end

%% STEP 2: Create matrices of the data per reference force per subject
DataSubject1_F2 = ...
    cell2mat([DataMatrix(1,1,1);DataMatrix(1,1,2);DataMatrix(1,1,3);DataMatrix(1,1,4)]);
DataSubject1_F4 = ...
    cell2mat([DataMatrix(1,2,1);DataMatrix(1,2,2);DataMatrix(1,2,3);DataMatrix(1,2,4)]);
DataSubject1_F6 = ...
    cell2mat([DataMatrix(1,3,1);DataMatrix(1,3,2);DataMatrix(1,3,3);DataMatrix(1,3,4)]);
DataSubject1_F8 = ...
    cell2mat([DataMatrix(1,4,1);DataMatrix(1,4,2);DataMatrix(1,4,3);DataMatrix(1,4,4)]);
%DataSubject1 = [DataSubject1_F2;DataSubject1_F4;DataSubject1_F6;DataSubject1_F8]

DataSubject2_F2 = ...
    cell2mat([DataMatrix(2,1,1);DataMatrix(2,1,2);DataMatrix(2,1,3);DataMatrix(2,1,4)]);
DataSubject2_F4 = ...
    cell2mat([DataMatrix(2,2,1);DataMatrix(2,2,2);DataMatrix(2,2,3);DataMatrix(2,2,4)]);
DataSubject2_F6 = ...
    cell2mat([DataMatrix(2,3,1);DataMatrix(2,3,2);DataMatrix(2,3,3);DataMatrix(2,3,4)]);
DataSubject2_F8 = ...
    cell2mat([DataMatrix(2,4,1);DataMatrix(2,4,2);DataMatrix(2,4,3);DataMatrix(2,4,4)]);

DataSubject3_F2 = ...
    cell2mat([DataMatrix(3,1,1);DataMatrix(3,1,2);DataMatrix(3,1,3);DataMatrix(3,1,4)]);
DataSubject3_F4 = ...
    cell2mat([DataMatrix(3,2,1);DataMatrix(3,2,2);DataMatrix(3,2,3);DataMatrix(3,2,4)]);
DataSubject3_F6 = ...
    cell2mat([DataMatrix(3,3,1);DataMatrix(3,3,2);DataMatrix(3,3,3);DataMatrix(3,3,4)]);
DataSubject3_F8 = ...
    cell2mat([DataMatrix(3,4,1);DataMatrix(3,4,2);DataMatrix(3,4,3);DataMatrix(3,4,4)]);

DataSubject4_F2 = ...
    cell2mat([DataMatrix(4,1,1);DataMatrix(4,1,2);DataMatrix(4,1,3);DataMatrix(4,1,4)]);
DataSubject4_F4 = ...
    cell2mat([DataMatrix(4,2,1);DataMatrix(4,2,2);DataMatrix(4,2,3);DataMatrix(4,2,4)]);
DataSubject4_F6 = ...
    cell2mat([DataMatrix(4,3,1);DataMatrix(4,3,2);DataMatrix(4,3,3);DataMatrix(4,3,4)]);
DataSubject4_F8 = ...
    cell2mat([DataMatrix(4,4,1);DataMatrix(4,4,2);DataMatrix(4,4,3);DataMatrix(4,4,4)]);

DataSubject5_F2 = ...
    cell2mat([DataMatrix(5,1,1);DataMatrix(5,1,2);DataMatrix(5,1,3);DataMatrix(5,1,4)]);
DataSubject5_F4 = ...
    cell2mat([DataMatrix(5,2,1);DataMatrix(5,2,2);DataMatrix(5,2,3);DataMatrix(5,2,4)]);
DataSubject5_F6 = ...
    cell2mat([DataMatrix(5,3,1);DataMatrix(5,3,2);DataMatrix(5,3,3);DataMatrix(5,3,4)]);
DataSubject5_F8 = ...
    cell2mat([DataMatrix(5,4,1);DataMatrix(5,4,2);DataMatrix(5,4,3);DataMatrix(5,4,4)]);

DataSubject6_F2 = ...
    cell2mat([DataMatrix(6,1,1);DataMatrix(6,1,2);DataMatrix(6,1,3);DataMatrix(6,1,4)]);
DataSubject6_F4 = ...
    cell2mat([DataMatrix(6,2,1);DataMatrix(6,2,2);DataMatrix(6,2,3);DataMatrix(6,2,4)]);
DataSubject6_F6 = ...
    cell2mat([DataMatrix(6,3,1);DataMatrix(6,3,2);DataMatrix(6,3,3);DataMatrix(6,3,4)]);
DataSubject6_F8 = ...
    cell2mat([DataMatrix(6,4,1);DataMatrix(6,4,2);DataMatrix(6,4,3);DataMatrix(6,4,4)]);

DataSubject7_F2 = ...
    cell2mat([DataMatrix(7,1,1);DataMatrix(7,1,2);DataMatrix(7,1,3);DataMatrix(7,1,4)]);
DataSubject7_F4 = ...
    cell2mat([DataMatrix(7,2,1);DataMatrix(7,2,2);DataMatrix(7,2,3);DataMatrix(7,2,4)]);
DataSubject7_F6 = ...
    cell2mat([DataMatrix(7,3,1);DataMatrix(7,3,2);DataMatrix(7,3,3);DataMatrix(7,3,4)]);
```

```
DataSubject7_F8 = ...
    cell2mat([DataMatrix(7,4,1);DataMatrix(7,4,2);DataMatrix(7,4,3);DataMatrix(7,4,4)]);

DataSubject8_F2 = ...
    cell2mat([DataMatrix(8,1,1);DataMatrix(8,1,2);DataMatrix(8,1,3);DataMatrix(8,1,4)]);
DataSubject8_F4 = ...
    cell2mat([DataMatrix(8,2,1);DataMatrix(8,2,2);DataMatrix(8,2,3);DataMatrix(8,2,4)]);
DataSubject8_F6 = ...
    cell2mat([DataMatrix(8,3,1);DataMatrix(8,3,2);DataMatrix(8,3,3);DataMatrix(8,3,4)]);
DataSubject8_F8 = ...
    cell2mat([DataMatrix(8,4,1);DataMatrix(8,4,2);DataMatrix(8,4,3);DataMatrix(8,4,4)]);

DataSubject9_F2 = ...
    cell2mat([DataMatrix(9,1,1);DataMatrix(9,1,2);DataMatrix(9,1,3);DataMatrix(9,1,4)]);
DataSubject9_F4 = ...
    cell2mat([DataMatrix(9,2,1);DataMatrix(9,2,2);DataMatrix(9,2,3);DataMatrix(9,2,4)]);
DataSubject9_F6 = ...
    cell2mat([DataMatrix(9,3,1);DataMatrix(9,3,2);DataMatrix(9,3,3);DataMatrix(9,3,4)]);
DataSubject9_F8 = ...
    cell2mat([DataMatrix(9,4,1);DataMatrix(9,4,2);DataMatrix(9,4,3);DataMatrix(9,4,4)]);

DataSubject10_F2 = ...
    cell2mat([DataMatrix(10,1,1);DataMatrix(10,1,2);DataMatrix(10,1,3);DataMatrix(10,1,4)]);
DataSubject10_F4 = ...
    cell2mat([DataMatrix(10,2,1);DataMatrix(10,2,2);DataMatrix(10,2,3);DataMatrix(10,2,4)]);
DataSubject10_F6 = ...
    cell2mat([DataMatrix(10,3,1);DataMatrix(10,3,2);DataMatrix(10,3,3);DataMatrix(10,3,4)]);
DataSubject10_F8 = ...
    cell2mat([DataMatrix(10,4,1);DataMatrix(10,4,2);DataMatrix(10,4,3);DataMatrix(10,4,4)]);

%% STEP 3: Count the times when the test force was identified as larger than the ...
    reference force
FactorsMatrix = [-0.175;-0.14;-0.105;-0.07;-0.035;0.035;0.07;0.105;0.14;0.175];
Matrix = length(FactorsMatrix);

% Create zeros matrices
Subject1F2 = zeros(10,1);
Subject1F4 = zeros(10,1);
Subject1F6 = zeros(10,1);
Subject1F8 = zeros(10,1);
Subject2F2 = zeros(10,1);
Subject2F4 = zeros(10,1);
Subject2F6 = zeros(10,1);
Subject2F8 = zeros(10,1);
Subject3F2 = zeros(10,1);
Subject3F4 = zeros(10,1);
Subject3F6 = zeros(10,1);
Subject3F8 = zeros(10,1);
Subject4F2 = zeros(10,1);
Subject4F4 = zeros(10,1);
Subject4F6 = zeros(10,1);
Subject4F8 = zeros(10,1);
Subject5F2 = zeros(10,1);
Subject5F4 = zeros(10,1);
Subject5F6 = zeros(10,1);
Subject5F8 = zeros(10,1);
Subject6F2 = zeros(10,1);
Subject6F4 = zeros(10,1);
Subject6F6 = zeros(10,1);
Subject6F8 = zeros(10,1);
Subject7F2 = zeros(10,1);
Subject7F4 = zeros(10,1);
Subject7F6 = zeros(10,1);
Subject7F8 = zeros(10,1);
Subject8F2 = zeros(10,1);
Subject8F4 = zeros(10,1);
Subject8F6 = zeros(10,1);
Subject8F8 = zeros(10,1);
Subject9F2 = zeros(10,1);
Subject9F4 = zeros(10,1);
Subject9F6 = zeros(10,1);
```

```
Subject9F8 = zeros(10,1);
Subject10F2 = zeros(10,1);
Subject10F4 = zeros(10,1);
Subject10F6 = zeros(10,1);
Subject10F8 = zeros(10,1);

% Calculate the count for each factor
% Subject 1
for i = 1 : Matrix
    Subject1F2(i,1) = sum(DataSubject1_F2(:,2)==1 & ...
        DataSubject1_F2(:,3)==FactorsMatrix(i,:));
    Subject1F4(i,1) = sum(DataSubject1_F4(:,2)==1 & ...
        DataSubject1_F4(:,3)==FactorsMatrix(i,:));
    Subject1F6(i,1) = sum(DataSubject1_F6(:,2)==1 & ...
        DataSubject1_F6(:,3)==FactorsMatrix(i,:));
    Subject1F8(i,1) = sum(DataSubject1_F8(:,2)==1 & ...
        DataSubject1_F8(:,3)==FactorsMatrix(i,:));
end

% divide the count by the number of trials.
yF2_S1 = Subject1F2/4;
yF4_S1 = Subject1F4/4;
yF6_S1 = Subject1F6/4;
yF8_S1 = Subject1F8/4;

% Subject 2
for i = 1 : Matrix
    Subject2F2(i,1) = sum(DataSubject2_F2(:,2)==1 & ...
        DataSubject2_F2(:,3)==FactorsMatrix(i,:));
    Subject2F4(i,1) = sum(DataSubject2_F4(:,2)==1 & ...
        DataSubject2_F4(:,3)==FactorsMatrix(i,:));
    Subject2F6(i,1) = sum(DataSubject2_F6(:,2)==1 & ...
        DataSubject2_F6(:,3)==FactorsMatrix(i,:));
    Subject2F8(i,1) = sum(DataSubject2_F8(:,2)==1 & ...
        DataSubject2_F8(:,3)==FactorsMatrix(i,:));
end

% Divide the count by the number of trials.
yF2_S2 = Subject2F2/4;
yF4_S2 = Subject2F4/4;
yF6_S2 = Subject2F6/4;
yF8_S2 = Subject2F8/4;

% Subject 3
for i = 1 : Matrix
    Subject3F2(i,1) = sum(DataSubject3_F2(:,2)==1 & ...
        DataSubject3_F2(:,3)==FactorsMatrix(i,:));
    Subject3F4(i,1) = sum(DataSubject3_F4(:,2)==1 & ...
        DataSubject3_F4(:,3)==FactorsMatrix(i,:));
    Subject3F6(i,1) = sum(DataSubject3_F6(:,2)==1 & ...
        DataSubject3_F6(:,3)==FactorsMatrix(i,:));
    Subject3F8(i,1) = sum(DataSubject3_F8(:,2)==1 & ...
        DataSubject3_F8(:,3)==FactorsMatrix(i,:));
end

% Divide the count by the number of trials.
yF2_S3 = Subject3F2/4;
yF4_S3 = Subject3F4/4;
yF6_S3 = Subject3F6/4;
yF8_S3 = Subject3F8/4;

% Subject 4
for i = 1 : Matrix
    Subject4F2(i,1) = sum(DataSubject4_F2(:,2)==1 & ...
        DataSubject4_F2(:,3)==FactorsMatrix(i,:));
    Subject4F4(i,1) = sum(DataSubject4_F4(:,2)==1 & ...
        DataSubject4_F4(:,3)==FactorsMatrix(i,:));
    Subject4F6(i,1) = sum(DataSubject4_F6(:,2)==1 & ...
        DataSubject4_F6(:,3)==FactorsMatrix(i,:));
    Subject4F8(i,1) = sum(DataSubject4_F8(:,2)==1 & ...
        DataSubject4_F8(:,3)==FactorsMatrix(i,:));
```

```
end

% Divide the count by the number of trials.
yF2_S4 = Subject4F2/4;
yF4_S4 = Subject4F4/4;
yF6_S4 = Subject4F6/4;
yF8_S4 = Subject4F8/4;

% Subject 5
for i = 1 : Matrix
    Subject5F2(i,1) = sum(DataSubject5_F2(:,2)==1 & ...
        DataSubject5_F2(:,3)==FactorsMatrix(i,:));
    Subject5F4(i,1) = sum(DataSubject5_F4(:,2)==1 & ...
        DataSubject5_F4(:,3)==FactorsMatrix(i,:));
    Subject5F6(i,1) = sum(DataSubject5_F6(:,2)==1 & ...
        DataSubject5_F6(:,3)==FactorsMatrix(i,:));
    Subject5F8(i,1) = sum(DataSubject5_F8(:,2)==1 & ...
        DataSubject5_F8(:,3)==FactorsMatrix(i,:));
end

% divide the count by the number of trials.
yF2_S5 = Subject5F2/4;
yF4_S5 = Subject5F4/4;
yF6_S5 = Subject5F6/4;
yF8_S5 = Subject5F8/4;

% Subject 6
for i = 1 : Matrix
    Subject6F2(i,1) = sum(DataSubject6_F2(:,2)==1 & ...
        DataSubject6_F2(:,3)==FactorsMatrix(i,:));
    Subject6F4(i,1) = sum(DataSubject6_F4(:,2)==1 & ...
        DataSubject6_F4(:,3)==FactorsMatrix(i,:));
    Subject6F6(i,1) = sum(DataSubject6_F6(:,2)==1 & ...
        DataSubject6_F6(:,3)==FactorsMatrix(i,:));
    Subject6F8(i,1) = sum(DataSubject6_F8(:,2)==1 & ...
        DataSubject6_F8(:,3)==FactorsMatrix(i,:));
end

% divide the count by the number of trials.
yF2_S6 = Subject6F2/4;
yF4_S6 = Subject6F4/4;
yF6_S6 = Subject6F6/4;
yF8_S6 = Subject6F8/4;

% Subject 7
for i = 1 : Matrix
    Subject7F2(i,1) = sum(DataSubject7_F2(:,2)==1 & ...
        DataSubject7_F2(:,3)==FactorsMatrix(i,:));
    Subject7F4(i,1) = sum(DataSubject7_F4(:,2)==1 & ...
        DataSubject7_F4(:,3)==FactorsMatrix(i,:));
    Subject7F6(i,1) = sum(DataSubject7_F6(:,2)==1 & ...
        DataSubject7_F6(:,3)==FactorsMatrix(i,:));
    Subject7F8(i,1) = sum(DataSubject7_F8(:,2)==1 & ...
        DataSubject7_F8(:,3)==FactorsMatrix(i,:));
end

% divide the count by the number of trials.
yF2_S7 = Subject7F2/4;
yF4_S7 = Subject7F4/4;
yF6_S7 = Subject7F6/4;
yF8_S7 = Subject7F8/4;

% Subject 8
for i = 1 : Matrix
    Subject8F2(i,1) = sum(DataSubject8_F2(:,2)==1 & ...
        DataSubject8_F2(:,3)==FactorsMatrix(i,:));
    Subject8F4(i,1) = sum(DataSubject8_F4(:,2)==1 & ...
        DataSubject8_F4(:,3)==FactorsMatrix(i,:));
    Subject8F6(i,1) = sum(DataSubject8_F6(:,2)==1 & ...
        DataSubject8_F6(:,3)==FactorsMatrix(i,:));
```

```
    Subject8F8(i,1) = sum(DataSubject8_F8(:,2)==1 & ...
        DataSubject8_F8(:,3)==FactorsMatrix(i,:));
end

% divide the count by the number of trials.
yF2_S8 = Subject8F2/4;
yF4_S8 = Subject8F4/4;
yF6_S8 = Subject8F6/4;
yF8_S8 = Subject8F8/4;

% Subject 9
for i = 1 : Matrix
    Subject9F2(i,1) = sum(DataSubject9_F2(:,2)==1 & ...
        DataSubject9_F2(:,3)==FactorsMatrix(i,:));
    Subject9F4(i,1) = sum(DataSubject9_F4(:,2)==1 & ...
        DataSubject9_F4(:,3)==FactorsMatrix(i,:));
    Subject9F6(i,1) = sum(DataSubject9_F6(:,2)==1 & ...
        DataSubject9_F6(:,3)==FactorsMatrix(i,:));
    Subject9F8(i,1) = sum(DataSubject9_F8(:,2)==1 & ...
        DataSubject9_F8(:,3)==FactorsMatrix(i,:));
end

% divide the count by the number of trials.
yF2_S9 = Subject9F2/4;
yF4_S9 = Subject9F4/4;
yF6_S9 = Subject9F6/4;
yF8_S9 = Subject9F8/4;

% Subject 10
for i = 1 : Matrix
    Subject10F2(i,1) = sum(DataSubject10_F2(:,2)==1 & ...
        DataSubject10_F2(:,3)==FactorsMatrix(i,:));
    Subject10F4(i,1) = sum(DataSubject10_F4(:,2)==1 & ...
        DataSubject10_F4(:,3)==FactorsMatrix(i,:));
    Subject10F6(i,1) = sum(DataSubject10_F6(:,2)==1 & ...
        DataSubject10_F6(:,3)==FactorsMatrix(i,:));
    Subject10F8(i,1) = sum(DataSubject10_F8(:,2)==1 & ...
        DataSubject10_F8(:,3)==FactorsMatrix(i,:));
end

% divide the count by the number of trials.
yF2_S10 = Subject10F2/4;
yF4_S10 = Subject10F4/4;
yF6_S10 = Subject10F6/4;
yF8_S10 = Subject10F8/4;

%% STEP 4: Fit a psychometric curve onto each subjects data, to be able to calculate ...
    the JND per subject
x=[-0.175, -0.140, -0.105, -0.070, -0.035, 0.035, 0.070, 0.105, 0.140, 0.175] ;
targets = [0.25, 0.5, 0.75]; % 25%, 50% and 75% performance
weights = ones(1,length(x)); % No weighting

% SUBJECT 1
% Reference force 2N
[coeffsF2S1, ¬, curveF2S1, thresholdF2S1] = ...
FitPsycheCurveLogit(x, yF2_S1, weights, targets);
% Reference force 4N
[coeffsF4S1, ¬, curveF4S1, thresholdF4S1] = ...
FitPsycheCurveLogit(x, yF4_S1, weights, targets);
% Reference force 6N
[coeffsF6S1, ¬, curveF6S1, thresholdF6S1] = ...
FitPsycheCurveLogit(x, yF6_S1, weights, targets);
% Reference force 8N
[coeffsF8S1, ¬, curveF8S1, thresholdF8S1] = ...
FitPsycheCurveLogit(x, yF8_S1, weights, targets);

% SUBJECT 2
[coeffsF2S2, ¬, curveF2S2, thresholdF2S2] = ...
FitPsycheCurveLogit(x, yF2_S2, weights, targets);
[coeffsF4S2, ¬, curveF4S2, thresholdF4S2] = ...
FitPsycheCurveLogit(x, yF4_S2, weights, targets);
```

```
[coeffsF6S2, ¬, curveF6S2, thresholdF6S2] = ...
FitPsycheCurveLogit(x, yF6_S2, weights, targets);
[coeffsF8S2, ¬, curveF8S2, thresholdF8S2] = ...
FitPsycheCurveLogit(x, yF8_S2, weights, targets);

% SUBJECT 3
[coeffsF2S3, ¬, curveF2S3, thresholdF2S3] = ...
FitPsycheCurveLogit(x, yF2_S3, weights, targets);
[coeffsF4S3, ¬, curveF4S3, thresholdF4S3] = ...
FitPsycheCurveLogit(x, yF4_S3, weights, targets);
[coeffsF6S3, ¬, curveF6S3, thresholdF6S3] = ...
FitPsycheCurveLogit(x, yF6_S3, weights, targets);
[coeffsF8S3, ¬, curveF8S3, thresholdF8S3] = ...
FitPsycheCurveLogit(x, yF8_S3, weights, targets);

% SUBJECT 4
[coeffsF2S4, ¬, curveF2S4, thresholdF2S4] = ...
FitPsycheCurveLogit(x, yF2_S4, weights, targets);
[coeffsF4S4, ¬, curveF4S4, thresholdF4S4] = ...
FitPsycheCurveLogit(x, yF4_S4, weights, targets);
[coeffsF6S4, ¬, curveF6S4, thresholdF6S4] = ...
FitPsycheCurveLogit(x, yF6_S4, weights, targets);
[coeffsF8S4, ¬, curveF8S4, thresholdF8S4] = ...
FitPsycheCurveLogit(x, yF8_S4, weights, targets);

% SUBJECT 5
[coeffsF2S5, ¬, curveF2S5, thresholdF2S5] = ...
FitPsycheCurveLogit(x, yF2_S5, weights, targets);
[coeffsF4S5, ¬, curveF4S5, thresholdF4S5] = ...
FitPsycheCurveLogit(x, yF4_S5, weights, targets);
[coeffsF6S5, ¬, curveF6S5, thresholdF6S5] = ...
FitPsycheCurveLogit(x, yF6_S5, weights, targets);
[coeffsF8S5, ¬, curveF8S5, thresholdF8S5] = ...
FitPsycheCurveLogit(x, yF8_S5, weights, targets);

% SUBJECT 6
[coeffsF2S6, ¬, curveF2S6, thresholdF2S6] = ...
FitPsycheCurveLogit(x, yF2_S6, weights, targets);
[coeffsF4S6, ¬, curveF4S6, thresholdF4S6] = ...
FitPsycheCurveLogit(x, yF4_S6, weights, targets);
[coeffsF6S6, ¬, curveF6S6, thresholdF6S6] = ...
FitPsycheCurveLogit(x, yF6_S6, weights, targets);
[coeffsF8S6, ¬, curveF8S6, thresholdF8S6] = ...
FitPsycheCurveLogit(x, yF8_S6, weights, targets);

% SUBJECT 7
[coeffsF2S7, ¬, curveF2S7, thresholdF2S7] = ...
FitPsycheCurveLogit(x, yF2_S7, weights, targets);
[coeffsF4S7, ¬, curveF4S7, thresholdF4S7] = ...
FitPsycheCurveLogit(x, yF4_S7, weights, targets);
[coeffsF6S7, ¬, curveF6S7, thresholdF6S7] = ...
FitPsycheCurveLogit(x, yF6_S7, weights, targets);
[coeffsF8S7, ¬, curveF8S7, thresholdF8S7] = ...
FitPsycheCurveLogit(x, yF8_S7, weights, targets);

% SUBJECT 8
[coeffsF2S8, ¬, curveF2S8, thresholdF2S8] = ...
FitPsycheCurveLogit(x, yF2_S8, weights, targets);
[coeffsF4S8, ¬, curveF4S8, thresholdF4S8] = ...
FitPsycheCurveLogit(x, yF4_S8, weights, targets);
[coeffsF6S8, ¬, curveF6S8, thresholdF6S8] = ...
FitPsycheCurveLogit(x, yF6_S8, weights, targets);
[coeffsF8S8, ¬, curveF8S8, thresholdF8S8] = ...
FitPsycheCurveLogit(x, yF8_S8, weights, targets);

% SUBJECT 9
[coeffsF2S9, ¬, curveF2S9, thresholdF2S9] = ...
FitPsycheCurveLogit(x, yF2_S9, weights, targets);
[coeffsF4S9, ¬, curveF4S9, thresholdF4S9] = ...
FitPsycheCurveLogit(x, yF4_S9, weights, targets);
[coeffsF6S9, ¬, curveF6S9, thresholdF6S9] = ...
```

```
FitPsycheCurveLogit(x, yF6_S9, weights, targets);
[coeffsF8S9, ¬, curveF8S9, thresholdF8S9] = ...
FitPsycheCurveLogit(x, yF8_S9, weights, targets);

% SUBJECT 10
[coeffsF2S10, ¬, curveF2S10, thresholdF2S10] = ...
FitPsycheCurveLogit(x, yF2_S10, weights, targets);
[coeffsF4S10, ¬, curveF4S10, thresholdF4S10] = ...
FitPsycheCurveLogit(x, yF4_S10, weights, targets);
[coeffsF6S10, ¬, curveF6S10, thresholdF6S10] = ...
FitPsycheCurveLogit(x, yF6_S10, weights, targets);
[coeffsF8S10, ¬, curveF8S10, thresholdF8S10] = ...
FitPsycheCurveLogit(x, yF8_S10, weights, targets);

%% STEP 5: Calculate the JND per reference force per subject
% REFERENCE FORCE 2N
JND_F2T = zeros(10,1);
JND_F4T = zeros(10,1); % reference force 4N
JND_F6T = zeros(10,1);
JND_F8T = zeros(10,1);
JND_F2 = zeros(10,1);
JND_F4 = zeros(10,1);
JND_F6 = zeros(10,1);
JND_F8 = zeros(10,1);

F2=2;
F4=4;
F6=6;
F8=8;

for i = 1: length(JND_F2T)
    JND_F2T(1,1) = (thresholdF2S1(1,3)-thresholdF2S1(1,1))/2;
    JND_F2T(2,1) = (thresholdF2S2(1,3)-thresholdF2S2(1,1))/2;
    JND_F2T(3,1) = (thresholdF2S3(1,3)-thresholdF2S3(1,1))/2;
    JND_F2T(4,1) = (thresholdF2S4(1,3)-thresholdF2S4(1,1))/2;
    JND_F2T(5,1) = (thresholdF2S5(1,3)-thresholdF2S5(1,1))/2;
    JND_F2T(6,1) = (thresholdF2S6(1,3)-thresholdF2S6(1,1))/2;
    JND_F2T(7,1) = (thresholdF2S7(1,3)-thresholdF2S7(1,1))/2;
    JND_F2T(8,1) = (thresholdF2S8(1,3)-thresholdF2S8(1,1))/2;
    JND_F2T(9,1) = (thresholdF2S9(1,3)-thresholdF2S9(1,1))/2;
    JND_F2T(10,1) = (thresholdF2S10(1,3)-thresholdF2S10(1,1))/2;
end

for i = length(JND_F2)
    JND_F2(1,1) = (curveF2S1(500,1)-curveF2S1(1,1))/2;
    JND_F2(2,1) = (curveF2S2(330,1)-curveF2S2(1,1))/2;
    JND_F2(3,1) = (curveF2S3(1,1)-curveF2S3(500,1))/2;
    JND_F2(4,1) = (curveF2S4(500,1)-curveF2S4(1,1))/2;
    JND_F2(5,1) = (curveF2S5(500,1)-curveF2S5(25,1))/2;
    JND_F2(6,1) = (curveF2S6(500,1)-curveF2S6(1,1))/2;
    JND_F2(7,1) = (curveF2S4(453,1)-curveF2S7(48,1))/2;
    JND_F2(8,1) = (curveF2S8(1,1)-curveF2S8(500,1))/2;
    JND_F2(9,1) = (curveF2S9(392,1)-curveF2S9(1,1))/2;
    JND_F2(10,1) = (curveF2S10(500,1)-curveF2S10(66,1))/2;
end

% REFERENCE FORCE 4N
for i = 1: length(JND_F4T)
    JND_F4T(1,1) = (thresholdF4S1(1,3)-thresholdF4S1(1,1))/2;
    JND_F4T(2,1) = (thresholdF4S2(1,3)-thresholdF4S2(1,1))/2;
    JND_F4T(3,1) = (thresholdF4S3(1,3)-thresholdF4S3(1,1))/2;
    JND_F4T(4,1) = (thresholdF4S4(1,3)-thresholdF4S4(1,1))/2;
    JND_F4T(5,1) = (thresholdF4S5(1,3)-thresholdF4S5(1,1))/2;
    JND_F4T(6,1) = (thresholdF4S6(1,3)-thresholdF4S6(1,1))/2;
    JND_F4T(7,1) = (thresholdF4S7(1,3)-thresholdF4S7(1,1))/2;
    JND_F4T(8,1) = (thresholdF4S8(1,3)-thresholdF4S8(1,1))/2;
    JND_F4T(9,1) = (thresholdF4S9(1,3)-thresholdF4S9(1,1))/2;
    JND_F4T(10,1) = (thresholdF4S10(1,3)-thresholdF4S10(1,1))/2;
end

for i = length(JND_F4)
```

```
    JND_F4(1,1) = (curveF4S1(401,1)-curveF4S1(198,1))/2;
    JND_F4(2,1) = (curveF4S2(500,1)-curveF4S2(1,1))/2;
    JND_F4(3,1) = (curveF4S3(1,1)-curveF4S3(500,1))/2;
    JND_F4(4,1) = (curveF4S4(500,1)-curveF4S4(1,1))/2;
    JND_F4(5,1) = (curveF4S5(425,1)-curveF4S5(114,1))/2;
    JND_F4(6,1) = (curveF4S6(482,1)-curveF4S6(139,1))/2;
    JND_F4(7,1) = (curveF4S4(500,1)-curveF4S7(89,1))/2;
    JND_F4(8,1) = (curveF4S8(305,1)-curveF4S8(10,1))/2;
    JND_F4(9,1) = (curveF4S9(273,1)-curveF4S9(1,1))/2;
    JND_F4(10,1) = (curveF4S10(407,1)-curveF4S10(94,1))/2;
end

% REFERENCE FORCE 6N
for i = 1: length(JND_F6T)
    JND_F6T(1,1) = (thresholdF6S1(1,3)-thresholdF6S1(1,1))/2;
    JND_F6T(2,1) = (thresholdF6S2(1,3)-thresholdF6S2(1,1))/2;
    JND_F6T(3,1) = (thresholdF6S3(1,3)-thresholdF6S3(1,1))/2;
    JND_F6T(4,1) = (thresholdF6S4(1,3)-thresholdF6S4(1,1))/2;
    JND_F6T(5,1) = (thresholdF6S5(1,3)-thresholdF6S5(1,1))/2;
    JND_F6T(6,1) = (thresholdF6S6(1,3)-thresholdF6S6(1,1))/2;
    JND_F6T(7,1) = (thresholdF6S7(1,3)-thresholdF6S7(1,1))/2;
    JND_F6T(8,1) = (thresholdF6S8(1,3)-thresholdF6S8(1,1))/2;
    JND_F6T(9,1) = (thresholdF6S9(1,3)-thresholdF6S9(1,1))/2;
    JND_F6T(10,1) = (thresholdF6S10(1,3)-thresholdF6S10(1,1))/2;
end

for i = length(JND_F6)
    JND_F6(1,1) = (curveF6S1(435,1)-curveF6S1(140,1))/2;
    JND_F6(2,1) = (curveF6S2(444,1)-curveF6S2(57,1))/2;
    JND_F6(3,1) = (curveF6S3(500,1)-curveF6S3(1,1))/2;
    JND_F6(4,1) = (curveF6S4(393,1)-curveF6S4(69,1))/2;
    JND_F6(5,1) = (curveF6S5(472,1)-curveF6S5(29,1))/2;
    JND_F6(6,1) = (curveF6S6(500,1)-curveF6S6(215,1))/2;
    JND_F6(7,1) = (curveF6S4(500,1)-curveF6S7(1,1))/2;
    JND_F6(8,1) = (curveF6S8(488,1)-curveF6S8(6,1))/2;
    JND_F6(9,1) = (curveF6S9(325,1)-curveF6S9(1,1))/2;
    JND_F6(10,1) = (curveF6S10(500,1)-curveF6S10(108,1))/2;
end

% REFERENCE FORCE 8N
for i = 1: length(JND_F8T)
    JND_F8T(1,1) = (thresholdF8S1(1,3)-thresholdF8S1(1,1))/2;
    JND_F8T(2,1) = (thresholdF8S2(1,3)-thresholdF8S2(1,1))/2;
    JND_F8T(3,1) = (thresholdF8S3(1,3)-thresholdF8S3(1,1))/2;
    JND_F8T(4,1) = (thresholdF8S4(1,3)-thresholdF8S4(1,1))/2;
    JND_F8T(5,1) = (thresholdF8S5(1,3)-thresholdF8S5(1,1))/2;
    JND_F8T(6,1) = (thresholdF8S6(1,3)-thresholdF8S6(1,1))/2;
    JND_F8T(7,1) = (thresholdF8S7(1,3)-thresholdF8S7(1,1))/2;
    JND_F8T(8,1) = (thresholdF8S8(1,3)-thresholdF8S8(1,1))/2;
    JND_F8T(9,1) = (thresholdF8S9(1,3)-thresholdF8S9(1,1))/2;
    JND_F8T(10,1) = (thresholdF8S10(1,3)-thresholdF8S10(1,1))/2;
end

for i = length(JND_F8)
    JND_F8(1,1) = (curveF8S1(393,1)-curveF8S1(69,1))/2;
    JND_F8(2,1) = (curveF8S2(361,1)-curveF8S2(66,1))/2;
    JND_F8(3,1) = (curveF8S3(493,1)-curveF8S3(1,1))/2;
    JND_F8(4,1) = (curveF8S4(407,1)-curveF8S4(94,1))/2;
    JND_F8(5,1) = (curveF8S5(500,1)-curveF8S5(112,1))/2;
    JND_F8(6,1) = (curveF8S6(500,1)-curveF8S6(69,1))/2;
    JND_F8(7,1) = (curveF8S4(500,1)-curveF8S7(159,1))/2;
    JND_F8(8,1) = (curveF8S8(375,1)-curveF8S8(89,1))/2;
    JND_F8(9,1) = (curveF8S9(379,1)-curveF8S9(1,1))/2;
    JND_F8(10,1) = (curveF8S10(286,1)-curveF8S10(120,1))/2;
end

%% STEP 6: Pool all the data together
yF2=(yF2_S1+yF2_S2+yF2_S3+yF2_S4+yF2_S5+yF2_S6+yF2_S7+yF2_S8+yF2_S9+yF2_S10)/10;
yF4=(yF4_S1+yF4_S2+yF4_S3+yF4_S4+yF4_S5+yF4_S6+yF4_S7+yF4_S8+yF4_S9+yF2_S10)/10;
yF6=(yF6_S1+yF6_S2+yF6_S3+yF6_S4+yF6_S5+yF6_S6+yF6_S7+yF6_S8+yF6_S9+yF2_S10)/10;
yF8=(yF8_S1+yF8_S2+yF8_S3+yF8_S4+yF8_S5+yF8_S6+yF8_S7+yF8_S8+yF8_S9+yF2_S10)/10;
```

```
%% STEP 7: Create the scattered data points
x=[-0.175, -0.140, -0.105, -0.070, -0.035, 0.035, 0.070, 0.105, 0.140, 0.175] ;

% Scatter the datapoints per reference force
% Reference force 2N
figure, scatter(x,yF2, 'filled', 'r')
hold on
% Reference force 4N
figure, scatter(x,yF4, 'MarkerEdgeColor',[0 0.7 0], 'MarkerFaceColor',[0 0.7 0])
% Reference force 6N
figure, scatter(x,yF6, 'MarkerEdgeColor', [0 0.5 1], 'MarkerFaceColor', [0 0.5 1])
% Reference force 8N
figure, scatter(x,yF8, 'filled', 'k')
ylabel('Response reference force > test force')
xlabel('Test force factor')
hold off

%% STEP 8: Create the psychometric function plot
%%%%% STEP 7: Fit the psychometric function%%%%%%
% Fit psychometric functions
targets = [0.25, 0.5, 0.75]; % 25%, 50% and 75% performance
weights = ones(1,length(x)); % No weighting

% Fit per reference force
% Reference force 2N
[coeffsF2, ¬, curveF2, thresholdF2] = ...
FitPsycheCurveLogit(x, yF2, weights, targets);
% Reference force 4N
[coeffsF4, ¬, curveF4, thresholdF4] = ...
FitPsycheCurveLogit(x, yF4, weights, targets);
% Reference force 6N
[coeffsF6, ¬, curveF6, thresholdF6] = ...
FitPsycheCurveLogit(x, yF6, weights, targets);
% Reference force 8N
[coeffsF8, ¬, curveF8, thresholdF8] = ...
FitPsycheCurveLogit(x, yF8, weights, targets);

stdcurve=std(curveF2)

%% STEP 9: Extrapolate the data
xbefore=-0.300:0.0001:-0.175;
xafter=0.175:0.0001:0.400;

ExtraF2_before=interp1(curveF2(:,1),curveF2(:,2),xbefore,'linear','extrap');
ExtraF2_after=interp1(curveF2(:,1),curveF2(:,2),xafter,'linear','extrap');

%% STEP 10: Calculate the JND and WF per reference force for the fitted curve
% JND & WF: F2
JND_F2_25 = curveF2(1,:);
JND_F2_75 = curveF2(500,:);

JND_F2total = (JND_F2_75(:,1)-JND_F2_25(:,1))/2;
JND_F2total_T = (thresholdF2(1,3)-thresholdF2(1,1))/2;

WF_F2=(JND_F2total/2)*100;
WF_F2_T=(JND_F2total_T/2)*100;

% JND & WF: F4
JND_F4_25 = curveF4(30,:);
JND_F4_75 = curveF4(471,:);

JND_F4total=(JND_F4_75(:,1)-JND_F4_25(:,1))/2;
JND_F4total_T = (thresholdF4(1,3)-thresholdF4(1,1))/2;

WF_F4= (JND_F4total/4)*100;
WF_F4_T=(JND_F4total_T/4)*100;

% JND & WF: F6
JND_F6_25 = curveF6(37,:);
JND_F6_75 = curveF6(500,:);
```

```
JND_F6total = (JND_F6_75(:,1)-JND_F6_25(:,1))/2;
JND_F6total_T = (thresholdF6(1,3)-thresholdF6(1,1))/2;

WF_F6=(JND_F6total/6)*100;
WF_F6_T=(JND_F6total_T/6)*100;

% JND & WF: F8
JND_F8_25 = curveF8(55,:);
JND_F8_75 = curveF8(469,:);

JND_F8total = (JND_F8_75(:,1)-JND_F8_25(:,1))/2;
JND_F8total_T = (thresholdF8(1,3)-thresholdF8(1,1))/2;

WF_F8=(JND_F8total/8)*100;
WF_F8_T=(JND_F8total_T/8)*100;

%% STEP 11: Plot psychometric fitted curves
x0=10;
y0=10;
width=1800;
height=1000;
set(gcf,'position',[x0,y0,width,height])

figure(1)
plot(curveF2(:,1), curveF2(:,2), 'LineStyle', '-', 'Color', 'r','LineWidth',6)
hold on
plot([xbefore,xafter],[ExtraF2_before,ExtraF2_after], 'LineStyle', '--', 'Color', ...
    'r','LineWidth',3)
scatter(x,yF2,100,'r')
plot(curveF4(:,1), curveF4(:,2), 'LineStyle', '-', 'Color', [0 0.7 0],'LineWidth',6)
scatter(x,yF4,100,'MarkerEdgeColor',[0 0.7 0])
plot(curveF6(:,1), curveF6(:,2), 'LineStyle', '-', 'Color', [0 0.5 1],'LineWidth',6)
scatter(x,yF6,100,'MarkerEdgeColor', [0 0.5 1])
plot(curveF8(:,1), curveF8(:,2), 'LineStyle', '-', 'Color', 'k','LineWidth',6)
scatter(x,yF8,100,'k')
ylim([0, 1])
xticks([-0.300,-0.175, -0.140, -0.105, -0.070, -0.035, 0, 0.035, 0.070, 0.105, 0.140, ...
    0.175,0.400])
yticks([0, 0.1, 0.2, 0.3, 0.4, 0.5, 0.6, 0.7, 0.8, 0.9, 1])
ax = gca;
ax.FontSize = 22;
set(gca, 'XTickLabelRotation', 45)
ylabel('Response test force > reference force','fontweight','bold','FontSize',26)
xlabel('Test force factor','fontweight','bold','FontSize',26)
%title('{\bf Psychometric curve of experiment 1}','fontsize',15)
legend({'2N fit -- JND = 0.35 -- WF = 18% *','Extrapolated data 2N','Scatter 2N','4N ...
    fit -- JND = 0.15 -- WF = 4% ','Scatter 4N','6N fit -- JND = 0.17 -- WF = 3% ...
    ','Scatter 6N','8N fit -- JND = 0.15 -- WF = 2%','Scatter 8N'},'FontSize',17, ...
    'Location','northwest') %northwest
hold off

%% STEP 12: Psychometric curves per reference force (to show variability between ...
    subjects)
% Reference force 2N
figure(2)
plot(curveF2S1(:,1), curveF2S1(:,2), 'LineStyle', '-', 'Color', 'r','LineWidth',3)
hold on
plot(curveF2S2(:,1), curveF2S2(:,2), 'LineStyle', '-', 'Color', [0 0.7 0],'LineWidth',3)
plot(curveF2S3(:,1), curveF2S3(:,2), 'LineStyle', '-', 'Color', [0 0.5 1],'LineWidth',3)
plot(curveF2S4(:,1), curveF2S4(:,2), 'LineStyle', '-', 'Color', 'k','LineWidth',3)
plot(curveF2S5(:,1), curveF2S5(:,2), 'LineStyle', '-', 'Color', 'g','LineWidth',3)
plot(curveF2S6(:,1), curveF2S6(:,2), 'LineStyle', '-', 'Color', 'b','LineWidth',3)
plot(curveF2S7(:,1), curveF2S7(:,2), 'LineStyle', '-', 'Color', 'm','LineWidth',3)
plot(curveF2S8(:,1), curveF2S8(:,2), 'LineStyle', '-', 'Color', 'c','LineWidth',3)
plot(curveF2S9(:,1), curveF2S9(:,2), 'LineStyle', '-', 'Color', 'y','LineWidth',3)
plot(curveF2S10(:,1), curveF2S10(:,2), 'LineStyle', '-', 'Color', [0.8 0 ...
    0.5],'LineWidth',3)
ylim([0, 1])
xticks([-0.175, -0.140, -0.105, -0.070, -0.035, 0, 0.035, 0.070, 0.105, 0.140, 0.175])
yticks([0, 0.1, 0.2, 0.3, 0.4, 0.5, 0.6, 0.7, 0.8, 0.9, 1])
```

```
ax = gca;
ax.FontSize = 14;
set(gcf,'position',[x0,y0,width,height])
ylabel('Response test force > reference force','fontweight','bold','FontSize',18)
xlabel('Test force factor','fontweight','bold','FontSize',18)
title('Psychometric curve per subject for reference force: 2N','fontsize',18)
legend({'Subject 1','Subject 2','Subject 3','Subject 4','Subject 5','Subject ...
    6','Subject 7','Subject 8','Subject 9','Subject 10'},'FontSize',14, ...
    'Location','northwest')
hold off

% Reference force 4N
figure(3)
plot(curveF4S1(:,1), curveF4S1(:,2), 'LineStyle', '-', 'Color', 'r','LineWidth',3)
hold on
plot(curveF4S2(:,1), curveF4S2(:,2), 'LineStyle', '-', 'Color', [0 0.7 0],'LineWidth',3)
plot(curveF4S3(:,1), curveF4S3(:,2), 'LineStyle', '-', 'Color', [0 0.5 1],'LineWidth',3)
plot(curveF4S4(:,1), curveF4S4(:,2), 'LineStyle', '-', 'Color', 'k','LineWidth',3)
plot(curveF4S5(:,1), curveF4S5(:,2), 'LineStyle', '-', 'Color', 'g','LineWidth',3)
plot(curveF4S6(:,1), curveF4S6(:,2), 'LineStyle', '-', 'Color', 'b','LineWidth',3)
plot(curveF4S7(:,1), curveF4S7(:,2), 'LineStyle', '-', 'Color', 'm','LineWidth',3)
plot(curveF4S8(:,1), curveF4S8(:,2), 'LineStyle', '-', 'Color', 'c','LineWidth',3)
plot(curveF4S9(:,1), curveF4S9(:,2), 'LineStyle', '-', 'Color', 'y','LineWidth',3)
plot(curveF4S10(:,1), curveF4S10(:,2), 'LineStyle', '-', 'Color', [0.8 0 ...
    0.5],'LineWidth',3)
ylim([0, 1])
xticks([-0.175, -0.140, -0.105, -0.070, -0.035, 0, 0.035, 0.070, 0.105, 0.140, 0.175])
yticks([0, 0.1, 0.2, 0.3, 0.4, 0.5, 0.6, 0.7, 0.8, 0.9, 1])
ax = gca;
ax.FontSize = 14;
set(gcf,'position',[x0,y0,width,height])
ylabel('Response test force > reference force','fontweight','bold','FontSize',18)
xlabel('Test force factor','fontweight','bold','FontSize',18)
title('Psychometric curve per subject for reference force: 4N','fontsize',18)
legend({'Subject 1','Subject 2','Subject 3','Subject 4','Subject 5','Subject ...
    6','Subject 7','Subject 8','Subject 9','Subject 10'},'FontSize',14, ...
    'Location','northwest')
hold off

% Reference force: 6N
figure(4)
plot(curveF6S1(:,1), curveF6S1(:,2), 'LineStyle', '-', 'Color', 'r','LineWidth',3)
hold on
plot(curveF6S2(:,1), curveF6S2(:,2), 'LineStyle', '-', 'Color', [0 0.7 0],'LineWidth',3)
plot(curveF6S3(:,1), curveF6S3(:,2), 'LineStyle', '-', 'Color', [0 0.5 1],'LineWidth',3)
plot(curveF6S4(:,1), curveF6S4(:,2), 'LineStyle', '-', 'Color', 'k','LineWidth',3)
plot(curveF6S5(:,1), curveF6S5(:,2), 'LineStyle', '-', 'Color', 'g','LineWidth',3)
plot(curveF6S6(:,1), curveF6S6(:,2), 'LineStyle', '-', 'Color', 'b','LineWidth',3)
plot(curveF6S7(:,1), curveF6S7(:,2), 'LineStyle', '-', 'Color', 'm','LineWidth',3)
plot(curveF6S8(:,1), curveF6S8(:,2), 'LineStyle', '-', 'Color', 'c','LineWidth',3)
plot(curveF6S9(:,1), curveF6S9(:,2), 'LineStyle', '-', 'Color', 'y','LineWidth',3)
plot(curveF6S10(:,1), curveF6S10(:,2), 'LineStyle', '-', 'Color', [0.8 0 ...
    0.5],'LineWidth',3)
ylim([0, 1])
xticks([-0.175, -0.140, -0.105, -0.070, -0.035, 0, 0.035, 0.070, 0.105, 0.140, 0.175])
yticks([0, 0.1, 0.2, 0.3, 0.4, 0.5, 0.6, 0.7, 0.8, 0.9, 1])
ax = gca;
ax.FontSize = 14;
set(gcf,'position',[x0,y0,width,height])
ylabel('Response test force > reference force','fontweight','bold','FontSize',18)
xlabel('Test force factor','fontweight','bold','FontSize',18)
title('Psychometric curve per subject for reference force: 6N','fontsize',18)
legend({'Subject 1','Subject 2','Subject 3','Subject 4','Subject 5','Subject ...
    6','Subject 7','Subject 8','Subject 9','Subject 10'},'FontSize',14, ...
    'Location','northwest')
hold off

% Reference force: 8N
figure(5)
plot(curveF8S1(:,1), curveF8S1(:,2), 'LineStyle', '-', 'Color', 'r','LineWidth',3)
hold on
```

```
plot(curveF8S2(:,1), curveF8S2(:,2), 'LineStyle', '-', 'Color', [0 0.7 0],'LineWidth',3)
plot(curveF8S3(:,1), curveF8S3(:,2), 'LineStyle', '-', 'Color', [0 0.5 1],'LineWidth',3)
plot(curveF8S4(:,1), curveF8S4(:,2), 'LineStyle', '-', 'Color', 'k','LineWidth',3)
plot(curveF8S5(:,1), curveF8S5(:,2), 'LineStyle', '-', 'Color', 'g','LineWidth',3)
plot(curveF8S6(:,1), curveF8S6(:,2), 'LineStyle', '-', 'Color', 'b','LineWidth',3)
plot(curveF8S7(:,1), curveF8S7(:,2), 'LineStyle', '-', 'Color', 'm','LineWidth',3)
plot(curveF8S8(:,1), curveF8S8(:,2), 'LineStyle', '-', 'Color', 'c','LineWidth',3)
plot(curveF8S9(:,1), curveF8S9(:,2), 'LineStyle', '-', 'Color', 'y','LineWidth',3)
plot(curveF8S10(:,1), curveF8S10(:,2), 'LineStyle', '-', 'Color', [0.8 0 ...
    0.5],'LineWidth',3)
ylim([0, 1])
xticks([-0.175, -0.140, -0.105, -0.070, -0.035, 0, 0.035, 0.070, 0.105, 0.140, 0.175])
yticks([0, 0.1, 0.2, 0.3, 0.4, 0.5, 0.6, 0.7, 0.8, 0.9, 1])
ax = gca;
ax.FontSize = 14;
set(gcf,'position',[x0,y0,width,height])
ylabel('Response test force > reference force','fontweight','bold','FontSize',18)
xlabel('Test force factor','fontweight','bold','FontSize',18)
title('Psychometric curve per subject for reference force: 8N','fontsize',18)
legend({'Subject 1','Subject 2','Subject 3','Subject 4','Subject 5','Subject ...
    6','Subject 7','Subject 8','Subject 9','Subject 10'},'FontSize',14, ...
    'Location','northwest')
hold off

%% Calculate standard deviation
STD_2 = zeros(10,1);
STD_2(1,1) = std(yF2_S1);
STD_2(2,1) = std(yF2_S2);
STD_2(3,1)=std(yF2_S3);
STD_2(4,1)=std(yF2_S4);
STD_2(5,1)=std(yF2_S5);
STD_2(6,1)=std(yF2_S6);
STD_2(7,1)=std(yF2_S7);
STD_2(8,1)=std(yF2_S8);
STD_2(9,1)=std(yF2_S9);
STD_2(10,1)=std(yF2_S10);

STD_2mean=sum(STD_2)/10;

STD_4 = zeros(10,1);
STD_4(1,1) = std(yF4_S1);
STD_4(2,1) = std(yF4_S2);
STD_4(3,1)=std(yF4_S3);
STD_4(4,1)=std(yF4_S4);
STD_4(5,1)=std(yF4_S5);
STD_4(6,1)=std(yF4_S6);
STD_4(7,1)=std(yF4_S7);
STD_4(8,1)=std(yF4_S8);
STD_4(9,1)=std(yF4_S9);
STD_4(10,1)=std(yF4_S10);

STD_4mean=sum(STD_4)/10;

STD_6 = zeros(10,1);
STD_6(1,1) = std(yF6_S1);
STD_6(2,1) = std(yF6_S2);
STD_6(3,1)=std(yF6_S3);
STD_6(4,1)=std(yF6_S4);
STD_6(5,1)=std(yF6_S5);
STD_6(6,1)=std(yF6_S6);
STD_6(7,1)=std(yF6_S7);
STD_6(8,1)=std(yF6_S8);
STD_6(9,1)=std(yF6_S9);
STD_6(10,1)=std(yF6_S10);

STD_6mean=sum(STD_6)/10;

STD_8 = zeros(10,1);
STD_8(1,1) = std(yF8_S1);
STD_8(2,1) = std(yF8_S2);
STD_8(3,1)=std(yF8_S3);
```

```
STD_8(4,1)=std(yF8_S4);
STD_8(5,1)=std(yF8_S5);
STD_8(6,1)=std(yF8_S6);
STD_8(7,1)=std(yF8_S7);
STD_8(8,1)=std(yF8_S8);
STD_8(9,1)=std(yF8_S9);
STD_8(10,1)=std(yF8_S10);

STD_8mean=sum(STD_8)/10;
%%
STD_2Fit = std(yF2)
STD_4Fit = std(yF4)
STD_6Fit = std(yF6)
STD_8Fit = std(yF8)

var_2Fit = var(yF2)
var_4Fit = var(yF4)
var_6Fit = var(yF6)
var_8Fit = var(yF8)

%%
figure(1)
plot(x,yF2_S1)
figure(2)
plot(x,yF2_S2)
figure(3)
plot(x,yF2_S3)

%%
yF2_totalmatrix = ...
    [yF2_S1,yF2_S2,yF2_S3,yF2_S4,yF2_S5,yF2_S6,yF2_S7,yF2_S8,yF2_S9,yF2_S10]
```

```
% ...
    http://matlaboratory.blogspot.co.uk/2015/04/introduction-to-psychometric-curves-and.html

function [coeffs, stats, curve, threshold] = ...
    FitPsycheCurveLogit(xAxis, yData, weights, targets)

% Transpose if necessary
if size(xAxis,1)<size(xAxis,2)
    xAxis=xAxis';
end
if size(yData,1)<size(yData,2)
    yData=yData';
end
if size(weights,1)<size(weights,2)
    weights=weights';
end

% Perform fit
[coeffs, ¬, stats] = ...
    glmfit(xAxis, [yData, weights], 'binomial','link','logit');
% glmfit(xAxis, [yData, weights], 'binomial','link','logit');

% Create a new xAxis with higher resolution
fineX = linspace(min(xAxis),max(xAxis),numel(xAxis)*50);
% Generate curve from fit
curve = glmval(coeffs, fineX, 'logit');
if max(weights)≤1
    % Assume yData was proportional
    curve = [fineX', curve];
else
    % Assume yData was % or actual number of trials
    curve = [fineX', curve*100];
end

% If targets (y) supplied, find threshold (x), else find 25, 50 and 75%
% values
if nargin==4
```

```
else
    targets = [0.25, 0.5, 0.75];
end
% Calculate
threshold = (log(targets./(1-targets))-coeffs(1))/coeffs(2);
```

11.2. Experiment 2

```
%% Results experiment 2: Displacement production and reproduction
% Jorrinde Lambers (4307283)
% Experiments took place: 8/7/2019 - 17/7/2019
clear all
close all
clc
%% Procedure
% 1. Load the data per subject for all the three displacements
% 2. Remove the first 2,5 seconds and the last 0,5 seconds to remove
% transition effects
% 3. Calculate the ADE, RDE and DV per subject for the visual production
% and for the blind reproduction
% 4. Pool all the results of all the subjects together, to find the total
% ADE, RDE and DV.
%% Define variables
target5=5; % target of 5 mm
target10=10; % target of 10 mm
target20=20; % target of 20 mm

%% Load in all the data of all subjects and put it into a matrix
NumberOfParticipants = 10;
Displacements = [5,10,20];
NumberOfDisplacements = 3;
DataMatrix = cell(NumberOfParticipants,NumberOfDisplacements);
for nParticipant = 1 : NumberOfParticipants
    k = 1;
        for displacement = Displacements
            for ndisplacements = 1 : NumberOfDisplacements
            FileName  = ...
                strcat('subject',num2str(nParticipant),'afstand',num2str(displacement),'.txt');
            TempOpenString = string(FileName);
            TempOpen  = fopen(TempOpenString);
            TempData  = textscan(TempOpen,'%f%f%f%f','CollectOutput',1);
            DataMatrix(nParticipant,k) = TempData;
            end
              k = k + 1;
        end
end
%% Match the right row and column to the right subject and displacement
DataSubject1_5 = cell2mat(DataMatrix(1,1));
DataSubject1_10 = cell2mat(DataMatrix(1,2));
DataSubject1_20 = cell2mat(DataMatrix(1,3));

DataSubject2_5 = cell2mat(DataMatrix(2,1));
DataSubject2_10 = cell2mat(DataMatrix(2,2));
DataSubject2_20 = cell2mat(DataMatrix(2,3));

DataSubject3_5 = cell2mat(DataMatrix(3,1));
DataSubject3_10 = cell2mat(DataMatrix(3,2));
DataSubject3_20 = cell2mat(DataMatrix(3,3));

DataSubject4_5 = cell2mat(DataMatrix(4,1));
DataSubject4_10 = cell2mat(DataMatrix(4,2));
DataSubject4_20 = cell2mat(DataMatrix(4,3));

DataSubject5_5 = cell2mat(DataMatrix(5,1));
DataSubject5_10 = cell2mat(DataMatrix(5,2));
DataSubject5_20 = cell2mat(DataMatrix(5,3));

DataSubject6_5 = cell2mat(DataMatrix(6,1));
```

```
DataSubject6_10 = cell2mat(DataMatrix(6,2));
DataSubject6_20 = cell2mat(DataMatrix(6,3));

DataSubject7_5 = cell2mat(DataMatrix(7,1));
DataSubject7_10 = cell2mat(DataMatrix(7,2));
DataSubject7_20 = cell2mat(DataMatrix(7,3));

DataSubject8_5 = cell2mat(DataMatrix(8,1));
DataSubject8_10 = cell2mat(DataMatrix(8,2));
DataSubject8_20 = cell2mat(DataMatrix(8,3));

DataSubject9_5 = cell2mat(DataMatrix(9,1));
DataSubject9_10 = cell2mat(DataMatrix(9,2));
DataSubject9_20 = cell2mat(DataMatrix(9,3));

DataSubject10_5 = cell2mat(DataMatrix(10,1));
DataSubject10_10 = cell2mat(DataMatrix(10,2));
DataSubject10_20 = cell2mat(DataMatrix(10,3));

%% SUBJECT 1
%%%%%%%%%%%%%%%%%%%%%% DISPLACEMENT 5 MM
DataS1V_5=zeros(41,40);
DataS1V_5(:,1:4)=DataSubject1_5(51:91,:); % First 2.5 and last 0.5 seconds are removed
DataS1V_5(:,5:8)=DataSubject1_5(253:293,:);
DataS1V_5(:,9:12)=DataSubject1_5(455:495,:);
DataS1V_5(:,13:16)=DataSubject1_5(657:697,:);
DataS1V_5(:,17:20)=DataSubject1_5(859:899,:);
DataS1V_5(:,21:24)=DataSubject1_5(1061:1101,:);
DataS1V_5(:,25:28)=DataSubject1_5(1263:1303,:);
DataS1V_5(:,29:32)=DataSubject1_5(1465:1505,:);
DataS1V_5(:,33:36)=DataSubject1_5(1667:1707,:);
DataS1V_5(:,37:40)=DataSubject1_5(1869:1909,:);

% ADE
Mean_ADE_S1V_5 = zeros(10,2);
mean=(sum(DataS1V_5(:,2)))/41;
Mean_ADE_S1V_5(1,1)=mean;
Mean_ADE_S1V_5(1,2)=abs(mean-target5);

mean=(sum(DataS1V_5(:,6)))/41;
Mean_ADE_S1V_5(2,1)=mean;
Mean_ADE_S1V_5(2,2)=abs(mean-target5);

mean=(sum(DataS1V_5(:,10)))/41;
Mean_ADE_S1V_5(3,1)=mean;
Mean_ADE_S1V_5(3,2)=abs(mean-target5);

mean=(sum(DataS1V_5(:,14)))/41;
Mean_ADE_S1V_5(4,1)=mean;
Mean_ADE_S1V_5(4,2)=abs(mean-target5);

mean=(sum(DataS1V_5(:,18)))/41;
Mean_ADE_S1V_5(5,1)=mean;
Mean_ADE_S1V_5(5,2)=abs(mean-target5);

mean=(sum(DataS1V_5(:,22)))/41;
Mean_ADE_S1V_5(6,1)=mean;
Mean_ADE_S1V_5(6,2)=abs(mean-target5);

mean=(sum(DataS1V_5(:,26)))/41;
Mean_ADE_S1V_5(7,1)=mean;
Mean_ADE_S1V_5(7,2)=abs(mean-target5);

mean=(sum(DataS1V_5(:,30)))/41;
Mean_ADE_S1V_5(8,1)=mean;
Mean_ADE_S1V_5(8,2)=abs(mean-target5);

mean=(sum(DataS1V_5(:,34)))/41;
Mean_ADE_S1V_5(9,1)=mean;
Mean_ADE_S1V_5(9,2)=abs(mean-target5);

```

```
mean=(sum(DataS1V_5(:,38)))/41;
Mean_ADE_S1V_5(10,1)=mean;
Mean_ADE_S1V_5(10,2)=abs(mean-target5);

totalADE_S1V_5 = sum(Mean_ADE_S1V_5(:,2))/10;

% RDE
RDE_S1V_5=zeros(10,1);
RDE_S1V_5(1,1) = Mean_ADE_S1V_5(1,2)/target5;
RDE_S1V_5(2,1) = Mean_ADE_S1V_5(2,2)/target5;
RDE_S1V_5(3,1) = Mean_ADE_S1V_5(3,2)/target5;
RDE_S1V_5(4,1) = Mean_ADE_S1V_5(4,2)/target5;
RDE_S1V_5(5,1) = Mean_ADE_S1V_5(5,2)/target5;
RDE_S1V_5(6,1) = Mean_ADE_S1V_5(6,2)/target5;
RDE_S1V_5(7,1) = Mean_ADE_S1V_5(7,2)/target5;
RDE_S1V_5(8,1) = Mean_ADE_S1V_5(8,2)/target5;
RDE_S1V_5(9,1) = Mean_ADE_S1V_5(9,2)/target5;
RDE_S1V_5(10,1) = Mean_ADE_S1V_5(10,2)/target5;
totalRDE_S1V_5 = sum(RDE_S1V_5)/10;

% DV
DV_S1V_5=zeros(10,1);
DV_S1V_5(1,1)=std(DataS1V_5(:,2));
DV_S1V_5(2,1)=std(DataS1V_5(:,6));
DV_S1V_5(3,1)=std(DataS1V_5(:,10));
DV_S1V_5(4,1)=std(DataS1V_5(:,14));
DV_S1V_5(5,1)=std(DataS1V_5(:,18));
DV_S1V_5(6,1)=std(DataS1V_5(:,22));
DV_S1V_5(7,1)=std(DataS1V_5(:,26));
DV_S1V_5(8,1)=std(DataS1V_5(:,30));
DV_S1V_5(9,1)=std(DataS1V_5(:,34));
DV_S1V_5(10,1)=std(DataS1V_5(:,38));
totalDV_S1V_5 = sum(DV_S1V_5)/10;

% Blind reproduction (10x)
DataS1B_5=zeros(41,40);
DataS1B_5(:,1:4) = DataSubject1_5(152:192,:);
DataS1B_5(:,5:8)  = DataSubject1_5(354:394,:);
DataS1B_5(:,9:12)  = DataSubject1_5(556:596,:);
DataS1B_5(:,13:16)  = DataSubject1_5(758:798,:);
DataS1B_5(:,17:20)  = DataSubject1_5(960:1000,:);
DataS1B_5(:,21:24)  = DataSubject1_5(1159:1199,:);
DataS1B_5(:,25:28)  = DataSubject1_5(1361:1401,:);
DataS1B_5(:,29:32)  = DataSubject1_5(1563:1603,:);
DataS1B_5(:,33:36)  = DataSubject1_5(1765:1805,:);
DataS1B_5(:,37:40)  = DataSubject1_5(1967:2007,:);

% ADE blind
Mean_ADE_S1B_5 = zeros(10,2);
mean=(sum(DataS1B_5(:,2)))/41;
Mean_ADE_S1B_5(1,1)=mean;
Mean_ADE_S1B_5(1,2)=abs(mean-target5);

mean=(sum(DataS1B_5(:,6)))/41;
Mean_ADE_S1B_5(2,1)=mean;
Mean_ADE_S1B_5(2,2)=abs(mean-target5);

mean=(sum(DataS1B_5(:,10)))/41;
Mean_ADE_S1B_5(3,1)=mean;
Mean_ADE_S1B_5(3,2)=abs(mean-target5);

mean=(sum(DataS1B_5(:,14)))/41;
Mean_ADE_S1B_5(4,1)=mean;
Mean_ADE_S1B_5(4,2)=abs(mean-target5);

mean=(sum(DataS1B_5(:,18)))/41;
Mean_ADE_S1B_5(5,1)=mean;
Mean_ADE_S1B_5(5,2)=abs(mean-target5);

mean=(sum(DataS1B_5(:,22)))/41;
Mean_ADE_S1B_5(6,1)=mean;
```

```
Mean_ADE_S1B_5(6,2)=abs(mean-target5);

mean=(sum(DataS1B_5(:,26)))/41;
Mean_ADE_S1B_5(7,1)=mean;
Mean_ADE_S1B_5(7,2)=abs(mean-target5);

mean=(sum(DataS1B_5(:,30)))/41;
Mean_ADE_S1B_5(8,1)=mean;
Mean_ADE_S1B_5(8,2)=abs(mean-target5);

mean=(sum(DataS1B_5(:,34)))/41;
Mean_ADE_S1B_5(9,1)=mean;
Mean_ADE_S1B_5(9,2)=abs(mean-target5);

mean=(sum(DataS1B_5(:,38)))/41;
Mean_ADE_S1B_5(10,1)=mean;
Mean_ADE_S1B_5(10,2)=abs(mean-target5);

totalADE_S1B_5 = sum(Mean_ADE_S1B_5(:,2))/10;

% RDE
RDE_S1B_5=zeros(10,1);
RDE_S1B_5(1,1) = Mean_ADE_S1B_5(1,2)/target5;
RDE_S1B_5(2,1) = Mean_ADE_S1B_5(2,2)/target5;
RDE_S1B_5(3,1) = Mean_ADE_S1B_5(3,2)/target5;
RDE_S1B_5(4,1) = Mean_ADE_S1B_5(4,2)/target5;
RDE_S1B_5(5,1) = Mean_ADE_S1B_5(5,2)/target5;
RDE_S1B_5(6,1) = Mean_ADE_S1B_5(6,2)/target5;
RDE_S1B_5(7,1) = Mean_ADE_S1B_5(7,2)/target5;
RDE_S1B_5(8,1) = Mean_ADE_S1B_5(8,2)/target5;
RDE_S1B_5(9,1) = Mean_ADE_S1B_5(9,2)/target5;
RDE_S1B_5(10,1) = Mean_ADE_S1B_5(10,2)/target5;
totalRDE_S1B_5 = sum(RDE_S1B_5)/10;

% DV
DV_S1B_5=zeros(10,1);
DV_S1B_5(1,1)=std(DataS1B_5(:,2));
DV_S1B_5(2,1)=std(DataS1B_5(:,6));
DV_S1B_5(3,1)=std(DataS1B_5(:,10));
DV_S1B_5(4,1)=std(DataS1B_5(:,14));
DV_S1B_5(5,1)=std(DataS1B_5(:,18));
DV_S1B_5(6,1)=std(DataS1B_5(:,22));
DV_S1B_5(7,1)=std(DataS1B_5(:,26));
DV_S1B_5(8,1)=std(DataS1B_5(:,30));
DV_S1B_5(9,1)=std(DataS1B_5(:,34));
DV_S1B_5(10,1)=std(DataS1B_5(:,38));
totalDV_S1B_5 = sum(DV_S1B_5)/10;

%%%%%%%%%%%%%%%%%%%%%%%%%%%%%%%%% DISPLACEMENT 10 MM
% Visual production (10x)
DataS1V_10 = zeros(41,40);
DataS1V_10(:,1:4)=DataSubject1_10(51:91,:); % First 2.5 and last 0.5 seconds are removed
DataS1V_10(:,5:8)=DataSubject1_10(253:293,:);
DataS1V_10(:,9:12)=DataSubject1_10(455:495,:);
DataS1V_10(:,13:16)=DataSubject1_10(657:697,:);
DataS1V_10(:,17:20)=DataSubject1_10(859:899,:);
DataS1V_10(:,21:24)=DataSubject1_10(1061:1101,:);
DataS1V_10(:,25:28)=DataSubject1_10(1263:1303,:);
DataS1V_10(:,29:32)=DataSubject1_10(1465:1505,:);
DataS1V_10(:,33:36)=DataSubject1_10(1667:1707,:);
DataS1V_10(:,37:40)=DataSubject1_10(1869:1909,:);

% ADE
Mean_ADE_S1V_10 = zeros(10,2);
mean=(sum(DataS1V_10(:,2)))/41;
Mean_ADE_S1V_10(1,1)=mean;
Mean_ADE_S1V_10(1,2)=abs(mean-target10);

mean=(sum(DataS1V_10(:,6)))/41;
Mean_ADE_S1V_10(2,1)=mean;
Mean_ADE_S1V_10(2,2)=abs(mean-target10);
```

```

mean=(sum(DataS1V_10(:,10)))/41;
Mean_ADE_S1V_10(3,1)=mean;
Mean_ADE_S1V_10(3,2)=abs(mean-target10);

mean=(sum(DataS1V_10(:,14)))/41;
Mean_ADE_S1V_10(4,1)=mean;
Mean_ADE_S1V_10(4,2)=abs(mean-target10);

mean=(sum(DataS1V_10(:,18)))/41;
Mean_ADE_S1V_10(5,1)=mean;
Mean_ADE_S1V_10(5,2)=abs(mean-target10);

mean=(sum(DataS1V_10(:,22)))/41;
Mean_ADE_S1V_10(6,1)=mean;
Mean_ADE_S1V_10(6,2)=abs(mean-target10);

mean=(sum(DataS1V_10(:,26)))/41;
Mean_ADE_S1V_10(7,1)=mean;
Mean_ADE_S1V_10(7,2)=abs(mean-target10);

mean=(sum(DataS1V_10(:,30)))/41;
Mean_ADE_S1V_10(8,1)=mean;
Mean_ADE_S1V_10(8,2)=abs(mean-target10);

mean=(sum(DataS1V_10(:,34)))/41;
Mean_ADE_S1V_10(9,1)=mean;
Mean_ADE_S1V_10(9,2)=abs(mean-target10);

mean=(sum(DataS1V_10(:,38)))/41;
Mean_ADE_S1V_10(10,1)=mean;
Mean_ADE_S1V_10(10,2)=abs(mean-target10);

totalADE_S1V_10 = sum(Mean_ADE_S1V_10(:,2))/10;

% RDE
RDE_S1V_10=zeros(10,1);
RDE_S1V_10(1,1) = Mean_ADE_S1V_10(1,2)/target10;
RDE_S1V_10(2,1) = Mean_ADE_S1V_10(2,2)/target10;
RDE_S1V_10(3,1) = Mean_ADE_S1V_10(3,2)/target10;
RDE_S1V_10(4,1) = Mean_ADE_S1V_10(4,2)/target10;
RDE_S1V_10(5,1) = Mean_ADE_S1V_10(5,2)/target10;
RDE_S1V_10(6,1) = Mean_ADE_S1V_10(6,2)/target10;
RDE_S1V_10(7,1) = Mean_ADE_S1V_10(7,2)/target10;
RDE_S1V_10(8,1) = Mean_ADE_S1V_10(8,2)/target10;
RDE_S1V_10(9,1) = Mean_ADE_S1V_10(9,2)/target10;
RDE_S1V_10(10,1) = Mean_ADE_S1V_10(10,2)/target10;
totalRDE_S1V_10 = sum(RDE_S1V_10)/10;

% DV
DV_S1V_10=zeros(10,1);
DV_S1V_10(1,1)=std(DataS1V_10(:,2));
DV_S1V_10(2,1)=std(DataS1V_10(:,6));
DV_S1V_10(3,1)=std(DataS1V_10(:,10));
DV_S1V_10(4,1)=std(DataS1V_10(:,14));
DV_S1V_10(5,1)=std(DataS1V_10(:,18));
DV_S1V_10(6,1)=std(DataS1V_10(:,22));
DV_S1V_10(7,1)=std(DataS1V_10(:,26));
DV_S1V_10(8,1)=std(DataS1V_10(:,30));
DV_S1V_10(9,1)=std(DataS1V_10(:,34));
DV_S1V_10(10,1)=std(DataS1V_10(:,38));
totalDV_S1V_10 = sum(DV_S1V_10)/10;

% Blind reproduction (10x)
DataS1B_10 = zeros(41,40);
DataS1B_10(:,1:4) = DataSubject1_10(152:192,:);
DataS1B_10(:,5:8) = DataSubject1_10(354:394,:);
DataS1B_10(:,9:12) = DataSubject1_10(556:596,:);
DataS1B_10(:,13:16) = DataSubject1_10(758:798,:);
DataS1B_10(:,17:20) = DataSubject1_10(960:1000,:);
DataS1B_10(:,21:24) = DataSubject1_10(1162:1202,:);
```

```
DataS1B_10(:,25:28) = DataSubject1_10(1364:1404,:);
DataS1B_10(:,29:32) = DataSubject1_10(1566:1606,:);
DataS1B_10(:,33:36) = DataSubject1_10(1768:1808,:);
DataS1B_10(:,37:40) = DataSubject1_10(1970:2010,:);

% ADE blind
Mean_ADE_S1B_10 = zeros(10,2);
mean=(sum(DataS1B_10(:,2)))/41;
Mean_ADE_S1B_10(1,1)=mean;
Mean_ADE_S1B_10(1,2)=abs(mean-target10);

mean=(sum(DataS1B_10(:,6)))/41;
Mean_ADE_S1B_10(2,1)=mean;
Mean_ADE_S1B_10(2,2)=abs(mean-target10);

mean=(sum(DataS1B_10(:,10)))/41;
Mean_ADE_S1B_10(3,1)=mean;
Mean_ADE_S1B_10(3,2)=abs(mean-target10);

mean=(sum(DataS1B_10(:,14)))/41;
Mean_ADE_S1B_10(4,1)=mean;
Mean_ADE_S1B_10(4,2)=abs(mean-target10);

mean=(sum(DataS1B_10(:,18)))/41;
Mean_ADE_S1B_10(5,1)=mean;
Mean_ADE_S1B_10(5,2)=abs(mean-target10);

mean=(sum(DataS1B_10(:,22)))/41;
Mean_ADE_S1B_10(6,1)=mean;
Mean_ADE_S1B_10(6,2)=abs(mean-target10);

mean=(sum(DataS1B_10(:,26)))/41;
Mean_ADE_S1B_10(7,1)=mean;
Mean_ADE_S1B_10(7,2)=abs(mean-target10);

mean=(sum(DataS1B_10(:,30)))/41;
Mean_ADE_S1B_10(8,1)=mean;
Mean_ADE_S1B_10(8,2)=abs(mean-target10);

mean=(sum(DataS1B_10(:,34)))/41;
Mean_ADE_S1B_10(9,1)=mean;
Mean_ADE_S1B_10(9,2)=abs(mean-target10);

mean=(sum(DataS1B_10(:,38)))/41;
Mean_ADE_S1B_10(10,1)=mean;
Mean_ADE_S1B_10(10,2)=abs(mean-target10);

totalADE_S1B_10 = sum(Mean_ADE_S1B_10(:,2))/10;

% RDE
RDE_S1B_10=zeros(10,1);
RDE_S1B_10(1,1) = Mean_ADE_S1B_10(1,2)/target10;
RDE_S1B_10(2,1) = Mean_ADE_S1B_10(2,2)/target10;
RDE_S1B_10(3,1) = Mean_ADE_S1B_10(3,2)/target10;
RDE_S1B_10(4,1) = Mean_ADE_S1B_10(4,2)/target10;
RDE_S1B_10(5,1) = Mean_ADE_S1B_10(5,2)/target10;
RDE_S1B_10(6,1) = Mean_ADE_S1B_10(6,2)/target10;
RDE_S1B_10(7,1) = Mean_ADE_S1B_10(7,2)/target10;
RDE_S1B_10(8,1) = Mean_ADE_S1B_10(8,2)/target10;
RDE_S1B_10(9,1) = Mean_ADE_S1B_10(9,2)/target10;
RDE_S1B_10(10,1) = Mean_ADE_S1B_10(10,2)/target10;
totalRDE_S1B_10 = sum(RDE_S1B_10)/10;

% DV
DV_S1B_10=zeros(10,1);
DV_S1B_10(1,1)=std(DataS1B_10(:,2));
DV_S1B_10(2,1)=std(DataS1B_10(:,6));
DV_S1B_10(3,1)=std(DataS1B_10(:,10));
DV_S1B_10(4,1)=std(DataS1B_10(:,14));
DV_S1B_10(5,1)=std(DataS1B_10(:,18));
DV_S1B_10(6,1)=std(DataS1B_10(:,22));
```

```
DV_S1B_10(7,1)=std(DataS1B_10(:,26));
DV_S1B_10(8,1)=std(DataS1B_10(:,30));
DV_S1B_10(9,1)=std(DataS1B_10(:,34));
DV_S1B_10(10,1)=std(DataS1B_10(:,38));
totalDV_S1B_10 = sum(DV_S1B_10)/10;

%%%%%%%%%%%%%%%%%%%%%%%%%%%%%%%%%%%%%%%%% DISPLACEMENT 20 MM
% Visual production (10x)
DataS1V_20 = zeros(41,40);
DataS1V_20(:,1:4)=DataSubject1_20(51:91,:); % First 2.5 and last 0.5 seconds are removed
DataS1V_20(:,5:8)=DataSubject1_20(253:293,:);
DataS1V_20(:,9:12)=DataSubject1_20(455:495,:);
DataS1V_20(:,13:16)=DataSubject1_20(657:697,:);
DataS1V_20(:,17:20)=DataSubject1_20(859:899,:);
DataS1V_20(:,21:24)=DataSubject1_20(1061:1101,:);
DataS1V_20(:,25:28)=DataSubject1_20(1263:1303,:);
DataS1V_20(:,29:32)=DataSubject1_20(1465:1505,:);
DataS1V_20(:,33:36)=DataSubject1_20(1667:1707,:);
DataS1V_20(:,37:40)=DataSubject1_20(1869:1909,:);

% ADE
Mean_ADE_S1V_20 = zeros(10,2);
mean=(sum(DataS1V_20(:,2)))/41;
Mean_ADE_S1V_20(1,1)=mean;
Mean_ADE_S1V_20(1,2)=abs(mean-target20);

mean=(sum(DataS1V_20(:,6)))/41;
Mean_ADE_S1V_20(2,1)=mean;
Mean_ADE_S1V_20(2,2)=abs(mean-target20);

mean=(sum(DataS1V_20(:,10)))/41;
Mean_ADE_S1V_20(3,1)=mean;
Mean_ADE_S1V_20(3,2)=abs(mean-target20);

mean=(sum(DataS1V_20(:,14)))/41;
Mean_ADE_S1V_20(4,1)=mean;
Mean_ADE_S1V_20(4,2)=abs(mean-target20);

mean=(sum(DataS1V_20(:,18)))/41;
Mean_ADE_S1V_20(5,1)=mean;
Mean_ADE_S1V_20(5,2)=abs(mean-target20);

mean=(sum(DataS1V_20(:,22)))/41;
Mean_ADE_S1V_20(6,1)=mean;
Mean_ADE_S1V_20(6,2)=abs(mean-target20);

mean=(sum(DataS1V_20(:,26)))/41;
Mean_ADE_S1V_20(7,1)=mean;
Mean_ADE_S1V_20(7,2)=abs(mean-target20);

mean=(sum(DataS1V_20(:,30)))/41;
Mean_ADE_S1V_20(8,1)=mean;
Mean_ADE_S1V_20(8,2)=abs(mean-target20);

mean=(sum(DataS1V_20(:,34)))/41;
Mean_ADE_S1V_20(9,1)=mean;
Mean_ADE_S1V_20(9,2)=abs(mean-target20);

mean=(sum(DataS1V_20(:,38)))/41;
Mean_ADE_S1V_20(10,1)=mean;
Mean_ADE_S1V_20(10,2)=abs(mean-target20);

totalADE_S1V_20 = sum(Mean_ADE_S1V_20(:,2))/10;

% RDE
RDE_S1V_20=zeros(10,1);
RDE_S1V_20(1,1) = Mean_ADE_S1V_20(1,2)/target20;
RDE_S1V_20(2,1) = Mean_ADE_S1V_20(2,2)/target20;
RDE_S1V_20(3,1) = Mean_ADE_S1V_20(3,2)/target20;
RDE_S1V_20(4,1) = Mean_ADE_S1V_20(4,2)/target20;
RDE_S1V_20(5,1) = Mean_ADE_S1V_20(5,2)/target20;
```

```
RDE_S1V_20(6,1) = Mean_ADE_S1V_20(6,2)/target20;
RDE_S1V_20(7,1) = Mean_ADE_S1V_20(7,2)/target20;
RDE_S1V_20(8,1) = Mean_ADE_S1V_20(8,2)/target20;
RDE_S1V_20(9,1) = Mean_ADE_S1V_20(9,2)/target20;
RDE_S1V_20(10,1) = Mean_ADE_S1V_20(10,2)/target20;
totalRDE_S1V_20 = sum(RDE_S1V_20)/10;

% DV
DV_S1V_20=zeros(10,1);
DV_S1V_20(1,1)=std(DataS1V_20(:,2));
DV_S1V_20(2,1)=std(DataS1V_20(:,6));
DV_S1V_20(3,1)=std(DataS1V_20(:,10));
DV_S1V_20(4,1)=std(DataS1V_20(:,14));
DV_S1V_20(5,1)=std(DataS1V_20(:,18));
DV_S1V_20(6,1)=std(DataS1V_20(:,22));
DV_S1V_20(7,1)=std(DataS1V_20(:,26));
DV_S1V_20(8,1)=std(DataS1V_20(:,30));
DV_S1V_20(9,1)=std(DataS1V_20(:,34));
DV_S1V_20(10,1)=std(DataS1V_20(:,38));
totalDV_S1V_20 = sum(DV_S1V_20)/10;

% Blind reproduction (10x)
DataS1B_20 = zeros(41,40);
DataS1B_20(:,1:4) = DataSubject1_20(152:192,:);
DataS1B_20(:,5:8) = DataSubject1_20(354:394,:);
DataS1B_20(:,9:12) = DataSubject1_20(556:596,:);
DataS1B_20(:,13:16) = DataSubject1_20(758:798,:);
DataS1B_20(:,17:20) = DataSubject1_20(960:1000,:);
DataS1B_20(:,21:24) = DataSubject1_20(1159:1199,:);
DataS1B_20(:,25:28) = DataSubject1_20(1361:1401,:);
DataS1B_20(:,29:32) = DataSubject1_20(1563:1603,:);
DataS1B_20(:,33:36) = DataSubject1_20(1765:1805,:);
DataS1B_20(:,37:40) = DataSubject1_20(1967:2007,:);

% ADE blind
Mean_ADE_S1B_20 = zeros(10,2);
mean=(sum(DataS1B_20(:,2)))/41;
Mean_ADE_S1B_20(1,1)=mean;
Mean_ADE_S1B_20(1,2)=abs(mean-target20);

mean=(sum(DataS1B_20(:,6)))/41;
Mean_ADE_S1B_20(2,1)=mean;
Mean_ADE_S1B_20(2,2)=abs(mean-target20);

mean=(sum(DataS1B_20(:,10)))/41;
Mean_ADE_S1B_20(3,1)=mean;
Mean_ADE_S1B_20(3,2)=abs(mean-target20);

mean=(sum(DataS1B_20(:,14)))/41;
Mean_ADE_S1B_20(4,1)=mean;
Mean_ADE_S1B_20(4,2)=abs(mean-target20);

mean=(sum(DataS1B_20(:,18)))/41;
Mean_ADE_S1B_20(5,1)=mean;
Mean_ADE_S1B_20(5,2)=abs(mean-target20);

mean=(sum(DataS1B_20(:,22)))/41;
Mean_ADE_S1B_20(6,1)=mean;
Mean_ADE_S1B_20(6,2)=abs(mean-target20);

mean=(sum(DataS1B_20(:,26)))/41;
Mean_ADE_S1B_20(7,1)=mean;
Mean_ADE_S1B_20(7,2)=abs(mean-target20);

mean=(sum(DataS1B_20(:,30)))/41;
Mean_ADE_S1B_20(8,1)=mean;
Mean_ADE_S1B_20(8,2)=abs(mean-target20);

mean=(sum(DataS1B_20(:,34)))/41;
Mean_ADE_S1B_20(9,1)=mean;
Mean_ADE_S1B_20(9,2)=abs(mean-target20);
```

```
mean=(sum(DataS1B_20(:,38)))/41;
Mean_ADE_S1B_20(10,1)=mean;
Mean_ADE_S1B_20(10,2)=abs(mean-target20);

totalADE_S1B_20 = sum(Mean_ADE_S1B_20(:,2))/10;

% RDE
RDE_S1B_20=zeros(10,1);
RDE_S1B_20(1,1) = Mean_ADE_S1B_20(1,2)/target20;
RDE_S1B_20(2,1) = Mean_ADE_S1B_20(2,2)/target20;
RDE_S1B_20(3,1) = Mean_ADE_S1B_20(3,2)/target20;
RDE_S1B_20(4,1) = Mean_ADE_S1B_20(4,2)/target20;
RDE_S1B_20(5,1) = Mean_ADE_S1B_20(5,2)/target20;
RDE_S1B_20(6,1) = Mean_ADE_S1B_20(6,2)/target20;
RDE_S1B_20(7,1) = Mean_ADE_S1B_20(7,2)/target20;
RDE_S1B_20(8,1) = Mean_ADE_S1B_20(8,2)/target20;
RDE_S1B_20(9,1) = Mean_ADE_S1B_20(9,2)/target20;
RDE_S1B_20(10,1) = Mean_ADE_S1B_20(10,2)/target20;
totalRDE_S1B_20 = sum(RDE_S1B_20)/10;

% DV
DV_S1B_20=zeros(10,1);
DV_S1B_20(1,1)=std(DataS1B_20(:,2));
DV_S1B_20(2,1)=std(DataS1B_20(:,6));
DV_S1B_20(3,1)=std(DataS1B_20(:,10));
DV_S1B_20(4,1)=std(DataS1B_20(:,14));
DV_S1B_20(5,1)=std(DataS1B_20(:,18));
DV_S1B_20(6,1)=std(DataS1B_20(:,22));
DV_S1B_20(7,1)=std(DataS1B_20(:,26));
DV_S1B_20(8,1)=std(DataS1B_20(:,30));
DV_S1B_20(9,1)=std(DataS1B_20(:,34));
DV_S1B_20(10,1)=std(DataS1B_20(:,38));
totalDV_S1B_20 = sum(DV_S1B_20)/10;
```

```
%% Make matrices of measurements of all subjects, to see variations
ADE_matrix_V = zeros(10,3); % rows are participants, columns are displacements
ADE_matrix_V(:,1) = [totalADE_S1V_5; totalADE_S2V_5; totalADE_S3V_5; totalADE_S4V_5; ...
    totalADE_S5V_5; totalADE_S6V_5; totalADE_S7V_5; totalADE_S8V_5; totalADE_S9V_5; ...
    totalADE_S10V_5];
ADE_matrix_V(:,2) = [totalADE_S1V_10; totalADE_S2V_10; totalADE_S3V_10; ...
    totalADE_S4V_10; totalADE_S5V_10; totalADE_S6V_10; totalADE_S7V_10; ...
    totalADE_S8V_10; totalADE_S9V_10; totalADE_S10V_10];
ADE_matrix_V(:,3) = [totalADE_S1V_20; totalADE_S2V_20; totalADE_S3V_20; ...
    totalADE_S4V_20; totalADE_S5V_20; totalADE_S6V_10; totalADE_S7V_20; ...
    totalADE_S8V_20; totalADE_S9V_20; totalADE_S10V_20];

ADE_matrix_B = zeros(10,3);
ADE_matrix_B(:,1) = [totalADE_S1B_5; totalADE_S2B_5; totalADE_S3B_5; totalADE_S4B_5; ...
    totalADE_S5B_5; totalADE_S6B_5; totalADE_S7B_5; totalADE_S8B_5; totalADE_S9B_5; ...
    totalADE_S10B_5];
ADE_matrix_B(:,2) = [totalADE_S1B_10; totalADE_S2B_10; totalADE_S3B_10; ...
    totalADE_S4B_10; totalADE_S5B_10; totalADE_S6B_10; totalADE_S7B_10; ...
    totalADE_S8B_10; totalADE_S9B_10; totalADE_S10B_10];
ADE_matrix_B(:,3) = [totalADE_S1B_10; totalADE_S2B_20; totalADE_S3B_20; ...
    totalADE_S4B_20; totalADE_S5B_20; totalADE_S6B_20; totalADE_S7B_20; ...
    totalADE_S8B_20; totalADE_S9B_20; totalADE_S10B_20];

RDE_matrix_V = zeros(10,3);
RDE_matrix_V(:,1) = [totalRDE_S1V_5;totalRDE_S2V_5; totalRDE_S3V_5; ...
    totalRDE_S4V_5;totalRDE_S5V_5; totalRDE_S6V_5; totalRDE_S7V_5; totalRDE_S8V_5; ...
    totalRDE_S9V_5; totalRDE_S10V_5];
RDE_matrix_V(:,2) = [totalRDE_S1V_10;totalRDE_S2V_10; totalRDE_S3V_10; ...
    totalRDE_S4V_10;totalRDE_S5V_10; totalRDE_S6V_10; totalRDE_S7V_10; totalRDE_S8V_10; ...
    totalRDE_S9V_10; totalRDE_S10V_10];
RDE_matrix_V(:,3) = [totalRDE_S1V_20;totalRDE_S2V_20; totalRDE_S3V_20; ...
    totalRDE_S4V_20;totalRDE_S5V_20; totalRDE_S6V_20; totalRDE_S7V_20; totalRDE_S8V_20; ...
    totalRDE_S9V_20; totalRDE_S10V_20];
RDE_matrix_V = RDE_matrix_V*100;
```

```
RDE_matrix_B = zeros(10,3);
RDE_matrix_B(:,1) = [totalRDE_S1B_5;totalRDE_S2B_5; totalRDE_S3B_5; ...
      totalRDE_S4B_5;totalRDE_S5B_5; totalRDE_S6B_5; totalRDE_S7B_5; totalRDE_S8B_5; ...
      totalRDE_S9B_5; totalRDE_S10B_5];
RDE_matrix_B(:,2) = [totalRDE_S1B_10;totalRDE_S2B_10; totalRDE_S3B_10; ...
      totalRDE_S4B_10;totalRDE_S5B_10; totalRDE_S6B_10; totalRDE_S7B_10; totalRDE_S8B_10; ...
      totalRDE_S9B_10; totalRDE_S10B_10];
RDE_matrix_B(:,3) = [totalRDE_S1B_20;totalRDE_S2B_20; totalRDE_S3B_20; ...
      totalRDE_S4B_20;totalRDE_S5B_20; totalRDE_S6B_20; totalRDE_S7B_20; totalRDE_S8B_20; ...
      totalRDE_S9B_20; totalRDE_S10B_20];
RDE_matrix_B = RDE_matrix_B*100;

DV_matrix_V = zeros(10,3);
DV_matrix_V(:,1) = [totalDV_S1V_5; totalDV_S2V_5; totalDV_S3V_5; totalDV_S4V_5; ...
      totalDV_S5V_5; totalDV_S6V_5; totalDV_S7V_5; totalDV_S8V_5; totalDV_S9V_5; ...
      totalDV_S10V_5];
DV_matrix_V(:,2) = [totalDV_S1V_10; totalDV_S2V_10; totalDV_S3V_10; totalDV_S4V_10; ...
      totalDV_S5V_10; totalDV_S6V_10; totalDV_S7V_10; totalDV_S8V_10; totalDV_S9V_10; ...
      totalDV_S10V_10];
DV_matrix_V(:,3) = [totalDV_S1V_20; totalDV_S2V_20; totalDV_S3V_20; totalDV_S4V_20; ...
      totalDV_S5V_20; totalDV_S6V_20; totalDV_S7V_20; totalDV_S8V_20; totalDV_S9V_20; ...
      totalDV_S10V_20];

DV_matrix_B = zeros(10,3);
DV_matrix_B(:,1) = [totalDV_S1B_5; totalDV_S2B_5; totalDV_S3B_5; totalDV_S4B_5; ...
      totalDV_S5B_5; totalDV_S6B_5; totalDV_S7B_5; totalDV_S8B_5; totalDV_S9B_5; ...
      totalDV_S10B_5];
DV_matrix_B(:,2) = [totalDV_S1B_10; totalDV_S2B_10; totalDV_S3B_10; totalDV_S4B_10; ...
      totalDV_S5B_10; totalDV_S6B_10; totalDV_S7B_10; totalDV_S8B_10; totalDV_S9B_10; ...
      totalDV_S10B_10];
DV_matrix_B(:,3) = [totalDV_S1B_20; totalDV_S2B_20; totalDV_S3B_20; totalDV_S4B_20; ...
      totalDV_S5B_20; totalDV_S6B_20; totalDV_S7B_20; totalDV_S8B_20; totalDV_S9B_20; ...
      totalDV_S10B_20];

%% Calculate the total ADE, RDE and DV
% sum and divide by the number of participants
ADE_V = sum(ADE_matrix_V)/10;
ADE_B = sum(ADE_matrix_B)/10;
RDE_V = sum(RDE_matrix_V)/10;
RDE_B = sum(RDE_matrix_B)/10;
DV_V = sum(DV_matrix_V)/10;
DV_B = sum(DV_matrix_B)/10;

%% Create the plots
x = 1:3;
data = [ADE_V; ADE_B];
data_matrix = [ADE_matrix_V; ADE_matrix_B];

x0=10;
y0=10;
width=1200;
height=600;
set(gcf,'position',[x0,y0,width,height])

% ADE
figure(1)
hBar = bar(x, data');
for k1 = 1:size(data,1)
      ctr(k1,:) = bsxfun(@plus, hBar(1).XData, [hBar(k1).XOffset]');
      ydt(k1,:) = hBar(k1).YData;
      set(hBar(1), 'FaceColor', [0.9 0 0])
      set(hBar(2), 'FaceColor', [0 0.5 0.5])
end
hold on
hScatter_ADE_V = gscatter(x-0.14, ADE_matrix_V');
hScatter_ADE_B = gscatter(x+0.14, ADE_matrix_B');
set(hScatter_ADE_V, 'Color', [0.3 0 0],'MarkerSize',25)
set(hScatter_ADE_B, 'Color', [0 0.6 0.8],'MarkerSize',25)
%errorbar(ctr,ydt, c,'.r', 'Color', [0 0 0], 'LineWidth', 3)
set(gca,'xtick', 1:length(ADE_V),'xticklabel', {'5 mm' '10 mm' '20 mm'})
```

```
ax = gca;
ax.FontSize = 22;
xlabel('Displacements (mm)','fontweight','bold','FontSize',26)
ylabel('Absolute displacement error (mm)','fontweight','bold','FontSize',26)
legend([hBar(1),hBar(2),hScatter_ADE_V(1),hScatter_ADE_B(1)],{'Visual feedback', 'Blind ...
    reproduction','Datapoints visual','Datapoints blind'},'FontSize',18, ...
    'Location','northwest')
hold off

datac = [RDE_V; RDE_B];
data_matrixc = [RDE_matrix_V; RDE_matrix_B];

% RDE
figure(2)
set(gcf,'position',[x0,y0,width,height])
hBar = bar(x, datac');
for k1 = 1:size(datac,1)
    ctr(k1,:) = bsxfun(@plus, hBar(1).XData, [hBar(k1).XOffset]');
    ydt(k1,:) = hBar(k1).YData;
    set(hBar(1), 'FaceColor', [0.9 0 0])
    set(hBar(2), 'FaceColor', [0 0.5 0.5])
end
hold on
hScatter_RDE_V = gscatter(x-0.14, RDE_matrix_V');
hScatter_RDE_B = gscatter(x+0.14, RDE_matrix_B');
set(hScatter_RDE_V, 'Color', [0.3 0 0],'MarkerSize',25)
set(hScatter_RDE_B, 'Color', [0 0.6 0.8],'MarkerSize',25)
%errorbar(ctr,ydt, c,'.r', 'Color', [0 0 0], 'LineWidth', 3)
set(gca,'xtick', 1:length(RDE_V),'xticklabel', {'5 mm' '10 mm' '20 mm'})
ax = gca;
ax.FontSize = 22;
xlabel('Displacements (mm)','fontweight','bold','FontSize',26)
ylabel('Relative displacement error (%)','fontweight','bold','FontSize',26)
%title('{\bf Relative Displacement Error (RDE)}','fontsize',15)
legend([hBar(1),hBar(2),hScatter_RDE_V(1),hScatter_RDE_B(1)],{'Visual feedback', 'Blind ...
    reproduction','Datapoints visual','Datapoints blind'},'FontSize',18, ...
    'Location','northwest')
hold off

datad = [DV_V; DV_B];
data_matrixd = [DV_matrix_V; DV_matrix_B];

% DV
figure(3)
set(gcf,'position',[x0,y0,width,height])
hBar = bar(x, datad');
for k1 = 1:size(datad,1)
    ctr(k1,:) = bsxfun(@plus, hBar(1).XData, [hBar(k1).XOffset]');
    ydt(k1,:) = hBar(k1).YData;
    set(hBar(1), 'FaceColor', [0.9 0 0])
    set(hBar(2), 'FaceColor', [0 0.5 0.5])
end
hold on
hScatter_DV_V = gscatter(x-0.14, DV_matrix_V');
hScatter_DV_B = gscatter(x+0.14, DV_matrix_B');
set(hScatter_DV_V, 'Color', [0.3 0 0],'MarkerSize',25)
set(hScatter_DV_B, 'Color', [0 0.6 0.8],'MarkerSize',25)
%errorbar(ctr,ydt, d,'.r', 'Color', [0 0 0], 'LineWidth', 3)
set(gca,'xtick', 1:length(DV_V),'xticklabel', {'5 mm' '10 mm' '20 mm'})
ax = gca;
ax.FontSize = 22;
xlabel('Displacements (mm)','fontweight','bold','FontSize',26)
ylabel('Displacement variability (mm)','fontweight','bold','FontSize',26)
%title('{\bf Displacement Variability (DV)}','fontsize',15)
legend([hBar(1),hBar(2),hScatter_DV_V(1),hScatter_DV_B(1)],{'Visual feedback', 'Blind ...
    reproduction','Datapoints visual','Datapoints blind'},'FontSize',18, ...
    'Location','northwest')
%legend({'Visual feedback', 'Blind reproduction'},'FontSize',18, 'Location','northwest')
hold off

%% Calculate the Standard Error (SE) and Standard Deviation (SD)
```

```
STD_ADE_V = std(ADE_matrix_V);
STD_ADE_B = std(ADE_matrix_B);

STD_RDE_V = std(RDE_matrix_V);
STD_RDE_B = std(RDE_matrix_B);

STD_DV_V = std(DV_matrix_V);
STD_DV_B = std(DV_matrix_B);

errorADE_V = STD_ADE_V / sqrt(10);
errorADE_B = STD_ADE_B / sqrt(10);
errorRDE_V = STD_RDE_V / sqrt(10);
errorRDE_B = STD_RDE_B / sqrt(10);
errorDV_V = STD_DV_V / sqrt(10);
errorDV_B = STD_DV_B / sqrt(10);
```

```
%% Calculate the speed of the first second for all the displacements to check stick&slip
%% Subject 1
% Displacement 5 mm
DataStickSlip_S1_5 = zeros(21,40);
DataStickSlip_S1_5(:,1:4)=DataSubject1_5(1:21,:);
DataStickSlip_S1_5(:,5:8)=DataSubject1_5(203:223,:);
DataStickSlip_S1_5(:,9:12)=DataSubject1_5(405:425,:);
DataStickSlip_S1_5(:,13:16)=DataSubject1_5(607:627,:);
DataStickSlip_S1_5(:,17:20)=DataSubject1_5(809:829,:);
DataStickSlip_S1_5(:,21:24)=DataSubject1_5(1011:1031,:);
DataStickSlip_S1_5(:,25:28)=DataSubject1_5(1213:1233,:);
DataStickSlip_S1_5(:,29:32)=DataSubject1_5(1415:1435,:);
DataStickSlip_S1_5(:,33:36)=DataSubject1_5(1617:1637,:);
DataStickSlip_S1_5(:,37:40)=DataSubject1_5(1819:1839,:);

Speed_S1_5 = zeros(10,1); % in mm per sec
Speed_S1_5(1,1)=(DataStickSlip_S1_5(21,2)-DataStickSlip_S1_5(1,2));
Speed_S1_5(2,1)=(DataStickSlip_S1_5(21,6)-DataStickSlip_S1_5(1,6));
Speed_S1_5(3,1)=(DataStickSlip_S1_5(21,10)-DataStickSlip_S1_5(1,10));
Speed_S1_5(4,1)=(DataStickSlip_S1_5(21,14)-DataStickSlip_S1_5(1,14));
Speed_S1_5(5,1)=(DataStickSlip_S1_5(21,18)-DataStickSlip_S1_5(1,18));
Speed_S1_5(6,1)=(DataStickSlip_S1_5(21,22)-DataStickSlip_S1_5(1,22));
Speed_S1_5(7,1)=(DataStickSlip_S1_5(21,26)-DataStickSlip_S1_5(1,26));
Speed_S1_5(8,1)=(DataStickSlip_S1_5(21,30)-DataStickSlip_S1_5(1,30));
Speed_S1_5(9,1)=(DataStickSlip_S1_5(21,34)-DataStickSlip_S1_5(1,34));
Speed_S1_5(10,1)=(DataStickSlip_S1_5(21,38)-DataStickSlip_S1_5(1,38));

meanSpeedS1_5 = (sum(Speed_S1_5))/10;

% Displacement 20 mm
DataStickSlip_S1_20 = zeros(21,40);
DataStickSlip_S1_20(:,1:4)=DataSubject1_20(1:21,:);
DataStickSlip_S1_20(:,5:8)=DataSubject1_20(203:223,:);
DataStickSlip_S1_20(:,9:12)=DataSubject1_20(405:425,:);
DataStickSlip_S1_20(:,13:16)=DataSubject1_20(607:627,:);
DataStickSlip_S1_20(:,17:20)=DataSubject1_20(809:829,:);
DataStickSlip_S1_20(:,21:24)=DataSubject1_20(1011:1031,:);
DataStickSlip_S1_20(:,25:28)=DataSubject1_20(1213:1233,:);
DataStickSlip_S1_20(:,29:32)=DataSubject1_20(1415:1435,:);
DataStickSlip_S1_20(:,33:36)=DataSubject1_20(1617:1637,:);
DataStickSlip_S1_20(:,37:40)=DataSubject1_20(1819:1839,:);

Speed_S1_20 = zeros(10,1);
Speed_S1_20(1,1)=(DataStickSlip_S1_20(21,2)-DataStickSlip_S1_20(1,2));
Speed_S1_20(2,1)=(DataStickSlip_S1_20(21,6)-DataStickSlip_S1_20(1,6));
Speed_S1_20(3,1)=(DataStickSlip_S1_20(21,10)-DataStickSlip_S1_20(1,10));
Speed_S1_20(4,1)=(DataStickSlip_S1_20(21,14)-DataStickSlip_S1_20(1,14));
Speed_S1_20(5,1)=(DataStickSlip_S1_20(21,18)-DataStickSlip_S1_20(1,18));
Speed_S1_20(6,1)=(DataStickSlip_S1_20(21,22)-DataStickSlip_S1_20(1,22));
Speed_S1_20(7,1)=(DataStickSlip_S1_20(21,26)-DataStickSlip_S1_20(1,26));
Speed_S1_20(8,1)=(DataStickSlip_S1_20(21,30)-DataStickSlip_S1_20(1,30));
Speed_S1_20(9,1)=(DataStickSlip_S1_20(21,34)-DataStickSlip_S1_20(1,34));
Speed_S1_20(10,1)=(DataStickSlip_S1_20(21,38)-DataStickSlip_S1_20(1,38));
```

```

meanSpeedS1_20 = (sum(Speed_S1_20))/10;
```

```
%% Pool data
% 5 mm
Speed_5 = ...
    [meanSpeedS1_5;meanSpeedS2_5;meanSpeedS3_5;meanSpeedS4_5;meanSpeedS5_5;meanSpeedS6_5;meanSpeedS7_5;meanS
TotalMeanSpeed_5 = sum(Speed_5)/10

% 20 mm
Speed_20 = ...
    [meanSpeedS1_20;meanSpeedS2_20;meanSpeedS3_20;meanSpeedS4_20;meanSpeedS5_20;meanSpeedS6_20;meanSpeedS7_2
TotalMeanSpeed_20 = sum(Speed_20)/10
```

```
%% Remove one outlier (subject 10)
ADE_matrix_V = zeros(9,3); % rows are participants, columns are displacements
ADE_matrix_V(:,1) = [totalADE_S1V_5; totalADE_S2V_5; totalADE_S3V_5; totalADE_S4V_5; ...
    totalADE_S5V_5; totalADE_S6V_5; totalADE_S7V_5; totalADE_S8V_5; totalADE_S9V_5];
ADE_matrix_V(:,2) = [totalADE_S1V_10; totalADE_S2V_10; totalADE_S3V_10; ...
    totalADE_S4V_10; totalADE_S5V_10; totalADE_S6V_10; totalADE_S7V_10; ...
    totalADE_S8V_10; totalADE_S9V_10];
ADE_matrix_V(:,3) = [totalADE_S1V_20; totalADE_S2V_20; totalADE_S3V_20; ...
    totalADE_S4V_20; totalADE_S5V_20; totalADE_S6V_10; totalADE_S7V_20; ...
    totalADE_S8V_20; totalADE_S9V_20];

ADE_matrix_B = zeros(9,3);
ADE_matrix_B(:,1) = [totalADE_S1B_5; totalADE_S2B_5; totalADE_S3B_5; totalADE_S4B_5; ...
    totalADE_S5B_5; totalADE_S6B_5; totalADE_S7B_5; totalADE_S8B_5; totalADE_S9B_5];
ADE_matrix_B(:,2) = [totalADE_S1B_10; totalADE_S2B_10; totalADE_S3B_10; ...
    totalADE_S4B_10; totalADE_S5B_10; totalADE_S6B_10; totalADE_S7B_10; ...
    totalADE_S8B_10; totalADE_S9B_10];
ADE_matrix_B(:,3) = [totalADE_S1B_10; totalADE_S2B_20; totalADE_S3B_20; ...
    totalADE_S4B_20; totalADE_S5B_20; totalADE_S6B_20; totalADE_S7B_20; ...
    totalADE_S8B_20; totalADE_S9B_20];

RDE_matrix_V = zeros(9,3);
RDE_matrix_V(:,1) = [totalRDE_S1V_5;totalRDE_S2V_5; totalRDE_S3V_5; ...
    totalRDE_S4V_5;totalRDE_S5V_5; totalRDE_S6V_5; totalRDE_S7V_5; totalRDE_S8V_5; ...
    totalRDE_S9V_5];
RDE_matrix_V(:,2) = [totalRDE_S1V_10;totalRDE_S2V_10; totalRDE_S3V_10; ...
    totalRDE_S4V_10;totalRDE_S5V_10; totalRDE_S6V_10; totalRDE_S7V_10; totalRDE_S8V_10; ...
    totalRDE_S9V_10];
RDE_matrix_V(:,3) = [totalRDE_S1V_20;totalRDE_S2V_20; totalRDE_S3V_20; ...
    totalRDE_S4V_20;totalRDE_S5V_20; totalRDE_S6V_20; totalRDE_S7V_20; totalRDE_S8V_20; ...
    totalRDE_S9V_20];
RDE_matrix_V = RDE_matrix_V*100;

RDE_matrix_B = zeros(9,3);
RDE_matrix_B(:,1) = [totalRDE_S1B_5;totalRDE_S2B_5; totalRDE_S3B_5; ...
    totalRDE_S4B_5;totalRDE_S5B_5; totalRDE_S6B_5; totalRDE_S7B_5; totalRDE_S8B_5; ...
    totalRDE_S9B_5];
RDE_matrix_B(:,2) = [totalRDE_S1B_10;totalRDE_S2B_10; totalRDE_S3B_10; ...
    totalRDE_S4B_10;totalRDE_S5B_10; totalRDE_S6B_10; totalRDE_S7B_10; totalRDE_S8B_10; ...
    totalRDE_S9B_10];
RDE_matrix_B(:,3) = [totalRDE_S1B_20;totalRDE_S2B_20; totalRDE_S3B_20; ...
    totalRDE_S4B_20;totalRDE_S5B_20; totalRDE_S6B_20; totalRDE_S7B_20; totalRDE_S8B_20; ...
    totalRDE_S9B_20];
RDE_matrix_B = RDE_matrix_B*100;

DV_matrix_V = zeros(9,3);
DV_matrix_V(:,1) = [totalDV_S1V_5; totalDV_S2V_5; totalDV_S3V_5; totalDV_S4V_5; ...
    totalDV_S5V_5; totalDV_S6V_5; totalDV_S7V_5; totalDV_S8V_5; totalDV_S9V_5];
DV_matrix_V(:,2) = [totalDV_S1V_10; totalDV_S2V_10; totalDV_S3V_10; totalDV_S4V_10; ...
    totalDV_S5V_10; totalDV_S6V_10; totalDV_S7V_10; totalDV_S8V_10; totalDV_S9V_10];
DV_matrix_V(:,3) = [totalDV_S1V_20; totalDV_S2V_20; totalDV_S3V_20; totalDV_S4V_20; ...
    totalDV_S5V_20; totalDV_S6V_20; totalDV_S7V_20; totalDV_S8V_20; totalDV_S9V_20];

```

```
DV_matrix_B = zeros(9,3);
DV_matrix_B(:,1) = [totalDV_S1B_5; totalDV_S2B_5; totalDV_S3B_5; totalDV_S4B_5; ...
    totalDV_S5B_5; totalDV_S6B_5; totalDV_S7B_5; totalDV_S8B_5; totalDV_S9B_5];
DV_matrix_B(:,2) = [totalDV_S1B_10; totalDV_S2B_10; totalDV_S3B_10; totalDV_S4B_10; ...
    totalDV_S5B_10; totalDV_S6B_10; totalDV_S7B_10; totalDV_S8B_10; totalDV_S9B_10];
DV_matrix_B(:,3) = [totalDV_S1B_20; totalDV_S2B_20; totalDV_S3B_20; totalDV_S4B_20; ...
    totalDV_S5B_20; totalDV_S6B_20; totalDV_S7B_20; totalDV_S8B_20; totalDV_S9B_20];

ADE_V = sum(ADE_matrix_V)/9;
ADE_B = sum(ADE_matrix_B)/9;
RDE_V = sum(RDE_matrix_V)/9;
RDE_B = sum(RDE_matrix_B)/9;
DV_V = sum(DV_matrix_V)/9;
DV_B = sum(DV_matrix_B)/9;

x = 1:3;
data = [ADE_V; ADE_B];
data_matrix = [ADE_matrix_V(1:9); ADE_matrix_B(1:9)];

x0=10;
y0=10;
width=1200;
height=600;
set(gcf,'position',[x0,y0,width,height])

% ADE
figure(1)
hBar = bar(x, data');
for k1 = 1:size(data,1)
    ctr(k1,:) = bsxfun(@plus, hBar(1).XData, [hBar(k1).XOffset]');
    ydt(k1,:) = hBar(k1).YData;
    set(hBar(1), 'FaceColor', [0.9 0 0])
    set(hBar(2), 'FaceColor', [0 0.5 0.5])
end
hold on
hScatter_ADE_V = gscatter(x-0.14, ADE_matrix_V');
hScatter_ADE_B = gscatter(x+0.14, ADE_matrix_B');
set(hScatter_ADE_V, 'Color', [0.3 0 0],'MarkerSize',25)
set(hScatter_ADE_B, 'Color', [0 0.6 0.8],'MarkerSize',25)
%errorbar(ctr,ydt, c,'.r', 'Color', [0 0 0], 'LineWidth', 3)
set(gca,'xtick', 1:length(ADE_V),'xticklabel', {'5 mm' '10 mm' '20 mm'})
ax = gca;
ax.FontSize = 22;
xlabel('Displacements (mm)','fontweight','bold','FontSize',26)
ylabel('Absolute displacement error (mm)','fontweight','bold','FontSize',26)
legend([hBar(1),hBar(2),hScatter_ADE_V(1),hScatter_ADE_B(1)],{'Visual feedback', 'Blind ...
    reproduction','Datapoints visual','Datapoints blind'},'FontSize',18, ...
    'Location','northwest')
hold off

datac = [RDE_V; RDE_B];
data_matrixc = [RDE_matrix_V; RDE_matrix_B];

% RDE
figure(2)
set(gcf,'position',[x0,y0,width,height])
hBar = bar(x, datac');
for k1 = 1:size(datac,1)
    ctr(k1,:) = bsxfun(@plus, hBar(1).XData, [hBar(k1).XOffset]');
    ydt(k1,:) = hBar(k1).YData;
    set(hBar(1), 'FaceColor', [0.9 0 0])
    set(hBar(2), 'FaceColor', [0 0.5 0.5])
end
hold on
hScatter_RDE_V = gscatter(x-0.14, RDE_matrix_V');
hScatter_RDE_B = gscatter(x+0.14, RDE_matrix_B');
set(hScatter_RDE_V, 'Color', [0.3 0 0],'MarkerSize',25)
set(hScatter_RDE_B, 'Color', [0 0.6 0.8],'MarkerSize',25)
%errorbar(ctr,ydt, c,'.r', 'Color', [0 0 0], 'LineWidth', 3)
set(gca,'xtick', 1:length(RDE_V),'xticklabel', {'5 mm' '10 mm' '20 mm'})
ax = gca;
```

```
ax.FontSize = 22;
xlabel('Displacements (mm)','fontweight','bold','FontSize',26)
ylabel('Relative displacement error (%)','fontweight','bold','FontSize',26)
%title('{\bf Relative Displacement Error (RDE)}','fontsize',15)
legend([hBar(1),hBar(2),hScatter_RDE_V(1),hScatter_RDE_B(1)],{'Visual feedback', 'Blind ...
    reproduction','Datapoints visual','Datapoints blind'},'FontSize',18, ...
    'Location','northwest')
hold off

datad = [DV_V; DV_B];
data_matrixd = [DV_matrix_V; DV_matrix_B];

% DV
figure(3)
set(gcf,'position',[x0,y0,width,height])
hBar = bar(x, datad');
for k1 = 1:size(datad,1)
    ctr(k1,:) = bsxfun(@plus, hBar(1).XData, [hBar(k1).XOffset]');
    ydt(k1,:) = hBar(k1).YData;
    set(hBar(1), 'FaceColor', [0.9 0 0])
    set(hBar(2), 'FaceColor', [0 0.5 0.5])
end
hold on
hScatter_DV_V = gscatter(x-0.14, DV_matrix_V');
hScatter_DV_B = gscatter(x+0.14, DV_matrix_B');
set(hScatter_DV_V, 'Color', [0.3 0 0],'MarkerSize',25)
set(hScatter_DV_B, 'Color', [0 0.6 0.8],'MarkerSize',25)
%errorbar(ctr,ydt, d,'.r', 'Color', [0 0 0], 'LineWidth', 3)
set(gca,'xtick', 1:length(DV_V),'xticklabel', {'5 mm' '10 mm' '20 mm'})
ax = gca;
ax.FontSize = 22;
xlabel('Displacements (mm)','fontweight','bold','FontSize',26)
ylabel('Displacement variability (mm)','fontweight','bold','FontSize',26)
%title('{\bf Displacement Variability (DV)}','fontsize',15)
legend([hBar(1),hBar(2),hScatter_DV_V(1),hScatter_DV_B(1)],{'Visual feedback', 'Blind ...
    reproduction','Datapoints visual','Datapoints blind'},'FontSize',18, ...
    'Location','northwest')
%legend({'Visual feedback', 'Blind reproduction'},'FontSize',18, 'Location','northwest')
hold off
```

References

[1] Body-powered prostheses. *Retrieved from: http://www.upperlimbprosthetics.info/index.php?p=*$1_{9_B}ody - Powered,$ 2019.

[2] P.G. Agache, C. Monneur, J.L. Leveque, and J. De Rigal. Mechanical properties and young's modulus of human skin in vivo. *Archives of Dermatological Research*, 269:221–232, 1980.

[3] C. Antfolk, M. D'Alonzo, B. Rosén, G. Lundborg, F. Sebelius, and C. Cipriani. Sensory feedback in upper limb prosthetics. *Expert Reviews of Medical Devices*, 0(1):45–54, 2013.

[4] Elaine A. Biddiss, D. Beaton, and Tom T. Chau. Consumer design priorities for upper limb prosthetics. *Disability and Rehabilitation: Assistive Technology*, 2(6):346–357, 2007.

[5] DINED. Dutch adults 2004, age 20-60, male and female. *Retrieved from https://dined.io.tudelft.nl/en/database/tool*, 2004.

[6] S. Diridollou, V. Vabre, M. Berson, I. Vaillant, D. Black, J.M. Lagarde, J.M. Grégoire, Y. Gall, and F. Patat. Skin ageing: changes of physical properties of human skin in vivo. *International Journal of Cosmetic Science*, 23:353–362, 2001.

[7] G. Dover and M.E. Powers. Reliability of joint position sense and force-reproduction measures during internal and external rotation of the shoulder. *Journal of Athletic Training*, 38(4):304–310, 2003.

[8] R.M. Enoka and J. Duchateau. Muscle fatigue: what, why and how it influences muscle function. *Journal Physiology*, pages 11–23, 2008.

[9] Festo. Proportional pressure regulators VEAA. *Retrieved from https://www.festo.com/cat/*$nl_n l/products_V EAA,$ 2019.

[10] S. Feyzabadi, S. Straube, M. Folgheraiter, E.A. Kirchner, S.K. Kim, and J.C. Albiez. Human force discrimination during active arm motion force feedback design. *IEEE Transactions on Haptics*, 6(3):309–319, 2013.

[11] M. Hichert. User capacities and operation forces. Requirements for body-powered upper-limb prostheses. *https://doi.org/10.4233/uuid:f46c5e6e-a21c-4bc2-b8ca-6175897e60e5*, 2017.

[12] A.L. Hicks, J. Kent-Braun, and D.S. Ditor. Sex differences in human skeletal muscle fatigue. *Exercise and Sport Sciences Reviews*, 29(3):109–112, 2001.

[13] S.H. Hussain, B. Limthongkui, and T.R. Humphreys. The biomechanical properties of the skin. *Dermatologic Surgery*, 39(2):193–203, 2013.

[14] K. Keller and M. Engelhardt. Strength and muscle mass loss with aging process. age and strength loss. *Muscles, Ligaments and Tendons Journal*, 3(4):346–350, 2013.

[15] F.P. Kendall and E.K. McCreary. Spieren. 2e druk, 1986.

[16] J.A. Kent-Braun, A.V. NG, J.W. Doyle, and T.F. Towse. Human skeletal muscle responses vary with age and gender during fatigue due to incremental isometric exercise. *Journal of Applied Physiology*, 93:1813–1823, 2002.

[17] Jones. L.A. and I.W. Hunter. Force sensation in isometric contractions: a relative force effect. *Brain Research*, 244:186–189, 1982.

[18] D. Latour, T. Sabolevski, and K. Lajoie-Weaver. Ipsilateral scapular cutaneous anchor. *Prooceedings of the 12th world congress of the International Society for Prosthetics and Orthotics*, page 555, 2007.

[19] D. A. Latour. Method for anchoring prosthetic and orthotic devices. *US8821588 B2 Patent*, 2014.

[20] Pyshio Logic. 5 exercises to improve scapular stabilization and prevent elbow, wrist and hand injuries.

[21] E.N. Marieb and K. Hoehn. *Human Anatomy Physiology*. Pearson Education Limited, tenth edition, 2016.

[22] M.L. McHugh. Standard error: meaning and interpretation. *Biochemia Medica*, 18(1): 7–13, 2008.

[23] Micro-epsilon. Sensors systems: Authority in displacement measurement.

[24] H. Monod. Contractility of muscle during prolonged static and repetitive dynamic activity. *Ergonomics*, 28(1):81–89, 1985.

[25] D.H. Plettenburg. A sizzling hand prosthesis: On the design and development of a pneumatically powered hand prosthesis for children. *PhD-thesis*, 2002.

[26] B. Radocy. Trs product catalog. page 32, 2018.

[27] F. Ribeiro and J. Oliveira. Factors influencing proprioception: What do they reveal? *Biomechanics in Applications*, ISBN: 978-953-307-969-1, 2011.

[28] H.S. Ryu, Y.H. Joo, S.O. Kim, K.C. Park, and S.W. Youn. Influence of age and regional differences on skin elasticity as measured by the cutometer. *Skin Research and Technology*, 14:354–358, 2008.

[29] J.I. Salles, B. Velasques, V. Cossich, E. Nicoliche, P. Ribeiro, M.V. Amaral, and G. Motta. Strength training and shoulder proprioception. *Journal of Athletic Training*, 50(3):277–280, 2015.

[30] S. Shimada, K. Fukuda, and K. Hiraki. Rubber hand illusion under delayed visual feedback. *PLoS one*, 4(7), 2009.

[31] G. Smit and D.H. Plettenburg. Efficiency of voluntary closing hand and hook prostheses. *Prosthetics and Orthotics International*, 34(4):411–427, 2010.

[32] G. Smit, D.H. Plettenburg, and F.C.T. Van der Helm. The lightweight delft cylinder hand, the first multi-articulating hand that meets the basic user requirements. *IEEE*, 2014.

[33] A.G.C. Van Boeijen, J.J. Daalhuizen, J.J.M. Zijlstra, and R.S.A. Van der Schoor. Delft design guide. 2013.

[34] A.N. Vardy and D.H. Plettenburg. Control locations for harnesses used in upper limb prostheses. *MEC14- Redefining the Norm*, pages 271–274, 2014.

[35] A.N. Vardy, M. Boone, and D.H. Plettenburg. Perceptual and control properties of a haptic upper-limb prosthetic interface. *MEC17 - A Sense of What's to Come*, 2017.

[36] H. Wirtl and U. Sixt. Piezo technology in pneumatic valves. *Retrieved from https://www.festo.com/net/SupportPortal/Files/346243/*$White_Paper_Piezo_EN.pdf$, 2017.

PART III

Literature study

A Pneumatic Force Transducer

Lambers, J.A.L.
Delft University of Technology

Abstract

Introduction: Body-powered prostheses are usually controlled via a harness. This design is often problematic as it is mostly uncomfortable. The Ipsilateral Scapular Cutaneous Anchor System has been designed as an alternative, where the harness is removed from the prosthesis. It shows a promising solution. However, the design still needs to be improved. It would be desirable to create a wireless system. This system needs to be placed on the back of the user, and therefore needs to be lightweight. It is thus chosen to use a pneumatic actuator.
Objective: The aim of this essay was to provide a complete overview of pneumatic actuators that are available. It was then checked whether the different actuators meet the requirements that were set. These requirements have been set, so that it can be checked whether the system is suitable for the design in the masters thesis; a pneumatic force transducer.
Study design: Literature review.
Methods: The databases of Scopus, Web Of Science and Google Patents were used. The research was divided into two main groups. The results of the first group represent all the pneumatic actuators available. The second group provides an overview of how force feedback can be provided.
Results: The pneumatic force transducer had to be lightweight, small, and should be able to provide a force of 50 N. The two most important groups were the McKibben muscles and Pneumatic Balloon Actuators (PBA). McKibben muscles are actuators that consist of a rubber tube with an outside sleeve and will contract when pressurized. Pneumatic Balloon Actuators (PBA) are small balloons that inflate when pressurized.
Conclusion: It can be concluded that a McKibben muscle actuator is a suitable system for the design of a pneumatic force transducer. Another system, the flexible active skin, shows to be suitable. Both these systems meet most of the requirements. To provide force feedback to the user, proprioceptive feedback will be integrated instead of tactile feedback.

body-powered prosthesis - pneumatic actuators - force control - force feedback - tactile feedback - proprioceptive feedback

1. Introduction

A body-powered prosthesis includes a harness, through which the user controls his/her device. The system provides force feedback through the harness, which is one of the main advantages of a body-powered prosthesis compared to other upper-limb prostheses.

Nonetheless, abandonment rates are high, namely up to 45%. According to a literature review on the use and abandonment of upper limb prostheses by Biddiss and Chau [14], subjects complained about discomfort, wire failure, abrasion of clothes and excessive wear temperatures. The discomfort is caused by the harness as it induces skin irritation. Biddiss et al. [15] also performed a different study on consumer design priorities for upper limb prostheses. It was concluded that for a body-powered hook, function and comfort were of most importance for users.

In literature, several options have been explored to overcome the problems mentioned and to design a more comfortable and durable body harness. An example is the axilla bypass ring, which relieves the irritation in the armpit [22]. This ring supports the armpit, to prevent the cables from sliding. In an alternative solution, the direction of the cables is changed, in order to remove irritations at certain areas.

A prosthesis of WILMER is a design where the prosthesis is controlled with the motions of the elbow instead of the shoulder [68]. In this way, no wires will be present on the back and shoulder. However, this solution is only usable for below-elbow defects.

Latour [52] came with a solution to remove the harness by designing a system that is attached to the scapula, see Figure 1. This design was called The Ipsilateral Scapular Cutaneous Anchor System [51]. The Anchor System is attached to the prosthesis via a wire.

A study by Hichert and Plettenburg [43], showed how this anchoring system performed comparable to the traditional body-powered harness. It was concluded that The Anchor System performs equally good in terms of perception and control. Therefore, it offers an alternative for the conventional body-powered prosthesis. However, more research and further improvements on the design are required. Criteria for this new design will be mentioned in this chapter after the research question is posed.

Figure 1: The Ipsilateral Scapular Cutaneous Anchor System [72].

To improve the anchoring system, it is preferred to redesign the harness and to lower the forces that are needed to control the prosthesis. Ideally, a body-powered prosthesis without any cables would be the solution. To accomplish this, a wireless connection between the prosthesis and force system should be present. In the masters thesis, a new version of the Anchor system will be designed. Figure 2 shows a schematic overview of the system that will be designed. It can be seen that the total system consists of a prosthesis and an apparatus, that will measure the displacement and will act as a force transducer. The system controls a prosthesis without any wires, which will be called 'Control loop 1'. The second control loop, 'Control loop 2', is the feedback from the prosthesis to the transducer. The importance of feedback will be explained later on.

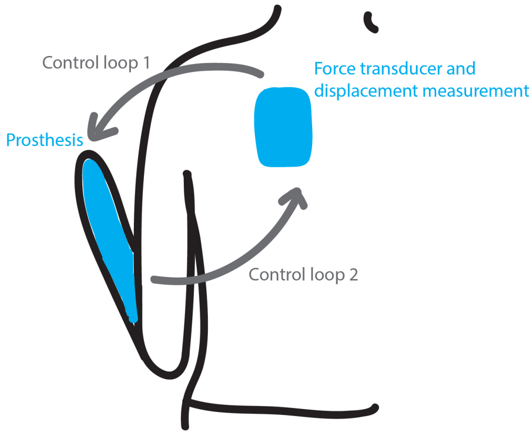

Figure 2: A schematic overview of the system that will be designed in the masters thesis. It consists of a pneumatic force transducer, that will also measure the displacement, and will control the prosthesis. This is Control loop 1. Control loop 2 will be the feedback from the prosthesis to the transducer.

As was stated before, the system will be wireless and needs to be placed on the back of the user. This means that it should be lightweight. Therefore, it is chosen to use a pneumatic actuator. Pneumatic actuators convert the energy of compressed gas into mechanical energy. This gas can be air or for example CO_2. Pistecky [67] used miniature CO_2 storage systems to provide a prosthesis with gas.

A pneumatic system is a relative simple technology and low of cost [7]. Furthermore, pneumatic systems are notably safer as compared to for example hydraulics and electronics. With hydraulics, care needs to be taken when chemical fluids are used. With electrical systems, attention should be paid that there are no sparks arising. A pneumatic system only uses gas and no other chemical fluids, thus making it the safest option [65].

An evaluation on pneumatic actuators done by Peerdeman et al. [66] shows that a pneumatic system can surpass electrical systems, with the correct design. It has a small size, and is lightweight. However, it is mentioned that a pneumatic cylinder can be difficult to control. This is caused by air compressibility, friction, and non-linear behaviour of the valves. Hence, the design of the cylinder requires attention, to make the system controllable.

The goal of this essay is to answer the research question:

Which pneumatic actuator is most suitable to control the (output) force of a pros-

thetic hand?

In this literature review it will be explored with what kind of pneumatic system a prosthetic hand can be controlled. In the follow-up of this study (a masters thesis), a redesign of The Anchor System of Latour [52] will be presented. This redesign should meet certain requirements. These requirements are important for this literature review, because the actuators have to be tested to see whether they meet the requirements. If they do, they are suitable for a system that will be designed in the follow-up.

In this paper, the different types of actuators will be considered and reviewed, and less attention will be paid to their system and control techniques.

Based on the two 'control loops' shown in Figure 2, two sub-questions will be posed.

1. **What types of pneumatic actuators are able to control a prosthesis?** ('Control loop 1')
2. **How can a pneumatic actuator provide force feedback?** ('Control loop 2')

A separate literature review will be conducted on these two sub-questions. Therefore, this literature review will be split up into two sections. One section (4.1) will be devoted to sub-question 1 ('Control loop 1'), and the other section (4.2) will be on sub-question 2 ('Control loop 2').

As mentioned before, the requirements for the final design in the masters thesis are also important in this literature review. Some of the requirements will be described first and eventually a list of all the criteria will be presented.

According to Plettenburg [68] a prosthetic device needs to meet three demands, namely: cosmesis, comfort and control. The first demand, cosmesis, will not be reviewed in this report, and will be discussed in the follow-up of this literature study. The second demand, comfort, will be considered. The system needs to be worn directly onto the body, which makes comfort a very important aspect. The last demand, control, will also be discussed in detail.

A comfortable system is created by using a soft material, because the actuator will be worn directly on the body. another important aspect in creating a comfortable system are the dimensions of the actuator. It is recommended that the system should be as small as possible. However, it should not be very thick. In this article, the thickness is the dimension perpendicular to the skin. If the actuator is thick, it will protrude, which makes it for example not practical to sit on a chair with a backrest. Therefore, it is desired to have a thin actuator.

A complete list of the criteria that the actuator should meet is listed below.

1. **The actuator should be pneumatically driven.**
   This requirement was part of the assignment provided by the TU Delft. In this chapter, it is widely discussed why a pneumatic system should be used.
2. **The actuator should be able to supply 50N.**
   The force of 50N is based on an article of Keller et al. [48], where the forces from objects, manipulated in the daily life activities, were measured. It is assumed in this literature review that there is a one on one relationship between the force at the transducer and at the prosthesis. This is assumed, because it then can be investigated whether the system can achieve the highest possible force. No concessions are made concerning the resolution of the force at the transducer and prosthesis. Most likely this relation will be different in the final design, which will result in the fact that a force of 50N will not have to be reached.
3. **The actuator should be maximally 223x346mm in width and height. The thickness should be limited.**
   The dimensions are retrieved from DINED [31]. The width is based on the shoulder breadth (445mm) divided by 2 (223mm), because the system will be placed on one of the two shoulders. The other dimension is the total height of the back. The system should at least be smaller than these dimensions, otherwise it would not fit. However, it needs to be stated that these maximum dimensions are not desired in the final design. It is certainly desirable that these dimensions will be a lot smaller.
   No dimension was set for the thickness, because no information was found. However, as was mentioned before, the thickness should be limited. More re-

search needs to be conducted in the follow-up of this literature research.

4. **The actuator should consists of a soft material.**
As mentioned above, according to Plettenburg [68] comfort is a very important aspect. A soft material makes it more pleasant for the user to wear the system.
5. **The actuator should be able to provide force feedback to the user.**
This is of importance because when controlling a body-powered prosthesis, it is desirable to receive force feedback. This will cause the user to 'feel' what he/she is doing and how much force needs to be provided.
6. **The latency time of the feedback should be less than 125ms. Preferably, it should be less than 50ms.**
The user should feel what is happening at the place of the prosthesis as fast as possible. It is not desired to have a large delay. The optimal time of delay was found to be between 100-125ms according to Farrel and Weir [37].
7. **The actuator should be practical in use.**
The actuator should not be too complicated or complicated in use. The total system is placed on the body of the user, which makes it desirable to make donning and doffing easy and quick. This requirement will be specified in detail in the follow-up of the literature review.
8. **The actuator should be as efficient as possible.**
The actuator should not use too much gas or air. The supply pressure level should be such that the minimum amount of gas is needed to fully activate the system. According to Plettenburg [69] this optimum pressure is at 12bar.

The results presented in this paper will be tested and discussed based on these criteria. At the end of this literature review, a recommendation will be made which kind of system (or systems) is suitable to be used. Another recommendation will be made on how the feedback should be provided to the user.

The structure of this article is as follows. In section 2 it will be explained how the literature research was conducted. In section 3, results will be presented. These will be showed per group, namely for the pneumatic actuators ('Control loop 1') (3.1) and for the physical feedback ('Control loop 2') (3.2). Each group is divided into subgroups. It is chosen to already discuss the results immediately afterwards in the same chapter. The complete discussion will be presented in section 4. Lastly, the conclusion will be presented in section 5.

2. Methods

To answer the research question posed in the section 1, a literature review has been conducted. Three search databases were used, namely Scopus, Web Of Science and Google Patents. In the introduction it was pointed out that the research conducted in this paper was divided into two parts. The methods used for these two parts will be discussed separately.

2.1 Control loop 1

The following search terms were used to find the relevant literature on sub-question 1:

(pneumatic AND actuat*) AND (control OR regulat* OR servo) AND (force OR power)*

This resulted in a total of 3316 articles and patents. After that, as a selection criterion it was chosen to only include articles with the English language and duplicates were removed. In Figure 3 the article selection is shown. As can be seen, articles were removed based on title, abstract and the full text. Articles were discarded when they did not specifically discuss the pneumatic system they used in their design. Also, many papers considered mathematical models of pneumatic systems. These articles were discarded, because they are not within the scope of this literature study. Further, many articles were not available in full text in the library of the TU Delft, so could not be included in this literature research.

During the abstract selection, 17 articles were removed and added to the group of Control loop 2, because they suited better there. In total, 27 papers were added from other sources. This resulted in a total of 124 articles that were used in this literature research.

2.2 Control loop 2

To find literature on sub-question 2, the following search terms were used:

pneumatic AND "force feedback"*

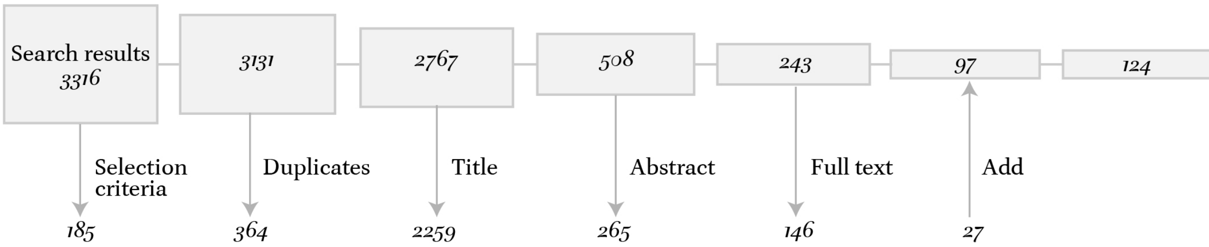

Figure 3: Article selection for the group on sub-question 1: What types of pneumatic actuators are able to control a prosthesis? The literature found will be grouped under the name: Control loop 1. The arrows pointing below show the articles that were discarded.

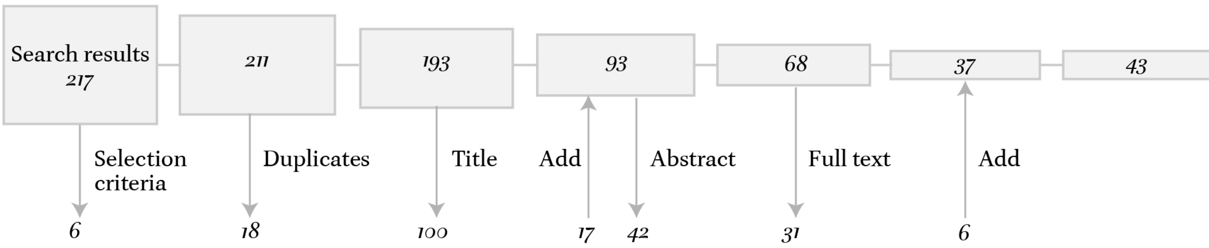

Figure 4: Article selection for the group on sub-question 2: How can a pneumatic actuator provide force feedback? The literature found will be grouped under the name: Control loop 2. The arrows pointing below show the articles that were discarded.

These terms resulted in a total of 217 articles and patents. The same selection criteria as above were used and also the same steps were taken to select the articles, see Figure 4. As mentioned above, 17 papers were included from the group on control loop 1. An amount of 6 articles was added from other sources. Again, many articles were not available in full text in the library of the TU Delft. After selection, 43 articles were used in this literature research.

The articles that are used in this review are listed in the References. All the articles that were included in the literature search are listed in the Appendix.

3. Results

The results will be presented in the two subgroups: Control loop 1 and Control loop 2. Each group was divided into subgroups. It is chosen to discuss certain elements immediately after the results of subgroup. This makes sure a clear overview of the results is kept. The complete discussion of the results will be presented in section 4: Discussion.

3.1 Control loop 1

The results on this group were divided into five groups, see Figure 5. These groups are divided based on types of pneumatic systems and on their properties.

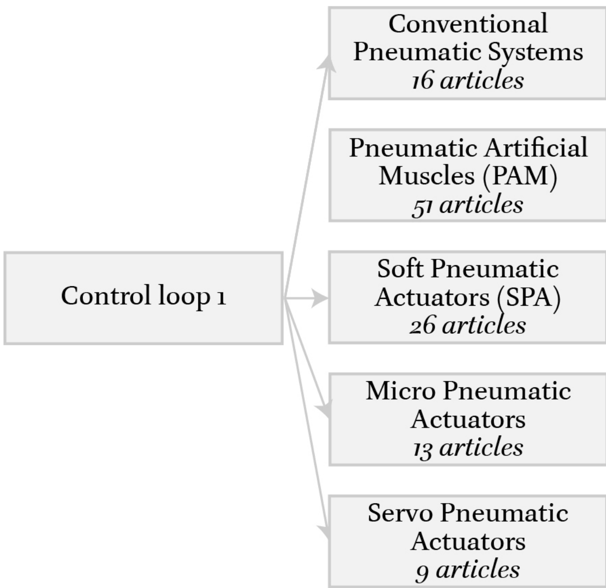

Figure 5: Division of results of the article search on Control loop 1. The results are divided into five groups. For each group, it is stated how many articles were found.

First, conventional pneumatic systems will be discussed to identify what kind of conventional pneumatic systems are now widely used. Second, pneumatic artificial muscles (PAM) are reviewed, because it is necessary to have an elaborate overview of the types of actuators that are suitable to be used. The third group contains soft actuators, which are very important due to the desired comfort of the user. The fourth group consists of micro pneumatic systems. They are of interest considering the size of the design should be as small as possible. Lastly, servo pneumatic systems were explored, to examine the possibilities of controlling a prosthetic device with a system like this.

Some of the selected literature were used in multiple groups, because a few designs fitted into more groups based on their properties.

3.1.1 Conventional Pneumatic Systems

There are several conventional types of pneumatic systems, three of which will be presented in this literature review. The three groups are piston actuators, screw actuators and rotary actuators. Figure 6 shows how the results were divided, and how many articles were found per subgroup.

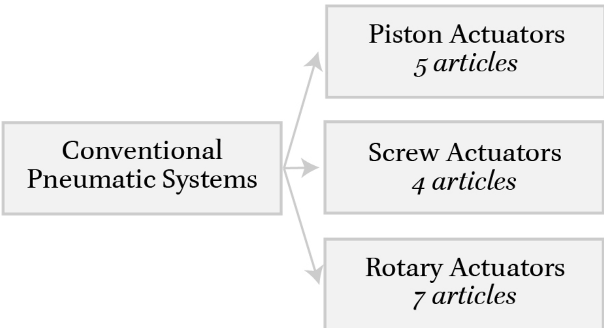

Figure 6: Division of results of the article search on Conventional Pneumatic Systems. The results are divided into three subgroups. For each subgroup, it is stated how many articles were found.

Piston Actuators

Piston-cylinder actuators are most commonly used for pneumatic systems [65]. They are applied in systems that require relative high pressures and low volumes. In Figure 7 a double-acting piston actuator can be seen. When air is supplied to one of the chambers (through the inlet valves), the sliding cross-head will move to the left. When the exhaust valves are opened, the air will escape through the outlet, causing the cross-head to slide to the right.

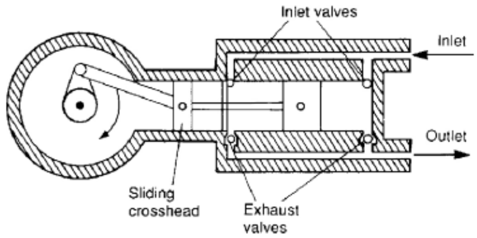

Figure 7: Double-acting piston actuator [65]. The air enters via the inlet. If the inlet valves are opened, the sliding cross-head will move to the left. If the exhaust valves are opened, the air escapes through the outlet.

Migliori [58] used a piston-cylinder actuator to design a pneumatically actuated gripping device. Figure 8 shows a patent of the design with number 13 and 14 as the inlet ports, through which the air is supplied to the chambers. The grippers are attached to the piston via a gear mechanism. When air is supplied to the lower chamber (12), the piston will move upwards. This, in turn, will cause the grippers to widen. When air is supplied to the upper chamber (11) via inlet port (13), the piston will lower, causing the grippers to close.

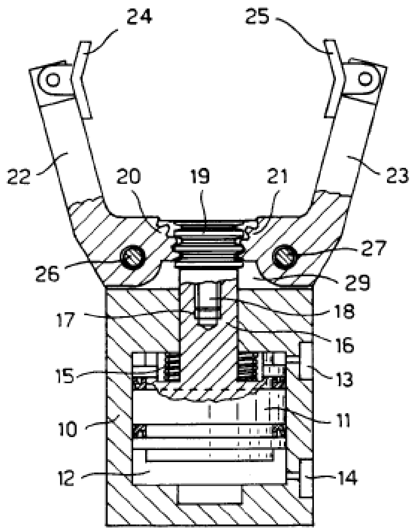

Figure 8: Patent of a piston-cylinder actuated gripping device [58]. When air is supplied through the inlet (14) to the lower chamber (12), the piston (16+17+18) will move upwards. The gear (19) will cause the grippers to move (20+21). When air is supplied through the inlet (13) to the upper chamber (11), the grippers will close.

Screw Actuators
Screw actuators are used when only medium pressure levels are required. Screw actuators have fewer moving parts than piston actuators, which makes them more simple [65]. This type of actuator consists of two rotating screws, one having a convex contour and the other having a concave contour (see Figure 9). When the screws rotate, air is drawn through the inlet port into the chamber. As a consequence, the air gets trapped between the screws, and will be compressed and transported to the outlet port [11].

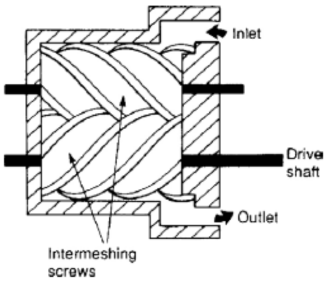

Figure 9: A screw actuator [65]. Air comes in through the inlet and gets trapped between the intermeshing screws. It causes the screws to rotate. The air can escape through the outlet.

Rotary Actuators
Rotary actuators are also called rotary vane actuators. Vanes (4) are attached to a rotor which rotates within the air chamber. Air comes into the air chamber via the inlet port (5), and gets trapped by the vanes (see Figure 10). Minimum amount of leakage is present when the vanes touch the surface of the chamber. While the vanes keep rotating, the air is transported to the outlet port (6) [82].

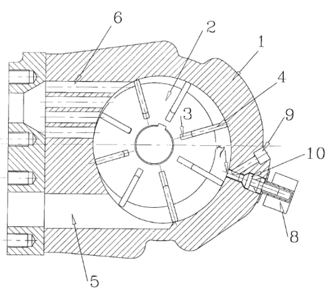

Figure 10: A rotary vane actuator with number 5 as the inlet port, and number 6 as the outlet port. Number 4 shows one of the vanes [82].

Egeresi [35] patented a design which uses a rotary vane motor (FIG 3) to supply a tooth brush with air, see Figure 11. The compressed air is eventually translated to a rotary motion of the brush (FIG 2). Egeresi [35] implemented this system also in a car-toy, where the wheels are rotating on air movement, and in many other products like a drill, shaver, screw et cetera.

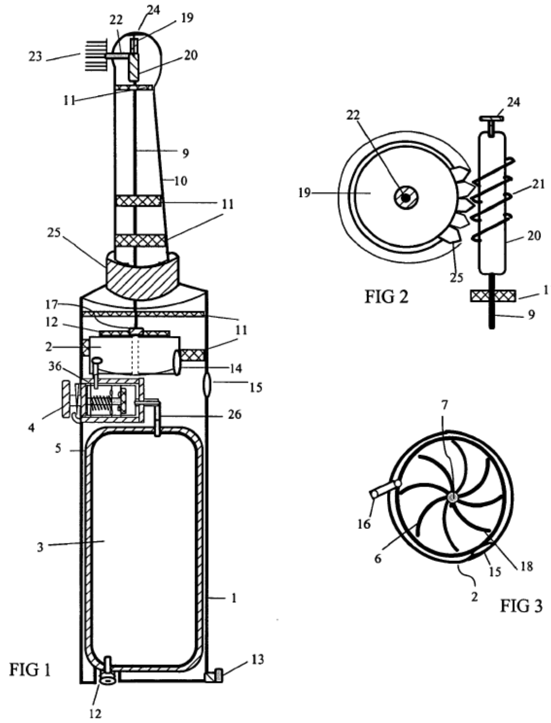

Figure 11: A tooth brush supplied with air via a rotary vane actuator. Air is supplied in the inlet (15) and vanes (6, 18) will move causing the system in FIG 2 to move [35].

Discussion – As mentioned in the introduction, cosmesis, comfort and control are essential when designing a prosthetic device. All three conventional pneumatic systems mentioned above have in common that they are rather bulky in size and produced out of hard materials, which is not desired and not comfortable. However, the systems discussed here can be used as a source of inspiration.

3.1.2 Pneumatic Artificial Muscles (PAM)

Pneumatic artificial muscles (PAM) were first invented by Joseph L. McKibben in 1950. They consist of an inner tube surrounded by a sleeve and will either contract or expand when pressurized [6].

Many different types of PAMs exist. The two major groups are McKibben muscle actuators and Pneumatic Balloon Actuators (PBA), see Figure 12. In this essay, these different types together with their specifications will be presented.

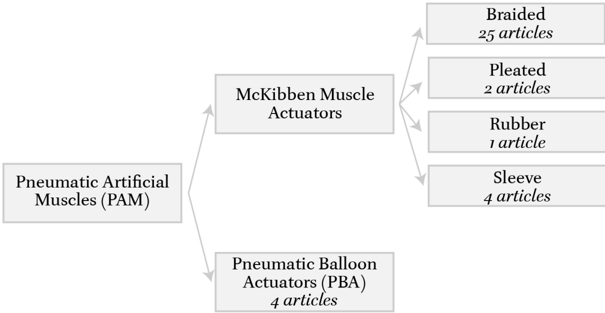

Figure 12: Division of results of the article search on pneumatic artificial muscles (PAM). The results are divided into subgroups. For each group, it is stated how many articles were found.

McKibben Artificial Muscles

As can be seen in Figure 12, the braided McKibben muscles were most frequently discussed in literature, because 44 out of the 51 articles on PAMs were devoted to McKibben muscle actuators. This type of artificial muscle consists of two layers, frequently with an inner layer of rubber and an outer layer of braided nylon fibers. The inner tube can be composed of natural or synthetic rubbers. The outer layer is a braided fiber shell. This shell protects the inner layer from blowing up too much and rupturing [18]. Nylon is widely used as a fiber material, but carbon is also applied [47].

The fibers are braided in such a way, that it determines how many the muscle will contract. Liu and Rahn [55] modeled the behaviour of braided McKibben muscles. The braid angle was measured longitudinally, see symbol α in Figure 13.

At a braid angle of 54.7, the circumferential and longitudinal stresses balance out, which causes the muscle to neither contract or extend when increasing the internal pressure. When this angle is lower, the muscle will contract. This, because the longitudinal forces are higher than the circumferential forces. It causes the muscle to contract and expand radially. When the braid angle is higher than 54.7, the muscle will extend. The circumferential force is higher than the longitudinal force. As a consequence, the muscle will contract radially and extend longitudinally (see Figure 14). However, this type of muscle is not used very often, because of buckling problems [55]. However, an extension muscle can be of use when designing a gripper, where the fingers need to be able to extent and contract. Al Abeach et al. [4] designed a gripper of which each finger was made of one extensor and three contractor muscles, which results in a multi degree of freedom (DOF) gripper.

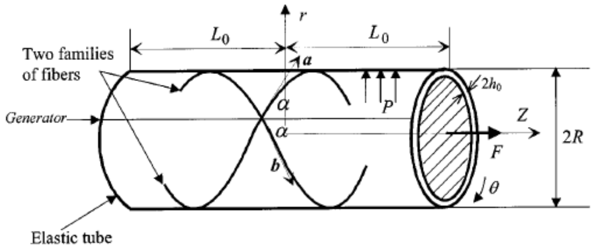

Figure 13: A McKibben actuator model, with α being the braid angle [55].

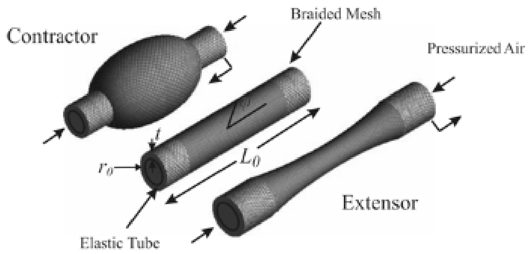

Figure 14: A contractor and extensor braided McKibben muscle, depending on their braid angle [57].

Hawkes et al. [40] designed an inverse PAM (IPAM), where where low pressure levels are needed to contract the muscle instead of high pressure levels. When pressurized, the muscle relaxes and will extend. Elastic energy is stored in the elastic membrane while extending. This energy is then used to contract, when the pressure is removed. It is claimed by Hawkes et al. [40] that the relation between the pressure and force is nearly linear, while this relation is non-linear in a conventional McKibben muscle.

It is also possible to design a straight-fiber artificial muscle, see Figure 15. When a straight-fiber muscle is pressurized, it will expand radially when contracted and not axially, as is the case in a non-straight-fiber muscle. This type of artificial muscle has a greater contraction ratio and has more power than the conventional braided McKibben muscle [47]. According to a study by Nakamura [60], a lower pressure is needed for a straight-fiber artificial muscle to get the same force in comparison to a braided McKibben type muscle.

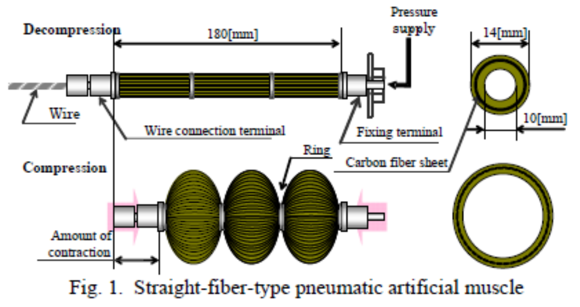

Figure 15: The design of a straight-fiber pneumatic artificial muscle. When pressurized, the muscle will expand radially and contract [47].

Another subgroup of the McKibben type muscles are the sleeve muscle actuators. Figure 16 shows the working principle of this kind of muscle. The muscle is placed around a rigid cylindrical element, with one end fixated. This causes the other side to be able to slide over the rigid element. When the muscle is pressurized, the muscle will contract and slide.

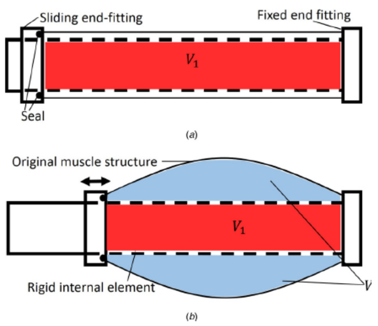

Figure 16: The working principle of a sleeve muscle actuator, where one side will slide over a cylindrical element when pressurized. This muscle has a higher efficiency because of the removal of the internal volume (V_1) [25].

An advantage of this design is the removal of internal muscle volume (V_1), because it is replaced by the rigid element. This leads to a higher efficiency, because the internal volume that needs to be filled with compressed air is lowered at each contraction length, see Figure 17b [25]. Approximately 20-37% energy can be saved with a sleeve muscle, which is desired, as stated in the criteria in section 1 [32].

One more advantage of this system is that a larger force capacity of the muscle is reached. When a conventional McKibben muscle is pressurized, the internal volume of the muscle (V) will push outward on the end fitting. This results in an elongation force, while it is desired that the muscle contracts. Simultaneously, the braided sleeve will oppose this force with a tensile force. In sleeve muscles, this internal volume (V_1) was removed, so the elongation force is not present. This results in a higher force capacity of the muscle, see Figure 17a [25]. However, what needs to be mentioned is that a new problem arises when using a sleeve muscle. There will be friction between the sliding seal and the rigid element. In the article of Cullinan et al. [25] this friction was not significant. Driver and Shen [33] used a specific U-Cup seal to decrease the friction and they used lubricants to further reduce the friction.

Another aspect that needs to be kept in mind when incorporating a sleeve muscle in a design, is the fact that the cylindrical rigid element has a fixed length. This could interfere with the external load when the muscle shortens [32].

The examples above are all single-acting sleeve muscle actuators. They can 'move' in one direction. Zheng and Shen [88] designed a double-acting sleeve muscle actuator, which can generate an extension force for bi-directional actuation. Two chambers are present in the actuator, which causes them both to individually being pressurized, see Figure 18. This makes it possible to move in two directions. Also, the double-sleeve has a higher force capacity than a conventional McKibben muscle according to Zheng and Shen [88].

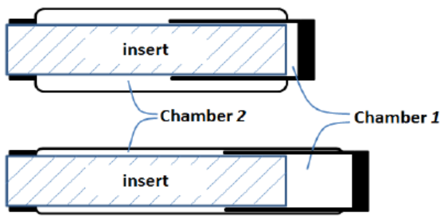

Figure 18: A double-sleeve muscle actuator, where two chambers are present. When Chamber 1 is pressurized, the muscle will elongate. When Chamber 2 is pressurized, the muscle will contract. The system therefore has a bi-directional actuation [88].

The last subgroup of the McKibben muscles were the pleated artificial muscles, designed by Daerden and Lefeber [26]. The muscle consists of a membrane that is folded into each other when there is no pressure. When the muscle is pressurized, the membrane will unfold and contract, see Figures 19c and 19d. In this process, no friction will

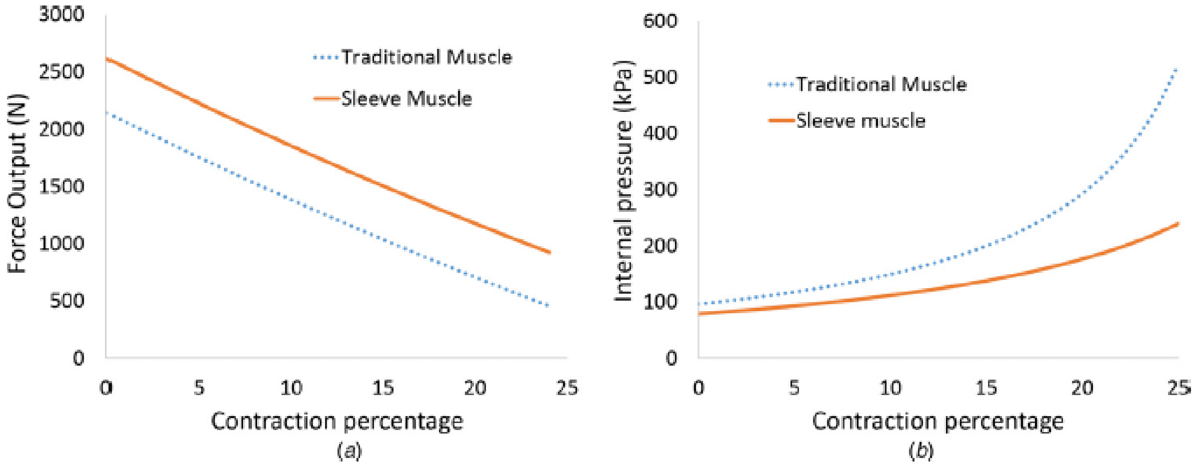

Figure 17: Results of experiments performed by Cullinan et al. [25] where a traditional McKibben muscle was compared to a sleeve muscle: (a) The force output with a constant internal pressure and (b) The pressure required at a constant output force over the contractile range.

occur because the folds are laid out radially [83]. This enables the muscle to work at low pressures and at large contractions.

Figure 19e shows a series pneumatic artificial muscles (sPAM) , placed on a robot's pneumatic backbone [39]. When the sPAMs are pressurized, they will exert a tension force on the backbone, causing a bending motion.

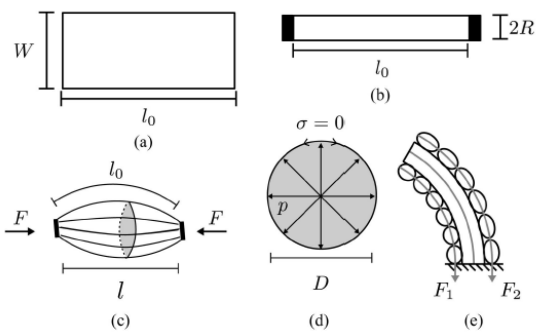

Figure 19: (a) The sPAM consists of a thin sheet. (b) O-rings are added on the sides, which causes the width to decrease, because the sheet will fold. (c) When pressurized, the pleats will unfold. (d) Cross-section of an inflated sPAM. (e) sPAMs are attached to a robot backbone [39].

As pleated muscles can only generate a pulling force, Versluys et al. [84] coupled two actuators antagonistically in order to generate a bidirectional motion.

Villegas et al. [85] improved the design of the pleated muscle by changing the manufacturing process and the design, to make it lighter and less sensitive to failure. The muscle is produced with the use of Fused Deposition Modeling (FDM), which is a rapid prototyping technology. This process makes complex designs cheaper and lightweight. In the new design, the arrangement of the pleated fibers was changed. In earlier generations of the pleated muscle, separate fibers are positioned in every pleat. In the design of Villegas et al. [85] a continuous fibre is placed over the folded membrane, which simplifies the production process. The muscle is also less prone to failure at the end fittings. With earlier generations, each fiber was attached to the end fitting with epoxy. This epoxy frequently came into the fibers, making them brittle and prone to break. In this new design, the fibers will not be saturated with epoxy because of its new structure.

Pneumatic Balloon Actuators (PBA)

As was presented in Figure 12, the other major group of the pneumatic artificial muscles were the Pneumatic Balloon Actuators (PBA). A PBA is commonly composed of two layers with a different stiffness. When the actuator is pressurized, it will bend, as a result of this difference in stiffness [89].

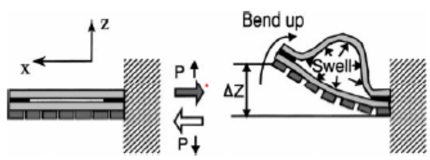

Figure 20: A pneumatic balloon actuator where two flexible films are attached with a cavity in between. When pressurized, the muscle will bend [49].

Konishi et al. [49] implemented a PBA by placing two thin flexible films together, with the upper one acting as a membrane, made of silicon rubber, and the bottom one acting as a substrate, made of polyimide. As can be seen in Figure 20, the two films are only connected on the sides, creating a cavity in between. When the actuator is pressurized, the balloon will expand and will create a bending motion.

Zheng et al. [89] incorporated the same principle of a PBA, but integrated a stiffness control channel (see Figure 21). For this control channel, they used a bismuth-based low-melting-point alloy. To make the actuator soft, thus having a low stiffness, the actuator is heated by placing it on a hot plate. The actuator becomes hard again when it is rested at room temperature. To create a partly soft actuator, a nichrome wire is used, which is electrically controlled. Joule heat will cause the actuator to partially melt. To make the actuator partially hard, ice is placed on the regions where it needs to harden.

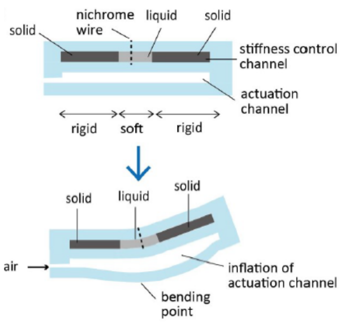

Figure 21: A pneumatic balloon actuator with a stiffness control channel made of a low-melting-point alloy [89].

Discussion – Sleeve muscles are of interest, because of their claimed high efficiency. This is one of the criteria set in section 2. The higher efficiency is caused by the reduction of internal volume. This way, less gas is needed, and thus reducing air consumption. However, this volume reduction is also possible with braided McKibben muscles. The volume can be reduced by filling the air chamber with granular, solid, and liquid fillers [87].

[25] stated that the friction between the sliding seal and rigid element of a sleeve muscle was not significant. Yet, they did not test the muscle at high speeds, which means it can potentially cause problems. This shows that to truly claim that a sleeve muscle has a high efficiency, more research should be conducted on the friction.

In this essay, it was mentioned that pleated muscles do not have any friction at all. Though, stated by Villegas et al. [85], there is still some friction between the fibres and the membrane and the unfolding of the pleats, which should be kept in mind.

Pneumatic balloon actuators are a feasible choice as an pneumatic actuator attached to the back of the user. Though, the incorporated stiffness control channel of Zheng et al. [89] will not be applicable to this system. It is not practical to cool and/or heat the system up with an external hot plate or ice while wearing the system on the back. Therefore, this type of actuator does not meet the criteria set in section 1.

3.1.3 Soft Pneumatic Actuators (SPA)

It is important for the pneumatic system to be soft, flexible, and wearable to meet the requirement of comfort stated by Plettenburg [68]. A requirement was set in section 1 (Introduction) that the system needs to be soft. Therefore, this group was created to explore the options on soft pneumatic actuators. For this topic, articles were included that specifically designed a pneumatic muscle to be flexible, wearable or soft. The results were divided into five groups, see Figure 22. One group consists of residual ideas, that did not fit in the other subgroups.

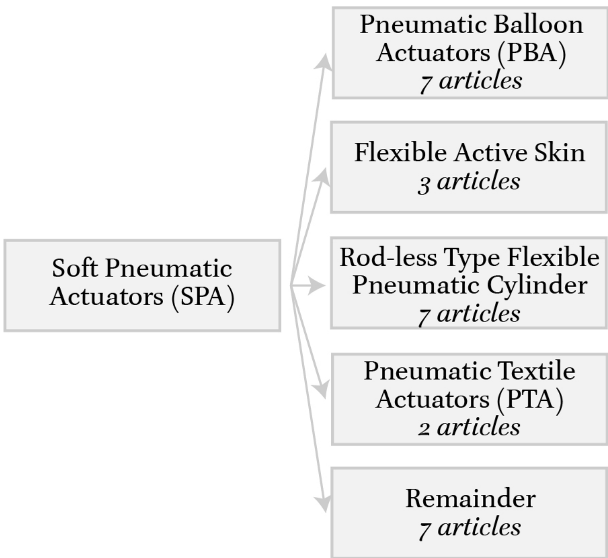

Figure 22: Division of results of the article search on soft pneumatic actuators (SPA). This group was divided into five subgroups. For each subgroup, it is stated how many articles were found.

Pneumatic Balloon Actuators (PBA)
PBAs are widely used as a soft actuator system, as they are very suitable. In this literature review, 7 out of the 26 articles on soft pneumatic actuators integrated PBAs. They are safe to use in wearable systems, because they can deflate when not actively providing power [61].

Schulz et al. [75] designed a prosthetic hand where joints are actuated with a PBA. When a finger needs to be extended, the balloon will be inflated, which causes a rotary motion, see Figure 23.

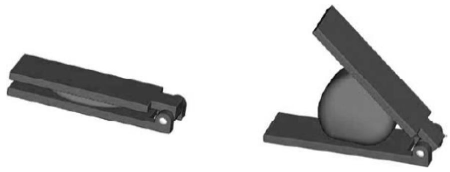

Figure 23: Extension principle of a pneumatic balloon actuator. A rotary motion is caused by the inflation of the balloon [75].

Nojiri et al. [62] used PBAs to create a soft five-fingered robotic hand. In Figure 24 a schematic representation is provided of the PBA used. In the design, two PBAs are placed opposite of each other, composing one of the joints of a finger. When the PBAs are pressurized, the fingers are flexed, and they are extended when the pressure is released.

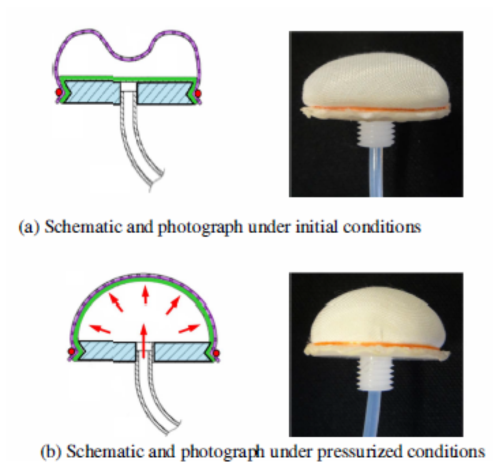

Figure 24: Representation of a pneumatic balloon actuator with (a) Not pressurized and (b) Pressurized [62].

Another design, created by Cho et al. [21], is a layer-type pneumatic actuator, composed of two balloons. The design resembles an airbag. It supports the lower back of the user when performing actions such as picking something up from the ground. The balloon is placed on the belly of the user and will bulge when pressurized, forcing the user to stand up straight.

Flexible Active Skin
Park et al. [63] designed a wearable sleeve of small pneumatic actuators. The sleeve monitors the motion of the user with the help of strain sensors, and will assist where needed. When the pneumatic actuators are pressurized, the sleeve will expand in radial direction, which will create a contraction in axial direction. In this way, it will for example assist in the walking motion, see Figure 25.

Figure 25: Working principle of a wearable sleeve, where the motion is measured with strain sensors. The sleeve will assist where needed, based on the signals of these sensors [64].

Besse et al. [13] designed a flexible active skin that consists of a shape memory polymer sheet, including many small actuators, connected to a stretchable pneumatic chamber. The actuators can be individually controlled by local Joule heating excited by the supply of pressure, see Figure 26. The surface is locally reshaped by a low-voltage signal, when simultaneously applying pressure to it. When the sheet is heated without the supply of pressure, it will go back to its original flat state. This design was used to make a Braille display.
The flexible active skin can exert high forces and can create a haptic interface.

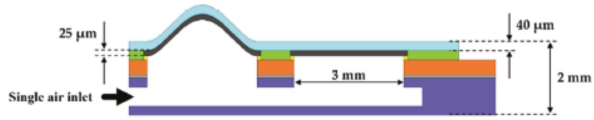

Figure 26: Flexible active skin, with a layer of shape memory polymer connected to a pneumatic chamber [13].

Rod-less Type Flexible Pneumatic Cylinder
The design of a rod-less type flexible pneumatic cylinder was first created by Akagi and Dohta [1]. The cylinder consists of a flexible

tube that functions as a cylinder and sealing, one steel ball that operates as a cylinder head, and a slide stage that is able to slide along the outside of the tube. Two rollers are placed on the outside, which deforms the tube, see Figure 27 [3].

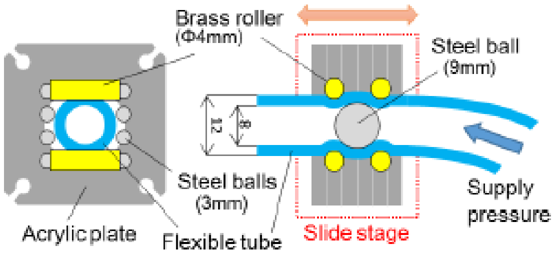

Figure 27: Working principle of the rod-less type flexible pneumatic cylinder. It contains brass rollers, a large steel ball ($9mm$), smaller steel balls ($3mm$), and a tube [3].

When pressure is supplied to one side of the cylinder, the steel ball will move along on the tube, and takes the slide stage with it. The design is implemented multiple times in a flexible and portable rehabilitation device, where the user needs to move the handling stages in a certain way to train the hands and arms (see Figure). Namely approximately 27% of the articles found on soft actuators discussed the use of the rod-less cylinder, see Figure 28 [3] [54] [56].

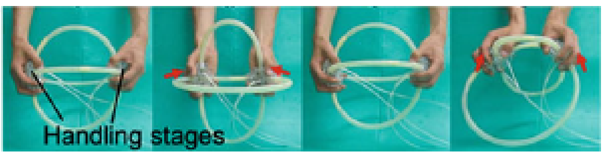

Figure 28: The rod-less type flexible pneumatic cylinder incorporated in a portable rehabilitation device [56].

Pneumatic Textile Actuator (PTA)
Belforte et al. [12] designed a pneumatic textile actuator (PTA) that is similar to a conventional McKibben muscle. The difference is that the outer layer is composed of fabric. The fabric needs to be anisotropic, causing it to be stiff in one direction and flexible in the orthogonal direction. This design was created because it can easily be integrated in clothing, which makes the actuator wearable and practical. This is desired as stated in the criteria.

Heidingsfeld et al. [42] went a step further and designed a new pneumatic textile actuator. The design consists of two layers of textiles, fabricated in one piece using the Jacquard weaving technology. This technology makes it possible to create flat fabrics. When the actuator is pressurized, it will expand and contract (Figure 29).

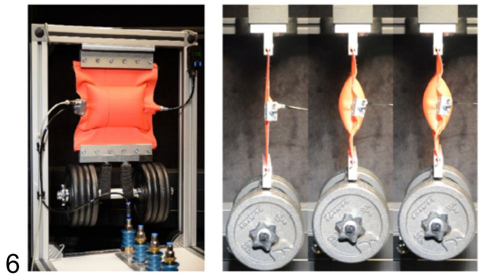

Figure 29: Pneumatic textile actuator (PTA) being pressurized [42].

PTAs achieve a higher contraction force compared to conventional McKibben muscles as a result of the whole surface of the pressure chamber working as a force transmitting element. In a conventional pneumatic cylinder, the piston surface determines the force, which is small compared to the surface of the pressure chamber. The maximum contraction of a pneumatic textile actuator (PTA) depends on the thickness of the inner tube. The thinner the tube, the higher the contraction, however the muscle will then be less durable [12].

As there is no piston present in a PTA, the energy dissipation is low, because there is no friction of the piston [42]. This makes the system more efficient.

Rest
Tsukagoshi et al. [80] designed a wearable tail-arm and leg. A flat tube made of urethane is used, to make it easy to integrate the design into clothes. A wound tube actuator (WTA) is created, which is similar to a sleeve that can be put around a body segment (e.g. the arm or leg) (Figure 30).

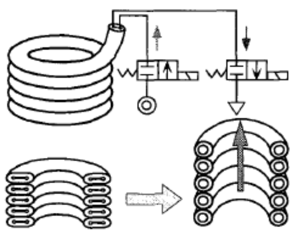

Figure 30: Wound Tube Actuator (WTA) [80].

Dameitry and Tsukagoshi [27] designed a gripper with a zig-zag driving mechanism

(Figure 31). When the gripper is pressurized, the flat tube will expand, and will push the gripper in a bend state, caused by the zig-zag at the joints. A similar design was already created many years before, namely in 1971 [23].

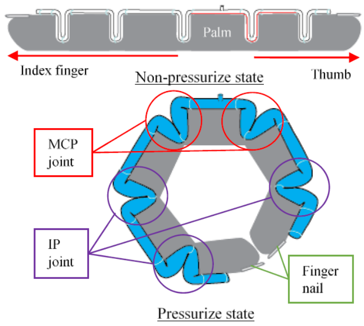

Figure 31: Zig-zag gripper. When the gripper is pressurized, it will bend because of the zig-zag design at the joints [27].

Wang et al. [86] designed a bidirectional pneumatic bending actuator for a rehabilitation glove. A spring is inserted into the glove to create a bidirectional actuator. The glove is bent when the pressure is 0. This bent position is caused by the spring. When the actuator is pressurized, it will overcome the spring torsional force to create an extended position of the hand, see Figure 32.

Figure 32: A pneumatic bending actuator with a spring inserted to create a bidirectional rehabilitation glove. (a) The actuator was not inflated, so the spring causes the bent position. (b) The actuator was inflated, which causes the extended position [86].

Discussion – The flexible active skin designed by Besse et al. [13] is perhaps not suitable for the design of a wireless prosthesis. Heat needs to be applied first, to be able to change the shape with the help of pressure. This does not meet the requirement that the system needs to be practical. When this actuator is used, the sheet needs to be heated first, before the shoulder can move and control the prosthesis. However, the study of Park et al. [64] shows a flexible skin that does not need heat to change its shape. This seems a potential solution. However the idea is in preliminary stage and more research should be conducted on this subject.

A rod-less type flexible pneumatic cylinder is a very flexible system. The system is used in a portable rehabilitation device in many articles, which is very large. As mentioned in the introduction, a criteria was set that the system should be small. This mechanism should be analysed more, to see if it could be integrated in a system where the shoulder controls the motion instead of the hands.

Pneumatic textile actuators (PTAs) are promising wearable actuators. However, more research should be conducted to look into the consequences of changing the conventional McKibben muscle into a PTA, for example the contraction ratio.

3.1.4 Micro Pneumatic Actuators

Micro pneumatic actuators are very small actuators. As was stated in the introduction, a small actuator is desired. It should maximally be 223x346mm in width and height. The thickness should be limited. In Figure 33, it can be seen how the articles were divided over the groups, namely in a group of miniature PAMs (MPAM) and a group of pneumatic balloon actuators (PBA). Both will be discussed in detail.

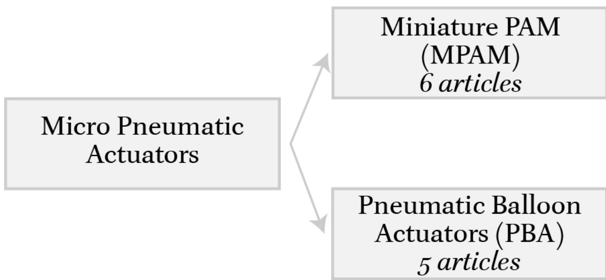

Figure 33: Division of the results of the article search on micro pneumatic actuators. The group is divided into two subgroups. For each subgroup, it is stated how many articles were found.

Miniature Pneumatic Artificial Muscles (MPAM)

By reducing the diameter of the silicone tube, a miniature PAM can be achieved. Though, when reducing this diameter, the contraction and force capacity of the muscle will also decrease. To compensate for these problems, it is wisely to choose a tube material with a very small wall thickness. Nonetheless, this will decrease the operating pressure, and consequently will cause a lower contraction force.

	Chakravarthy et al. [20]	De Volder et al. [28]	Al-Ibadi et al. [5]
Type of actuator	MPAM	MPAM	Conventional PAM
Length	97mm	62mm	200mm
Inner diameter tube	0.5mm	0.5mm	12.0mm
Outer diameter tube	0.9mm	1.0mm	16.4mm
Thickness sleeve	0.1mm	0.09mm	0.5mm
Maximum pressure	1.0MPa	1.0MPa	1MPa
Maximum force	4.2N	6.0N	50N

Table 1: Results from two studies on micro pneumatic artificial actuators [20] [28] compared to a conventional McKibben artifical muscle [5].

Chakravarthy et al. [20] and De Volder et al. [28] performed experiments with miniature pneumatic artificial muscles (MPAMs). Both studies used an actuator with braided nylon sleeves and an inner silicone tube. Table 1 shows the results of these two studies. Another study is also added to the table, showing the results of a conventional McKibben muscle. In the discussion, these results will be compared. However, as can be seen in Table 1, the results cannot be compared directly, because the lengths of the muscles differ.
Chakravarthy et al. [20] experimented with different muscle lengths, which showed that when increasing the muscle length, the force would decrease. This could be the reason why Chakravarthy et al. [20] has a lower maximum force (4.2N) than De Volder et al. [28] (6.0N). In Table 1, it can also be seen how small a micro-actuator can be made. The total diameter, and thus the thickness, can be can be as small as 1.2mm.

A micro pneumatic artificial muscle (MPAM) does not by definition ensure that the total system will be small in size. This is caused by the valves that regulate the air pressure. These valves can still be of a (comparatively) large size. For that reason, attention must also be paid to the valves, to make them as small as possible.

Lee and Shimoyama [53] and Akagi et al. [2] designed micro valves, which have dimensions of approximately 19x25x2mm and 33x19.6x10mm. Though, when using a micro valve, the maximum pressure will decrease. Table 1 shows that the maximum pressure of a MPAM with a normal-sized valve was 1.0MPa, while with micro valves of Lee and Shimoyama [53] and Akagi et al. [2] a maximum pressure of 0.5-0.6MPa can be reached.

In a human being, there is a variable recruitment of muscles, meaning that more motor units will be recruited when a force becomes larger. DeLaHunt et al. [29] tried to mimic this variable recruitment with the use of MPAMs that are placed together in parallel. One single MPAM will represent a muscle fiber, a pair of MPAMs will represent a motor unit, and the total bundle of MPAMs will represent a muscle bundle.

DeLaHunt et al. [29] showed that there was a nonlinear increase in force as the number of activated parallel MPAMs increased. A minor loss in force generation was found due to inactive MPAMs, when not all muscles were recruited. This loss was caused by variations in the resting length. The article of DeLaHunt et al. [29] stated that variable recruitment has benefits, but attention should be paid to the production process, to decrease the effects of force loss due to the inactive MPAMs.

Pneumatic Balloon Actuators (PBA)
Pneumatic balloon actuators (PBA) are widely used in bio-medical applications, for example in surgery. In surgery it is desired that the devices are small. Hence they are designed in micro-scale. A bending PBA was used for cellular manipulation, where micro-fingers were opened and closed by the inflation and deflation of the PBAs. The dimensions of the PBA at the fingertip were 160x600μm. Clusters of cells of several hundred μm were pinched and released by the micro-fingers [49]. Alogla et al. [8] designed a similar micro-gripper with PBAs.

Alogla et al. [9] designed another micro-gripper which can be produced even smaller than 100μm for single cell manipulation (see Figure 34). The outside cantilevers are the micro-fingers that will manipulate the cell. The tip could maximally open to a length of 1mm and could provide a maximum force of 50mN.

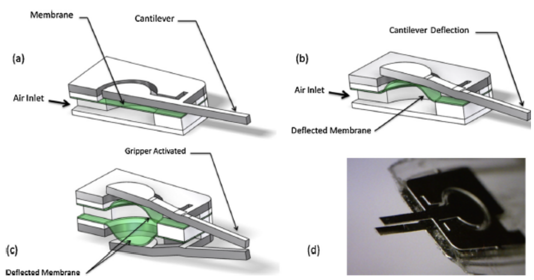

Figure 34: A PBA micro-gripper, with (a) and (b) showing a one-arm bearing onto a fixed plate, or with two arm-bearings (c) [9].

Discussion – This paragraph showed that when changing the thickness and diameter of the tube, a miniature PAM can be created. However, lower maximum forces are reached. In Table 1, the results of the study performed by Al-Ibadi et al. [5] can be seen, together with the two studies on the micro PAMs. The results from Al-Ibadi et al. [5] were approximated from a graph provided in their article. The maximum possible pressure was $5MPa$, but the results with a pressure of $1MPa$ were used, to be able to compare the results to the MPAMs.
It can be seen that the dimensions of the micro PAMs are smaller than the conventional McKibben muscle. This results in a lower maximum force. This force depends on the pressure and area. In Table 1, the difference between the muscles is the area of the actuator, which is larger for a conventional McKibben muscle. This results in a larger force. In the criteria, it was set that a force of $50N$ should be reached. This means that the MPAMs are not applicable. However, these actuators show the possibility of creating a smaller actuator and that there is a trade-off between size and force.

A criteria was also set for the size of the system. When this size of the valve decreases, the total size of the system will be smaller. The dimensions provided in this literature research were approximately 19x25x2mm and 33x19.6x10mm. However, this micro-term can be debated. Valves created by The Lee Company [79], have a size of 7.6x22.4x7.6mm, which is in some dimensions even smaller than the valves claimed to be of micro size. It can be questioned if the claimed micro-valves are really that small. Though, compared to conventional valves, they are smaller. A solenoid valve designed by Festo has a size of 77x42x31.5mm, which is definitely larger than the micro-valves in this literature review [38].

3.1.5 Servo Pneumatic Actuators

On the subject of servo pneumatic actuators 9 articles were found. These articles were not subdivided into groups.

Servo pneumatic actuators provide position control by being integrated in a feedback control system, see Figure 35. The position is measured by a sensor, which is fed back to the controller. This position is then compared to desired value, which gives an error signal. The servo valves use this error signal as a control signal, which will increase the accuracy of the system [65].

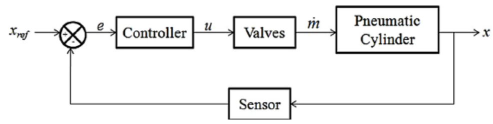

Figure 35: Closed-loop feedback control of a pneumatic cylinder with servo-controlled valves. The output(x) is measured by the sensor and fed back [73].

Jouppila et al. [46] conducted experiments comparing the performance of pneumatic muscles and pneumatic cylinders (both servo controlled) to see if pneumatic muscles are suitable for this type of control. The performance of both actuators was tested by a single positioning task and with sinusoidal position tracking tasks. It was concluded that cylinders have a higher bandwidth, based on the time of the response. A larger bandwidth, yields a faster closed-loop dynamics. This was the case with cylinders. Cylinders also have fewer modelling errors than pneumatic muscles, which causes the cylinder to outperform the muscle actuators at high tracking frequencies. The muscle actuators were very robust when increasing the payload, leading to a minimal change in performance. The cylinder actuator performance decreased at when the payload was increased. This was caused by friction at smaller tracking frequencies.

Jouppila et al. [46] concluded that pneumatic muscle actuators are suitable to be controlled with servo position systems, with good modelling and a choice of control law.

Many articles devote their attention to the use of two servo-valves instead of one, see Figure 36. When only using one servo-valve, the pneumatic stiffness can vary significantly with the system state, because the pressure dynamics of both cylinder chambers are coupled [34]. The pneumatic stiffness depends on the piston position and the pneumatic force inside each chamber. When only using one servo-valve, this stiffness is also velocity-dependent. This disadvantage is visible at zero velocity, where a large sudden change in pneumatic stiffness can occur with a change in velocity sign. This velocity-dependency is not desired, because the controller should be able to account for this sudden large change [19]. To decouple the chambers, two servo-valves can be used to achieve independent motion and pressure control, see Figure 36.

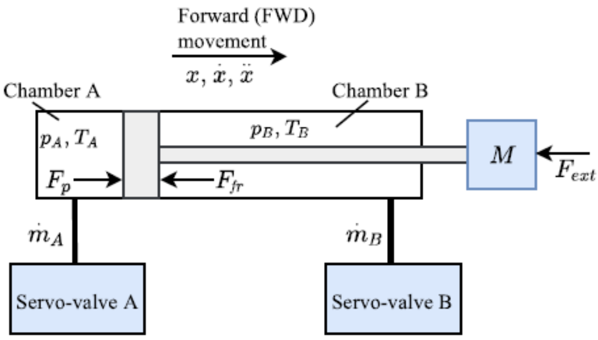

Figure 36: A schematic representation of a pneumatic actuator with two servo-valves [34].

3.2 Control loop 2

Physical feedback is important for the user when controlling the prosthesis, as was set in the criteria. Physical feedback can be provided in two ways, namely as tactile feedback or as proprioceptive feedback. Proprioceptive information is the sense of the state of the human body, such as the angles/position of the joints. In this case, the proprioceptive information is the state of the prosthesis. Tactile information is the sense of pressure, temperature, vibration et cetera.

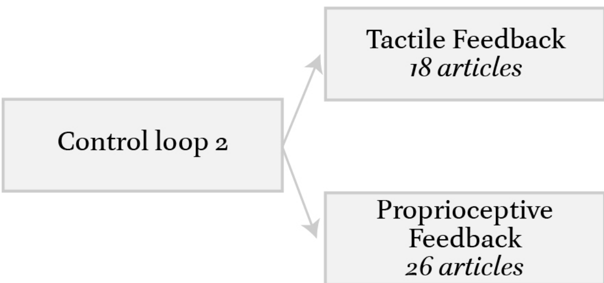

Figure 37: Division of results of the article search on Control loop 2. The results are divided into two groups. For each group, it is stated how many articles were found.

The results were divided in these two subgroups, see Figure 37. Designs that use these types of feedback are presented and discussed.

3.2.1 Tactile feedback

Tactile feedback using pneumatic balloon actuators (PBAs) with different magnitude levels can be provided in three ways, namely via amplitude modulation, position modulation and frequency modulation [59]. For amplitude manipulation, the pressure in the balloon was differed. In position modulation, three small balloons were used. When the feedback level increased, more balloons were inflated. For frequency modulation the time between two periods of inflation was varied. When it took shorter for the balloon to inflate for the second time, the feedback level was higher.
The modulation techniques were tested by 10 healthy subjects and the results can be seen in Figure 38. In the left chart, the percentage correctly identified feedback levels can be seen for all the three modalities. Figure 38 shows that subjects performed the best with the frequency modulation, and that it outperforms the other two modalities. This means that there is a high level of discrimination in the frequency modulation. In the chart on the right, the differences between modalities are smaller. Nonetheless, frequency modulation still achieved the highest results.

PBAs are also used in robotic surgery as a tactile feedback mechanism. Culjat et al. [24] used PBAs to provide tactile feedback to the fingers of the surgeon. The PBAs are placed on the controls of a Da Vinci surgery system. The force sensed by the robotic grasper is translated into proportional inflation pressures. In this way, the mechanoreceptors in the finger are stimulated. These PBAs are very small, as they will need to provide feedback on a small surface, namely the tip of the finger. A balloon-diameter of 3*mm* was tested to be the smallest effective balloon.

Fan et al. [36] created a haptic feedback system for lower-limb prostheses, to improve balance during gait. Four force sensors were placed on the bottom of the foot, which controlled the four corresponding balloon actuators (see Figure 39). The PBAs are placed on the inside of a cuff, that will be worn on the thigh. Thus when only the heel touches the ground, one PBA will be inflated.

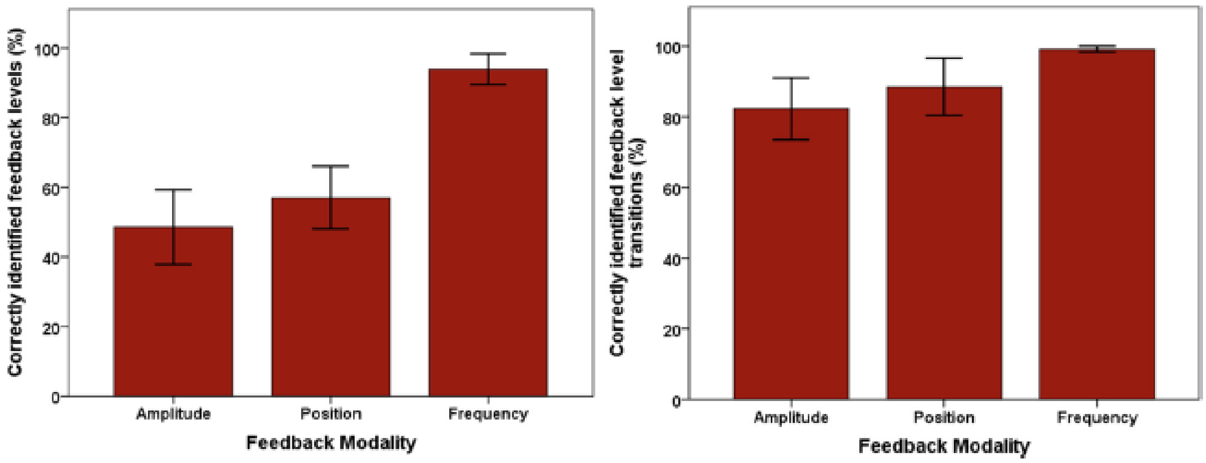

Figure 38: The results of the feedback modulation study performed by Muijzer-Witteveen et al. [59]. With in the left chart made visible the percentage correctly identified feedback levels and the right chart the percentage correctly identified feedback level transitions.

Figure 39: Conceptual model of the lower-limb prosthesis with a cuff placed around the thigh. In this cuff PBAs are placed. Sensors on the bottom of the foot translate pressure information into the inflation of the PBAs [36].

Two accuracy tests were performed on this design. This resulted in an accuracy of 99% in a test where subjects needed to tell the sequence of actuation and an accuracy of 94,8% in a directional actuation task, where subjects needed to indicate which balloon(s) was/were actuated.

PBAs can also integrated in clothing or wristbands. Delazio et al. [30] incorporated pneumatic balloons in a jacket, for virtual reality purposes. The force jacket is incorporated with 26 internal airbags with force sensitive resistors. Micro-controllers controlled each individual airbag to reach a certain target force. This target force is measured by the force sensors in the balloons. Experiments were conducted with subjects. It resulted in the fact that the shoulders were the most sensitive to pressure, while the back was relatively insensitive.

He et al. [41] and Pohl et al. [71] designed something similar, namely a pneumatic balloon armband. When inflated, compression feedback will be provided to the user. Subjects were able to distinguish between stimuli with an accuracy of 93% and 95%.

3.2.2 Proprioceptive feedback

The second way of providing feedback is through proprioceptive feedback. This was the sense of the state of the human body, and in this case the state of the prosthesis. In this paragraph, some designs will be presented that use proprioceptive feedback in their system.

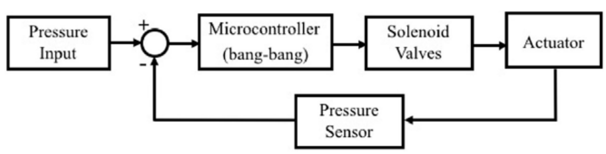

Figure 40: Feedback control loop scheme with a micro controller to turn the solenoid valves on or off to have pressure relation, using the information from the measured by the pressure sensor [76].

Figure 40 shows an example of a control loop, where a pressure sensor sends information back to the micro controller, which will in turn regulate the pressure. This control loop is used in a design by Sebastian et al. [76], where a soft robotic interface was created (see Figure 41). The user needs to pinch the interface. This pinch force is measured and fed back to the micro controller, which in turn regulates the valves for pressure regulation.

Figure 41: A soft robotic interface with force-control [76].

Suh et al. [78] created a soft and flexible pneumatic actuator skin with embedded sensors. The skin consists of three layers, a stretchable layer, a mask layer and an unstretchable layers (see Figure 42). In the mask layer, a very thin air chamber is made. The strain of the skin is measured with the sensors, and fed back to the controller that regulates the pressure. The user will sense proprioceptive feedback, through the inflated balloons. In the design shown in Figure 42 only four actuation points are shown, but many more can be distributed over a larger area.

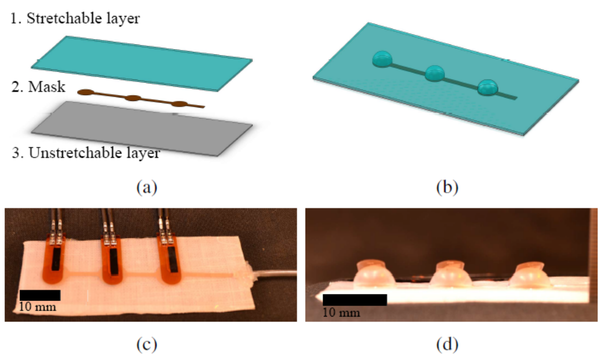

Figure 42: Fabrication and working principle of the soft pneumatic actuator skin. (a) Three component layers. (b) The combined layers. (c) Top view with the embedded sensors. (d) Side view of the inflated design [78].

Many force feedback systems are used in virtual reality (VR). Bouzit et al. [17] designed a force feedback glove for virtual environments. A patent for this design was granted in 2006 [16], see Figure 43. The adduction/abduction angles of the finger are measured with Hall-effect sensors, while the translation of the piston inside the cylinder (22) is measured with an infrared sensor. In this way, the position of the hand is measured and can be related to the virtual environment to provide force feedback.

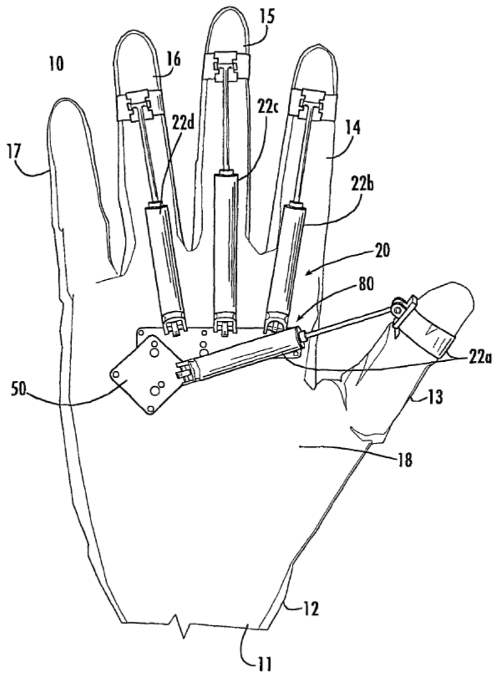

Figure 43: A hand force feedback and sensing system patent [16].

Jadhav et al. [44] created a glove that measures the position of the fingers with infrared cameras. This information is fed back to the controller. The position of the fingers is then related to the virtual reality environment. Based on this relation, haptic feedback will be provided. This will be created by for example changing the pressure level inside the glove. The user then feels more resistance when moving their finger. For example, when playing the piano in the virtual environment, the user will feel a pressure on the fingers that 'touch' the piano keys.
Kuusisto et al. [50] designed a similar glove, where he finger position was tracked with a magnetic tracker instead of infrared cameras.

Uddin et al. [81] also created a glove that provided physical force feedback. Force sensitive resistance sensors are placed on the robotic fingers of the glove. The sensors send the force measurements to the controller.

When there is no force exerted on the sensors, the valves are fully open and thus have a duty cycle of 100%. When a force is exerted, the duty cycle of the valves will decrease, which in turn resists the motion of the piston. When maximum force is sensed, the duty cycle will go to 0%, which causes the piston to be immobile. As a consequence, the robotic fingers are also immobile. The user will 'feel' that it cannot provide any more force. This system is able to provide force feedback between 0 and $9N$.

Discussion – Pneumatic balloon actuators used as tactile feedback sounds promising. However, this assumption should be explored more. The study performed by Muijzer-Witteveen et al. [59] showed that frequency modulation provided the best feedback. The highest percentage correctly identified feedback levels was found here, as also in the percentage correctly identified feedback level transitions. Though, it needs to be mentioned that the level transition experiment was not done optimally. In the article of Fan et al. [36] a value of 94.4% of discrimination accuracy can be found, where three levels were used. In the article of Muijzer-Witteveen et al. [59] a value of 83% was found, where four levels were used. This value could be lower, due to the higher number of feedback levels or due to a less efficient setup. This shows that more research should be conducted in this field, to fully show how the discrimination accuracy is and on what it depends.
However, the study of Fan et al. [36] also has a remark. Only six subjects were included in this research. To fully test the system and check the accuracy, more subjects are needed.

Other research has been conducted on vibrotactile feedback by Antfolk et al. [10]. It is stated that this type of feedback improves the users performance in a grip force task, but task execution time is longer. There is a time-delay in the feedback, which causes the user to work slower. Another problem with this type of sensory feedback, and also with mechanotactile feedback, is that it can lead to adaptation. This means that the stimulation is less perceived over time. One more aspect that needs to be considered when integrating mechanoreceptorsensing, is the sensibility of the human body. As mentioned in the introduction, the final design will be placed on the users back. According to the sensory map on the cortex of Penfield and Rasmussen in 1950, the back does not have a large representation in the cortex, see Figure 44 [74]. This agrees with a study by Delazio et al. [30], where experiment were conducted on the sensibility of the human body.

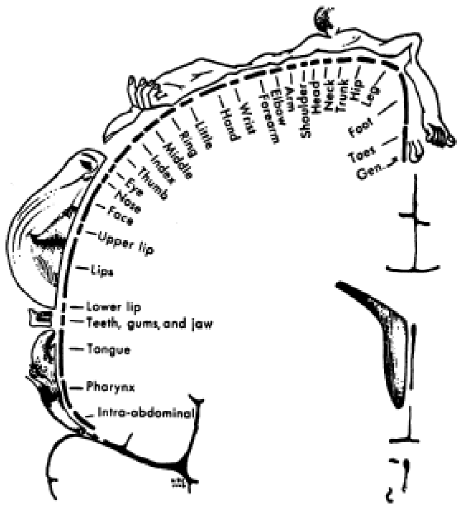

Figure 44: Sensory Homunculus: representation on the cerebral cortex [74].

4. Discussion

As mentioned before, some of the results were discussed in section 4: Results. The complete discussion will be presented in this section. The results will be discussed per Control loop.

4.1 Control loop 1

In the literature found, it was often stated that pneumatic artificial muscles surpass conventional piston-cylinder actuators. PAMs, according to many, would have a higher energy-to-mass ratio. However, a study by Plettenburg [70] showed that a proper piston-cylinder design surpasses pneumatic artificial muscles, with a superior energy-to-mass ratio. The conception that PAMs have a higher ratio than conventional systems, stems from the fact piston-cylinders are frequently over-dimensioned. This negatively affects the energy-to-mass ratio.

In this article, a comparison was made between servo controlled pneumatic cylinders and servo controlled pneumatic muscles. It was shown that servo controlled cylinders have a higher bandwidth than servo controlled muscles. However, it is not known how high the bandwidth in the final design needs to be. Therefore, the level of bandwidth should be captured more thorough in future research.

Braided McKibben muscles were frequently found in literature. Not only in paragraph 3.1.2 (Pneumatic Artificial Muscles (PAM)), but also in other paragraphs, where this type of muscle was used as a basis for their design. Different rubber materials can be used for the inner layer, as also different materials can be used for the outer layer. Nylon, carbon and textiles (in PTA) can operate as the outside layer. In the follow-up of this study, more literature should be explored on this subject. The effects of different materials should be analyzed intensively.

Pneumatic balloon actuators (PBAs) were widely discussed in literature. It was shown that PBAs can be soft, and can be made very small. They can be made smaller than $100\mu m$. However, the maximum force is then $50mN$, which is extremely small and thus not useful in the focus of this literature research. This type of actuator does not meet the requirement set that the maximum force should be 50 N. Nonetheless, this shows that a even a very small size is able to function correctly.

In paragraph 3.1.4, it was shown shown that with micro PAMs the maximum force decreased. It was discussed that these forces were too low and that the micro PAMs do not meet the requirement of providing a force of $50N$. However, it was stated that the relation between the force at the actuator (input) and the force at the prosthesis (output) is assumed to be one on one. Nonetheless, a gain can be implemented. When for example using a MPAM, it is needed to have a gain factor between the input and output. This shows that MPAMs can still be used when a there is a gain between the input and the output. However, this reduces the resolution at the output, which decreases the accuracy. A too high gain should therefore not be recommended.

Servo pneumatic systems were mostly position controlled. This is not desired in this literature review, where the prosthesis is force controlled. However, the principle of position control could be transferred to a force controlled prosthesis.

4.2 Control loop 2

Pneumatic Balloon Actuators (PBAs) could be used to provide tactile feedback to the user. In section 3.1 (Control loop 1), it was shown that PBAs have a wide range of applications. Furthermore, it was extensively discussed in 3.2 (Control loop 2) that PBAs can also be useful when designing a haptic interface. However, adaptation can arise, which causes the pressure signal to be less over time [10]. This means that the design should adjust its level of stimulation every certain period of time.

Different modalities of feedback were studied by Muijzer-Witteveen et al. [59]. This study showed that frequency modulation was the most effective. The pneumatic balloon should inflate and deflate at a certain frequency. The question is, if this is operable in a system that is used on a daily basis. How will the balloons behave when inflated and deflated many times a day? How durable will they be? Will the accuracy be constant over time? These are all questions that need to be explored more.

Other results of the article of Muijzer-Witteveen et al. [59] showed that amplitude modulation or position modulation was not successful. A very small amount of subjects correctly identified the feedback levels.

When force feedback is integrated in a control system, it is desired to have a short latency time. Thus, the time between measuring the force and feeding it back to the user needs to be short, such that the user almost immediately feels the force that he/she is applying with the device. Antfolk et al. [10] conducted a literature study on sensory feedback in upper limb prosthetics. Tactile feedback takes approximately 14-28ms to be fed back to the user Johansson and Flanagan [45]. In the experiments conducted by [10], response time for tactile feedback is higher than for proprioceptive feedback. This causes the task execution time to be lower for direct proprioceptive feedback than with vibrotactile feedback [10] [36].

As mentioned before, it is desirable to have a short latency time. Is it then feasible to use tactile feedback as a mechanism, while it has

Actuator	Subgroup	Criteria							
		Pneumatic	50N	223 x 346mm	Soft	Feedback	Latency time 50ms	Practical	Efficient
3Conventional	Piston	+	+	-	-	+	+	-	?
	Rotary	+	+	-	-	+	+	-	?
	Screw	+	+	-	-	+	+	-	?
PAM	McKibben	+	+	+	+	+	+	+	+
	PBA	+	+	+	+	+	-	+	?
Soft	PBA	+	+	+	+	+	-	+	?
	Flexible active skin	+	?	?	+	+	?	+	?
	Rodless	+	?	?	+	+	?	?	?
	PTA	+	+	+	+	+	+	+	+
	Rest	+	?	?	+	+	?	?	?
Micro	MPAM	+	-	+	+	+	+	+	?
	PBA	+	-	+	+	+	-	+	?
Servo		+	+	?	?	+	+	?	?

Table 2: All the actuators discussed in this report on Control loop 1, are verified if they meet the criteria set, with + = Yes, - = No, ? = Not discussed/known.

a slow response time? Additionally, Delazio et al. [30] stated that the back was not very sensitive. This could induce problems in the final design when using pressure as a feedback mechanism.

Considering the slow response time of tactile feedback, and the insensibility of the back, proprioceptive feedback would be the better solution to provide force feedback to the user.

Antfolk et al. [10] mentioned different ways to provide efficient feedback. First, modality-matched feedback is explained. This means that when a force is applied to the prosthesis, this information should be fed back to the user as force, and not for example as pressure. As mentioned in the introduction, the goal is to feed back the force to the user. This also shows that pneumatic balloon actuators are not a suitable choice, as they provide tactile information (pressure).

Secondly, Simpson [77] mentioned the method of extended physiologic proprioception. The body's own physiological mechanisms need to be directly related to the activation and sensing of the controlled device. For example when a grip reaction force is provided at the prosthesis, it will be fed back to the user as a reaction torque about the elbow. This increases efficacy of control.

Above two methods can be of use when designing a wireless force transducer.

5. Conclusion

The research question of this essay was the following:

Which pneumatic actuator is most suitable to control the (output) force of a prosthetic hand?

To answer this question, the system was divided into two systems: Control loop 1 and Control loop 2. A separate literature review was conducted on both these control loops. This provided an elaborate overview of all the types of pneumatic actuators and its possibilities to provide feedback. All the information found was linked to a harness-less body-powered prosthesis, that will be designed in the follow-up of this literature research.

All the systems discussed in this literature study are reviewed if they meet the requirements set in section 1: Introduction. In Table 2 it can be seen, for the results on Control loop 1, which systems meet the requirement (+), does not meet the requirement (-), or if it

Actuator	Criteria							
	Pneumatic	50N	223 x 346mm	Soft	Feedback	Latency time 50ms	Practical	Efficient
Tactile	+	+	+	+	+	-	?	?
Proprioceptive	+	+	+	+	+	+	?	?

Table 3: All the actuators discussed in this report on Control loop 2, are verified if they meet the criteria set, with + = Yes, - = No, ? = Not discussed/known.

was not discussed and/or known (?). In Table 3 it can be seen, for the results on Control loop 2, which system meets the requirements or not.

Conventional pneumatic systems do not meet the three basic requirements of cosmesis, comfort and control. They are generally rather bulky and are produced out of hard materials. That is why McKibben muscles are a better choice. McKibben muscles meet all the requirements (see Table 2). Braided muscles have a high freedom in movement, caused by their variability in braid angle. This can be of use when designing a muscle that needs to contract or bent in a certain direction. This creates a large range of design possibilities, which can be of use in the design of a pneumatic system attached to the back of the user in my thesis.

Instead of using McKibben muscles, flexible active skin is also an opportunity as it meets most of the requirements (see Table 2). However, some of the criteria could not be tested, because not all information was present. Therefore, this system should be explored more in the future, to fully conclude if it is useful in the follow-up of this study.

Some articles were found on micro pneumatic systems. However, this term was debated, as was explained in section 4 (Discussion). However, it shows that many research is performed on this subject, with some promising results. Pneumatic systems are becoming smaller and smaller, which is preferable in a wearable system. The system needs to be comfortable, and should therefor not be too heavy and too large. With the use of micro pneumatic systems, a device as small as possible can be achieved. Nevertheless, a gain factor then needs to be integrated between the input and output force, to reach a force of 50N.

As explained in this literature study, it is preferred to provide proprioceptive feedback instead of tactile feedback (see Table 3). The possibility of using a pneumatic balloon actuator in this system will be eliminated, mainly due to the incompatibility of providing sufficient force feedback and the long latency time. It can be concluded from this article, that force feedback controlled systems will be the best option to provide the subject with physical feedback. It is extensively explained why pneumatic balloon actuators are not suitable. Therefore, in the masters thesis following this literature study, a force-controlled pneumatic system will be used. Inspiration can be obtained from information on servo pneumatic systems, as these systems show similarities.

To conclude, this literature review presented an extensive overview of all the possible options for a pneumatic force transducer. It provides a good starting point for the design of a pneumatic force transducer for a wireless prosthetic device. The design will consist of a McKibben muscle or flexible active skin. Research needs to be conducted on the material choice for McKibben muscles, and whether it is possible to use a fabric material as in a pneumatic textile muscle (PTA). Furthermore, feedback will be provided through proprioceptive feedback.

References

[1] T. Akagi and S. Dohta. Development of small sized multi-port pressure control valve for wearable actuator. *IEEE International Workshop on Robot and Human Interactive Communication*, pages 649–654, 2004.

[2] T. Akagi, S. Dohta, F. Zhao, and K. Fujita. Development and analysis of small-

sized quasi-servo valve using on/off valves. *SICE Annual Conference*, pages 783–790, 2010.

[3] T. Akagi, S. Dohta, Y. Matsui, H. Tamaki, and N. Kato. Low-cost wearable rehabilitation devices using flexible pneumatic cylinder with built-in pneumatic driving system. *IEEE International Conference on Advanced Intelligent Mechatronics (AIM)*, pages 89–93, 2016.

[4] L.A.T. Al Abeach, S. Nefti-Meziani, and S. Davis. Design of a variable stiffness soft dexterous gripper. *Soft Robotics*, 4 (3):274–284, 2017.

[5] A. Al-Ibadi, S. Nefti-Meziani, and S. Davis. Efficient structure-based models for the mckibben contraction pneumatic muscle actuator: The full description of the behaviour of the contraction pma. *Actuators*, 6(4), 2017.

[6] A. Al-Ibadi, S. Nefti-Meziani, and S. Davis. A circular pneumatic muscle actuator (cpma) inspired by human skeletal muscles. *IEEE International Conference on Soft Robotics (RoboSoft)*, 2018.

[7] H. Ali, S.M. Bashi, S. Noor, and M.H. Marhaban. A review of pneumatic actuators (modeling and control). *Australian Journal of Basic and Applied Sciences*, 3 (2):440–454, 2009.

[8] A.F. Alogla, P. Scanlan, W.M. Shu, and R.L. Reuben. A scalable syringe-actuated microgripper for biological manipulation. *Sensors and Actuators A: Physical*, 202:135–139, 2013.

[9] A.F. Alogla, F. Amalou, C. Balmer, P. Scanlan, W. Shu, and R.L. Reuben. Micro-tweezers: Design, fabrication, simulation and testing of a pneumaticaly actuated micro-gripper for micromanipulation and microtactile sensing. *Sensors and Actuators A: Physical*, 236:394–404, 2015.

[10] C. Antfolk, M. D'Alonzo, B. Rosén, G. Lundborg, F. Sebelius, and C. Cipriani. Sensory feedback in upper limb prosthetics. *Expert Reviews of Medical Devices*, 0(1):45–54, 2013.

[11] A. Barber. Pneumatic handbook 8th edition. 1997.

[12] G. Belforte, G. Eula, and S. Appendino. Design and development of innovative textile pneumatic muscles. *Journal of The Textile Institute*, 103(7):733–743, 2012.

[13] N. Besse, S. Rosset, Zarate J.J., and H. Shea. Flexible active skin: Large reconfigurable arrays of individually addressed shape memory polymer actuators. *Advanced Materials Technologies*, 2, 2017.

[14] Elaine A. Biddiss and Tom T. Chau. Upper limb prosthesis use and abandonment: A survey of the last 25 years. *Prosthetics and Orthotics International*, 31(3): 236–257, 2007.

[15] Elaine A. Biddiss, D. Beaton, and T. Chau. Consumer design priorities for upper limb prosthetics. *Disability and Rehabilitation: Assistive Technology*, 2 (6):346–357, 2007.

[16] M. Bouzit and G.C. Burdea. Hand force feedback and sensing system. *US7138976 B1 Patent*, 2006.

[17] M. Bouzit, G. Burdea, G. Popescu, and R. Boian. The rutgers master ii - new design force-feedback glove. *IEEE/ASME Transactions on Mechatronics*, 7(2):256–263, 2002.

[18] D.G. Caldwell, N. Tsagarakis, and G.A. Medrano-Cerda. Bio-mimetic actuators: polymeric pseudo muscular actuators and pneumatic muscle actuators for biological emulation. *Mechatronics*, 10: 499–530, 2000.

[19] J.F. Carneiro and F.G. De Almeida. Using two servovalves to improve pneumatic force control in industrial cylinders. *The International Journal of Advanced Manufacturing Technology*, 66: 283–301, 2013.

[20] S. Chakravarthy, K. Aditya, and A. Ghosal. Experimental characterization and control of miniaturized pneumatic artificial muscle. *Journal of Medical Devices*, 8, 2014.

[21] F. Cho, R. Sugimoto, T. Noritsugu, and X. Li. Improvement of wearable power assist wear for low back support using pneumatic actuator. *IOP Conference Series: Materials Science and Engineering*, 249, 2017.

[22] M. Collier and M. LeBlanc. Axilla bypass ring for shoulder harnesses for upper-limb prostheses. *Journal Prosthetics and Orthotics*, 8(4):130–131, 1996.

[23] J.C. Cool and J.O. Van Hooreweder. Hand prosthesis with adaptive internally powered fingers. *Medical Biological Engineering*, 9:33–36, 1971.

[24] M. Culjat, C. King, M. Franco, J. Bisley, W. Grundfest, and E. Dutson. Pneumatic balloon actuators for tactile feedback in robotic surgery. *Industrial Robot: An International Journal*, 31(6):449–455, 2008.

[25] M.F. Cullinan, E. Bourke, K. Kelly, and C. McGinn. A mckibben type sleeve pneumatic muscle and integrated mechanism for improved stroke length. *Journal of Mechanisms and Robotics*, 9, 2017.

[26] F. Daerden and D. Lefeber. The concept and design of pleated artificial muscles. *International Journal Of Fluid Power*, 2 (3):41–50, 2001.

[27] A. Dameitry and H. Tsukagoshi. Lightweight underactuated pneumatic fingers capable of grasping various objects. *IEEE International Conference on Robotics and Automation (ICRA)*, pages 2009–2014, 2016.

[28] M. De Volder, A.J.M. Moers, and D. Reynaerts. Fabrication and control of miniature mckibben actuators. *Sensors and Actuators*, 166:111–116, 2011.

[29] S.A. DeLaHunt, T.E. Pillsbury, and N.M. Wereley. Variable recruitment in bundles of miniature pneumatic artificial muscles. *Bioinspiration Biomimetics*, 11, 2016.

[30] A. Delazio, K. Nakagi, R.L. Klatzky, S.E. Hudson, J.F. Lehman, and A.P. Sample. Force jacket: Pneumatically-actuated jacket for embodied haptic experiences. *CHI*, 2018.

[31] DINED. Dutch adults 2004, age 20-60, male and female. *Retrieved from https://dined.io.tudelft.nl/en/database/tool*, 2004.

[32] T. Driver and X. Shen. Sleeve muscle actuator: Concept and prototype demonstration. *Journal of Bionic Engineering*, 10:222–230, 2013.

[33] T.A. Driver and X. Shen. Design and control of a sleeve muscle-actuated robotic elbow. *Journal of Dynamic Systems, Measurement and Control*, 136, 2014.

[34] P. Dólleman, J.F. Carneiro, and F.G. De Almeida. Exploring the use of two servo-valves for servo-pneumatic control. *The International Journal of Advanced Manufacturing Technology*, 97: 3963–3980, 2018.

[35] Z. Egeresi. Compressed air pressure driven tooth brush, toy, shaver, drill, grinder, screw, driver, engraver, sander. *US0044848 A1 Patent*, 2005.

[36] R.E. Fan, M.O. Culjat, S. King, M.L. Franco, R. Boryk, J.W. Bisley, E. Dutson, and W.S. Grundfest. A haptic feedback system for lower-limb prostheses. *IEEE Transactions on Neural Systems and Rehabilitation Engineering*, 16 (3):270–277, 2008.

[37] T.R. Farrel and R.F. Weir. The optimal controller delay for myoelectric prostheses. *IEEE Transactions on neural systems and rehabilitation engineering*, 15 (1):111–118, 2007.

[38] Festo. Solenoid/pneumatic valves, iso 5599-1. *Retrieved from: http://pdf.directindustry.com/pdf/festo/solenoid-pneumatic-valves-iso-5599-1/4735-181221.html*, 2018.

[39] J.D. Greer, T.K. Morimoto, A.M. Okamura, and E.W. Hawkes. Series pneumatic artificial muscles (spams) and application to a soft continuum robot. *IEEE International Conference Robot Automation*, pages 5503–5510, 2017.

[40] E.W. Hawkes, D.L. Christensen, and A.M. Okamura. Design and implementation of a 300% strain soft artificial muscle. *IEEE International Conference on Robotics and Automation (ICRA)*, pages 4022–4029, 2016.

[41] L. He, C. Xu, D. Xu, and R. Brill. Pneuhaptic: Delivering haptic cues with a pneumatic armband. *ISWC*, pages 47–48, 2015.

[42] M. Heidingsfeld, R. Horio, B. Baesch, C. Riethmüller, G.T. Gresser, and O. Sawodny. Introduction, mathematical modelling and motion control of the novel pneumatic textile actuator. *International Journal of Fluid Power*, 2016.

[43] M. Hichert and D. H. Plettenburg. Ipsilateral scapular cutaneous anchor system: An alternative for the harness in body-powered upper-limb prostheses. *Prosthetics and Orthotics International*, 42(1):101–106, 2017.

[44] S. Jadhav, V. Kannanda, B. Kang, M.T. Tolley, and J.P. Schulze. Soft robotic glove for kinesthetic haptic feedback in virtual reality environments. *International Symposium on Electronic Imaging*, pages 19–24, 2017.

[45] RS. Johansson and JR. Flanagan. Coding and use of tactile signals from the fingertips in object manipulation tasks. *Nat. Rev. Neursci.*, 10(5):345–359, 2009.

[46] V. Jouppila, S.A. Gadsden, and A. Ellman. Experimental comparisons of sliding mode controlled pneumatic muscle and cylinder actuators. *Journal of Dynamic Systems, Measurement and Control*, 136, 2014.

[47] D. Kamo, M. Maehara, D. Tanaka, and T. Nakamura. Development of a manipulator with straight-fiber-type artificial muscle and differential gear mechanism. *IECON 2011 - 37th Annual Conference of the IEEE Industrial Electronics Society*, pages 98–103, 2011.

[48] A.D. Keller, C.L. Taylor, and V. Zahm. Studies to determine the functional requirements for hand and arm prosthesis. pages 1–73, 1947.

[49] S. Konishi, F. Kawai, and P. Cusin. Thin flexible end-effector using pneumatic balloon actuator. *Sensor and Actuators*, 89:28–35, 2001.

[50] J. Kuusisto, A. Ellman, J. Reunamo, and J. Kuosa. Manipulating virtual objects with a haptic glove based on soft pneumatic muscles. *Proceedings of the ASME 2009 International Design Engineering Technical Conferences Computers and Information in Engineering Conference*, 2009.

[51] D. Latour, T. Sabolevski, and K. Lajoie-Weaver. Ipsilateral scapular cutaneous anchor. *Prooceedings of the 12th world congress of the International Society for Prosthetics and Orthotics*, page 555, 2007.

[52] D. A. Latour. Method for anchoring prosthetic and orthotic devices. *US8821588 B2 Patent*, 2006.

[53] Y.K. Lee and I. Shimoyama. A multichannel micro valve for micro pneumatic artificial muscle. *Fifteenth IEEE International Conference on Micro Electro Mechanical Systems*, pages 702–705, 2002.

[54] C. Liu, S. Dohta, T. Akagi, and A. Ando. Development of flexible spherical actuator using flexible pneumatic cylinder. *IEEE International Conference on Advanced Mechatronic Systems*, pages 81–86, 2012.

[55] W. Liu and C.R. Rahn. Fiber-reinforced membrane models of mckibben actuators. *Journal of Applied Mechanics*, 70: 853–859, 2003.

[56] Y. Matsui, T. Akagi, S. Dohta, and S. Fujimoto. Development of flexible pneumatic cylinder with string-type displacement sensor for flexible spherical actuator. *Proceedings on the 3rd International Conference on Intelligent Technologies and Engineering Systems*, pages 75–81, 2016.

[57] W. McMahan, V. Chitrakaran, M. Csencsits, D. Dawson, L.D. Walker, B.A. Jones, M. Pritts, D. Dienno, M. Grissom, and C.D. Rahn. Field trials and testing of the octarm continuum manipulator. *IEEE International Conference on Robotics and Automation*, pages 2336–2341, 2006.

[58] L. Migliori. Pneumatically actuated gripping device. *EP0619166 A1 Patent*, 1994.

[59] H. Muijzer-Witteveen, F. Guerra, V. Sluiter, and H. Van der Kooij. Pneumatic feedback for wearable lower limb exoskeletons further explored. *EuroHaptics*, pages 90–98, 2016.

[60] T. Nakamura. Experimental comparisons between mckibben type artificial muscles and straight fibers type artificial muscles. *SPIE Smart Materials, Nano- and Micro-Smart Systems III*, 2007.

[61] C.R. Nesler, T.A. Swift, and E.J. Rouse. Initial design and experimental evaluation of a pneumatic interference actuator. *Soft Robotics*, 2017.

[62] Y. Nojiri, N. Tsujiuchi, T. Koizumi, T. Mizuno, Y. Ichakawa, and M. Shimizu. Modeling and force control of membrane pneumatic actuators. *38th Annual Conference on IEEE Industrial Electronics Society*, pages 2607–2612, 2012.

[63] Y. Park, B. Chen, C. Majidi, R.J. Wood, R. Nagpal, and E. Goldfield. Active modular elastomer sleeve for soft wearable assistance robots. *International Conference on Intelligent Robots and Systems*, pages 1595–1602, 2012.

[64] Y. Park, D. Young, B. Chen, R.J. Wood, R. Nagpal, and E.C. Goldfield. Networked bio-inspired modules for sensorimotor control of wearable cyber-physical devices. *International Conference on Computing, Networking and Communications*, pages 92–96, 2013.

[65] A. Parr. *Hydraulics and Pneumatics: A Technician's and Engineer's Guide*. Elsevier, 2011.

[66] B. Peerdeman, G. Smit, S. Stramigioli, D. Plettenburg, and S. Misra. Evaluation of pneumatic cylinder actuators for hand prostheses. *IEEE RAS/EMBS International Conference on Biomedical Robotics and Biomechatronics*, 2012.

[67] P.V. Pistecky. Ontwerpen van armprotesen. 20(1):20–28, 1983.

[68] D.H. Plettenburg. Basic requirements for upper extremity prostheses: The wilmer approach. *Proceedings of the 20th Annual Conference of the IEEE Engineering in Medicine and Biology Society*, 20 (5):2276–2281, 1998.

[69] D.H. Plettenburg. A sizzling hand prosthesis: On the design and development of a pneumatically powered hand prosthesis for children. *PhD-thesis*, 2002.

[70] D.H. Plettenburg. Pneumatic actuators: a comparison of energy-to-mass ratio's. *Proceedings of the 2005 IEEE 9th International Conference on Rehabilitation Robotics*, pages 545–549, 2005.

[71] H. Pohl, P. Brandes, H.N. Quang, and M. Rohs. Squeezeback: Peumatic compression for notifications. *CHI*, pages 5318–5330, 2017.

[72] B. Radocy. Trs product catalog. page 32, 2018.

[73] D. Saravanakumar, B. Mohan, and T. Muthuramalingam. A review on recent research trends in servo pneumatic positioning systems. *Precision Engineering*, 49:481–492, 2017.

[74] G.D. Schott. Penfield's homunculus: a note on cerebral cartography. *Journal of Neurology, Neurosurgery, and Psychiatry*, 56:329–333, 1993.

[75] S. Schulz, C. Pylatiuk, M. Reischl, J. Martin, R. Mikut, and G. Bretthauer. A hydraulically driven multifunctional prosthetic hand. *Robotica*, 23:293–299, 2005.

[76] F. Sebastian, Q. Fu, M. Santello, and P. Polygerinos. Soft robotic haptic interface with variable stiffness for rehabilitation of neurologically impaired hand function. *Frontiers in Robotics and AI*, 4 (69), 2017.

[77] DC. Simpson. The control and supply of a multimovement externally powered upper limb prosthesis. *Proceedings of the Fifth International Symposium on Advances in External Control of Human Extremities*, pages 247–245, 1975.

[78] C. Suh, J.C. Margarit, Y.S. Song, and J. Paik. Soft pneumatic actuator skin with embedded sensors. *IEEE International Conference on Intelligent Robots and Systems*, pages 2783–2788, 2014.

[79] The Lee Company. 2-port face mount: Conventional models. *Retrieved from: https://www.theleeco.com/products/electro-fluidic-systems/solenoid-valves/control-valves/lhd-series/2-port/face-mount/*, 2018.

[80] H. Tsukagoshi, K. Shirato, M. Ido, and A. Kitagawa. Tail-arm: a wearable unit

to stimulate exercise. *IEEE International Workshop on Robot and Human Interactive Communication*, pages 667–672, 2004.

[81] M.W. Uddin, X. Zhang, and D. Wang. A pneumatic-driven haptic glove with force and tactile feedback. *International Conference on Virtual Reality and Visualization*, pages 304–311, 2016.

[82] I. Vaisman. Rotary vane compressor with economizer port for capacity control. *US6428284 B1 Patent*, 2002.

[83] B. Verrelst, R. Van Ham, B. Vanderborght, D. Lefeber, and F. Daerden. Second generation pleated pneumatic artificial muscle and its robotic applications. *Advanced robotics*, 20(7):783–805, 2006.

[84] R. Versluys, A. Desomer, G. Lenaerts, O. Paret, B. Vanderborght, G. Van der Perre, L. Peeraer, and D. Lefeber. A biomechatronical transtibial prosthesis powerd by pleated pneumatic artificial muscles. *International Journal Modelling, Identification and Control*, 4(4): 394–405, 2008.

[85] D. Villegas, M. Van Damme, B. Vanderborght, P. Beyl, and D. Lefeber. Third-generation pleated pneumatic artificial muscles for robotic applications: Developent and comparison with mckibben muscle. *Advanced Robotics*, 26(11-12): 1205–1227, 2012.

[86] B. Wang, A. McDaid, K.C. Aw, and M. Biglari-Abhari. Design and development of a skinny bidirectional soft glove for post-stroke hand rehabilitation. *Intelligent Systems Conference*, pages 979–987, 2017.

[87] Z. Zhang and M. Philen. Pressurized artificial muscles. *Journal of Intelligent Material Systems and Structures*, 23(3): 255–268, 2011.

[88] H. Zheng and X. Shen. Concept, design and application of sleeve muscle actuator. *Proceedings of the ASME 2014 International Design Engineering Technical Conferences Computers and Information in Engineering Conference*, 2014.

[89] L. Zheng, S. Yoshida, Y. Morimoto, H. Onoe, and S. Takeuchi. Pneumatic balloon actuator with tunable bending points. *IEEE Internationl Conferene on Micro Electro Mechanical Systems (MEMS)*, pages 18–21, 2015.

Appendix

[1] T. Akagi and S. Dohta. Development of small sized multi-port pressure control valve for wearable actuator. *IEEE International Workshop on Robot and Human Interactive Communication*, pages 649–654, 2004.

[2] T. Akagi, S. Dohta, Y. Matsui, H. Tamaki, and N. Kato. Low-cost wearable rehabilitation devices using flexible pneumatic cylinder with built-in pneumatic driving system. *IEEE International Conference on Advanced Intelligent Mechatronics (AIM)*, pages 89–93, 2016.

[3] T. Akagi, S. Dohta, F. Zhao, and K. Fujita. Development and analysis of small-sized quasi-servo valve using on/off valves. *SICE Annual Conference*, pages 783–790, 2010.

[4] L.A.T. Al Abeach, S. Nefti-Meziani, and S. Davis. Design of a variable stiffness soft dexterous gripper. *Soft Robotics*, 4(3):274–284, 2017.

[5] H. Al-Fahaam, S. Davis, and S. Nefti-Meziani. Power assistive and rehabilitation wearable robot based on pneumatic soft actuators. *2016 21st International Conference on Methods and Models in Automation and Robotics (MMAR)*, pages 472–477, 2016.

[6] A. Al-Ibadi, S. Nefti-Meziani, and S. Davis. Efficient structure-based models for the mckibben contraction pneumatic muscle actuator: The full description of the behaviour of the contraction pma. *Actuators*, 6(4), 2017.

[7] A. Al-Ibadi, S. Nefti-Meziani, and S. Davis. A circular pneumatic muscle actuator (cpma) inspired by human skeletal muscles. *IEEE International Conference on Soft Robotics (RoboSoft)*, 2018.

[8] A. Al-Ibadi, S. Nefti-Meziani, and

S. Davis. A circular pneumatic muscle actuator (cpma) inspired by human skeletal muscles. *IEEE International Conference on Soft Robotics (RoboSoft)*, 2018.

[9] H. Ali, S.M. Bashi, S. Noor, and M.H. Marhaban. A review of pneumatic actuators (modeling and control). *Australian Journal of Basic and Applied Sciences*, 3(2):440–454, 2009.

[10] A.F. Alogla, F. Amalou, C. Balmer, P. Scanlan, W. Shu, and R.L. Reuben. Micro-tweezers: Design, fabrication, simulation and testing of a pneumaticaly actuated micro-gripper for micromanipulation and microtactile sensing. *Sensors and Actuators A: Physical*, 236:394–404, 2015.

[11] A.F. Alogla, P. Scanlan, W.M. Shu, and R.L. Reuben. A scalable syringe-actuated microgripper for biological manipulation. *Sensors and Actuators A: Physical*, 202:135–139, 2013.

[12] C. Antfolk, M. D'Alonzo, B. Rosén, G. Lundborg, F. Sebelius, and C. Cipriani. Sensory feedback in upper limb prosthetics. *Expert Reviews of Medical Devices*, 0(1):45–54, 2013.

[13] Diane J. Atkins, Denise C.Y. Heard, and William H. Donocan. Epidemiologic overview of individuals with upper-limb loss and their reported research priorities. *Prosthetics and Orthotics*, 8(1):2–11, 1996.

[14] G. Bao, P. Yao, Z. Xu, K. Li, Z. Wang, L. Zhang, and Q. Yang. Pneumatic bio-soft robot module: Structure, elongation and experiment. *International Journal Agriculture Biology Engineering*, 10(2):114–122, 2017.

[15] J. Barak, Y. Naveh, and S. Ehrlich. Portable ambulant pneumatic compression system. *US6494852 B1 Patent*, 2002.

[16] A. Barber. Pneumatic handbook 8th edition. 1997.

[17] H.D. Baumann. Rotary pneumatic actuator. *US6772528 B2 Patent*, 2004.

[18] B.A. Baydere, S.K. Talas, and E. Samur. A novel highly-extensible 2-dof pneumatic actuator for soft robot applications. *Sensors and Actuators A: Physical*, 281:84–94, 2018.

[19] G. Belforte, G. Eula, and S. Appendino. Design and development of innovative textile pneumatic muscles. *Journal of The Textile Institute*, 103(7):733–743, 2012.

[20] D. Ben-Dov and S.E. Salcudean. A force-controlled pneumatic actuator. *IEEE Transactions on Robotics and Automation*, 11(6):906–911, 1995.

[21] S. Besoiu, M. Vistrian, and D. Radu. Mechatronic design of a planar parallel robot actuated by pneumatic artificial muscles. *Solid State Phenomena*, pages 57–62, 2010.

[22] N. Besse, S. Rosset, Zarate J.J., and H. Shea. Flexible active skin: Large reconfigurable arrays of individually addressed shape memory polymer actuators. *Advanced Materials Technologies*, 2, 2017.

[23] Elaine A. Biddiss, D. Beaton, and T. Chau. Consumer design priorities for upper limb prosthetics. *Disability and Rehabilitation: Assistive Technology*, 2(6):346–357, 2007.

[24] Elaine A. Biddiss and Tom T. Chau. Upper limb prosthesis use and abandonment: A survey of the last 25 years. *Prosthetics and Orthotics International*, 31(3):236–257, 2007.

[25] M. Bochen and T. Ehre. Piston-cylinder unit. *US8286545 B2 Patent*, 2012.

[26] M. Bouzit, G. Burdea, G. Popescu, and R. Boian. The rutgers master ii - new design force-feedback glove. *IEEE/ASME Transactions on Mechatronics*, 7(2):256–263, 2002.

[27] M. Bouzit and G.C. Burdea. Hand force feedback and sensing system. *US7138976 B1 Patent*, 2006.

[28] D. Bruder, A. Sedal, R. Vasudevan, and C.D. Remy. Force generation by parallel combinations of fiber-reinforced fluid-driven actuators. *IEEE Robotics and Automation Letters*, 3(4):3999–4006, 2018.

[29] G.C. Burdea and D. Gomez. Actuator system for providing force feedback to portable master support. *US5354162A Patent*, 1994.

[30] G.C. Burdea and J. Zhuang. Actuator system for providing force feedback to a dextrous master glove. *US5143505A Patent*, 1992.

[31] D.G. Caldwell, U. Andersen, C.J. Bowler, and A.J. Wardle. A higher power/weight dexterous manipulator using 'sensory glove' based motion control and tactile feedback. *Transactions of the Institute of Measurement and Control*, 17(5):234–241, 1995.

[32] D.G. Caldwell, P.Y. Chua, and M.Z. Amran. 'soft' actuation for dextrous hands - a 23 DOF anthropomorphic hand powered by pneumatic muscle actuators. *International Journal of Modelling, Identification and Control*, 4(4):383–393, 2008.

[33] D.G. Caldwell, G.A. Medrano-Cerda, and M.J. Goodwin. Braided pneumatic actuator control of a multi-jointed manipulator. *Proceedings of IEEE Systems Man and Cybernetics Conference - SMC*, pages 423–428, 1993.

[34] D.G. Caldwell and N. Tsagarakis. Biomimetic actuators in prosthetic and rehabilitation applications. *Technology and Health Care*, pages 107–120, 2002.

[35] D.G. Caldwell, N. Tsagarakis, and G.A. Medrano-Cerda. Bio-mimetic actuators: polymeric pseudo muscular actuators and pneumatic muscle actuators for biological emulation. *Mechatronics*, 10:499–530, 2000.

[36] D.G. Caldwell, N.G. Tsagarakis, S. Kousidou, N. Costa, and I. Sarakoglou. "soft" exoskeletons for upper and lower body rehabilitation - design, control and testing. *International Journal of Humanoid Robotics*, 4(3):549–573, 2007.

[37] B.D. Camaron, C. De la Malla, and J. López-Moliner. The role of differential delays in integrating transient visual and proprioceptive informatio. *Frontiers in Psychology*, 5(50), 2014.

[38] J.F. Carneiro and F.G. De Almeida. Pneumatic servo valve models based on artificial neural networks. *Journal Systems and Control Engineering*, 225(1):393–411, 2011.

[39] J.F. Carneiro and F.G. De Almeida. Using two servovalves to improve pneumatic force control in industrial cylinders. *The International Journal of Advanced Manufacturing Technology*, 66:283–301, 2013.

[40] J.F. Carneiro and F.G. De Almeida. Friction characteristics and servo control of a linear peristaltic actuator. *The International Journal of Advanced Manufacturing Technology*, 96:2117–2126, 2018.

[41] W. Carrigan, R. Stein, M. Mittal, and M.B.J. Wijesundara. Conformal grasping using feedback controlled bubble actuator array. *Proceedings of SPIE*, 9116, 2014.

[42] D. Chakarov, I. Veneva, M. Tsveov, and E. Zlatanov. Adjusting the natural stiffness of a pneumatic powered exoskeleton designed as a virtual reality haptic device. *International Journal Of Advanced Robotic Systems*, pages 1–13, 2017.

[43] S. Chakravarthy, K. Aditya, and A. Ghosal. Experimental characterization and control of miniaturized pneumatic artificial muscle. *Journal of Medical Devices*, 8, 2014.

[44] C. Chen, Y. Wu, F. Chen, and M. Chen. Pneumatic artificial muscle-driven control loading system (ifuzzy2017). *International Journal Fuzzy Systems*, 20(6):1779–1789, 2018.

[45] T. Chen and Z. Zhang. Design and research of tele-operation manipulator with force feedback. *International Conference on Intelligent Computation Technology and Automation*, pages 979–983, 2008.

[46] F. Cho, R. Sugimoto, T. Noritsugu, and X. Li. Improvement of wearable power assist wear for low back support using pneumatic actuator. *IOP Conference Series: Materials Science and Engineering*, 249, 2017.

[47] T. Choi, J. Kim, and J. Lee. An artificial pneumatic muscle control method on the limited space. *SICE-ICASE International Joint Conference*, pages 4738–4743, 2016.

[48] M. Cinq-Mars and H. Gurocak. Pneumatic cylinder with magnetorheological brake using serpentine and helix flux guide as a linear hybrid actuator for haptics. *Journal of Intelligent Material Systems and Structures*, 28(10):1303–1321, 2016.

[49] R. Colbrunn and R.D. Quinn. Design and control of a robotic leg with braided pneumatic actuators. 2001.

[50] M. Collier and M. LeBlanc. Axilla bypass ring for shoulder harnesses for upper-limb prostheses. *Journal Prosthetics and Orthotics*, 8(4):130–131, 1996.

[51] J.C. Cool and J.O. Van Hooreweder. Hand prosthesis with adaptive internally powered fingers. *Medical Biological Engineering*, 9:33–36, 1971.

[52] F. Cordella, A. L. Ciancia, R. Sacchetti, A. Davalli, A. G. Cutti, E. Guglielmelli, and L. Zollo. Literature review on needs of upper limb prosthesis users. *Frontiers of Neuroscience*, 10(209):1–14, 2016.

[53] M. Culjat, C. King, M. Franco, J. Bisley, W. Grundfest, and E. Dutson. Pneumatic balloon actuators for tactile feedback in robotic surgery. *Industrial Robot: An International Journal*, 31(6):449–455, 2008.

[54] M.O. Culjat, R.E. Fan, and W.S. Grundfest. Optimization of a tactile feedback system to aid the rehabilitation of lower-limb amputees. page 62, 2008.

[55] M.F. Cullinan, E. Bourke, K. Kelly, and C. McGinn. A mckibben type sleeve pneumatic muscle and integrated mechanism for improved stroke length. *Journal of Mechanisms and Robotics*, 9, 2017.

[56] F. Daerden and D. Lefeber. The concept and design of pleated artificial muscles. *International Journal Of Fluid Power*, 2(3):41–50, 2001.

[57] A. Dameitry and H. Tsukagoshi. Lightweight underactuated pneumatic fingers capable of grasping various objects. *IEEE International Conference on Robotics and Automation (ICRA)*, pages 2009–2014, 2016.

[58] S. Davis and D.G. Caldwell. Braid effects on contractile range and friction modeling in pneumatic muscle actuators. *The International Journal of Robotics Research*, 25(4):359–369, 2006.

[59] S. Davis, N. Tsagarakis, J. Canderle, and D.G. Caldwell. Enhanced modelling and performance in braided pneumatic muscle actuators. *The International Journal of Robotics Research*, 22(3-4):213–227, 2003.

[60] M. De Volder, A.J.M. Moers, and D. Reynaerts. Fabrication and control of miniature mckibben actuators. *Sensors and Actuators*, 166:111–116, 2011.

[61] A. Deaconescu and T. Deaconescu. Contributions to the behavioural study of pneumatically actuated artificial muscles. *6th International DAAAM Baltic Conference*, 2008.

[62] S.A. DeLaHunt, T.E. Pillsbury, and N.M. Wereley. Variable recruitment in bundles of miniature pneumatic artificial muscles. *Bioinspiration Biomimetics*, 11, 2016.

[63] A. Delazio, K. Nakagi, R.L. Klatzky, S.E. Hudson, J.F. Lehman, and A.P. Sample. Force jacket: Pneumatically-actuated jacket for embodied haptic experiences. *CHI*, 2018.

[64] DINED. Dutch adults 2004, age 20-60, male and female. *Retrieved from https://dined.io.tudelft.nl/en/database/tool*, 2004.

[65] B.G. Do Nascimento, C.B.S. Vimieiro, D.A.P. Nagem, and M. Pinotti. Hip orthosis powered by pneumatic artificial muscle: Voluntary activation in absence of myoelectrical signal. *Artificial Organs*, 32(4):317–322, 2008.

[66] E. Doh, H. Lee, J. Park, and K. Yun. Three-axis tactile display using pdms

pneumatic actuator for robot-assisted surgery. *Transducers*, pages 2418–2421, 2011.

[67] T. Driver and X. Shen. Sleeve muscle actuator: Concept and prototype demonstration. *Journal of Bionic Engineering*, 10:222–230, 2013.

[68] T.A. Driver and X. Shen. Design and control of a sleeve muscle-actuated robotic elbow. *Journal of Dynamic Systems, Measurement and Control*, 136, 2014.

[69] T.A. Driver and X. Shen. Design and control of a sleeve muscle-actuated robotic elbow. *Journal of Dynamic Systems, Measurement, and Control*, 136, 2014.

[70] H. Du, Z. Wang, and L. Chen. Design of a new type of pneumatic force feedback data glove. *Proceedings of 2011 International Conference on Fluid Power and Mechatronics*, pages 292–296, 2011.

[71] S. Díaz-Zagal, C. Gutiérrez-Estrada, E. Rendón-Lara, I. Abundez-Barrera, and J.H. Pacheco-Sánchez. Pneumatic artificial mini-muscles conception: Medical robotics applications. *Applied Mechanics and Materials*, 15:49–54, 2009.

[72] P. Dólleman, J.F. Carneiro, and F.G. De Almeida. Exploring the use of two servo-valves for servo-pneumatic control. *The International Journal of Advanced Manufacturing Technology*, 97:3963–3980, 2018.

[73] Z. Egeresi. Compressed air pressure driven tooth brush, toy, shaver, drill, grinder, screw, driver, engraver, sander. *US0044848 A1 Patent*, 2005.

[74] Y. Eguchi, T. Akagi, S. Dohta, and W. Kobayashi. Improvement of flexible linear stepping actuator driven by pneumatic balloons and brakes. *MATEC Web of Conferences*, 82, 2016.

[75] R.E. Fan, M.O. Culjat, S. King, M.L. Franco, R. Boryk, J.W. Bisley, E. Dutson, and W.S. Grundfest. A haptic feedback system for lower-limb prostheses. *IEEE Transactions on Neural Systems and Rehabilitation Engineering*, 16(3):270–277, 2008.

[76] T.R. Farrel and R.F. Weir. The optimal controller delay for myoelectric prostheses. *IEEE Transactions on neural systems and rehabilitation engineering*, 15(1):111–118, 2007.

[77] Festo. Solenoid/pneumatic valves, iso 5599-1. *Retrieved from: http://pdf.directindustry.com/pdf/festo/solenoid-pneumatic-valves-iso-5599-1/4735-181221.html*, 2018.

[78] C. Gaudeni, L. Meli, and D. Prattichizzo. A novel pneumatic force sensor for robot-assisted surgery. *EuroHaptics*, pages 587–599, 2018.

[79] J.D. Greer, T.K. Morimoto, A.M. Okamura, and E.W. Hawkes. Series pneumatic artificial muscles (spams) and application to a soft continuum robot. *IEEE International Conference Robot Automation*, pages 5503–5510, 2017.

[80] Y. Hao, Z. Gong, Z. Xie, S. Guan, X. Yang, T. Wang, and L. Wen. A soft bionic gripper with variable effective length. *Journal of Bionic Engineering*, 15:220–235, 2018.

[81] E.W. Hawkes, D.L. Christensen, and A.M. Okamura. Design and implementation of a 300% strain soft artificial muscle. *IEEE International Conference on Robotics and Automation (ICRA)*, pages 4022–4029, 2016.

[82] L. He, C. Xu, D. Xu, and R. Brill. Pneuhaptic: Delivering haptic cues with a pneumatic armband. *ISWC*, pages 47–48, 2015.

[83] M. Heidingsfeld, R. Horio, B. Baesch, C. Riethmüller, G.T. Gresser, and O. Sawodny. Introduction, mathematical modelling and motion control of the novel pneumatic textile actuator. *International Journal of Fluid Power*, 2016.

[84] M. Hichert and D. H. Plettenburg. Ipsilateral scapular cutaneous anchor system: An alternative for the harness in body-powered upper-limb prostheses. *Prosthetics and Orthotics International*, 42(1):101–106, 2017.

[85] S. Honda, Y. Tsujimura, and S. Konishi. Design and characterization of contraction motion actuator converted

from swelling pneumatic balloon actuator for large deformation and force. *Transducers*, pages 2140–2143, 2015.

[86] Y. Hwang, O.H. Paydar, and R.N. Candler. Pneumatic microfinger with balloon fins for linear motion using 3d printed molds. *Sensors and Actuators A: Physical*, 234:65–71, 2015.

[87] M. Iltanen, A. Ellman, and J. Laitinen. Wearable haptic device for an ipt system based on pneumatic muscles. *Proceedings of the ASME 2007 International Design Engineering Technical Conferences Computers and Information in Engineering Conference*, 2007.

[88] S. Jadhav, V. Kannanda, B. Kang, M.T. Tolley, and J.P. Schulze. Soft robotic glove for kinesthetic haptic feedback in virtual reality environments. *International Symposium on Electronic Imaging*, pages 19–24, 2017.

[89] RS. Johansson and JR. Flanagan. Coding and use of tactile signals from the fingertips in object manipulation tasks. *Nat. Rev. Neursci.*, 10(5):345–359, 2009.

[90] V. Jouppila and A. Ellman. Effect of load disturbances on multiplexed force control of mckibben actuators. *ASME International Mechanical Engineering Congress and Exposition*, 2007.

[91] V. Jouppila, S.A. Gadsden, and A. Ellman. Experimental comparisons of sliding mode controlled pneumatic muscle and cylinder actuators. *Journal of Dynamic Systems, Measurement and Control*, 136, 2014.

[92] D. Kamo, M. Maehara, D. Tanaka, and T. Nakamura. Development of a manipulator with straight-fiber-type artificial muscle and differential gear mechanism. *IECON 2011 - 37th Annual Conference of the IEEE Industrial Electronics Society*, pages 98–103, 2011.

[93] R. Kang, Y. Guo, K. Cheng, and L. Chen. Design and control of a soft actuator driven by pneumatic muscles. *2014 International Conference on Industrial Automation, Information and Communications Technology*, pages 26–30, 2014.

[94] A.D. Keller, C.L. Taylor, and V. Zahm. Studies to determine the functional requirements for hand and arm prosthesis. pages 1–73, 1947.

[95] P.M. Khin, H.K. Yap, M.H. Ang, and C. Yeow. Fabric-based actuator modules for building soft pneumatic structures with high payload-to-weight ratio. *2017 IEEE/RSJ International Conference on Intelligent Robots and Systems (IROS)*, pages 2744–2750, 2017.

[96] S. Konishi. Small, soft and safe micromachines for biomedical applications. *Transducers*, pages 863–866, 2015.

[97] S. Konishi, F. Kawai, and P. Cusin. Thin flexible end-effector using pneumatic balloon actuator. *Sensor and Actuators*, 89:28–35, 2001.

[98] I. Koo, K. Jung, J. Koo, J. Nam, Y. Lee, and H.R. Choi. Wearable tactile display based on soft actuator. *Proceedings of the 2006 IEEE International Conference on Robotics and Automation*, pages 2220–2225, 2006.

[99] J.F. Kramer. Force feedback and texture simulating interface device. *US6979164 B2 Patent*, 2005.

[100] J. Kuusisto, A. Ellman, J. Reunamo, and J. Kuosa. Manipulating virtual objects with a haptic glove based on soft pneumatic muscles. *Proceedings of the ASME 2009 International Design Engineering Technical Conferences Computers and Information in Engineering Conference*, 2009.

[101] D. Latour, T. Sabolevski, and K. Lajoie-Weaver. Ipsilateral scapular cutaneous anchor. *Prooceedings of the 12th world congress of the International Society for Prosthetics and Orthotics*, page 555, 2007.

[102] D. A. Latour. Method for anchoring prosthetic and orthotic devices. *US8821588 B2 Patent*, 2006.

[103] Y.K. Lee and I. Shimoyama. A multichannel micro valve for micro pneumatic artificial muscle. *Fifteenth IEEE International Conference on Micro Electro Mechanical Systems*, pages 702–705, 2002.

[104] M. Lemire, L. Boni, and B. Furnish. The straight story on linear actuators. 2007.

[105] M. Li, S. Luo, T. Nanayakkara, L.D. Seneviratne, P. Dasgupta, and K. Althoefer. Multi-fingered haptic palpation using pneumatic feedback actuators. *Sensors and Actuators A: Physical*, 218:132–141, 2014.

[106] C. Liao, P.B. Gladen, and K. Hochhalter. Precision servo control system for a pneumatic actuator. *US6523451 B1 Patent*, 2003.

[107] C. Liu, S. Dohta, T. Akagi, and A. Ando. Development of flexible spherical actuator using flexible pneumatic cylinder. *IEEE International Conference on Advanced Mechatronic Systems*, pages 81–86, 2012.

[108] W. Liu and C.R. Rahn. Fiber-reinforced membrane models of mckibben actuators. *Journal of Applied Mechanics*, 70:853–859, 2003.

[109] D. Majoe, L. Widmes, and J. Gutknecht. Pneumatic air muscle and pneumatic sources for light weight autonomous robots. *IEEE International Conference on Robotics and Automation*, pages 3243–3250, 2011.

[110] S.R. Majumdar. Pneumatic systems: Principles and maintenance. 1995.

[111] R.V. Martinez, J.L. Branch, C.R. Fish, L. Jin, R.F. Shepherd, R.M.D. Nunes, Suo Z., and G.M. Whitesides. Robotic tentacles with three-dimensional mobility based on flexible elastomers. *Advanced Materials*, 25:205–212, 2013.

[112] Y. Matsui, T. Akagi, S. Dohta, and S. Fujimoto. Development of flexible pneumatic cylinder with string-type displacement sensor for flexible spherical actuator. *Proceedings on the 3rd International Conference on Intelligent Technologies and Engineering Systems*, pages 75–81, 2016.

[113] V.P. McCarrol, R.E. Howe, B.D. Carter, and D.S. Cook. Servo-pneumatic actuator. *US7401541 B2 Patent*, 2008.

[114] W. McMahan, V. Chitrakaran, M. Csencsits, D. Dawson, L.D. Walker, B.A. Jones, M. Pritts, D. Dienno, M. Grissom, and C.D. Rahn. Field trials and testing of the octarm continuum manipulator. *IEEE International Conference on Robotics and Automation*, pages 2336–2341, 2006.

[115] L. Migliori. Pneumatically actuated gripping device. *EP0619166 A1 Patent*, 1994.

[116] J. Misumi, S. Wakimoto, and K. Suzumori. Experimental investigation of conductive fibers for a smart pneumatic artificial muscle. *Proceedings of the 2015 IEEE Conference on Robotics and Biomimetics*, pages 2335–2340, 2015.

[117] R. Miyazaki, T. Terata, T. Kanno, T. Tsuji, G. Endo, and K. Kawashima. Compact haptic device using a pneumatic bellows for teleoperation of a surgical robot. *International Conference on Intelligent Robots and Systems (IROS)*, pages 2018–2023, 2015.

[118] J. Morrow, H. Shin, J. Torrey, R. Larkins, S. Dang, C. Phillips-Grafflin, Y. Park, and D. Berenson. Improving soft pneumatic actuator fingers through integration of soft sensors, position and force control, and rigid fingernails. *2016 IEEE International Conference on Robotics and Automation (ICRA)*, 218, 2016.

[119] H. Muijzer-Witteveen, F. Guerra, V. Sluiter, and H. Van der Kooij. Pneumatic feedback for wearable lower limb exoskeletons further explored. *EuroHaptics*, pages 90–98, 2016.

[120] T. Nakamura. Experimental comparisons between mckibben type artificial muscles and straight fibers type artificial muscles. *SPIE Smart Materials, Nano- and Micro-Smart Systems III*, 2007.

[121] T. Nango, T. Akagi, S. Dohta, and H. Matsushita. Development of flexible robot arm using rod-less type flexible pneumatic cylinders. *SICE-ICASE International Joint Conference*, pages 451–454, 2006.

[122] C.R. Nesler, T.A. Swift, and E.J. Rouse. Initial design and experimental evalua-

tion of a pneumatic interference actuator. *Soft Robotics*, 2017.

[123] Y. Nojiri, N. Tsujiuchi, T. Koizumi, T. Mizuno, Y. Ichakawa, and M. Shimizu. Modeling and force control of membrane pneumatic actuators. *38th Annual Conference on IEEE Industrial Electronics Society*, pages 2607–2612, 2012.

[124] T. Noritsugu, M. Takaiwa, and D. Sasaki. Power assist wear driven with pneumatic rubber artificial muscles. *19th International Conference on Mechatronics and Machine Vision in Practice*, pages 539–544, 2009.

[125] Y. Park, B. Chen, C. Majidi, R.J. Wood, R. Nagpal, and E. Goldfield. Active modular elastomer sleeve for soft wearable assistance robots. *International Conference on Intelligent Robots and Systems*, pages 1595–1602, 2012.

[126] Y. Park, D. Young, B. Chen, R.J. Wood, R. Nagpal, and E.C. Goldfield. Networked bio-inspired modules for sensorimotor control of wearable cyberphysical devices. *International Conference on Computing, Networking and Communications*, pages 92–96, 2013.

[127] A. Parr. *Hydraulics and Pneumatics: A Technician's and Engineer's Guide*. Elsevier, 2011.

[128] B. Peerdeman, G. Smit, S. Stramigioli, D. Plettenburg, and S. Misra. Evaluation of pneumatic cylinder actuators for hand prostheses. *IEEE RAS/EMBS International Conference on Biomedical Robotics and Biomechatronics*, 2012.

[129] P.V. Pistecky. Ontwerpen van armprotesen. 20(1):20–28, 1983.

[130] D.H. Plettenburg. Basic requirements for upper extremity prostheses: The wilmer approach. *Proceedings of the 20th Annual Conference of the IEEE Engineering in Medicine and Biology Society*, 20(5):2276–2281, 1998.

[131] D.H. Plettenburg. A sizzling hand prosthesis: On the design and development of a pneumatically powered hand prosthesis for children. *PhD-thesis*, 2002.

[132] D.H. Plettenburg. Pneumatic actuators: a comparison of energy-to-mass ratio's. *Proceedings of the 2005 IEEE 9th International Conference on Rehabilitation Robotics*, pages 545–549, 2005.

[133] H. Pohl, P. Brandes, H.N. Quang, and M. Rohs. Squeezeback: Peumatic compression for notifications. *CHI*, pages 5318–5330, 2017.

[134] B. Radocy. Trs product catalog. page 32, 2018.

[135] N. Saga. Development of a tendon driven system using a pneumatic balloon. *Journal of Intelligent Material Systems and Structures*, 18:171–174, 2007.

[136] N. Saga, J. Nagase, and T. Saikawa. Pneumatic artificial muscles based on biomechanical characteristics of human muscles. *Applied Bionics and Biomechanics*, 3(3):191–197, 2006.

[137] N. Saga and N. Saito. Rehabilitation instrument for prevent contracture of ankle using the pneumatic balloon actuator. *30th Annual International IEEE EMBS Conference*, pages 4294–4297, 2008.

[138] D. Saravanakumar, B. Mohan, and T. Muthuramalingam. A review on recent research trends in servo pneumatic positioning systems. *Precision Engineering*, 49:481–492, 2017.

[139] B.M. Schena and L.B. Rosenberg. Method for providing high bandwidth force feedback with improved actuator feel. *US7236157 B2 Patent*, 2007.

[140] G.D. Schott. Penfield's homunculus: a note on cerebral cartography. *Journal of Neurology, Neurosurgery, and Psychiatry*, 56:329–333, 1993.

[141] S. Schulz, C. Pylatiuk, M. Reischl, J. Martin, R. Mikut, and G. Bretthauer. A hydraulically driven multifunctional prosthetic hand. *Robotica*, 23:293–299, 2005.

[142] F. Sebastian, Q. Fu, M. Santello, and P. Polygerinos. Soft robotic haptic interface with variable stiffness for rehabilitation of neurologically impaired

hand function. *Frontiers in Robotics and AI*, 4(69), 2017.

[143] J. Shaperman and M. LeBlanc. Prehensor grip for children: A survey of the literature. *JPO: Journal of Prosthetics and Orthotics*, 7(2):61–64, 1995.

[144] X. Shen and M. Goldfarb. On the enhanced passivity of pneumatically actuated impedance-type haptic interfaces. *IEEE Transactions on Robotics*, 22(3):470–480, 2006.

[145] S. Shimada, K. Fukuda, and K. Hiraki. Rubber hand illusion under delayed visual feedback. *PLoS one*, 4(7), 2009.

[146] A. Shiva, A. Stilli, Y. Noh, A. Faragasso, I. De Falco, G. Gerboni, M. Cianchetti, A. Menciassi, K. Althoefer, and H.A. Wurdemann. Tendon-based stiffening for a pneumatically actuated soft manipulator. *IEEE Robotics and Automation Letters*, 1(2):632–637, 2016.

[147] DC. Simpson. The control and supply of a multimovement externally powered upper limb prosthesis. *Proceedings of the Fifth International Symposium on Advances in External Control of Human Extremities*, pages 247–245, 1975.

[148] D.V. Sriramamurty and D.E. Brzezinski. Fluid power piston actuators. *4056043 Patent*, 1977.

[149] C. Suh, J.C. Margarit, Y.S. Song, and J. Paik. Soft pneumatic actuator skin with embedded sensors. *IEEE International Conference on Intelligent Robots and Systems*, pages 2783–2788, 2014.

[150] Z. Sun, X. Miao, and X. Li. Design of a bidirectional force feedback dataglove based on pneumatic artificial muscles. *Proceedings of the 2009 IEEE International Conference on Mechatronics and Automation*, pages 1767–1771, 2009.

[151] K. Suzumori, N. Osaki, J. Misumi, A. Yamamoto, and T. Kanda. A multiplex pneumatic actuator drive method based on acoustic communication in air supply line. *IEEE International Conference on Intelligent Robots and Systems*, pages 2795–2800, 2014.

[152] K. Tadano and K. Kawashima. Development of 4-dofs forceps with force sensing using pneumatic servo system. *Proceedings of the 2006 IEEE International Conference on Robotics and Automation*, pages 2250–2255, 2006.

[153] K. Tadano and K. Kawashima. Development of a master-slave system with force-sensing abilities using pneumatic actuators for laparoscopic surgery. *Advanced Robotics*, 24(12):1763–1783, 2010.

[154] H. Tamaki, S. Dohta, T. Akagi, W. Kobayashi, and Y. Matsui. Development of hybrid type flexible pneumatic cylinder for considering less air consumption. *MATEC Web of Conferences*, 82, 2016.

[155] T. Taniguchi, S. Sakurai, T. Nojima, and K. Hirota. Multi-point pressure sensation display using pneumatic actuators. *EuroHaptics*, pages 58–67, 2018.

[156] The Lee Company. 2-port face mount: Conventional models. *Retrieved from: https://www.theleeco.com/products/electro-fluidic-systems/solenoid-valves/control-valves/lhd-series/2-port/face-mount/*, 2018.

[157] L.O. Tiziani, T.W. Cahoon, and F.L. Hammond. Sensorized pneumatic muscle for force and stiffness control. *IEEE International Conference on Robotics and Automation*, pages 5545–5552, 2017.

[158] N. Tsagarakis, D.G. Caldwell, and G.A. Medrano-Cerda. A 7 dof pneumatic muscle actuator (pma) powered exoskeleton. *Proceedings of the 1999 IEEE International Workshop on Robot and Human Interaction*, pages 327–333, 1999.

[159] H. Tsukagoshi, K. Shirato, M. Ido, and A. Kitagawa. Tail-arm: a wearable unit to stimulate exercise. *IEEE International Workshop on Robot and Human Interactive Communication*, pages 667–672, 2004.

[160] M.W. Uddin, X. Zhang, and D. Wang. A pneumatic-driven haptic glove with force and tactile feedback. *International*

Conference on Virtual Reality and Visualization, pages 304–311, 2016.

[161] I. Vaisman. Rotary vane compressor with economizer port for capacity control. *US6428284 B1 Patent*, 2002.

[162] O. Van der Niet, H.A. Reinders-Messelink, R.M. Bongers, H. Bouwsema, and C.K. Van der Sluis. The i-limb hand and the dmc plus hand compared: A case report. *Prosthetics and Orthotics International*, 34(2):216–220, 2010.

[163] M. Vazquez, E. Brockmeyer, R. Desai, C. Harrison, and S.E. Hudson. 3d printing pneumatic device controls with variable activation force capabilities. *CHI*, pages 1295–1304, 2015.

[164] A.J. Veal, I.A. Anderson, and S.Q. Xie. The smart peano fluidic muscle: a low profile flexible orthosis actuator that feels pain. *Proceedings of SPIE*, 2015.

[165] B. Verrelst, R. Van Ham, B. Vanderborght, D. Lefeber, and F. Daerden. Second generation pleated pneumatic artificial muscle and its robotic applications. *Advanced robotics*, 20(7):783–805, 2006.

[166] R. Versluys, A. Desomer, G. Lenaerts, O. Paret, B. Vanderborght, G. Van der Perre, L. Peeraer, and D. Lefeber. A biomechatronical transtibial prosthesis powerd by pleated pneumatic artificial muscles. *International Journal Modelling, Identification and Control*, 4(4):394–405, 2008.

[167] D. Villegas, M. Van Damme, B. Vanderborght, P. Beyl, and D. Lefeber. Third-generation pleated pneumatic artificial muscles for robotic applications: Developent and comparison with mckibben muscle. *Advanced Robotics*, 26(11-12):1205–1227, 2012.

[168] B. Wang, A. McDaid, K.C. Aw, and M. Biglari-Abhari. Design and development of a skinny bidirectional soft glove for post-stroke hand rehabilitation. *Intelligent Systems Conference*, pages 979–987, 2017.

[169] J. Wirekoh and Y. Park. Design of flat pneumatic artificial muscles. *Smart Materials and Structures*, 26, 2017.

[170] C. Xiang, J. Guo, Y. Chen, L. Hao, and S. Davis. Development of a sma-fishing-line-mckibben bending actuator. *IEEE Access*, 6, 2018.

[171] K. Xing, J. Huang, Q. Xu, and Y. Wang. Design of a wearable rehabilitation robotic hand actuated by pneumatic artificial muscles. *Proceedings of the 7th Asian Control Conference*, pages 740–744, 2009.

[172] C. Ying, Z. Jia-fan, Y. Can-jun, and N. Bin. Design and hybrid control of the pneumatic force-feedback systems for arm-exoskeleton by using on/off valve. *Mechatronics*, 17:325–335, 2007.

[173] J. Yuan, X. Li, C. Romaniello, K. Wu, E. Cook, T. Suzuki, and Y. Shi. Pneumatic micro-hand actuator for future space manipulation and robotics. *Proceedings of the ASME 2014 International Design Engineering Technical Conferences Computers and Information in Engineering Conference*, 2014.

[174] J. Zhang, C. Yang, Y. Chen, Y. Zhang, and Y. Dong. Modeling and control of a curved pneumatic muscle actuator for wearable elbow exoskeleton. *Mechatronics*, 18:448–457, 2008.

[175] W. Zhang, M.L. Accorsi, and J.W. Leonard. Analysis of geometrically nonlinear anisotropic membranes: application to pneumatic muscle actuators. *Finite Elements in Analysis and Design*, 41:944–962, 2005.

[176] X. Zhang and G. Krishnan. A nested pneumatic muscle arrangement for amplified stroke and force behavior. *Journal of Intelligent Material Systems and Structures*, 29(6):1139–1156, 2018.

[177] Y Zhang, D. Wang, Z. Wang, Y. Wang, L. Wen, and Y. Zhang. A two-fingered force feedback glove using soft actuators. *Haptics Symposium*, pages 186–191, 2018.

[178] Z. Zhang and M. Philen. Pressurized artificial muscles. *Journal of Intelligent Material Systems and Structures*, 23(3):255–268, 2011.

[179] H. Zheng and X. Shen. Concept, design and application of sleeve muscle actuator. *Proceedings of the ASME 2014 International Design Engineering Technical Conferences Computers and Information in Engineering Conference*, 2014.

[180] H. Zheng, M. Wu, and X. Shen. Pneumatic variable series elastic actuator. *Journal of Dynamic Systems, Measurement, and Control*, 138, 2016.

[181] L. Zheng, S. Yoshida, Y. Morimoto, H. Onoe, and S. Takeuchi. Pneumatic balloon actuator with tunable bending points. *IEEE Internationl Conferene on Micro Electro Mechanical Systems (MEMS)*, pages 18–21, 2015.